Mechanistic investigations of organocatalytic and gold-catalyzed reactions and synthetic approach towards a chiral bifunctional catalyst

Dissertation

Kim Heike Schuppener

Bonn 2023

Mechanistic investigations of organocatalytic and gold-catalyzed reactions and synthetic approach towards a chiral bifunctional catalyst

Dissertation

zur

Erlangung des Doktorgrades (Dr. rer. nat.)

der

Mathematisch-Naturwissenschaftlichen Fakultät

der

Rheinischen Friedrich-Wilhelms-Universität Bonn

vorgelegt von

Kim Heike Schuppener

geboren in

Andernach

Bonn 2023

Angefertigt mit der Genehmigung der Mathematisch-Naturwissenschaftlichen Fakultät der Rheinischen Friedrich-Wilhelms-Universität Bonn

1.Gutachter: PD Dr. Marianne Engeser

2.Gutachter: Prof. Dr. Arne Lützen

Tag der Promotion: 27.04.2023

Erscheinungsjahr: 2023

Ich versichere hiermit, dass ich die vorliegende Arbeit unter Einhaltung der Regeln guter wissenschaftlicher Praxis selbstständig verfasst habe. Für die inhaltliche Erstellung habe ich keine fremde Hilfe, insbesondere keine entgeltliche Hilfe, in Anspruch genommen. Es wurden keine anderen Quellen und Hilfsmittel als die von mir angegebenen benutzt. Stellen, die dem Wortlaut oder Sinn nach anderen Arbeiten entnommen wurden, sind durch Angabe der Quellen als Zitate kenntlich gemacht. Außerdem versichere ich, dass die vorgelegte Arbeit nicht bereits anderweitig als Dissertation eingereicht oder veröffentlicht worden ist und kein früherer Promotionsversuch unternommen worden ist.

Kim Heike Schuppener

Plaidt, 2023

Danksagung

Zunächst möchte ich PD Dr. Marianne Engeser meinen Dank aussprechen, nicht nur dafür, dass Sie mir ermöglicht hat, meine Dissertation in ihrem Arbeitskreis anzufertigen, sondern auch dafür, dass sie mich in die Welt der Analytik eingeführt hat. Ich danke ihr für die bereichernden Gespräche über Massenspektrometrie und andere ergänzende Methoden, die mich immer wieder selbst dazu angeregt haben, alles aus einer neuen Perspektive zu betrachten. Ich konnte mich dank ihrer empathischen Betreuung immer mit Problemen an sie wenden und hatte stets das Gefühl, selbst an allen Gedankengängen und Vorgängen beteiligt zu sein.

Des Weiteren danke ich Prof. Dr. Arne Lützen, der sich bereit erklärt hat, das Zweitgutachten meiner Arbeit anzufertigen. Dabei sind einige seiner Anregungen schon im Vorfeld in die Projekte eingeflossen und haben des Öfteren dazu geführt, einen neuen Weg zu beschreiten.

Außerdem danke ich Prof. Dr. Bredow und Prof. Dr. Imhof dafür, dass sie als Dritt- und Viertprüfer diese Arbeit erst ermöglicht haben.

Der Jürgen Manchot Stiftung danke ich an dieser Stelle für die finanzielle Unterstützung, ohne die meine Promotion nicht möglich gewesen wäre. Dabei möchte ich mich vor allem für den unkomplizierten und netten Kontakt bedanken.

Ein weiterer Dank geht an Dr. Roland Schlesinger für die finanzielle Unterstützung durch das PC-Praktikum. Es hat mir all die Jahre viel Freude gemacht, dort lehren zu dürfen. Ich möchte mich bei Lilly Hofmann bedanken, deren unzählige GC-MS-Messungen ein wichtiger Bestandteil dieser Arbeit sind. Zudem danke ich Andreas Schneider für die extrem kompetente Unterstützung mit der UHPLC. Dem NMR-Team möchte ich für die erfüllten Sonderwünsche danken. Ein besonderer Dank gilt Lukas Lauterbach, der mir sehr bei meinen GC-MS-Messungen geholfen hat. Außerdem möchte ich Luca Denkler als erweitertes Mitglied der Arbeitskreisfamilie für die vielen tollen Mittagspausen danken.

Zudem danke ich dem gesamten Arbeitskreis für die vielen tollen Erlebnisse auch abseits des Laboralltags. Johann Alexander Willms danke ich dafür, dass er mich durch seine herzliche Art schon während meines Bachelorstudiums für diesen Arbeitskreis begeistert hat. Julius Nimzyk sei gedankt für die witzigen Momente, die unseren Arbeitsalltag immer wieder erfrischt haben. Des Weiteren bedanke ich mich bei Anne Müller-Feyen für die angeregten Diskussionen über Gott und die Welt. Es war mir immer ein Vergnügen. Außerdem danke ich Anne Schnell für die Gespräche über organisatorische und analytische Probleme aller Art. Ein besonderer Dank gilt Aron Janusko, der mir stets mit Rat und Tat, vor allem bei Syntheseproblemen, zur Seite stand. Auch wenn ich nicht immer sofort oder manchmal auch nach einiger Zeit einsehen wollte, dass man sich das Leben leichter machen kann, habe ich durch seine Vorschläge am Ende oftmals mein Ziel erreicht. Danke für die Geduld.

Wiebke Rautenberg möchte ich für die monatelange Morgenbetreuung danken. Außerdem danke ich ihr für die stundenlangen Gespräche über Themen aller Art. Dabei habe ich mich immer über ein offenes Ohr und angeregten Diskussionen über Probleme des Laboralltags und darüber hinaus sehr gefreut. Des Weiteren danke ich Marius Herbst für die enorme Unterstützung. Ich bedanke mich für die oft langen und tiefgründigen Gespräche und die Empathie, die ich dabei erfahren durfte, für das immer da sein, auch bei trivialen Problemen und Geduld, die er stets mit mir hat.

Außerdem möchte ich Frederike Malburg und Lea Bergweiler für die jahrelange Unterstützung in allen Bereichen des Lebens danken, ohne die ich nicht so weit gekommen wäre. Danke für immer wieder aufbauende und verständnisvolle Worte, aber auch für die ein oder andere gerechtfertigte Schelte. Ich

danke beiden für den langen Weg, den sie schon mit mir gegangen sind und hoffe, dass ein noch längerer vor uns liegt.

Zuletzt geht noch ein stiller Dank, an die beiden Menschen, die dies hier leider nicht mehr lesen können.

Abstract

The first part of this thesis focuses on the mechanistic studies of an intermolecular cyclization reaction between an *α*,*β*-unsaturated aldehyde and an electron deficient primary alkyne to a cyclopentene carbaldehyde. Based on the concept of dual activation, a combination of a chiral secondary amine and a gold(I) catalyst are applied to induce the reaction. Precisely, the *L*-proline-derived base catalyst first enables a 1,4-addition of both substrates (Michael addition). Afterwards, a 5-*exo*-*dig*-cyclization occurs. Since the mechanism of the first reaction is already well explored, this thesis mainly focuses on the cyclization process. To obtain information of the mechanistic events, reaction monitoring was performed *via* a combination of ESI-MS and GC-MS. By means of ESI-MS, it was possible to detect transient species directly from the reaction solution. On one hand, the ESI-MS experiments enabled simultaneous detection of many components. On the other hand, this technique could not deliver precise information about the species' concentration in solution. As a consequence, the kinetic behavior of the components was monitored with GC-MS measurements in parallel.

At the starting point, two general mechanisms were conceivable. The first suggestions included the formation of an iminium ion that activates the aldehyde moiety in parallel to the Lewis acid activation of the primary alkyne. In the second approach, the secondary amine merely reacts as a base. Thus, only the gold(I) complex binds to the Michael product. Nevertheless, the need of assistance from the *L*-proline derivative was uncontroversial. The reaction monitoring *via* ESI-MS provided spectra containing species that were in accordance with both catalytic cycles suggested. The characterization of those species was supported by CID experiments. Additionally, an interesting deprotoaurated molecule was detected. However, the hypothesis that the gold catalyst would bind to the alkyne before the cyclization occurs could be ruled out by isotopic labeling of the primary alkyne's proton and later by successful application of a phenyl-substituted alkyne. Thereby, it was possible to demonstrate that the scope of substrates can be extended to substituted alkynes. Interestingly, mono- and diaurated species were detected simultaneously for every substrate combination. The gold-containing molecules were observable with and without an amine attached to them. In accordance with other mechanistic studies, all species containing two gold atoms were identified as *gem*-diaurated species that emerge as product of the ESI process and do not participate in the reaction itself. Finally, base exchange experiments with pyridine and triethylamine demonstrated that binding of the *L*-proline derivative is crucial for the cyclization reaction. Thus, the iminium ion cycle was confirmed and completed. Additionally, GC-MS monitoring showed that the reaction is limited by the rate determining step (RDS) of the Michael addition which is the addition to the first iminium ion. The cyclization's RDS could be revealed to be the release of the amine catalyst. Both RDS could be determined due to variation of the reaction solution's pH value.

Inspired by the efficiency of the dual activation reaction, attempts were made to synthesize a gold catalyst that also enables iminium and enamine formation. Precisely, it was planned to combine an *N*-heterocyclic carbene ligand with an *L*-proline moiety. To connect both fragments, an ether bridge with a simple alkyl chain was used that promised maximum flexibility of the ligand. With this approach, a favorable alignment of both catalytic moieties was anticipated. The first synthetic steps could be conducted successfully. Thereafter, the connection of the alkyl linker to the proline moiety proved to be challenging. At least two side products were identified by means of ESI-MS. Nevertheless, two following reaction steps were performed successfully. Even though, only small amounts of the ligand precursor could be obtained, this demonstrated that the general route is viable. However, the connection of the two fragments most probably occurs more efficiently if the leaving group is placed on the proline-fragment instead of the alkyl chain.

Abstract

In the third part of this thesis a kinetic study of a domino cyclization with oxidative coupling induced by aurochloric acid is presented. Prior mechanistic investigations of this working group *via* ESI-MS already provided insights into the mechanistic events. While simultaneous ESI-MS measurements showed no differences to the first study, reaction monitoring with quantitative UHPLC-coupled UV/Vis spectroscopy in parallel debunked the hypothesis that reaction times of several hours are required. Moreover, the reaction proved to occur too fast to be monitored by the original setup. Finally, a significant deceleration of the whole reaction was provoked by dilution of the initial reaction solution. This confirmed that the domino cyclization with oxidative coupling is terminated within minutes.

Table of content

1 Introduction 1
1.1 Homogenous gold catalysis 1
1.2 Organocatalysis 7
1.3 Dual activation principle 10
2 Instrumental analytics 13
2.1 First mass spectrometers and common mass analyzers 13
2.2 Electron ionization 14
2.3 Gas chromatography 15
2.4 Electrospray ionization 16
2.5 Tandem mass spectrometry 19
3 Mechanistic investigations of a dual activation reaction: Interplay between metal and organocatalysis 21
3.1 Introduction 21
3.2 Synthesis 23
3.2.1 Synthesis of the starting materials 23
3.2.2 Synthesis of the cyclic products 24
3.2.3 Synthesis of the acyclic Michael products 28
3.2.4 Preparations for the gas-chromatographic reaction monitoring 29
3.3 Overall reaction – ESI-MS experiments 31
3.4 Overall reaction – GC-MS experiments 44
3.5 Stepwise approach 49
3.6 Base exchange experiments 52
3.7 Acid and base influence 55
3.8 Conclusions 61
4 Synthetic approach towards an *L*-proline-coupled NHC-gold(I) complex 63
4.1 Introduction 63
4.2 First synthetic ideas 63
4.3 First synthetic approach 65
4.4 Further synthetic ideas and new synthetic strategy 66
4.5 Second synthetic approach 71
4.6 Conclusions and outlook 76
5 Kinetic investigations of a domino cyclization with oxidative coupling catalyzed by aurochloric acid 79
5.1 Introduction 79

5.2 Quantitative ^{1}H NMR experiments ... 81
5.3 Quantitative UHPLC-UV/Vis experiments ... 86
5.4 Conclusions ... 88
6 Conclusions of this thesis ... 91
7 Experimental section ... 93
7.1 General indications ... 93
7.2 Instruments, methods and chemicals ... 93
7.2.1 Thin-layer chromatography ... 93
7.2.2 Column chromatography ... 93
7.2.3 NMR spectroscopy ... 94
7.2.4 Mass spectrometry ... 94
7.2.5 UHPLC-coupled UV/Vis ... 97
7.2.6 Chemicals ... 98
7.3 Experimental procedures for the synthesis ... 99
7.4 Experimental procedures for the ESI-MS and GC-coupled EI-MS experiments of chapter 3 and 4 ... 103
7.4.1 For chapter 3.3, 3.4 and 3.7 ... 104
7.4.2 For chapter 3.5 ... 104
7.4.3 For chapter 3.6 ... 104
7.4.4 For chapter 3.7 ... 105
7.4.5 For chapter 4.4 ... 105
7.5 Experimental procedures for the quantitative ^{1}H NMR and UHPLC-coupled UV/Vis experiments of chapter 5 ... 105
7.5.1 For chapter 5.2 ... 106
7.5.2 For chapter 5.3 ... 106
8 Literature ... 109
9 Appendix ... I
9.1 List of abbreviations – General abbreviations ... I
9.2 List of substances ... III
9.3 Additional spectra, tables and fragmentation schemes ... VI
9.4 Data tables of all graphs ... XV
9.5 List of reaction names – Original data in the lab journals ... XXXIX

1 Introduction

1.1 Homogenous gold catalysis

Homogenous gold catalysis has been known for over a century but was not in the center of interest for a long time.[1,2] In contrast to palladium or platinum, gold cannot chemisorb or dissociate oxygen or hydrogen.[3] This led to a severe misjudgment: Gold was regarded as chemically inert.[4] In the 1980s, the group of *Hutchings*[5,6] was able to invert this image completely, recognizing gold's excellent and superior potential for electrophilic activations of alkynes.[2] They discovered that supported cationic gold can be applied in the hydrochlorination of acetylene.[6] Thereby, the highly toxic mercury chloride catalyst, used in chemical industry up to that time, could be avoided.[4] Single-side gold(I) and gold(III) cations were revealed to be the active species by *Malta et al.*,[7] who presented X-ray spectroscopic studies of the working catalyst in combination with computational modeling. In 1987, *Haruta* and co-workers[8] found that gold nanoparticles can also be of use for CO oxidation reactions. They presented vast combinations of aurochloric acid with transition metals that form reactive catalysts.[8] This extended the field of gold catalysis to hydrogenation reactions.[9] Based on these discoveries, the interest in gold-mediated reactions increased significantly.[4] Thus, gold catalysis is nowadays a well-established tool in organic synthesis.[10] More precisely, gold catalysts do not only convince by their excellent reactivity but also by their facile handling since they are usually neither sensitive to water nor oxygen.[1,11] Additionally, the application of gold catalysts can protect the environment from unnecessary pollution and contamination with toxic transition metal catalysts and their remnants, supporting the concept of green chemistry.[1,4]

In general, gold catalysis can either be heterogeneous[5,6,8,9,12] or homogeneous.[13,14] Heterogeneous gold catalysis usually includes supplementary redox chemistry.[12] This requires an additional oxidant if the oxidation is not induced by a dehydrogenation.[12] In contrast, homogeneous gold catalysts typically activate carbon-carbon multiple bonds like alkenes, allenes or alkynes.[15] Usually, π-coordination by mono- or dinuclear catalysts occurs.[16,17] In this process, the strong but mild carbophilic π-Lewis acidity of cationic gold(I) and gold(III) catalysts is exploited.[18–20] The π-complex can then be attacked by a broad scope of nucleophiles.[4,21] Thereby, the nucleophiles as well as the electrophile itself can be offered inter- or intramolecularly delivering access to a vast field of reactivity patterns.[17]

For a long time, homogeneous gold catalysis usually involved only one gold atom.[10] Until *Toste* and co-workers[22] reported computational mechanistic studies supported by experimental data in 2008, which gave first evidence of a dual π,σ-activation of an 1,5-allenyne by a single gold catalyst (scheme 1.1). Additionally, they postulated that a *gem*-diaurated complex was involved in releasing the newly formed cycloisomer.[22,23] The first *gem*-diaurated species had already been reported by the group of *Nesmeyanov*[24] in 1973, but did not gain much attention in context of gold catalysis at that time. Later, the field of dual gold catalysis was opened by *Hashmi et al.*[25] and the group of *Zhang*.[26] In 2012, both reported a simultaneous activation of electrophile and nucleophile independently.[25,26] The synergistic interplay (chapter 1.3) of a π-coordinated electrophile and a σ-bonded nucleophile revolutionized the whole perspective of gold catalysis as well as transition metal catalysis in general.[10] In accordance with these reactions, later studies postulated that the *gem*-diaurated species found were catalyst resting states.[27–30]

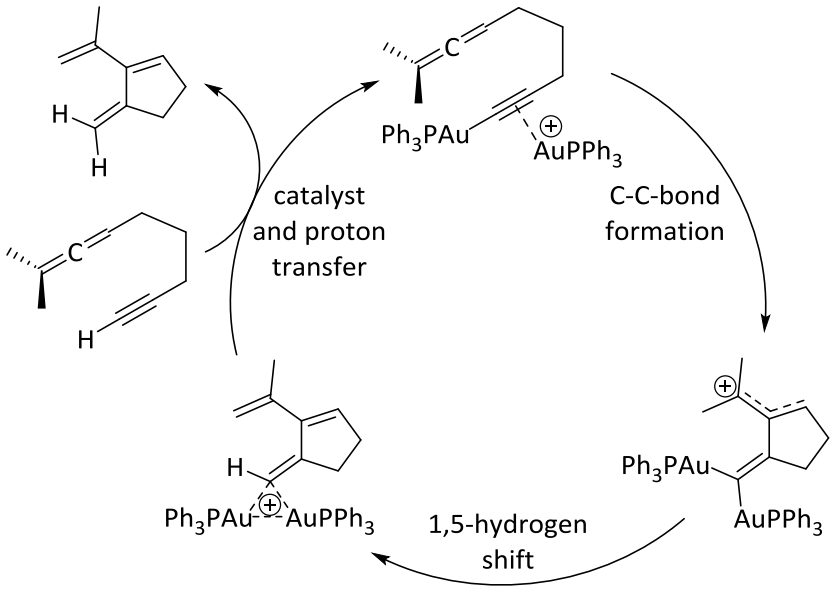

Scheme 1.1. Mechanism postulated for the gold-catalyzed cycloisomerization of an 1,5-allenyne *via* dual activation of an ene reaction by the group of *Toste*.[22]

In general, *gem*-diaurated compounds can be formed by a simple equilibrium of the active catalyst and a monoaurated vinyl species.[31] Scheme 1.2 depicts a general mechanism for a gold(I)-catalyzed nucleophilic addition to an alkyne.[22] The cycle can be sectioned into four steps: First, the π-coordination of the alkyne moiety to the active gold(I) catalyst takes place.[22] Then, the nucleophilic attack occurs.[22] The resulting monoaurated vinyl cation is deprotonated in the next step.[22] Finally, after a protodeauration, the product is released and the catalyst is regained.[22] Since other molecules of the active catalyst are present in the reaction solution, a second gold(I) cation can reversibly react with the neutral monoaurated vinyl species and form a *gem*-diaurated compound.[22] In contrast to the neutral monoaurated vinyl molecule, the *gem*-diaurated complex is stable towards acid and thus difficult to protodeaurate.[31] As a consequence, the product is not released from this molecule.

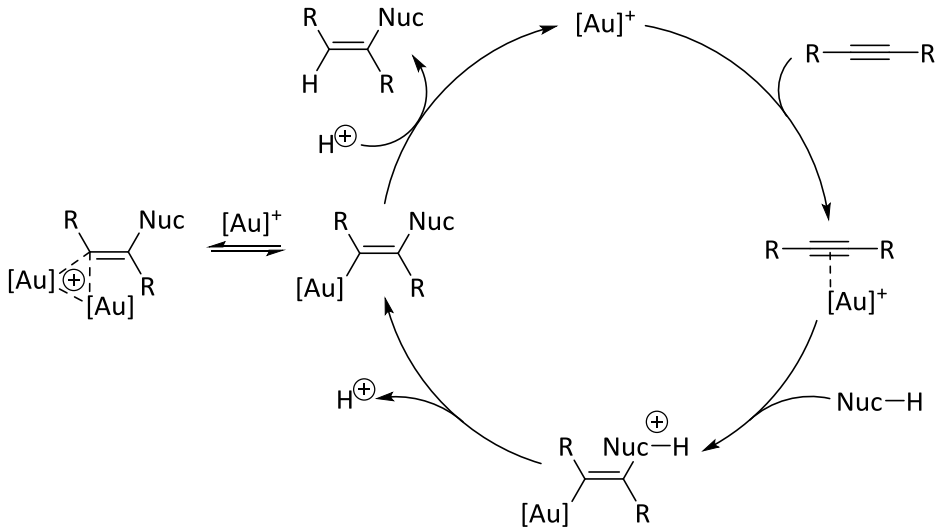

Scheme 1.2. Equilibrium of a monoaurated vinyl species and the corresponding *gem*-diaurated molecule during the addition of a nucleophile (Nuc) to an alkyne.[31]

Compared to monoaurated vinyl species obtained by primary alkynes, the formation of a *gem*-diaurated complex with a secondary monoaurated C-C double bond possesses a different binding motif (scheme 1.3). If a hetero atom is connected in α-position to the gold complex, the formation of a σ-Au-C bond is observed.[29,31,32] By means of X-ray analyses combined with *nuclear magnetic resonance* (NMR)

spectroscopy, it was possible to determine bond lengths of different diaurated compounds and compare them to the measurements of the corresponding monoaurated molecules.[33] The C-C double bond proved to be elongated after the second gold atom was attached.[33] On the other hand, the C-hetero bond was contracted and possessed higher double bond character.[33] Thus, it can be assumed that the *σ*-character of an Au-C bond is significant if a heteroatom is involved.[31]

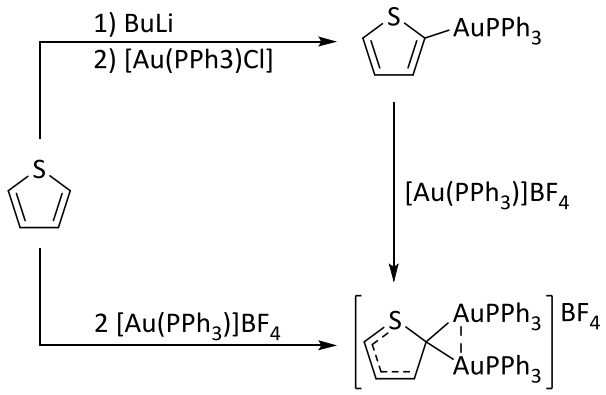

Scheme 1.3. Example of a *gem*-diaurated complex with *σ*-Au-C bond for diraurated thiophene. The monoaurated molecule as well as the diaurated complex were isolated and characterized *via* NMR spectroscopy by *Schmidbaur* and co-workers.[31,33]

In contrast, NMR studies of diaurated vinyl species indicated that the three-center-two-electron bond is stabilized by aurophilic interactions (5-10 kcal/mol).[34] As a result, the *gem*-diaurated complex is very stable and can even resist acids.[31] Only if bulky phosphine ligands are applied, the bond lengths were similar to the ones of the *σ*,*π*-complexes, that are formed when heteroatom substituents are involved.[35] In this case, the propensity to react with Brønsted acids is diminished even further.[35] In general, most of the numerous studies on the vinyl-type *gem*-diaurated species have concluded that the stable cationic complexes are off-cycle catalyst resting states.[27–30,36] Contrarily, the groups of *Hashmi*,[25,37,38,39] *Roithová*[40,41] and *Gagosz*[42] found evidence for an active role of this interesting type of molecule in the catalytic cycle.

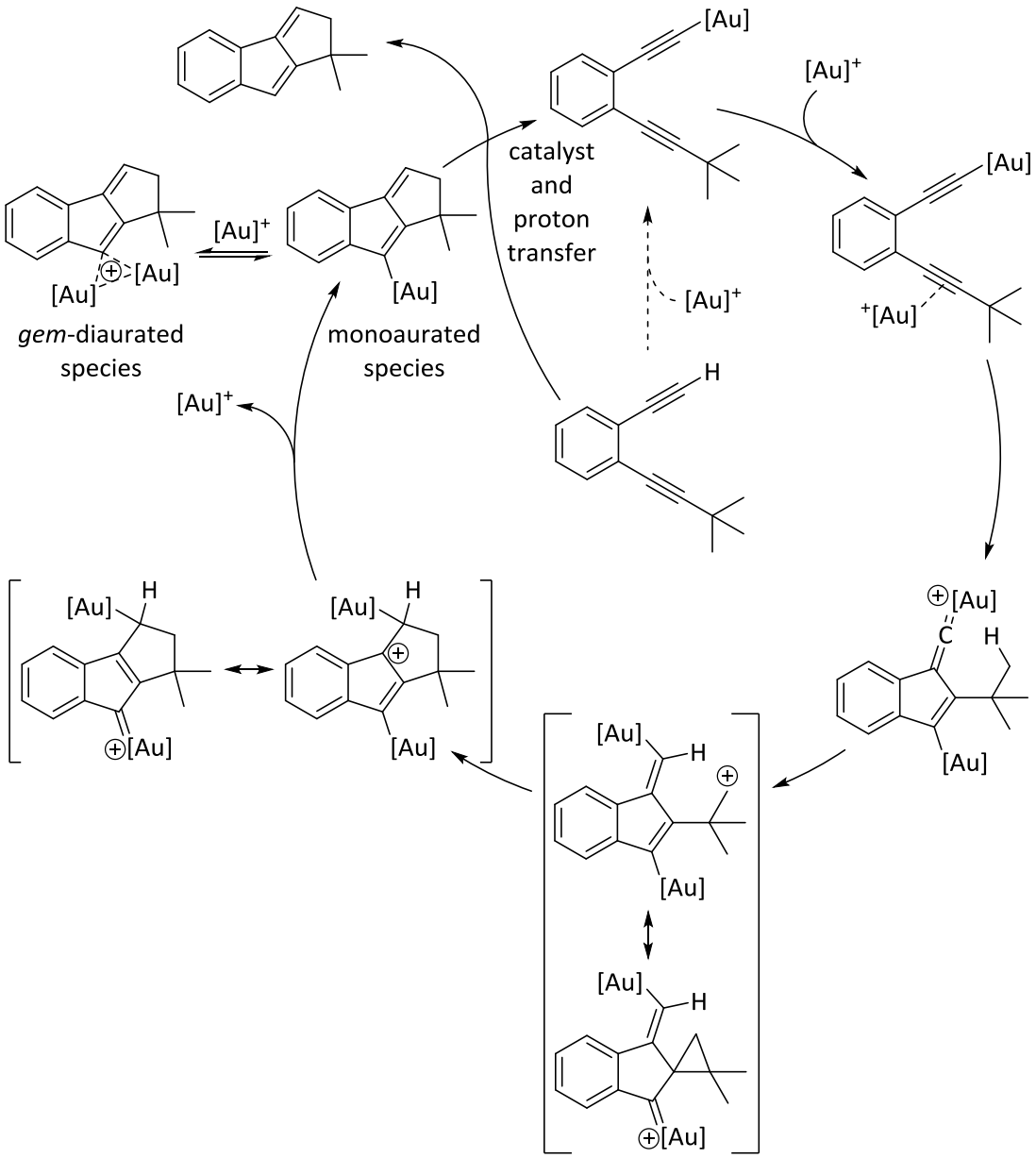

Scheme 1.4. Mechanistic suggestion of the dual gold activation reaction by the group of *Hashmi*.[39] The *gem*-diaurated species serves as catalyst supply.

In 2012, *Hashmi* and co-workers[39] presented a synthetic approach towards benzofulvenes. During this reaction, two five-membered rings are formed by the reaction of a primary and a secondary alkyne in *ortho*-position (scheme 1.4).[39] On one hand, this classical dual gold catalysis involves a deprotoauration at the primary alkyne.[39] Thereby, the *β*-carbon of the alkyne moiety is activated to react as a nucleophile.[39] On the other hand, the secondary alkyne coordinates to another gold atom which enables the nucleophilic attack on this alkyne.[39] As already described for scheme 1.2, the monoaurated gold molecule at the end of the catalytic cycle can either form a *gem*-diaurated complex (resting state) or release the product.[39] The product release is induced by a second substrate molecule on which the catalyst is transferred to.[39] Interestingly, if the *gem*-diaurated molecule is used directly as catalyst, the reaction proceeds three times faster than with the original catalyst molecule.[39] This can be explained by the fact that the probability of catalyst molecules reacting with one substrate is significantly increased by this approach. It has to be mentioned that initial formation of the gold acetylene by the substrate and the free catalyst is considered to be slow.[25] Therefore, the catalyst transfer is essential for an efficient reaction. Starting from the stable *gem*-diaurated catalyst, this species can only form the active

monoaurated molecule. This equilibrium acts as a supply for the catalyst transfer step and increases the concentration of the catalyst transfer substrate.[31] As a result, the attachment of the first catalytic unit to the original substrate (catalyst transfer – product release) is enhanced significantly when a high concentration of the *gem*-diaurated species is present.

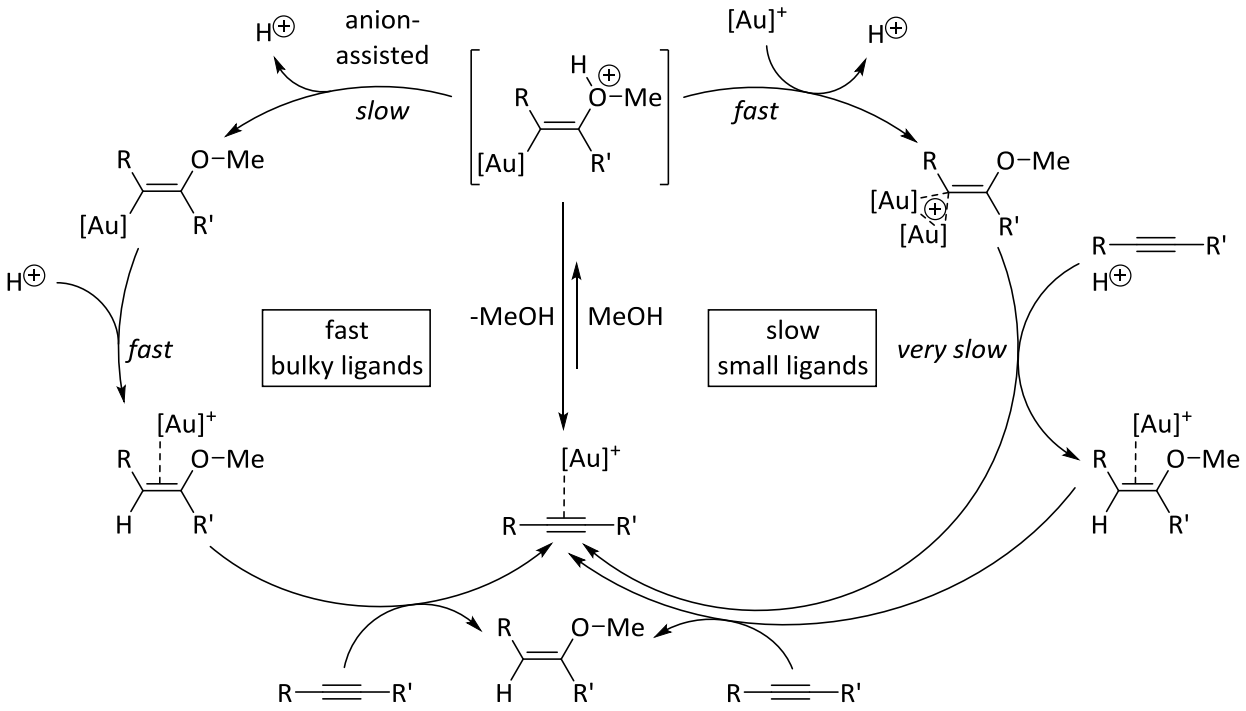

Scheme 1.5. Mechanism of the gold-catalyzed addition of methanol to an alkyne by *Roithová* and co-workers.[40] The slow pathway *via* a *gem*-diaurated complex can be suppressed by bulky ancillary ligands.

Based on this work, the group of *Roithová*[40] investigated a gold-mediated addition of methanol to an alkyne by means of ESI-MS (*electrospray ionization mass spectrometry*) and NMR spectroscopy combined with *density functional theory* (DFT) *calculations* (scheme 1.5). In these studies, the noble metal's ligands proved to play a decisive role.[40] In case of a small phosphine ligand (PPh_3), the mechanism proceeds *via* a *gem*-diaurated species.[40] This cycle's driving force is the exchange of the proton bound to the oxygen atom.[40] Afterwards, the transmetallation to another alkyne is extremely hindered by electronical effects since protodeauration of already cationic *gem*-diaurated compounds is not favored.[37,40] The second cycle represents the anion-assisted mechanism.[40] This pathway occurs if a bulky ancillary *N*-heterocyclic carbene (NHC) ligand (for example IPr) is applied.[40,43] The steric demand of the ligand suppresses the attachment of the second gold center.[40,44] Thus, the slow deprotonation of the monoaurated intermediate can take place.[40] In contrast to the cationic *gem*-diaurated intermediate, the neutral monoaurated species can easily be protonated thereafter.[40] Interestingly, the anion-assisted reaction is generally faster, but inhibited if the substrate is trapped by the immediate formation of the stable *gem*-diaurated intermediate.[39,40]

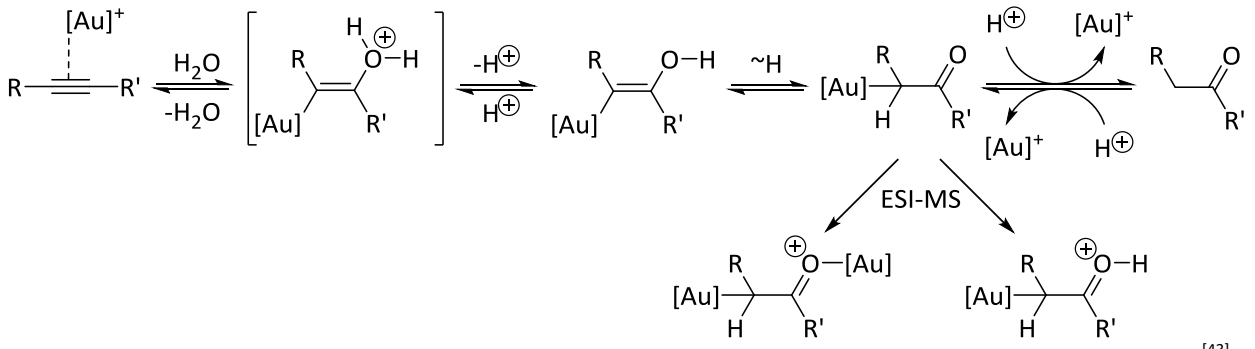

Scheme 1.6. Reaction pathway of the gold-catalyzed addition of water to an alkyne by the group of *Roithová*.[43] During the ESI process, a diaurated species is formed along with the protonated species of the monoaurated intermediate.

Recently, the same group presented a related mechanistic study about the gold-catalyzed addition of water to an alkyne (scheme 1.6).[43] For their experiments, a combination of ESI-MS with *infrared* (IR) *spectroscopy* (*infrared multiphoton dissociation* – IRMPD)[45,46] was used.[45,47] IRMPD provides IR spectra for mass-selected species in the gas phase which allows a structural insight into the individual ions.[41] Additionally, they performed isotopic labeling experiments. With the *delayed reactant labeling* method[48] the kinetics of reaction intermediates in solution can be monitored by ESI-MS. This is very exceptional since ESI-MS usually does not provide quantitative information about species in solution (chapter 2.4).[41] Based on these modern tools and with assistance of DFT calculations, the formation of *gem*-diaurated species during the anion-assisted mechanism was revealed (scheme 1.6).[40,43] After the nucleophilic attack and the subsequent deprotonation of the resulting cationic molecule, a proton shift occurs.[43] This step has already been postulated by the group of *Hashmi*[39] and proven by isotopic labeling experiments of G*agosz* and co-workers.[42] In accordance with these results, the *Roithová* group[43] found that a fast tautomerization occurs, stabilizing the ketone. Interestingly, the IR spectra did not show any C-O bond stretching for the mass-selected diaurated species.[43] Thus, the formation of a *gem*-diaurated intermediate in solution was excluded.[43] If no C-C double bond is present in the diaurated molecules, the second gold atom has to bind to the oxygen instead.[43] Additional acid and base experiments supported this hypothesis and revealed the first-order dependence on the gold catalyst concentration.[43] All this led to the conclusion that only monoaurated species are present in the reaction solution and the diaurated molecules are merely artifacts of the ESI process.[43] For a similar system with a small PPh_3 ligand, *Lu et al.*[49] detected a diaurated intermediate by means of ESI-MS. Their DFT calculations showed that in this case, the formation of a *gem*-diaurated complex is energetically favored compared to the attachment of the second gold atom to the nucleophile's heteroatom.[49] This again demonstrated that the formation and binding character of diaurated species heavily depends on the gold catalyst's ligand.

Concerning the addition to alkynes, *Roithová* and co-workers[40,43] chose an NHC ligand for their experiments with bulky ligands. In 1991, *Arduengo et al.*[50] reported the synthesis of the first stable NHC ligand. It took another decade until the first applications in gold catalysis were presented.[51] Nowadays, this type of ligand is used for numerous applications, including the introduction of chirality into gold catalysis.[20,52] NHC ligands convince by their unique electronic qualities as *σ*-donors and steric features.[53–57] Therefore, they overcome shortcomings of phosphine ligands that are often applied in the field of gold catalysis.[31,57,58] Since gold(I) complexes possess a linear geometry, small phosphine ligands are not able to limit the complexes' rotation around the Au-ligand bond.[18,59] This complicates the transfer of chiral information from the ligand to the substrate and makes enantioselective gold catalysis challenging.[20]

1.2 Organocatalysis

For a long period of time, selective catalysis was synonymous with either transition-metal-induced reactions or enzyme-mediated processes, while organocatalytic reactions only attracted little attention.[60] This changed dramatically at the beginning of the new millennium when the groups of *List*[61] and *MacMillan*[62] pushed this topic to the fore. While *List* and co-workers[61] gained much attention with an *L*-proline-mediated asymmetric aldol reaction, the group of *MacMillan*[62] presented a highly enantioselective Diels-Alder reaction catalyzed by a chiral imidazolidinone. In both reactions, small organic molecules were applied as catalysts that simultaneously induce stereoinformation into the products.[63] In 2021, their research was honored with the Nobel Prize in Chemistry.[64] Due to these works, the publications concerning organocatalysis rose tremendously.[63,65,66] At the beginning, the low reactivity of most organocatalysts caused high catalyst loadings.[61,67] Later, accurate catalyst design enabled lower catalyst concentrations outperforming even some of the most reactive metal and biocatalysts.[60,68]

In general, organocatalysts are small organic molecules that can be used to either activate electrophilic or nucleophilic substrates.[69,70] The principles of green chemistry can be easily complied, not only since the concept of catalysis itself enhances a reaction's effectiveness and efficiency.[71] The application of organocatalysts bears also other advantages compared to for example transition metal catalysts.[63,71] Most organocatalysts are inexpensive and readily available.[60,72] In contrast to the majority of transition metal catalysts, they are usually non-toxic and do not require toxic substances in addition.[63,72] Further, most of the organocatalytic reactions do not need to be carried out under inert gas since organocatalysts are usually neither sensitive to air nor moisture.[60,63,69,72] Moreover, the resulting products are also not contaminated with traces of metal that would require complex purification additionally to the expensive disposal of metallic waste.[63,72] These two facts are especially important if the product is applied in medicinal chemistry which does not tolerate metal contamination.[72] Another important fact for the green chemistry principle is that most of the reactions can be carried out under mild conditions.[63,71] Thus, less energy is required.[71] Furthermore, organocatalysts are only sensitive to some functional groups.[71] As a result, the need of protecting groups is reduced, lowering the number of reaction steps.[71] Additionally, organocatalytic reactions can easily be carried out in large scale.[63] All these points do not only facilitate the handling, but also reduce the costs of the individual processes. Nowadays, countless organocatalysts with many different reactivity patterns and mechanisms are established.[63,65,73]

A very popular example for this class of catalysts is proline which was used by the group of *List*.[61] This secondary amine is readily available in both enantiomeric forms and can be easily obtained from natural sources.[74] Additionally, the amino acid possesses a high nucleophilicity, making it an attractive tool for functionalizations of electron-deficient carbonyl compounds.[75] Nowadays, carbonyls are also activated by many well designed pyrrolidines and proline-based catalysts in context of organic synthesis.[76] If primary or secondary amines are applied, enamines and iminium ions are formed.[63,65] Thus, for carbonyl compounds, activation by *α*-, *β*- or *γ*-functionalization can be observed.[65,77] In case of saturated carbonyl compounds, usually an *α*-functionalization with an electrophile occurs.[65] This mechanistic approach is called *enamine catalysis*.[78] A general mechanistic cycle for the reaction of an aldehyde with an electrophile is shown in scheme 1.7.[65] First, the chiral secondary amine catalyst attaches to the aldehyde *via* condensation.[65] As a result, a highly acidic iminium ion is formed.[65] After deprotonation, the reactive nucleophilic enamine species can attack an electrophile and reform an iminium ion.[65] Finally, the *α*-functionalized product and the catalyst are released by hydrolysis.[65]

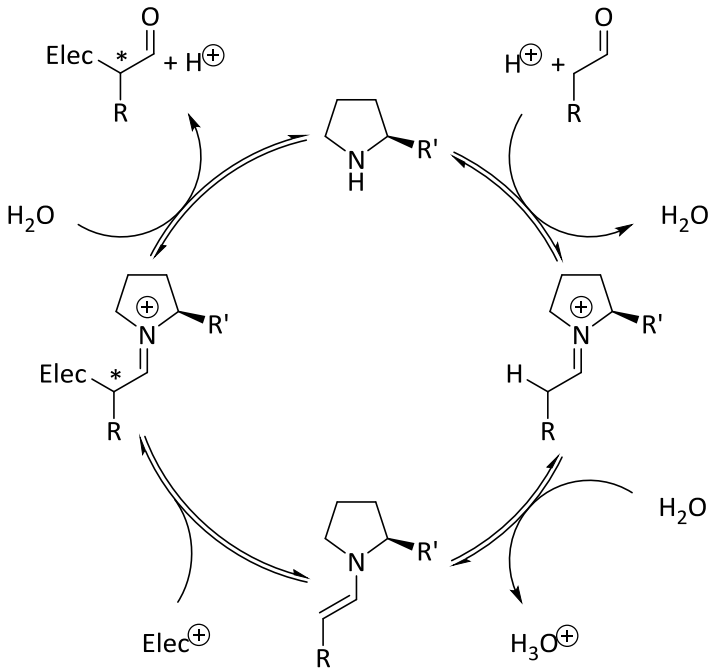

Scheme 1.7. Mechanistic cycle for the pyrrolidine-catalyzed *α*-functionalization of saturated aldehydes with electrophiles (Elec).[65]

The structure of the *σ*-bonded *trans*-enamine and the transition states have already been studied by *Houk* and *Cheong*[79] as well as the group of *Jørgensen*.[80] Since the HOMO (*highest occupied molecular orbital*) of the enamine species is higher in energy than the HOMO of the initial carbonyl compound, the interaction with the electrophile's LUMO (*lowest unoccupied molecular orbital*) or SOMO (*singly occupied molecular orbital*) is facilitated.[77] A high enantioselective control can be achieved by applying chiral amines.[77] Thereby, the catalysts can induce the chiral information by two opposite methods. In case of *L*-proline, the carboxylic acid can form a hydrogen bond which enables a *Re*-face attack from above (scheme 1.8a).[63,81] If a bulky group is attached to the pyrrolidine ring instead, the attack from above is sterically hindered and a *Si*-face attack occurs (scheme 1.8b).[63,81] The group of *Seebach*[82] additionally suggested that the oxazolidinone species, which is formed when *L*-proline is applied, plays a crucial role for the mechanism. In this approach, the formation of a five-membered heterocycle initiates the enamine's attack on the electrophile, while in the classic model the nitrogen's lone pair electrons are regarded as the trigger of the nucleophilic attack.[65,82] The discussion was intensified by the synthetic results of *Blackmod et al.*,[83] extensive NMR experiments on the oxazolidinone species conducted by *Gschwind* and co-workers[84] as well as other experimental and theoretical studies.[85,86,87] Recently, the *Engeser* group[88] was able to characterize this interesting species by means of ESI-MS and IRMPD. Nevertheless, the exact role of the oxazolidinone is still under discussion in the scientific field.[87,89]

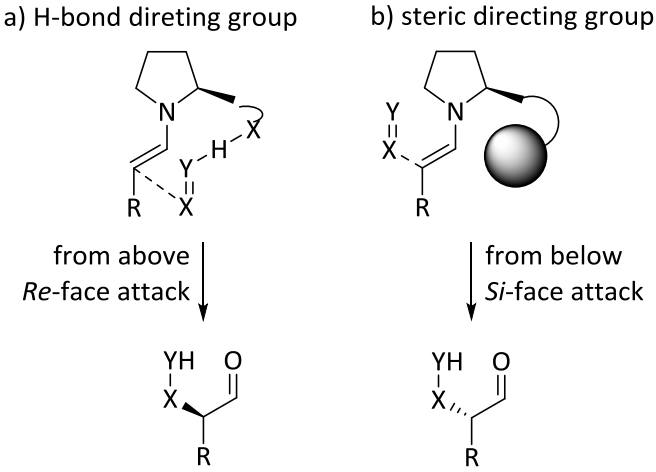

Scheme 1.8. Enamine intermediates of the electrophilic *α*-functionalization of saturated aldehydes with (a) hydrogen bond directed *Re*-face attack and (b) steric directed *Si*-face attack.[65,81]

In contrast to saturated aldehydes or ketones, *α*,*β*-unsaturated carbonyl compounds are activated by functionalization in *β*-position to react with nucleophiles.[63,65] The mechanism of the so-called *iminium ion catalysis*[62] is shown in scheme 1.9.[65] As in the enamine approach, the iminium ion mechanism starts with a condensation of the amine catalyst and the carbonyl moiety.[65] Since the carbonyl compound is *α*,*β*-unsaturated, a conjugated iminium ion results.[65] Subsequently, the nucleophilic attack occurs and an enamine is formed.[65] Under acidic conditions, another iminium ion emerges.[65] Afterwards, the catalyst is cleaved off and the product is released.[65] The structure and character of the iminium ion intermediates as well as their reactivity were investigated by the group of *Jørgensen*.[90] Their computational studies suggested that a *trans*-*trans*-iminium ion is energetically favored.[90] As a consequence, a *Re*-face attack occurs.[90] In contrast to the enamine in the *α*-functionalization, the iminium ion controls the enantioselectivity by steric hindrance, only shielding one diastereotopic face (scheme 1.10).[63,65] The formation of hydrogen bonds was excluded by X-ray studies of the *Seebach* group.[91]

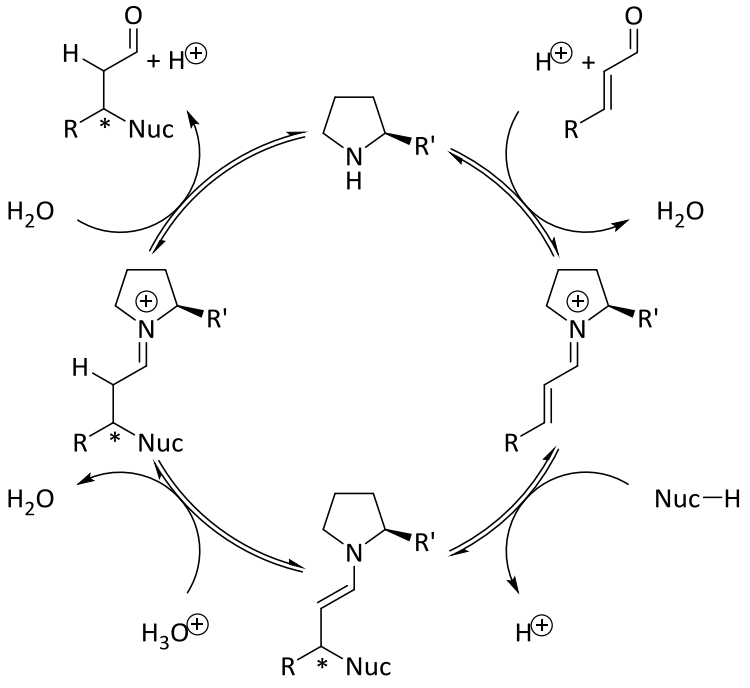

Scheme 1.9. Mechanistic cycle for the pyrrolidine-catalyzed *β*-functionalization of *α*,*β*-unsaturated aldehydes with nucleophiles (Nuc).[65]

In general, the LUMO of the iminium ion is lower in energy than the LUMO of the initial carbonyl compound.[63,77] Thus, the iminium ion's electrophilic character is increased and the subsequent nucleophilic attack is facilitated.[77] Since all processes shown in the mechanistic cycle of scheme 1.9 are reversible, attention must be paid to the chemical properties of the nucleophile to prevent undesired 1,2-additions.[65] This is especially the case for hard heteroatomic nucleophiles that attach more easily at the harder electrophilic carbon atom in 2-position compared to the one in 4-position.[65] Further, it is possible to invert the reactivity of *α*,*β*-unsaturated carbonyls.[92] For this purpose, the transient iminium ion must be deprotonated in the *γ*-position rendering an electron-rich dienamine that can react with electrophiles.[92] In this case the HOMO of the dienamine species is higher in energy than the HOMO of the *α*,*β*-unsaturated carbonyl compound.[93] As a result, the attack on an electrophile is facilitated.[93]

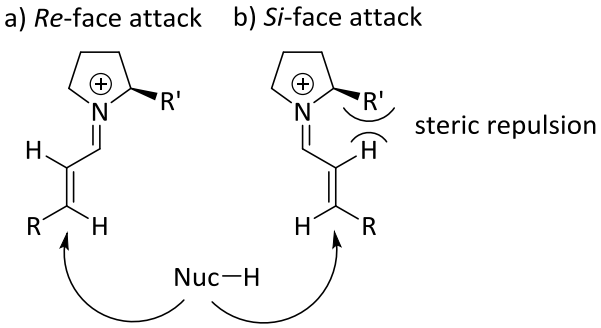

Scheme 1.10. Iminium ion intermediates of the *β*-functionalization of *α*,*β*-unsaturated aldehydes with nucleophiles (Nuc) with (a) favored *Re*-face attack and (b) unflavored *Si*-face attack.[65,81]

Mayr and co-workers[75,94–96] investigated the nucleophilicity and electrophilicity of iminium ions and enamines derived from pyrrolidines. For the *Jørgensen-Hayashi* catalyst (chapter 3, scheme 3.1, molecule **3**),[97] they found that the enamine derived from the diphenylprolinol silyl ether (nucleophilicity = 10.56)[95] is almost two orders of magnitude less reactive than the corresponding enamine formed by pyrrolidine (nucleophilicity = 12.25).[95] On the other hand, the iminium ion of the functionalized pyrrolidine catalyst (electrophilicity = -8.2)[94] proved to be 20 times more electrophilic than the one of pyrrolidine (electrophilicity = -9.8).[94] These results most probably originate from the electron-withdrawing aryl groups of the diphenylprolinol silyl ether and their negative inductive effect.[63,94,95] This proves that an individual catalyst design is essential for a successful synthesis favoring one mechanistic pathway over the other.

1.3 Dual activation principle

Transformations *via* monocatalytic concepts in transition metal (chapter 1.1) or organocatalysis (chapter 1.2) are limited since the catalytic unit usually only reacts with one single substrate.[98,99] Thereby, the energetic barrier for the new bond formation is only lowered by one side, the other substrate usually remains inactivated.[98] If the second reactant can in principle be activated by the same catalyst, the activation often requires the use of stoichiometric or even larger amounts of the catalytic unit or prior functional group manipulation.[99] As a consequence, not only higher amounts of potential environmentally harmful waste are generated, but also the economic effectiveness and efficiency is impaired.[72,100] To prevent these problems, two different catalysts can be applied in one single reaction opening access to many difficult and new transformations.[98,99,101–105,106] In general, these multi-catalytic systems can be assigned to four different catalytic principles. In case of *bifunctional catalysis*,[107] both

reaction partners are activated separately in individual catalytic cycles by discrete functional groups of the same catalyst.[108] Another approach is called *double activation catalysis*.[109] Thereby, two different catalyst molecules cooperate to activate the same substrate.[110] If this catalytic interplay occurs sequentially, in the sense that the second catalyst activates the intermediate of the first one, *cascade*[111] (*tandem*[112] and *domino*)[113] *catalysis* emerges. The fourth form of catalytic interplay is *synergistic*[98] (or *cooperative*)[114] *catalysis.* In this case, both reaction partners are activated simultaneously by two separate catalytic units.[99,102,103,105] As a result, the activation energy is lowered twice since both electrophile and nucleophile are activated (scheme 1.11).[103,104,115] More precisely, one catalyst lowers the LUMO (or SOMO) of the electrophile while the other elevates the energy level of the nucleophile's HOMO.[98] Thus, the activation energy gap between both energy levels is subsequently reduced compared to the activation energy of the original starting materials.[98]

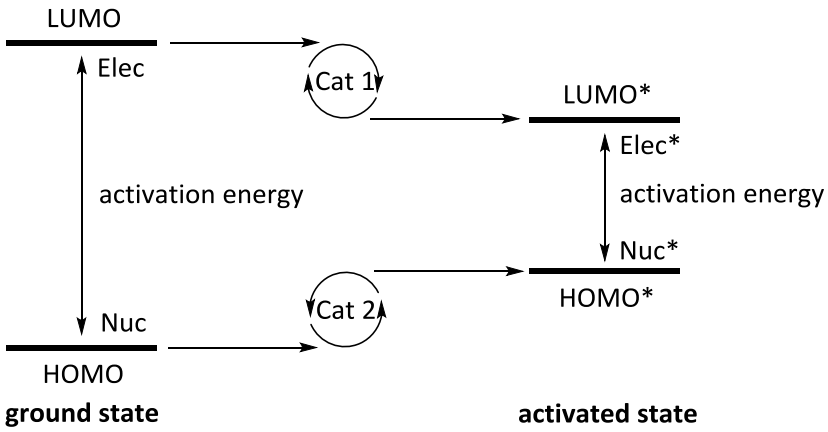

Scheme 1.11. Lowering of the activation energy by synergistic catalysis. The electrophile's (Elec) LUMO is lowered by catalyst (Cat 1) while the nucleophile's (Nuc) HOMO is elevated by the other catalyst (Cat 2).[104,115]

With the synergistic approach, the reactivity of the two reaction partners can be controlled simultaneously but separately.[103] As a result, the modulation of the HOMO-LUMO gap can be optimized and reactions are enabled under mild conditions.[103] A thoughtful choice of the two catalysts is essential for an optimized overall catalytic system.[98] In contrast to enzymatic processes *in vivo*, chemical reactions in organic synthesis do not imply a spatial separation of the two reactive catalytic moieties.[98] As a consequence, self-inhibition or even self-quenching of the catalytic system can occur, rendering both catalysts inactive.[98,116] For example irreversible complexation of a Lewis acid and base or spontaneous redox events take place.[98,114,116] Additionally, the increased reactivity of the reactants can enable possible side reactions, for example the reaction between an activated electrophile and an inactivated nucleophile.[98,105] This is especially adverse if the interaction with the catalytic unit induces the desired chirality into the molecule.[105]

In general, asymmetric transformations in organic synthesis are often performed, combining transition metals and organocatalysts.[101,116,117,118] The origin of chiral information can either be the transition metal catalyst or the organocatalyst or both.[103] In the last example, the application of two chiral catalytic units opens up the field of stereodivergent catalysis.[119] This gives access to all possible stereoisomers of the product by selection of the appropriate enantiomer of the catalysts.[119] If only one stereoisomer is targeted, the application of one chiral catalyst is usually sufficient.[118] In such cases, the advantages of the easily accessible chiral pool of amines are often combined with the efficiency of highly reactive transition metal catalysts.[63,101,103] As one particular example, chiral amine catalysts enable the activation of *α*,*β*-unsaturated carbonyl compounds, forming iminium ions that can easily be targeted by transition metal-activated alkynes.[103] Often, the chiral amine catalyst is a proline derivative like the *Jørgensen-Hayashi* catalyst which is nowadays particularly popular.[120]

2 Instrumental analytics

2.1 First mass spectrometers and common mass analyzers

In 1911, *Thomson*[121] presented the first mass spectroscope. Ions were sent through a combination of electric and magnetic fields separating them into several ion beams.[121,122] All ions of one beam possessed the same mass-to-charge ratio (*m*/*z*) which was detected by impact on a photographic plate.[121,122] The black traces' position on the plate correlated to the mass of the molecules, while the intensity of the spots gave information about the species' abundance.[121,122] The first mass spectrometer, though, was constructed by *Dempster*.[123] In this device, the detection no longer occurred by photographic plates, but *via* electrometers or electroscopes.[122,123] Later, *Bleakney*[124] isolated the electrons from the acceleration voltage for the ions and *Nier*[125] finally established the sector field mass spectrometer (Nier-type geometry).[122,126]

Nowadays, many different types of ion sources and mass analyzers can be coupled which enables the detection of a wide variety of analytes.[126] Some ionization methods that are relevant for this thesis are presented in detail later on (chapter 2.2 and 2.4). The most common mass analyzers of these days are *quadrupole*[127–129] (Q), *ion trap*[127–129] (IT), *time-of-flight*[130] (TOF) and Fourier transform analyzers like *Orbitrap* devices.[131,132] The analyte, the desired *m*/*z* range, the required resolving power and limit of detection as well as the interface with the ion source are relevant for the choice of a suitable analyzer since each device has its individual advantages.[133]

In general, the Q and IT instruments are related.[134] Both analyzer types employ a radio frequency (RF) potential and a superpositioned direct current (DC) potential.[126,133] Thus, ion oscillation within the device is induced.[133] As a result of distinct RF and DC potentials, only ions of a particular *m*/*z* value can pass though the analyzer.[126,133] In contrast, if the DC potential is reduced and solely the RF potential is applied (RF only mode), all ions can traverse the device.[126,133] In case of ITs, it is also possible to accumulate ions over time.[133] Thus, the sensitivity is enhanced.[133] However, all Q and IT analyzers are not suitable for accurate mass measurements and suffer from poor one unit resolution.[126,133]

Another important analyzer type is the TOF analyzer.[133] Within it, ions of different masses are accelerated by a voltage.[126] As a result, they possess the same kinetic energy but different velocities.[126] When they travel through a field-free drift path of a given length (flight tube),[133] their arrival time at the detector varies.[126,133] Thus, the individual time of flight can be used to calculate the ionic mass.[126,133] Compared to Q and IT devices, TOF analyzers are equipped with a high mass accuracy (0.2 u to 0.001 u)[126] and reasonable resolution (R = 1000 to 30,000).[126] Additionally, TOF instruments can achieve the widest mass range of all mass analyzers.[135]

The third category is represented by devices that apply Fourier transformation to convert an oscillation into an individual *m*/*z* value.[126] Nowadays, Orbitrap analyzers are a very popular example of these devices.[133] They are composed of an inner spindle electrode covered by two hollow outer concave electrodes facing each other.[131,132] The two outer electrodes are separated by a dielectric ring.[133] When ions enter tangentially, they can be trapped in a spiral path around the spindle.[132] Thereby, the electrical field within the device induces a harmonic oscillation.[131–133] This oscillation possesses a characteristic frequency for the individual mass of the ions.[132] Finally, the oscillation frequency obtained by Fourier transformation can be used to calculate the ions' *m*/*z* values and abundances.[126,132] While Orbitrap analyzers are significantly slower than TOF instruments, their high resolving power

(R = 20,000 to 200,000)[126] and extreme mass accuracy (10^{-6} u)[126] is unachieved by non-Fourier-transforming devices.[126,131]

As mentioned before, Q and IT instruments can also be used to guide ions into another analyzer.[126,132] A common example of combination is the quadrupole time-of-flight (Q/TOF) analyzer.[132] Thereby, ions are first filtered by the Q before entering the TOF analyzer orthogonally.[136] Combining both devices, a high mass accuracy and higher resolution compared to a simple Q or IT analyzer can be obtained.[133] Additionally, this facilitates the interface of TOF and continuous flow ion sources.[133] Typically, this pairing is a mismatch since TOF instruments usually require a package of ions.[133]

2.2 Electron ionization

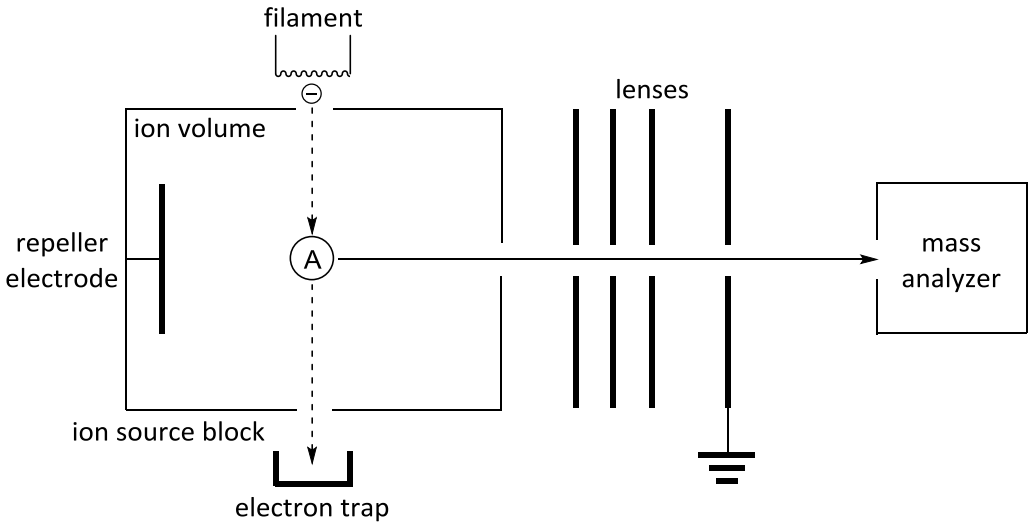

Figure 2.1. Schematic setup of an EI ion source with analyte (A).[126]

Electron ionization[126] (EI), formerly also termed *electron impact ionization*[137] or short *electron impact*,[138] is a highly efficient and extremely sensitive ionization method.[126] During the ionization process, neutral molecules have to be introduced into the highly diluted gas phase and are shot with a beam of electrons to form radical cations (figure 2.1).[126] For the sample introduction, any system or inlet can be utilized that is suitable for the evaporation of the individual analytes.[126] The gas phase can be regarded as highly diluted when the mean free distance between the particles becomes too long for intermolecular interactions which is usually realized at pressures below 10^{-4} Pa.[126] Afterwards, the gas beam of neutral analyte molecules is fed into the *ionization chamber* (*ion volume*).[126] There, the analyte beam crosses a beam of energetic electrons.[126] This electron beam is generated by thermionic emission. For this purpose, a metal filament typically consisting of (thoriated) rhenium or tungsten is heated resistively.[126,139] During operation, temperatures up to 2000 °C can be reached.[126] Concerning the filament's shape, many different arrangements can be tolerated like straight wires, ribbons or even small coins.[126] After the ionization has occurred by collision of the analytes with the primary electrons, an oriented ion beam is formed by a capacitor with two oppositely charged plates.[126] The generated cations are accelerated towards the negatively charged plate that possesses a slit or a round hole.[126] Thus, only ions with parallel pathway to the electric field can pass into the analyzer. To optimize this process, optical lenses are positioned in front of the mass analyzer and the acceleration voltage is applied in two or more stages.[126,140] In order to minimize loss of ions by collision with the chamber's

walls, a low voltage is applied by a *repeller electrode*[141] pushing the ions immediately out of the chamber.[126] As a result, the ions are focused and accelerated towards the mass analyzer of the spectrometer.[126]

During the ionization process, some of the colliding electron's kinetic energy is transferred to the analyte molecule and transferred into internal energy, while an electron is expelled from the analyte.[126] Thereby, molecules with an even-electron amount (closed-shell) usually lose one electron and an odd-electron (open-shell) radical cation emerges.[126,142] In contrast, odd-electron radical analytes generate even-electron cations.[126,142] In some cases, the primary electron's energy is high enough to cause doubly or even triply charged ions, although, these processes are usually of rather low abundance.[126,143] Beside molecular and multiply charged ions, also fragment, metastable and rearranged ions as well as ion pairs can be observed.[144] If the collision is not effective enough, the neutral molecule is merely transformed into an electronically excited state while no ionization occurs.[126] To prevent such events, the energy of the primary electron must be at least as high as the analyte's *ionization energy*,[145] the minimum amount of energy that is required to eject an electron from the molecule.[126] The ionization energy strongly differs depending on the structure and electronic character of the molecule, but mainly amounts to 10 eV. In general, the stabilization of the charge is the key point to a stable cation and thus to a low ionization energy.[126] Therefore, molecules with lone pairs (heteroatoms) and π-bonds possess low ionization energies.[126,146] Additionally, aromatic systems are favored over large π-systems.[126,146] In contrast, analytes, possessing only σ-bonds, have higher ionization energies.[126,146] Large alkyl chains are easier to ionize than short hydrocarbons due to their hyperconjugative effect.[126,146,147] In accordance with that, small diatomic molecules like F_2, N_2 or H_2 possess very high ionization energies.[126,146] The most unlikely to ionize are the closed-shell noble gas molecules.[126,146]

If the primary electron's energy is exactly equal to the ionization energy of the analyte, ionization only occurs in case of extremely effective collision and quantitative energy transfer to the molecule.[126] This event is of very low probability.[126] To improve the ionization efficiency significantly, a slight increase of the electron's kinetic energy suffices.[126] Thereby, the ionization efficiency depends on the *ionization cross section*,[148] an area through which electrons have to travel in order to effectively interact with the neutral molecule.[126,144] When the ionization cross section is plotted against the electron energy, a maximum of around 70 eV emerges for all molecules with only small variations.[126] As a result, EI spectra are usually measured at this energy level.[126] This not only ensures ionization of all species, but also provides spectra of high reproducibility.[126]

2.3 Gas chromatography

The combination of separation techniques with mass-spectrometric methods is the key to the analysis of complex analyte mixtures.[149] In 1959, *Gohlke*[150] described the first direct combination of *gas chromatography*[151] (GC) with EI-MS.[152] Nowadays, *gas chromatography-coupled mass spectrometry*[126] (GC-MS) is a routine method for mixture analysis.[153] The original name *gas-liquid chromatography*[150] already explains how the method proceeds. Like every other column chromatography, GC combines a mobile phase with a stationary phase in order to separate the complex analyte mixture.[126,154] The mobile phase is a gas.[126,154] Originally, nitrogen was used as *carrier gas*,[154] but nowadays, helium or hydrogen are more common.[126] On the other hand, the stationary phase, responsibly for the separation, is a liquid thin film (alkyl or aryl polysiloxanes) bound to a solid support (silica).[126,154] The fine capillary

tube columns with 0.1 to 0.5 mm inner diameter are normally coated with 0.2 to 0.5 µm of the stationary phase.[124,126] The whole column bears a length of 5 to 100 m.[154] Thus, it is technically not a column, but rather a coil.[126]

More often, the analyte is diluted in a volatile solvent, including samples taken from reaction solutions.[126,155] Afterwards, injection with a hot glass tube provokes spontaneous evaporation.[126] In doing so, the sample vapor is mixed with the carrier gas.[124,126] Thereafter, the carrier gas is induced with a flow of about 1 bar.[126] Due to the high flow resistance of the capillary column, a gas flow of approximately 1 mL/min results.[126,155] During operation, the column's temperature is controlled by an oven that can reach up to at least 350 °C.[126] Often a temperature gradient is applied in order to ensure an efficient separation.[126] However, the temperature at the injector and the transfer line has to be higher as the highest temperature of the program to prevent condensation and thus remixing of the analyte's components in the column.[126] After the mass-spectrometric detection, a chromatogram is obtained in which the relative peak intensities are shown as a function of the species' retention times.[126]

The separation is successful if all species of the mixture analyzed are represented by discrete peaks.[126] Sometimes, chromatograms show unsatisfactory results, when peaks overlap due to insufficient resolution or a general baseline drift is observed.[126] Frequently, peak tailing is noted, especially in case of polar components.[126] Additionally, diffusion can provoke a general peak broadening towards the end of the separation.[126] To identify the individual peaks of a complex mixture, an EI database can be consulted.[156] Another helpful tool for peak assignment is the calibration to an internal standard.[157–160] This approach additionally provides access to a quantitative analysis of the components.[157–160]

2.4 Electrospray ionization

Electrospray ionization[161] (ESI) is one of the most prominent ionization techniques in the field of mass spectrometry.[43,162] This soft ionization method allows the direct transfer of analytes from liquid solutions into the gas phase within milliseconds.[126] A vast variety of compounds of a wide range of molecular mass can be analyzed starting from monoatomic ions or small polar molecules up to soluble inorganic compounds as well as polymers and large proteins.[163–165,166] In contrast to EI (chapter 2.2), ESI also provides access to negatively charged ions and highly transient intermediate species.[167,168] The technique's principles date back to the work of *Zeleny*[169] in 1917 and *Taylor*[170] in 1964. However, it took several decades and numerous scientists to develop highly efficient devices.[163] Based on the work of the group of *Dole*,[161,171] the *Fenn* group[172] as well as *Gall* and co-workers[173] successfully developed the first ESI-MS interfaces in the 1980s. However, *Gall's*[173] work remained almost completely unnoted until it was translated from Russian to English in 2008.[174] As a consequence, only *Fenn*'s[163] dedication to this topic was awarded the Nobel Prize in Chemistry in 2002.[175]

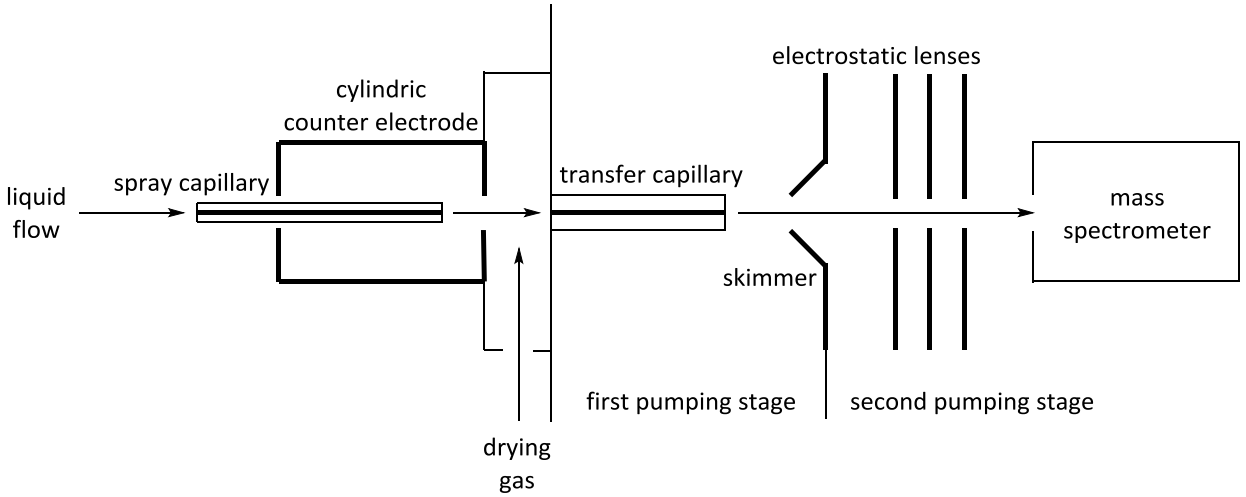

Figure 2.2. Schematic setup of an early ESI ion source.[126,165]

The principle setup of the first ESI ion source is depicted in figure 2.2 and described in the following.[165] The diluted sample solution is fed through a thin, conductive needle.[126,165] Between this spray capillary and the surrounding cylindrical counter electrode a constant potential of about 3 to 4 kV is applied.[126,165] Thus, when the analyte solution passes through the needle, it experiences the electric field at the conductive capillary's tip.[126,165] Afterwards, the resulting electrospray aerosol is evaporated by a stream of hot inert gas.[126,164] Driven by the electric field, small amounts of the sprayed substance enter the transfer capillary.[126,165] The atmospheric pressure zone is left behind and a major part of the gas expands due to reduced pressure.[126,165] At the transfer capillary's end, the first pumping stage with a pressure of approximately 10^{-2} Pa is reached.[126] Thereafter, a minor part of the material passes the orifice of the cone-shaped *skimmer*[165] (first electrostatic lens) and enters the high vacuum of 10^{-3} to 10^{-4} Pa.[126,165] At this point, the ions are completely dissolved.[126,164] Finally, they are focused and transferred through electrostatic lenses into the mass analyzer.[126,165]

Modern ESI ion sources all originate from this design, but possess slight deviations to enhance the devices' robustness, sensitivity as well as the spray and signal stability and increase the signal to noise ratio.[176,177] The first conventional difference is the application of an inert gas with a concentric flow enclosing the spray capillary.[178–180] Reducing influences of the surface tension, the nebulizer gas stream allows higher liquid flows (10 to 200 µL/min instead of 1 to 20 µL/min) of the analyte solution.[165,179,181] As a result, the *pneumatically assisted ESI*[178] enables the direct connection of a liquid chromatography system to the ion source.[180] Another standard deviation from the initial setup is the alignment of the interface.[182] Originally, the components were arranged intuitively in one line from the spray capillary to the mass analyzer.[126,165] Nowadays, the devices exhibit a sometimes almost orthogonal angle at the vacuum entrance.[182] By this approach, possible contaminations and especially clogging of the capillaries as well as the skimmers is reduced.[126] Additionally, some devices possess *ion funnels*[183] instead of skimmer cone electrodes.[184,185] The ion funnels are composed of many ring electrodes aligned in one axis.[183–185] The inner diameter of the rings is decreasing from 20 mm at the entrance to 1 mm at the exit.[183] Thus, a funnel shape emerges. During operation, an equal voltage with opposite phase of about 200 to 400 V is applied between the adjoining electrodes.[183,185] This induces an electrical field that transfers the ions more effectively, focusing them in the central axis.[183,186] As a result, the sensitivity of the apparatus is increased at least ten times compared to a skimmer-containing interface, providing spectra of higher signal to noise ratio.[187]

In general, the mechanism of ion formation after the spray capillary (figure 2.2) proceeds *via* three principal steps.[177] First, a spray of an electrostatically charged aerosol is formed.[177] Then, the droplets' solvent is evaporated to reduce the droplets' size until microdroplets emerge.[177] In the end, the

completely dissolved ions are emitted to the gas phase.[177] The process starts when the analyte solution is exposed to the high electric field at the spray capillary's tip.[165,177] As a consequence, a so-called *Taylor cone*[170] is formed by the solution in interaction with the nearby counter electrode.[126,177] Thereby, the high electric field of about 10^6 V/m causes a charge separation in the electrolytic solution.[177] This provokes a sharper curvature of the liquid's meniscus into a cone as soon as a critical electric field strength is reached.[126,177] With increasing field strength, the surface tension is overcompensated and a fine beam of highly charged liquid droplets is emitted towards the counter electrode.[126,188] Since the jet is dispersed by Coulomb forces into a fine spray of charged droplets, the name *electrospray ionization* emerged intuitively.[165] To accelerate the subsequent solvent evaporation, a heated inert gas stream is applied.[126,189] Thus, the charge density on the shrinking droplets' surface increases continuously until the *Rayleigh limit*[190] is reached.[165,177] At this point, the *Coulomb explosion*[165] of the unstable droplets leads to a cascade-like ejection of smaller offspring droplets.[177] These highly charged offspring droplets retain only about 1 to 2% of the parent droplets' mass but 10 to 18% of their charge.[189,191]

The droplet jet fission process does not lead directly to a spray of emitted ions.[126] The formation of the final gas phase ions can be described by two different models.[126] The older thesis is called *charge residue model* (CRM), postulated by *Dole et al.*[161] According to this model, successive loss of solvent by evaporation leads to tiny droplets that only contain one analyte molecule.[161] Finally, the charge of these small droplets is transferred to the analyte.[161] This process is especially favored if the analyte molecule possesses a functional group that can stabilize the charge.[192] Later on, the *ion evaporation model* (IEM) was presented by *Iribarne* and *Thomson*.[193] This approach suggests the direct evaporation of single analyte ions from the surface of highly charged microdroplets.[194] This process is induced by a strong electric field.[126] The increasing charge density of the shrinking droplets brings more charges within reach of an analyte molecule.[195,196] As a consequence, the direct evaporation of the analyte can occur for small molecules.[126] The concept was further supported by *Fenn* and co-workers[196] who found that the charge distribution strongly depends on the sample concentration. Thereby, higher concentrations led to multiply charged ions.[196] This shows that a comparably fixed number of charges in a droplet is distributed among many or few analytes resulting in singly or multiply charged ions.[126,196]

The ionization efficiency for electrospray ionization is named *ESI response factor* or short *ESI response*.[197] This topic is of special interest if complex mixtures like reaction solutions are analyzed. In contrast to EI (chapter 2.2), the analytes' individual ionization efficiency of ESI varies widely and does not correlate directly to the molecules' concentrations in solution.[198] Intuitively, the ESI response of already charged species is significantly higher than the one of neutral molecules that require adduct formation or have to undergo electrochemical transformations.[198,199] Additionally, a neutral analyte can be ionized more easily if the molecule exhibits functional moieties that facilitate the ion formation.[200] In positive ion mode, electron rich functional groups like amines can add a proton or a sodium cation spontaneously and form cationic species of the type $[M+H]^+$ or $[M+Na]^+$.[200] In contrast, mere alkanes are barely detectable.[198] Besides the analyte's very own structural properties, also the ESI parameters of the interface as well as the composition of the sample solution play key roles.[198,201] Thus, spectra are often dominated by species of high ESI response instead of high concentration in the sample solution.[202] Thereby, analytes with a low ESI response can be suppressed and vanish completely into the spectra's baseline noise.[202]

ESI-MS can be used to explore complex reaction solutions.[168,203–205] Many different types of organic reactions have already been studied by this analytical tool.[168,203–205,206] A decisive advantage of this method is that the samples only require dilution, but do not need prior work-up.[207] Additionally, minimal fragmentation allows detection of intact molecules as well as highly transient intermediate species.[126,207] In case of fast reactions, the group of *Metzger*[202] suggested a *continuous flow* setup that

includes a dilution step connecting the reaction solution directly to the mass spectrometer. *McIndoe* and co-workers[208] presented another interesting approach with their *pressurized sample infusion* method for reactions that are highly sensitive towards air or moisture. For this method, the sample is pushed out of a sealed reaction container by a slight overpressure and fed directly into the device.[209] To circumvent the problems of widely varying ESI response factors of the components and additives, reactants or catalysts can be equipped with functional groups or charge-tagging moieties.[86,200,210,211] In case of reaction monitoring with ESI-MS, this increases the ionization efficiency of all species of interest to the same magnitude. The correlation of peak intensity and concentration was verified by *McIndoe* and co-workers,[207,210] who performed ESI-MS, NMR and UV/Vis (*ultraviolet and visible light*)[212] experiments in parallel. Thus, the application of a charge-tagged reactant allows a deeper insight into the mechanistic events which has already been demonstrated by the mechanistic studies of our group.[213]

2.5 Tandem mass spectrometry

An additional tool that enriches the state of information on a complex mass spectrum or a specific species is *tandem mass spectrometry*.[214] Thereby, mass-selected ions (parent ions) of a spectrum can be isolated and subsequently fragmented into product ions.[126] As a result, further structural information of the parent ion is obtained.[126] This allows for the characterization of isomers that can be distinguished by their individual fragmentation patterns.[215] Since mass spectrometry is generally abbreviated MS, tandem mass spectrometry is usually called MS/MS or MS^2.[126] In general, tandem mass spectrometry can be divided into two different classes: *tandem-in-space* and *tandem-in-time*.[216] The first approach uses two mass analyzers.[216] Thus, detection of the parent ion and the product ion fragments occurs spatially separated.[216] This method is applied in bream transmitting devices like the Q/TOF analyzer that was used for the experiments of this thesis.[126,216] The second technique uses only one mass analyzer.[216] Since no spatial separation is given, the ion selection, activation and product detection occurs sequently in time.[216] This approach can be found in ion trap mass spectrometers.[216] Since the fragmentation stages are not limited to the number of analyzers, the tandem-in-time method also allows for multiple stage mass spectrometry (MS^n).[217] By fragmentation of gaseous ions further information about the species' structure can be obtained.[126,218] Usually, this is combined with soft ionization methods like ESI that render perfectly stable gas phase ions.[126] In principle, many different techniques can be applied to induce the dissociation of the parent ion like *infrared multiphoton dissociation* (IRMPD), *electron transfer dissociation*[219] (ETD), *electron detachment dissociation*[220] (EDD) or *blackbody infrared radiative dissociation*[221] (BIRD). A very prominent method is the *collision induced dissociation*[218,222] (CID). If a beam of selected ions is passed through a collision cell, they collide with an inert gas like helium, nitrogen or argon and dissociate into smaller fragments.[126] The fragmentation process can be regarded as sequential events.[223] First, the selected species is activated.[223] Afterwards, the additional internal energy transferred from the gas to the molecule is randomized.[223] Finally, the species dissociates along any fragmentation pathway possible at this specific energy level.[223] Thus, the amount of energy transferred to the molecule is crucial for the fragmentation pattern observed.[126]

3 Mechanistic investigations of a dual activation reaction: Interplay between metal and organocatalysis

3.1 Introduction

In 2010, the group of *Jørgensen*[224] presented an interesting synthetic approach towards cyclopentene carbaldehydes (scheme 3.1). Based on the work of *Kirsch* and co-workers,[225] they employed a synergistic dual activation system (chapter 1.3) consisting of a chiral secondary amine catalyst (*Jørgensen-Hayashi catalyst*)[226] and a metal catalyst (gold or copper). This catalytic system induces an intermolecular Michael addition of an *α,β*-unsaturated aldehyde and a functionalized malononitrile. Subsequently, a 5-*exo*-*dig*-cyclization occurs (scheme 3.2). Thereby, high enantioselectivity is provided by the chiral information of the *L*-proline derivative **3**.

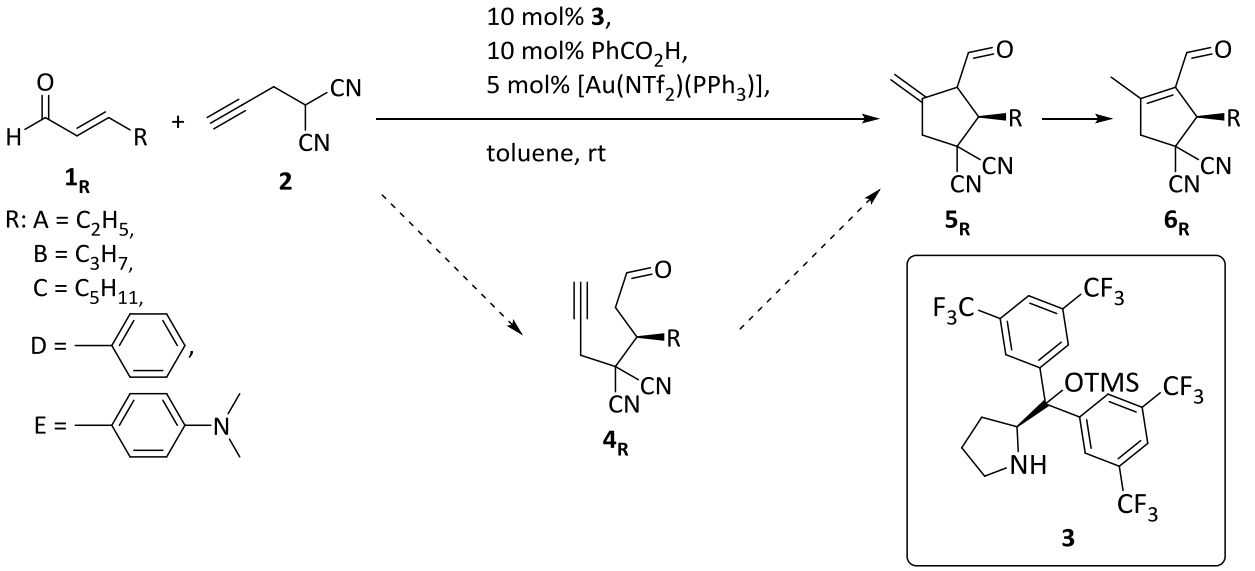

Scheme 3.1. Intermolecular 5-*exo*-*dig*-cyclization of *α,β*-unsaturated aldehydes $\mathbf{1_R}$ and an electron deficient alkyne **2** with subsequent isomerization presented by the group of *Jørgensen*.[224]

In case of the Michael addition, the secondary amine **3** enables the formation of an iminium ion $\mathbf{I_R^+}$ (scheme 3.2). The mechanism of this reaction step has already been investigated by *Jørgensen* and co-workers[90,227] and is generally accepted.[63,65] However, the second part of the reaction could not be elucidated completely so far. By a stepwise approach, the group of *Jørgensen*[224] revealed that the cyclization process is significantly more efficient if both catalysts are applied. The exact role of the amine catalyst **3** though could not be determined. The group of *Kirsch*[225] suggested two possible pathways for the 5-*exo*-*dig*-cyclization (scheme 3.2). In the first one (cycle (**A**)), the formation of an iminium/enamine species ($\mathbf{II_R^+}$/$\mathbf{III_R}$) is required to activate the aldehyde moiety for the ring closure. This hypothesis is supported by condensation reactions of aldehydes and amines observed under the same reaction conditions.[225] In contrast, the amine catalyst **3** solely reacts as a base in cycle (**B**). In this case, the cyclization is exclusively induced by the metal catalyst. Although experiments with silver(I) triflate and triethylamine as base supported this pathway, the transfer to a similar gold(I) system was not successful.[225] For both cycles suggested, the exact form of the gold catalyst in solution has not been elucidated so far. Note that $[Au]^+$ is not necessarily one specific catalyst form, but is used to mark the

expected positions and functions of the gold catalyst within the mechanistic suggestions of scheme 3.2. It is possible, that the gold catalyst changes its ligand sphere after binding to the substrate. Additionally to the type of cycle relevant for this reaction, it has to be investigated whether the gold catalyst binds covalently to the substrate or is first attached by coordination after a ligand exchange. Thus, the gold catalyst was named $[Au]^+$ for every reaction step with no specifications of the ligand sphere.

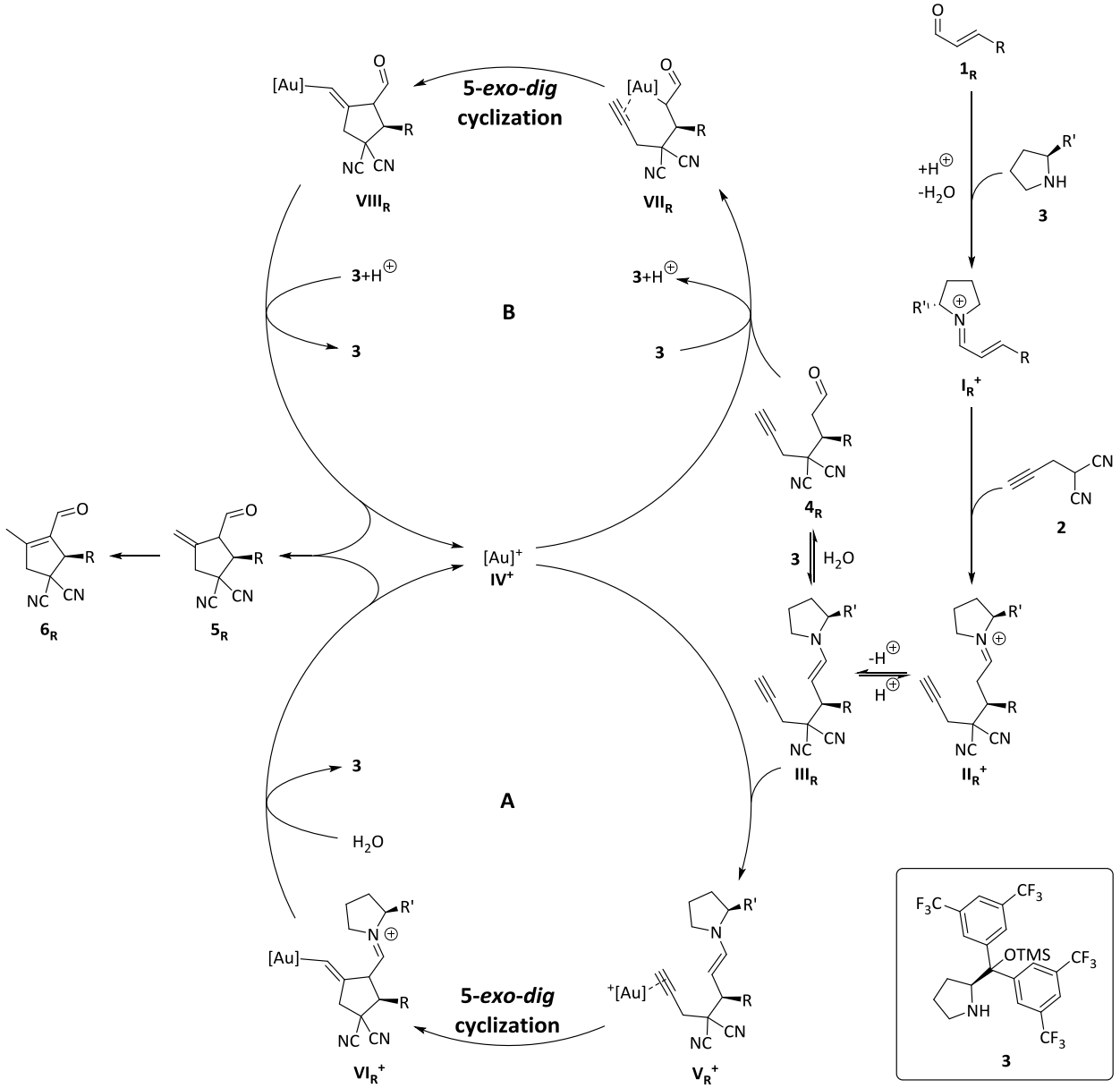

Scheme 3.2. Two proposed mechanisms for the 5-*exo*-*dig*-cyclization of *α*,*β*-unsaturated aldehydes with an alkyne promoted by gold(I) and a secondary amine.[224,225,228]

Since the previous studies were solely based on synthetic results and NMR characterization of the products,[224,225] direct ESI-MS monitoring of the reaction solution promised a deeper insight into the mechanistic events. ESI-MS (chapter 2.4) allows a simultaneous detection of distinct signals for every component rendering an overview of the complex reaction mixture. Additionally, the method does not require previous work-up of the samples. As a result, also transient intermediate species can be detected. ESI-MS seemed particularly suited to detect the amine, enamine and iminium species during the reaction. In contrast, neither the starting materials nor the products possess functional groups that enable facile ionization *via* ESI. Therefore, a complementary tool was required. GC-MS (chapter 2.3) appeared suitable to control the components' individual conversion. Contrary to ESI-MS, this technique provides a quantitative insight into the reaction because of the extremely unselective and highly

sensitive detection by EI-MS. Thus, GC-MS was used for the quantitative reaction monitoring of the reactants and products.

In the study described in the following, most experiments were performed using *trans*-2-pentenal $\mathbf{1_A}$ and alkyne **2** under the reaction conditions presented by the group of *Jørgensen*.[224] In addition, the effects of other substrates were investigated with compounds $\mathbf{1_B}$ to $\mathbf{1_E}$ (scheme 3.1). Preceding the experiments designed to elucidate the mechanism of the reaction, starting materials and references had to be synthesized if not commercially available.

3.2 Synthesis

3.2.1 Synthesis of the starting materials

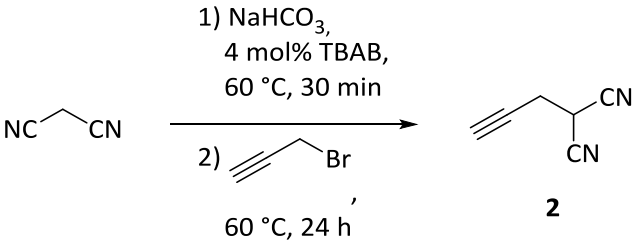

(3.1)

Scheme 3.3. Nucleophilic substitution on propargyl bromide with malononitrile according to *Díez-Barra et al.*[229]

All starting materials needed for the reaction published by *Jensen et al.*[224] (scheme 3.1) were commercially available except for the prop-2-ynylmalononitrile **2**. The synthesis had already been published in 1991 by *Díez-Barra et al.*[229] with moderate yields (51%), starting from malononitrile and propargyl bromide (scheme 3.3). They presented a solvent-free setup with TBAB (*tetra*-butylammonium bromide) as phase transfer catalyst. Unfortunately, propargyl bromide could not be obtained in a pure form. Only solutions were accessible. Thus, an 80 wt% solution in toluene from Aldrich was used for all reactions. This diminished the yield significantly. However, it was possible to enhance the conversion, optimizing the substrates' ratios. Originally, malononitrile was used in a twofold excess. This only rendered alkyne **2** with a yield of 17%. Later on, this result could be significantly improved using a fourfold excess of malononitrile. Thereby, the amounts of base used to deprotonate the malononitrile acidic proton were also adapted to ensure complete deprotonation. With this approach, alkyne **2** was obtained in 37% yield.

Since gold and the other elements present in the dual activation reaction presented by the group of *Jørgensen*[224] show no characteristic isotope pattern in mass spectra, two other derivatives of the original alkyne **2** were additionally used to obtain more information from the MS experiments (chapter 3.3 *et seq*.). Thus, the primary proton was substituted by a deuterium cation (scheme 3.4) as well as by a phenyl group (scheme 3.5). Systematic variation of one of the two starting materials facilitated the assignment of the various species in mass spectra dramatically and rendered further information of the species' structure.

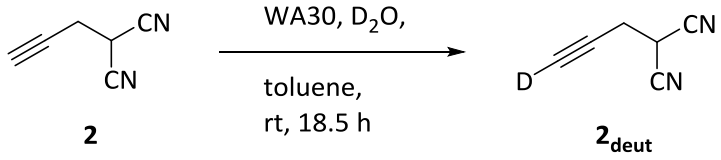

2 $\quad$ $\mathbf{2_{deut}}$ $\quad$ **79%** (41% D) **(3.2)**

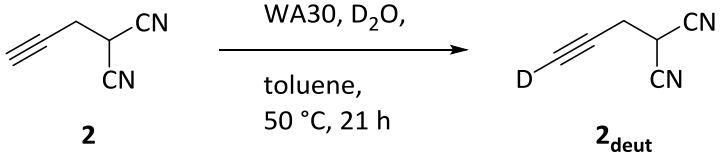

2 $\quad$ $\mathbf{2_{deut}}$ $\quad$ **80%** (94% D) **(3.3)**

Scheme 3.4. Deuteration of prop-2-ynylmalononitrile **2** analogous to *Yamada et al.*[230]

The deuteration of alkyne **2** was performed according to *Yamada et al.*[230] (scheme 3.4) who presented deuteration experiments with several primary alkynes. Alkyne **2** was stirred overnight in deuterium oxide in presence of Diaion® WA30 free base. This polystyrene polymer with a tertiary amine residue on the aromatic nuclei can be used as a basic anion exchange resin. Since *Yamada et al.*[230] reported that heating the reaction mixture can be required in some cases, two different setups with these resin beads in heavy water were tested. The first one was stirred at room temperature, while the second one was heated up to 50 °C. As alkyne **2** is not soluble in deuterium oxide, toluene was added as co-solvent to both setups as suggested by *Yamada et al.*[230] The colorless base beads turned crimson within an hour, indicating that the H-D-exchange had occurred. Afterwards, the amount of deuteration could be determined by GC-coupled EI-MS measurements (appendix, figure 9.1 and 9.2). As expected, deuterated product $\mathbf{2_{deut}}$ showed the same retention time as for **2** (chapter 3.2.4, table 3.1). While the room temperature setup showed only a deuteration of 41%, the heated reaction mixture rendered $\mathbf{2_{deut}}$ in 94% deuteration rate.

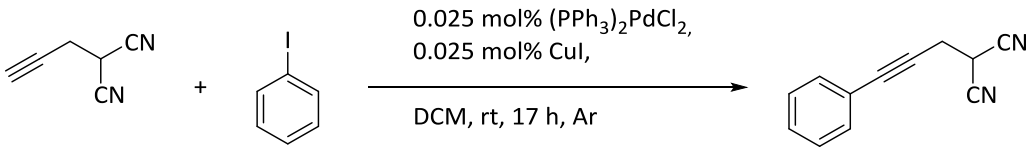

2 $\quad$ $\mathbf{2_{Ph}}$ $\quad$ **50%** **(3.4)**

Scheme 3.5. Sonogashira-Cross-Coupling reaction of alkyne **2** and iodobenzene according to *Schiller et al.*[231]

Phenylated alkyne $\mathbf{2_{Ph}}$ was synthesized by attaching the phenyl group to the primary alkyne *via* a Sonogashira-Cross-Coupling reaction (scheme 3.5) according to *Schiller et al.*[231] who published this phenylation with good yields in 2004. The Cross-Coupling product was obtained in 50% yield.

3.2.2 Synthesis of the cyclic products

According to *Jørgensen* and co-workers,[224] the different cyclopentene carbaldehydes $\mathbf{6_R}$ were generated by cycloaddition of prop-2-ynylmalononitrile **2** and the respective aldehyde $\mathbf{1_R}$ in the presence of benzoic acid and the two catalysts (scheme 3.6). Due to better practicability, the reaction

times of the aliphatic aldehydes were extended to two days (four days for the alternative setups with $\mathbf{2_{deut}}$ and $\mathbf{2_{Ph}}$), while the reaction times for the aromatic aldehydes were extended to five days.

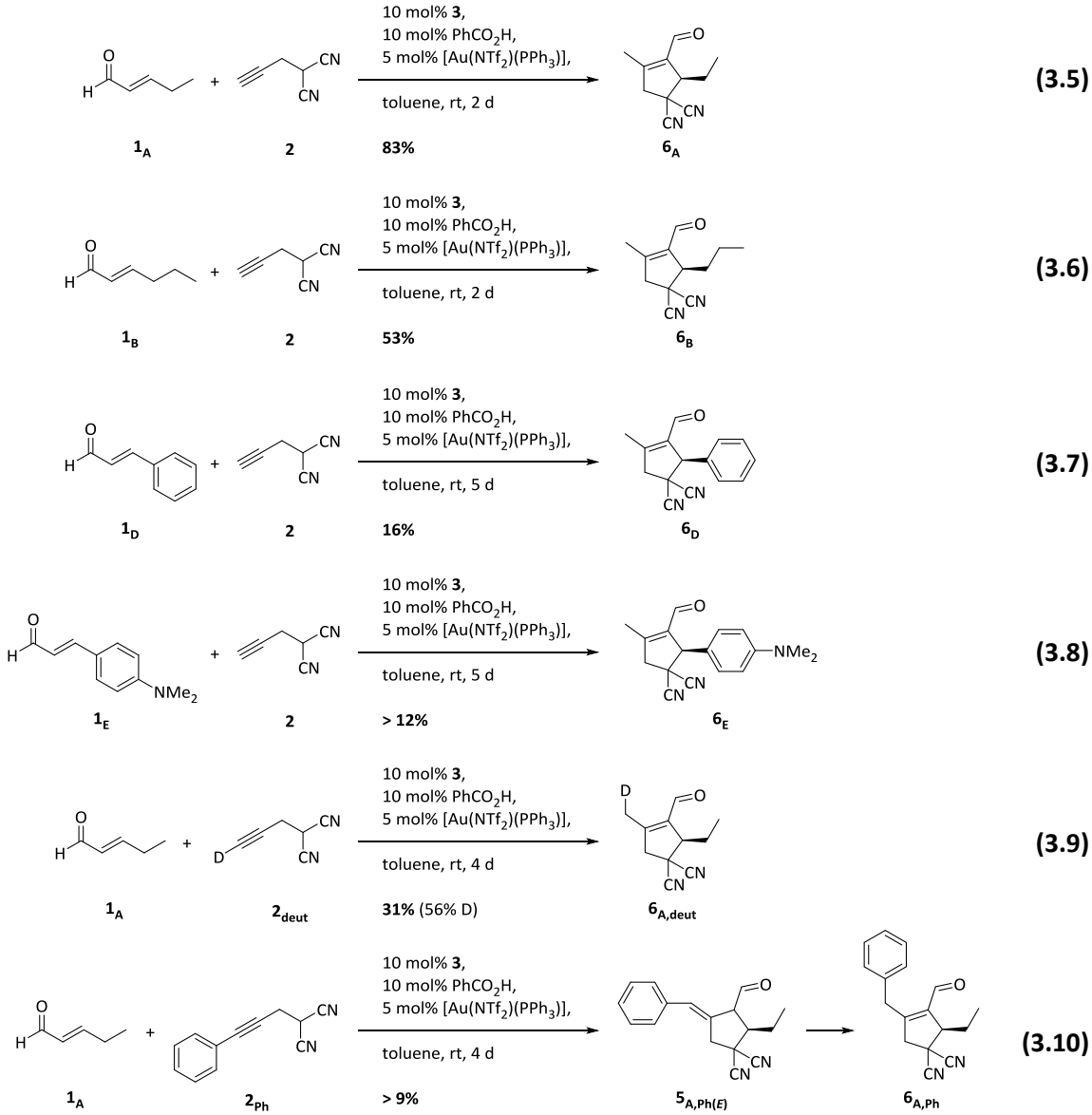

Scheme 3.6. Synthesis of the different cyclopentene carbaldehydes. Stereoinformation was assumed according to the results of the *Jørgensen* group.[224] Due to purification problems an exact yield could not be determined for reaction 3.8 and reaction 3.10. All products were detected by GC-coupled EI-MS.

The yields reported in the literature could not be reproduced (appendix, table 9.1). Again, the deuteration rate of the deuterated cyclization product $\mathbf{6_{A,deut}}$ was determined by GC-coupled EI-MS measurements (appendix, figure 9.3). Since the preparative setup of the one-pot reactions only varied in the reaction time, the main loss of product is attributed to the difficult purification by column chromatography. It was observed that the cyclopentene carbaldehydes tend to adhere to the silica gel when purification with a preparative *thin-layer chromatography* (TLC) plate was performed. Thus, the main problem appeared to be the loss of product, which would not separate from the column's silica gel. Additionally, one might suspect that the extended reaction times provoked partial decomposition of the carbocycles. Albeit, this is rather improbable as shown in the GC-MS experiments later on (chapter 3.4) which proved that shorter reaction times would also not increase the conversion. Nevertheless, the amounts of substance obtained by these synthetic attempts were sufficient for the mechanistic

investigations presented in chapter 3.3 to 3.7. Since the main object of this thesis focuses on the exploration of the mechanistic events, the synthetic procedures were not further optimized.

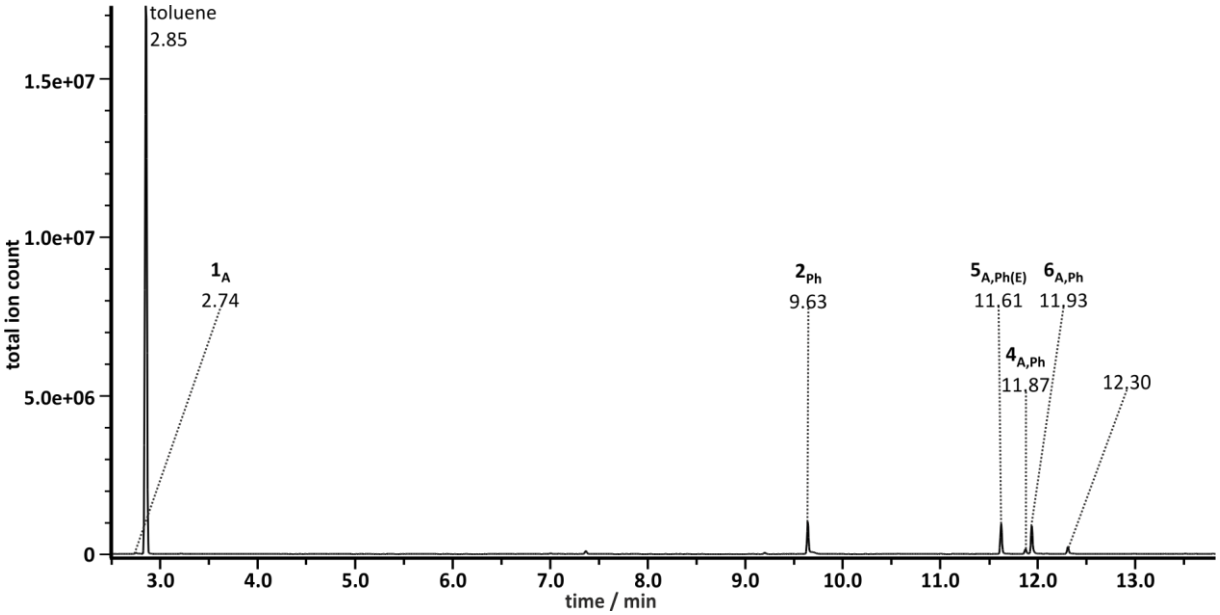

Figure 3.1. Gas chromatogram of the reaction solution of the cyclization reaction with alkyne $\mathbf{2_{Ph}}$ and *trans*-2-pentenal $\mathbf{1_A}$ (reaction 3.5) recorded with GC-MS instrument (a) (chapter 7.2.4). The sample was taken after three days reaction time, filtered over silica gel and evaporated from dichloromethane.

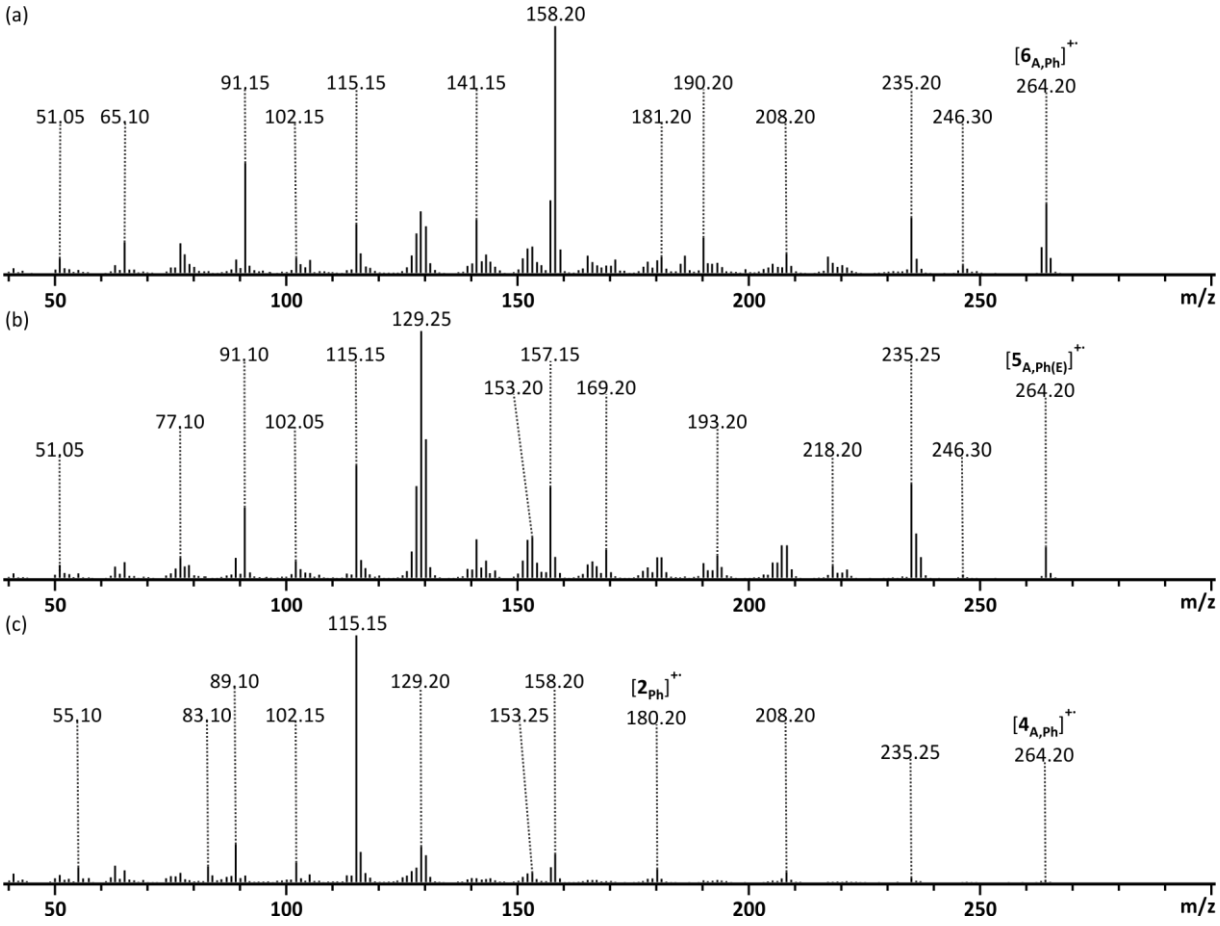

Figure 3.2. EI mass spectra of (a) phenylated cyclopentene carbaldehyde $\mathbf{6_{A,Ph}}$, (b) vinyl product $\mathbf{5_{A,Ph(\mathit{E})}}$ and (c) Michael product $\mathbf{4_{A,Ph}}$ obtained with the gas chromatogram of figure 3.1 recorded with GC-MS instrument (a) (chapter 7.2.4).

In case of reaction 3.10, additionally to the expected cyclopentene carbaldehyde **6**$_{A,Ph}$ two products could be observed during the GC-MS measurements (figure 3.1 and 3.2). Unfortunately, isolation of the additional products by column chromatography was not successful. It was solely possible to obtain cyclization product **6**$_{A,Ph}$ in pure form. NMR spectroscopy measurements were performed to characterize the isolated product. Figure 3.3 shows the *distortionless enhancement by polarization transfer* (DEPT-135) spectrum of the isolated substance. As the CH_2-groups show down and CH- as well as CH_3-groups show up in this NMR experiment, the substance measured possesses three different CH_2-groups. This is only possible if the isomerization to the cyclopentene species **6**$_{A,Ph}$ has occurred (further NMR spectra: appendix, figure 9.4 and 9.5). Thus, the spectrum cannot originate from the vinyl isomers **5**$_{A,Ph(E)}$ or **5**$_{A,Ph(Z)}$ (figure 3.4).

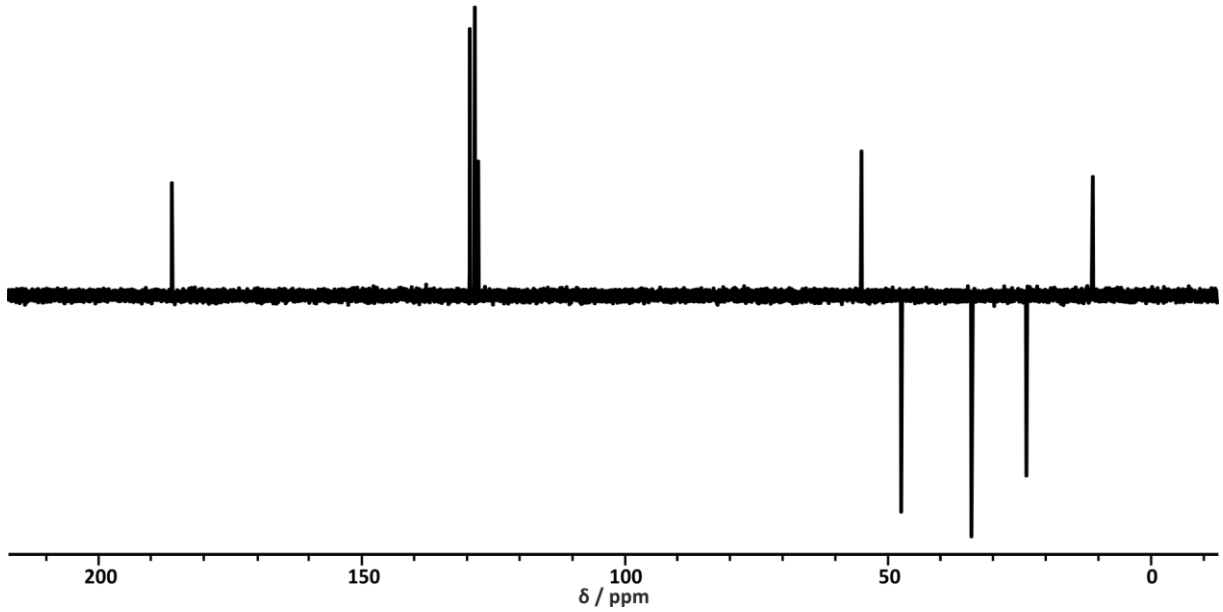

Figure 3.3. DEPT-135 spectrum of the isolated cyclopentene carbaldehyde **6**$_{A,Ph}$ in $CDCl_3$ measured with NMR instrument (a) (chapter 7.2.3). CH_2-groups show down. CH_3- and CH-groups show up.

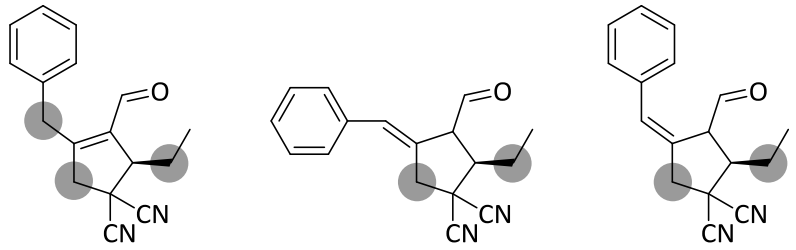

6$_{A,Ph}$ **5**$_{A,Ph(E)}$ **5**$_{A,Ph(Z)}$

Figure 3.4. Possible products of reaction 3.10. The CH_2 groups are marked for every molecule.

Comparison to the standards of chapter 3.2.3 enabled the identification of one peak as Michael product **4**$_{A,Ph}$. Moreover, it can be assumed that the third product is the cyclic carbaldehyde **5**$_{A,Ph(E)}$. In case of the phenyl-substituted alkyne **2**$_{Ph}$, a C-C-double bond in benzylic position enlarges the π-system of the aromatic ring and an isomerization to **6**$_{A,Ph}$ becomes less favorable. Since the aldehyde most probably hinders the formation of the (*Z*)-product sterically, the (*E*)-isomer should be formed during cyclization selectively. Afterwards, the isomerization to **6**$_{A,Ph}$ occurs only partially.

3.2.3 Synthesis of the acyclic Michael products

To investigate the two mechanistic steps (scheme 3.1) of the overall reaction separately, the acyclic product $\mathbf{4_A}$ was also synthesized (scheme 3.7). The Michael addition was already published by the group of *Jørgensen*.[224] They performed the reaction at 4 °C before heating up to room temperature overnight. However, the experiments showed that there is no need of cooling. When the reaction mixture was stirred at room temperature, no differences in the crude products were observed. Additionally, the yield was identical in both cases. Reaction 3.13 with phenylated alkyne $\mathbf{2_{Ph}}$ was also performed under these simplified conditions.

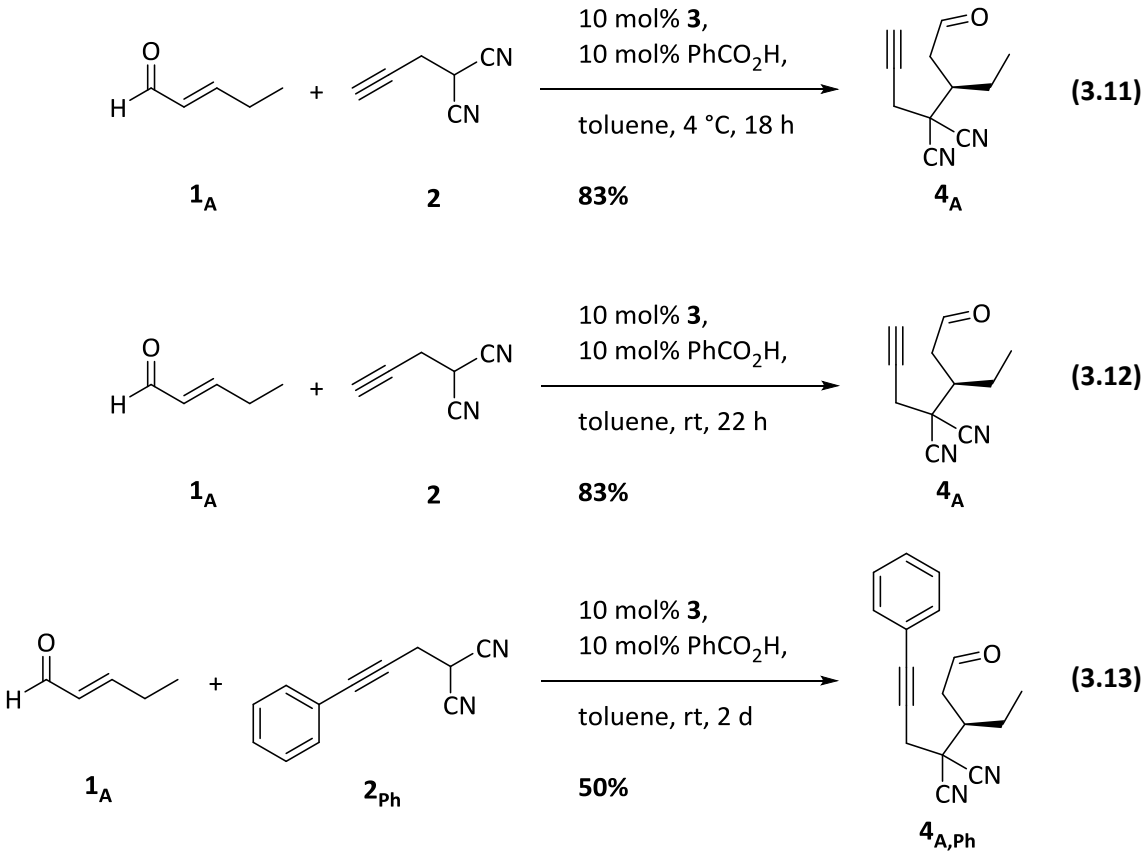

Scheme 3.7. Synthesis of different acyclic carbaldehydes according to the group of *Jørgensen*.[224]

Purification of the acyclic carbaldehydes proved to be challenging. The separation of the products from the starting materials appeared to be excellent by TLC, but GC-MS measurements of the assumed pure fractions always showed significant amounts of both starting materials. Further purification attempts did not change this result noticeably. Thus, a *retro* Michael addition might take place after separation. This behavior might also have been supported by the GC's high temperatures. In contrast, the ^{1}H NMR spectra did not show substantial amounts of aldehyde $\mathbf{1_R}$ and alkyne **2**. However, the presence of small traces of the starting materials could not be excluded because of a significantly high chemical noise base line. Nevertheless, the setups shed light on the individual Michael products' retention times that were required for the mechanistic and kinetic studies discussed in the following.

3.2.4 Preparations for the gas-chromatographic reaction monitoring

All reactions were monitored with GC-MS in parallel to the ESI-MS measurements. Assigning an exact reaction time to every sample, the components' individual conversion could be controlled. However, the conditions of the gas chromatography column did not allow a direct sample measurement from the reaction solution. All polar components were separated beforehand by means of a small silica column (0.6 cm diameter, 1 cm height) and diluted in dichloromethane. Each chromatographic peak was allocated by the peak's individual EI spectra. To assign every component correctly, GC-MS of the isolated and fully characterized product cyclopentene carbaldehydes $\mathbf{6_R}$ as well as the Michael products $\mathbf{4_R}$ were measured. This ensured accurate assignment of every species during the monitoring of the reactions.

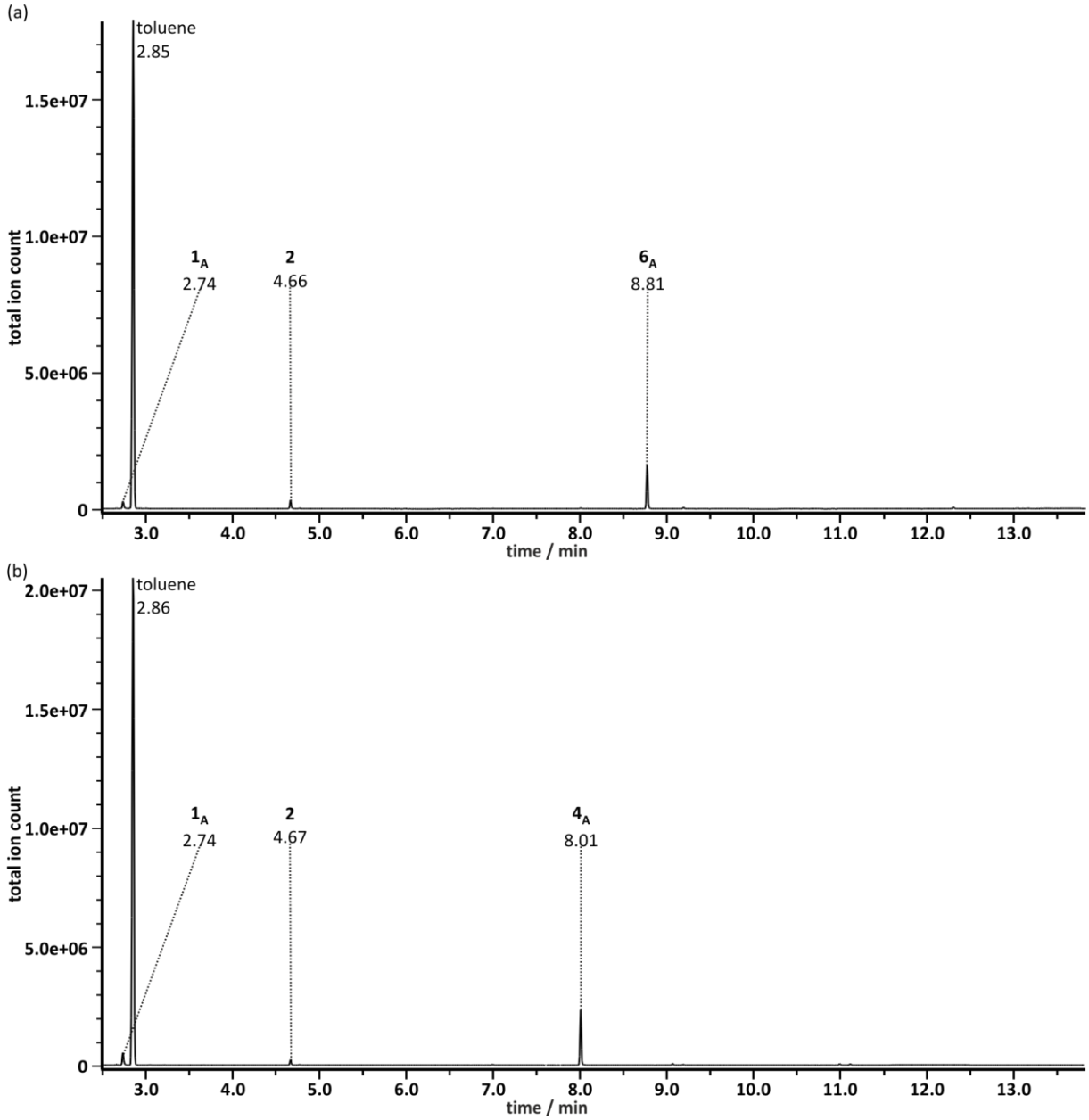

Figure 3.5. Gas chromatograms of the reaction solution of (a) the cyclization reaction with alkyne **2** and *trans*-2-pentenal $\mathbf{1_A}$ to cyclization product $\mathbf{6_A}$ (reaction 3.5) and (b) the Michael addition with alkyne **2** and *trans*-2-pentenal $\mathbf{1_A}$ to acyclic product $\mathbf{4_A}$ (reaction 3.6) recorded with GC-MS instrument (a) (chapter 7.2.4). The samples were taken after 22 h reaction time, filtered over silica gel and evaporated from dichloromethane.

Figure 3.5 represents the gas chromatograms recorded for the reaction solution of (a) cyclization reaction 3.5 and (b) Michael addition 3.11 after 22 hours reaction time. Since toluene is the reactions' solvent, the peak of the aromatic molecule is predominant in all chromatograms. The two substrates *trans*-2-pentenal $\mathbf{1_A}$ (2.74 minutes) and alkyne **2** (4.66 minutes) were identified in addition to the two products $\mathbf{6_A}$ and $\mathbf{4_A}$. The assignment of the species was supported by the individual EI spectra (figure 3.6) with the *m*/*z* value of their parent ions. Note that the EI spectra of the products $\mathbf{4_A}$ and $\mathbf{6_A}$ do not show significant differences in their fragmentation pattern. Thus, it was indispensable to determine the species' individual retention times for each of the two GC instruments used (table 3.1).

Table 3.1. Different retention times $t_{ret,\mathbf{i}}$ of all substances measured with the GC-MS instrument (a) (chapter 7.2.4) for the monitoring of the 5-*exo*-*dig*-cyclisation reaction presented by the groups of *Jørgensen*.[224] *Measurements with the device GC-MS instrument (b) (chapter 7.2.4) with different retention times. **4-(Dimethylamino)-cinnamaldehyde $\mathbf{1_E}$.

substrate	$t_{ret,\mathbf{i}}$ /min	acyclic product	$t_{ret,\mathbf{i}}$ /min	cyclic product	$t_{ret,\mathbf{i}}$ /min
alkyne **2**	4.66				
alkyne **2**	10.17*				
trans-2-pentenal $\mathbf{1_A}$	2.74	$\mathbf{4_A}$	8.03	$\mathbf{6_A}$	8.81
trans-2-pentenal $\mathbf{1_A}$	3.96*	$\mathbf{4_A}$	17.16*	$\mathbf{6_A}$	18.68*
trans-2-hexenal $\mathbf{1_B}$	3.56	$\mathbf{4_B}$	8.50	$\mathbf{6_B}$	9.22
trans-2-octenal $\mathbf{1_D}$	5.34	$\mathbf{4_D}$	9.58	$\mathbf{6_D}$	10.25
trans-2-cinnamaldehyde $\mathbf{1_D}$	7.09	$\mathbf{4_D}$	10.30	$\mathbf{6_D}$	11.14
DMAC** $\mathbf{1_E}$	10.73	$\mathbf{4_E}$	12.53	$\mathbf{6_E}$	13.24
alkyne $\mathbf{2_{deut}}$	4.66	$\mathbf{4_{A,deut}}$	8.03	$\mathbf{6_{A,deut}}$	8.81
alkyne $\mathbf{2_{Ph}}$	9.63	$\mathbf{4_{A,Ph}}$	11.87	$\mathbf{6_{A,Ph}}$	11.93
				$\mathbf{5_{A,Ph(}}\boldsymbol{E}\mathbf{)}$	11.61

The example of figure 3.5 shows that the two reaction products $\mathbf{6_A}$ and $\mathbf{4_A}$ can be distinguished easily by their individual retention times. In general, it was observed that the acyclic Michael products have a shorter retention time compared to the final carbaldehydes (table 3.1). In case of the reactions with phenylated alkyne $\mathbf{2_{Ph}}$, it was possible to additionally detect the vinyl product $\mathbf{5_{A,Ph(}}\boldsymbol{E}\mathbf{)}$. As for the non-phenylated reaction, all three product species show the same EI fragmentation pattern (chapter 3.2.3, figure 3.2), but they possess different base peaks. In figure 3.1 (chapter 3.2.3) the small differences in the species' individual retention times are visible. The vinyl product $\mathbf{5_{A,Ph(}}\boldsymbol{E}\mathbf{)}$ has an even shorter retention time than the Michael product $\mathbf{4_{A,Ph}}$.

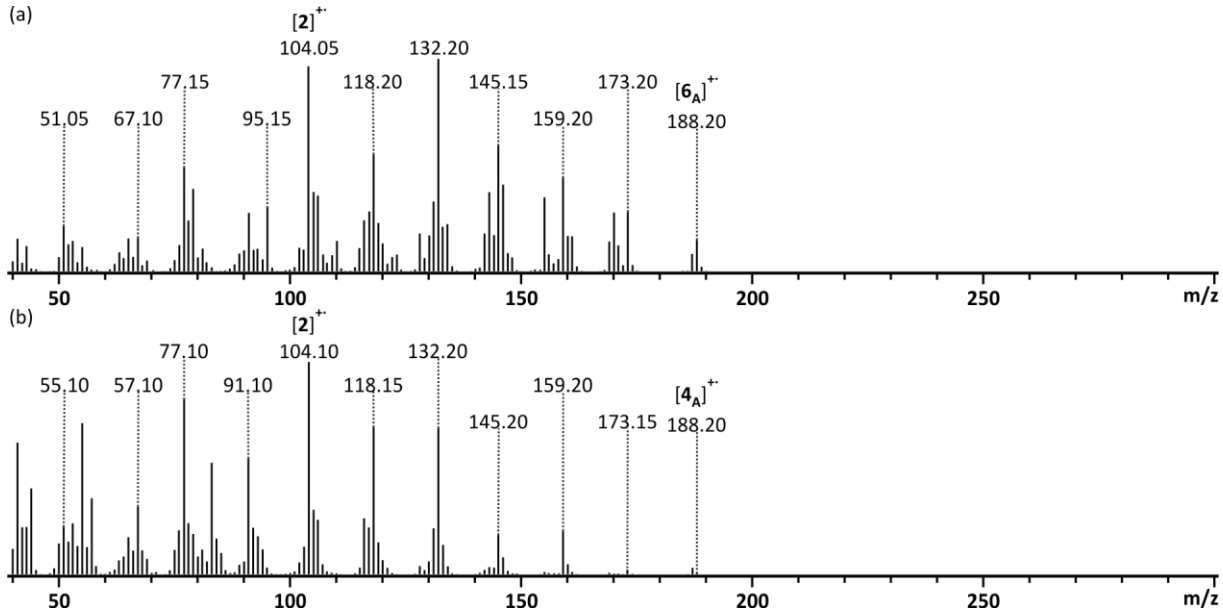

Figure 3.6. EI mass spectra of (a) cyclopentene carbaldehyde $\mathbf{6_A}$ and (b) Michael product $\mathbf{4_A}$ obtained with the gas chromatograms of figure 3.5 recorded with GC-MS instrument (a) (chapter 7.2.4).

3.3 Overall reaction – ESI-MS experiments

For the ESI-MS measurements, small samples of 5 µL were taken directly from the reaction solution, diluted in 500 µL acetonitrile and fed into the mass spectrometer. Since the exact reaction time was recorded for every single sample, possible temporal variations did not go unnoticed. By this technique, the detection of highly transient species present in the reaction solution was possible. Aldehydes and their resulting species and products were named as shown in scheme 3.1 (chapter 3.1). All transient species observed during the ESI-MS measurements were detected as $[M+H]^+$ or $[M]^+$ ions. Additionally, CID experiments were performed to gain more information about the species' individual structure and to facilitate the assignment.

Scheme 3.8 shows the overall reactions of different *α,β*-unsaturated aldehydes and alkyne **2** that were investigated by means of ESI-MS and GC-coupled EI-MS (chapter 3.4). Since only the spectra of the reactions with DMAC $\mathbf{1_E}$ differed widely, this setup was not investigated further for this study. Instead, *trans*-2-octenal $\mathbf{1_C}$ was used to evaluate possible variations according to the length and bulkiness of the aldehyde's substituent. *trans*-2-Pentenal $\mathbf{1_A}$ was chosen for detailed mechanistic experiments. Thus, modifications of the starting materials were only applied on setups including *trans*-2-pentenal $\mathbf{1_A}$ and assumed to be representative for reactions of other *α,β*-unsaturated aldehydes. A typical ESI(+) spectrum of the overall reaction of *trans*-2-pentenal $\mathbf{1_A}$ with alkyne **2** (reaction 3.14) can be found in figure 3.7.

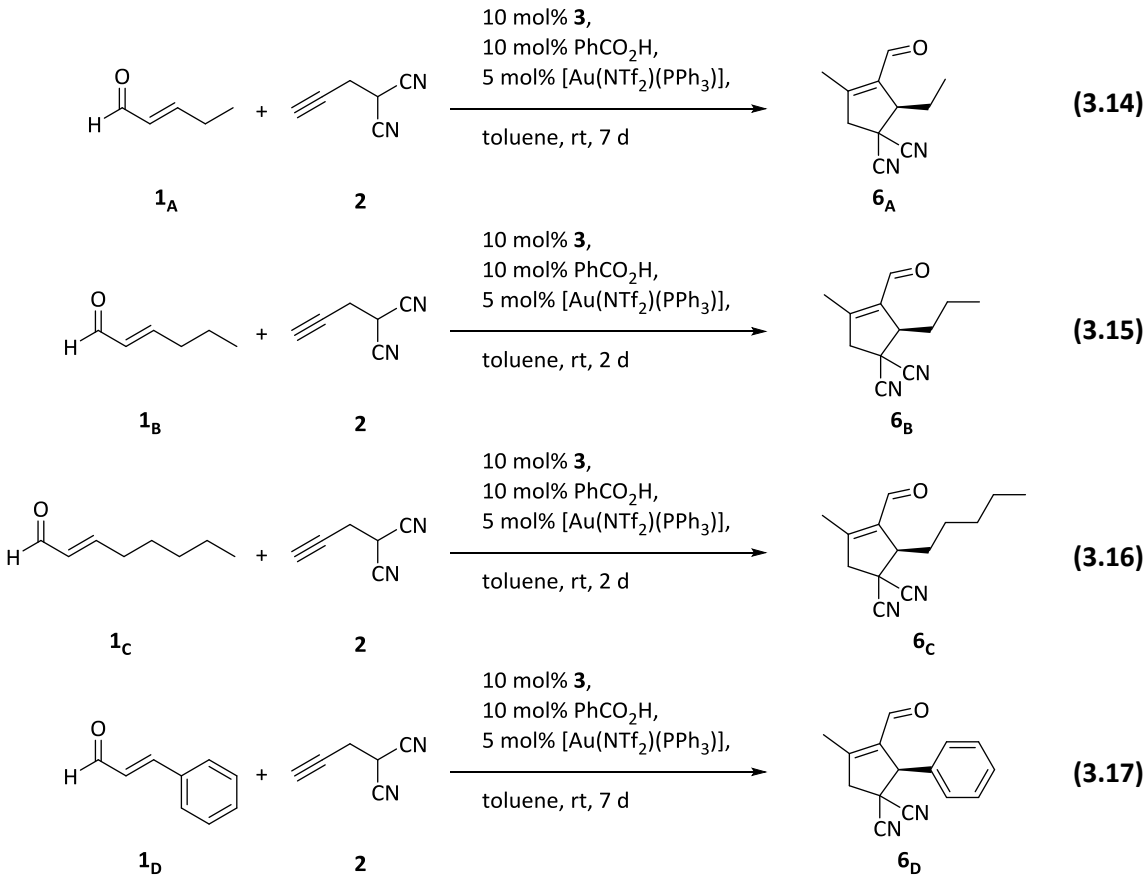

Scheme 3.8. Overall reactions of *α,β*-unsaturated aldehydes and alkyne **2** measured *via* ESI-MS and GC-MS prepared according to the group of *Jørgensen*.[224]

The *L*-proline-derived catalyst's protonated form [**3**+H]$^+$ can be identified as the spectrum's base peak with *m/z* 598. The structural similarity of this molecule to the iminium/enamine species [$\mathbf{I_A}$]$^+$ (*m/z* 664) and [$\mathbf{II_A}$]$^+$/[$\mathbf{III_A}$+H]$^+$ (*m/z* 768) can be seen in their CID spectra (figure 3.8). Note that the species [$\mathbf{II_A}$]$^+$ and [$\mathbf{III_A}$+H]$^+$ have the same molecular formula and thus the same mass. Therefore, they cannot be distinguished by ESI-MS. If fragmented by CID (figure 3.8), all three species (*m/z* 589, 664 and 768) show the typical loss of the TMS-protecting group as TMSOH. This fragmentation additionally occurs to some extent already in the ESI process. As a consequence, catalyst **3** also causes a signal [**3**+H-TMSOH]$^+$ in all ESI(+) spectra. Further, a mass difference of *m/z* = 72 was observed for all proline-derivative **3**-containing molecules. Instead of the TMS-group, the molecules thus incorporate a hydroxyl-group. In contrast to the loss of TMSOH, this hydrolysis has to occur in the reaction solution itself. The assignment of those species and the original TMS-containing ones was proved by additional CID measurements (figure 3.9). The molecules showed an analogous fragmentation as the respective species in figure 3.8. As before, most of those species show the same fragment *m/z* 508 which proves that the base catalyst **3** is involved. To indicate the close relation between the species, these molecules were named in the same manner, for example **3**' (with OH) instead of **3** (with TMS).

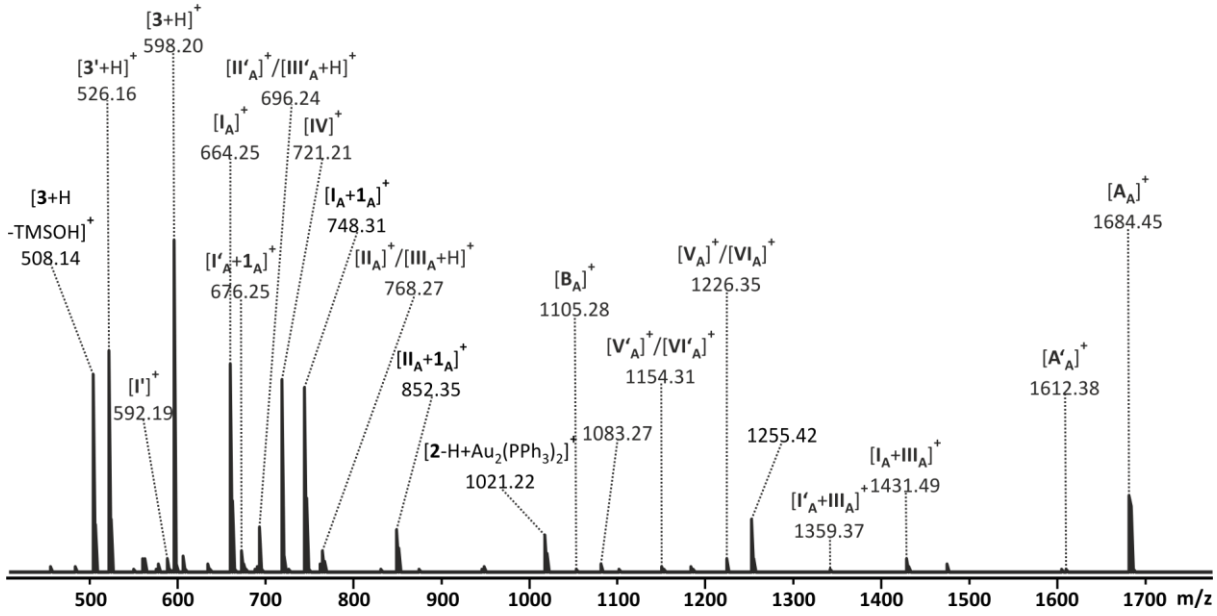

Figure 3.7. ESI(+) mass spectrum of the reaction solution of *trans*-2-pentenal $\mathbf{1_A}$ and alkyne **2** in toluene (reaction 3.14) recorded with Q/TOF mass spectrometer (a) (chapter 7.2.4). The sample was taken after one minute reaction time and diluted 1:100 in acetonitrile.

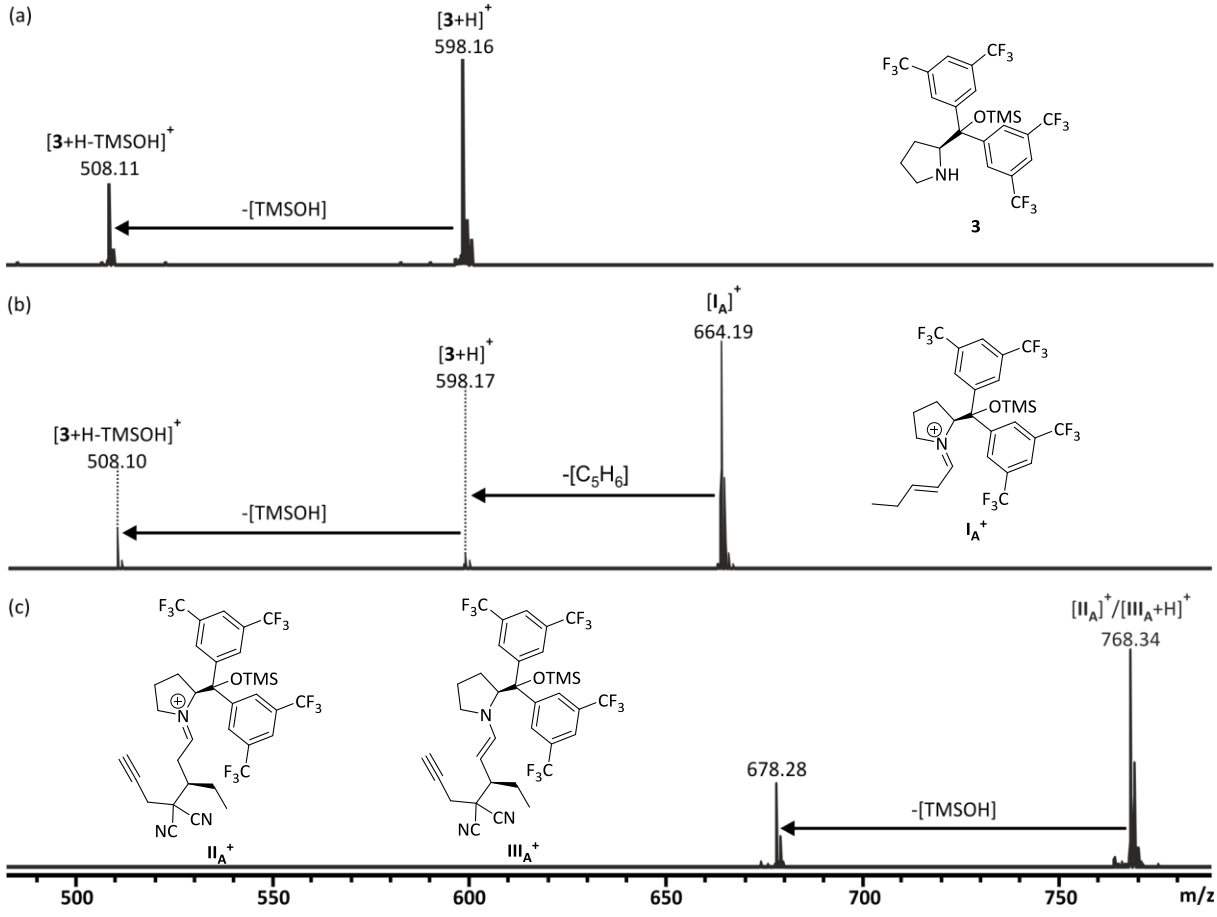

Figure 3.8. ESI(+) CID spectra of the mass-selected species (a) $[\mathbf{3}+H]^+$ (collision energy 5 eV), (b) $[\mathbf{I_A}]^+$ (collision energy 10 eV) and (c) $[\mathbf{II_A}]^+/[\mathbf{III_A}+H]^+$ (collision energy 10 eV) recorded with Q/TOF mass spectrometer (a) (chapter 7.2.4).

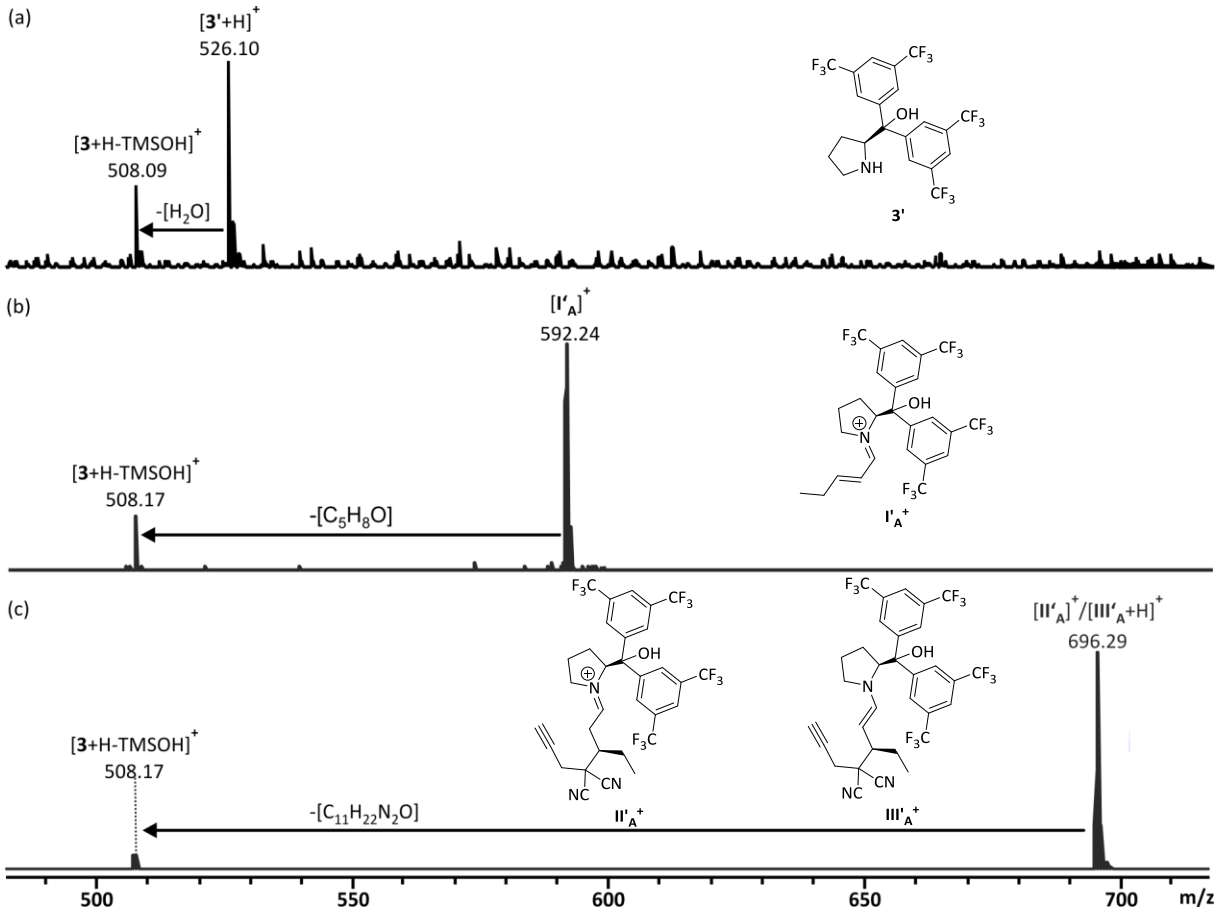

Figure 3.9. ESI(+) CID spectra of the mass-selected species (a) [**3'**+H]$^+$ (collision energy 15 eV), (b) [**I'$_A$**]$^+$ (collision energy 5 eV) and (c) [**II'$_A$**]$^+$/[**III'$_A$**+H]$^+$ recorded (collision energy 10 eV) recorded with Q/TOF mass spectrometer (a) (chapter 7.2.4).

Another signal present in all ESI(+) spectra is *m/z* 721 which can be assigned to the gold catalyst's free form in solution [**IV**]$^+$. For this molecule, two PPh_3 ligands coordinate to one gold(I) cation forming a $[Au(PPh_3)_2]^+$ complex. The molecule's structure could be revealed by CID (figure 3.10). During the fragmentation, the gold(I) complex loses one PPh_3 ligand leaving a monoligated $[Au(PPh_3)]^+$ species (*m/z* 459) behind.

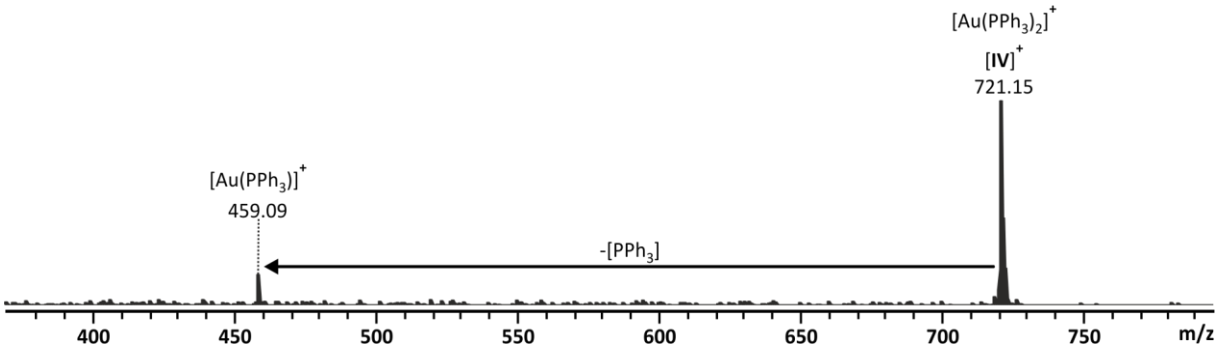

Figure 3.10. ESI(+) CID spectrum of the mass-selected species [**IV**]$^+$ (collision energy 25 eV) recorded with Q/TOF mass spectrometer (a) (chapter 7.2.4).

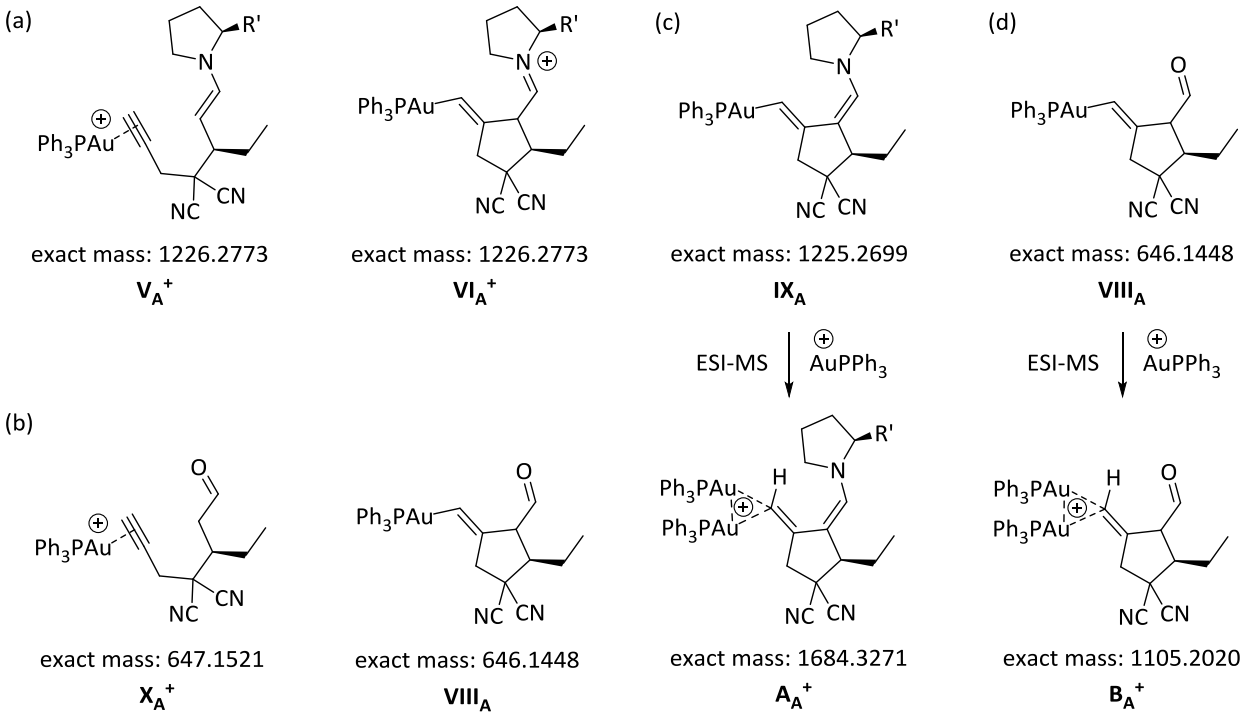

Scheme 3.9. Possible structures for (a) *m/z* 1226, (b) *m/z* 647, (c) *m/z* 1684 and (d) *m/z* 1105.

Interestingly, several species in accordance to both mechanistic suggestions of *Kirsch* and co-workers[225] (chapter 3.1, scheme 3.2) were detectable as well. Thereby, three different kinds of cations were observed. The two species $[\mathbf{V_A}]^+/[\mathbf{VI_A}]^+$ (scheme 3.9a) with *m/z* 1226 and $[\mathbf{A_A}]^+$ (scheme 3.9c) with *m/z* 1684 are based on iminium/enamine $\mathbf{II_A}^+/\mathbf{III_A}$. As a result, they participate in an (**A**)-type cycle. Species $[\mathbf{A_A}]^+$ can be assigned to a $Au(PPh_3)^+$ adduct of neutral $\mathbf{IX_A}$. In similar fashion, species $[\mathbf{B_A}]^+$ (scheme 3.9d) with *m/z* 1105 can be interpreted a $Au(PPh_3)^+$ adduct of neutral $\mathbf{VIII_A}$. Thus, it can be assigned to mechanistic cycle (**B**). Note that $\mathbf{X_A}^+$ and $\mathbf{VIII_A}$ (figure 3.9b) were not detected for the overall reaction depicted in figure 3.7. They will be discussed in chapter 3.6 (figure 3.24). For the proline derivative-containing species, two types of molecules were observed: One with an intact TMS-group ($[\mathbf{V_A}]^+/[\mathbf{VI_A}]^+$ and $[\mathbf{A_A}]^+$) and one with a hydroxyl-function instead ($[\mathbf{V'_A}]^+/[\mathbf{VI'_A}]^+$ and $[\mathbf{A'_A}]^+$). This is consistent with catalyst **3** and the iminium/enamine species (figure 3.8 and 3.9) which also showed this behavior. Interestingly, the two proline derivative-containing molecules $[\mathbf{V_A}]^+/[\mathbf{VI_A}]^+$ and $[\mathbf{A_A}]^+$ do not contain the same amount of gold(I) ions. While species $[\mathbf{V_A}]^+$ consists of one PPh_3 ligand and an alkyne enamine $\mathbf{III_A}$ that coordinates to the gold(I) atom ($[\mathbf{V_A}]^+$), cation $[\mathbf{A_A}]^+$ consists of two PPh_3 ligands and two gold(I) atoms bound to the enamine $\mathbf{III_A}$.

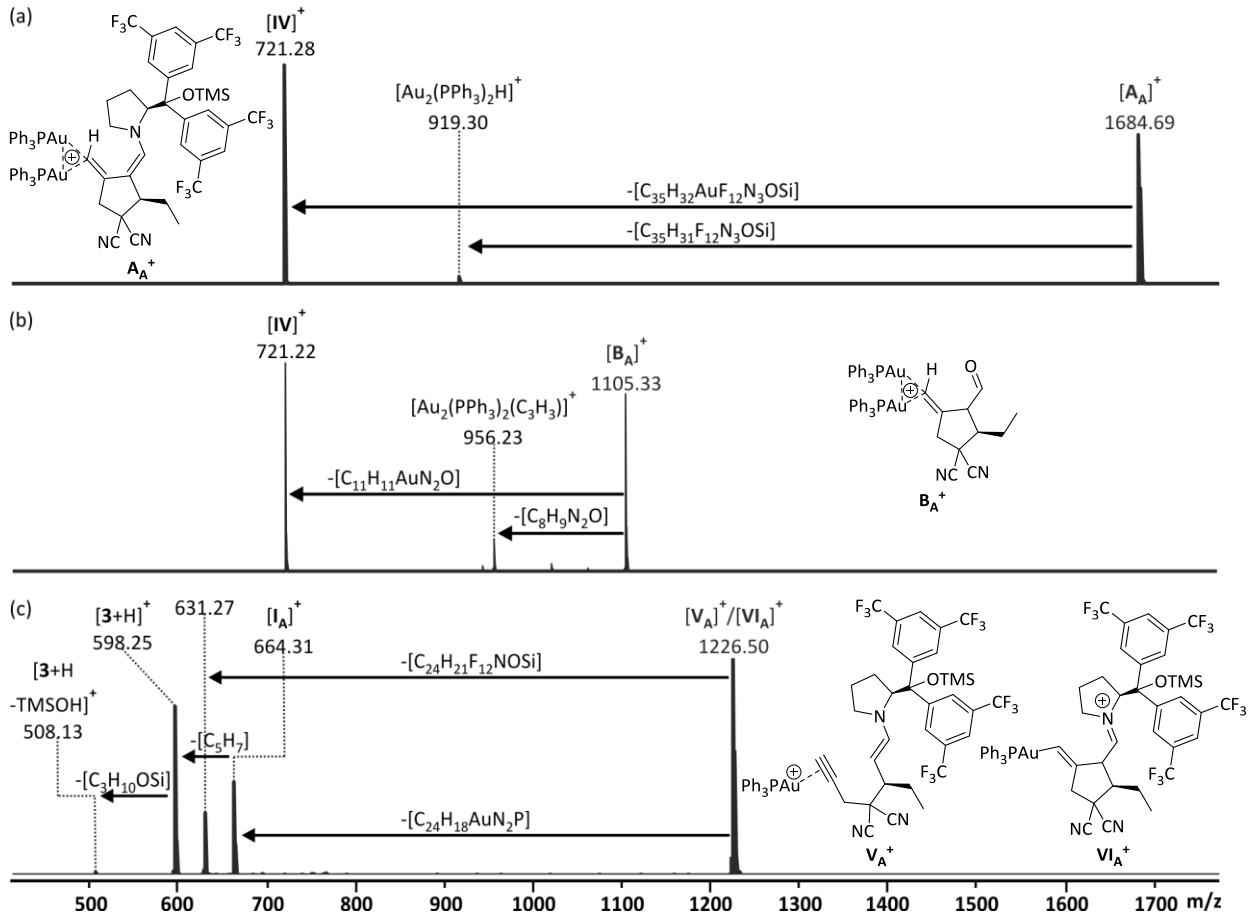

Figure 3.11. ESI(+) CID spectra of the mass-selected species (a) $[\mathbf{A_A}]^+$ (collision energy 30 eV), (b) $[\mathbf{B_A}]^+$ (collision energy 10 eV) and (c) $[\mathbf{V_A}]^+/[\mathbf{VI_A}]^+$ (collision energy 5 eV) recorded with Q/TOF mass spectrometer (a) (chapter 7.2.4).

The CID experiments of the base-containing species $[\mathbf{V_A}]^+/[\mathbf{VI_A}]^+$ (figure 3.11c) could not prove if the molecule is exclusively of acyclic ($[\mathbf{V_A}]^+$) or cyclic ($[\mathbf{VI_A}]^+$) character or if both forms are detected as a mixture. Nevertheless, the absence of a Au(PPh_3) fragment (*m/z* 459) suggests a covalent bond of the gold atom, since a coordinative bond is expected to break easily. A possible fragmentation scheme for $[\mathbf{V_A}]^+$ and $[\mathbf{VI_A}]^+$ is illustrated in scheme 3.10. The left fragmentation ($[\mathbf{V_A}]^+$) is less probable because of the coordinative bond. A cyclic structure appears rather plausible. This is further supported by the assumption that the intramolecular 5-*exo*-*dig*-cyclization is a fast process compared to the other intermolecular reactions. Additionally, it was not possible to determine if the two gold atoms of molecule $[\mathbf{A_A}]^+$ are connected to the same carbon or if they bind separately (figure 3.11a). This is also the case for the solely gold-containing species $[\mathbf{B_A}]^+$ (figure 3.11b). Nevertheless, a close proximity of the second gold atom to the first one is rather probable for $[\mathbf{A_A}]^+$ and $[\mathbf{B_A}]^+$ since the main fragment (*m/z* 721) consists of two PPh_3 ligands and not only one. In summary, the ESI-MS experiments could not reveal if one of the two suggested pathways is an off-cycle.

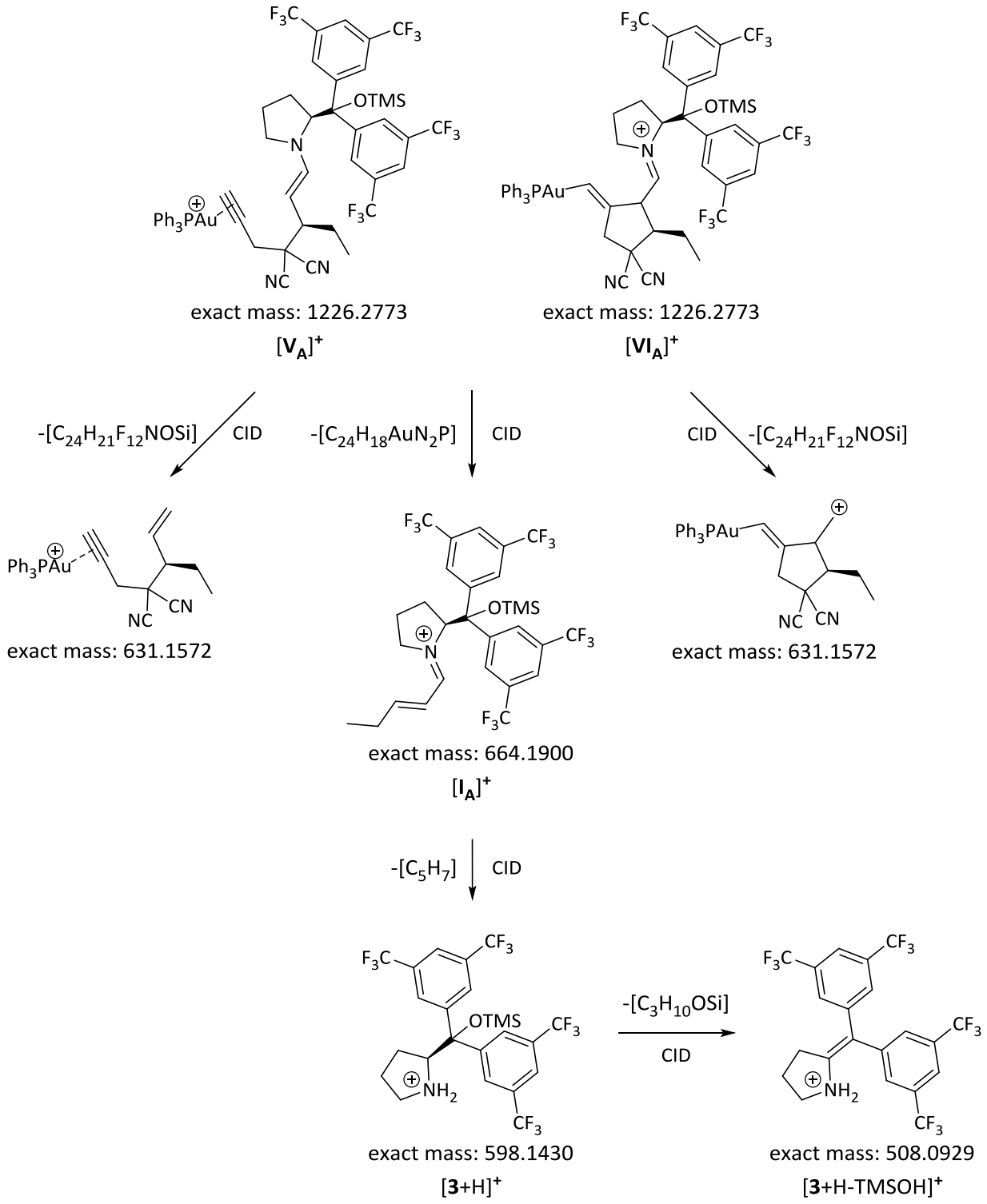

Scheme 3.10. Proposed structural fragmentation scheme of $[\mathbf{V_A}]^+/[\mathbf{VI_A}]^+$ based on accurate mass. The structural suggestion of *m/z* 631 differs depending on the parent ion. Since the coordinative bond of $[\mathbf{V_A}]^+$ is expected to break easily, the right fragmentation and thus the cyclic parent ion $[\mathbf{VI_A}]^+$ is more probable.

As visible in figure 3.7, several additive molecules were detected. Their accumulation (appendix, figure 9.6) during the reaction indicates that they are not gas phase artifacts but covalently bound molecules that are present in the reaction solution. Figure 3.12a shows the fragmentation spectrum gained by a CID experiment of *m/z* 1431 (adduct species $[\mathbf{I_A}+\mathbf{III_A}]^+$). The most interesting fragments are *m/z* 664 ($[\mathbf{I_A}]^+$) and *m/z* 768 ($[\mathbf{II_A}]^+/[\mathbf{III_A}+H]^+$). They result from a cleavage of the original adduct and represent the two parts of which it is formed. With this, it was possible to mimic the formation or rather the inverted reaction to the adduct species itself in the gas phase. To render *m/z* 834, one of the bases **3**

has to be cleaved off. Only one possibility is depicted here (scheme 3.11), but the cleavage of the base can also take place on the other side. The fragment *m*/*z* 610 is obtained from the base catalyst section. By variation of the starting materials, it was possible to determine which fragments correspond to which part of the molecule (figure 3.12b and c). That again proves the worth of substrate variation during mechanistic studies utilizing mass spectrometry.

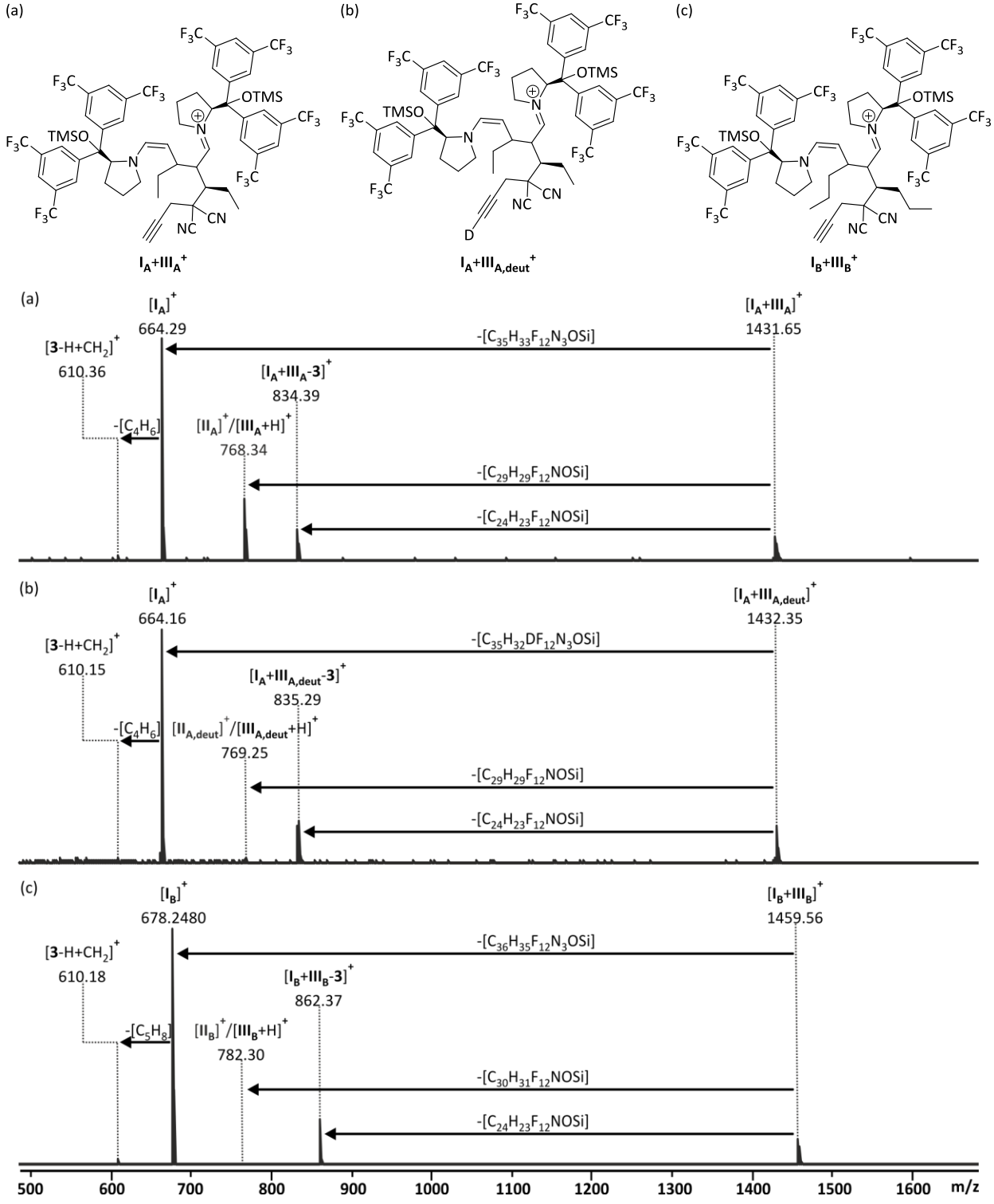

Figure 3.12. ESI(+) CID spectra of the mass-selected species (a) $[\mathbf{I_A+III_A}]^+$ (collision energy 5 eV), (a) $[\mathbf{I_A+III_{A,deut}}]^+$ (collision energy 18 eV) and (a) $[\mathbf{I_B+III_B}]^+$ (collision energy 5 eV) recorded with Q/TOF mass spectrometer (a) (chapter 7.2.4).

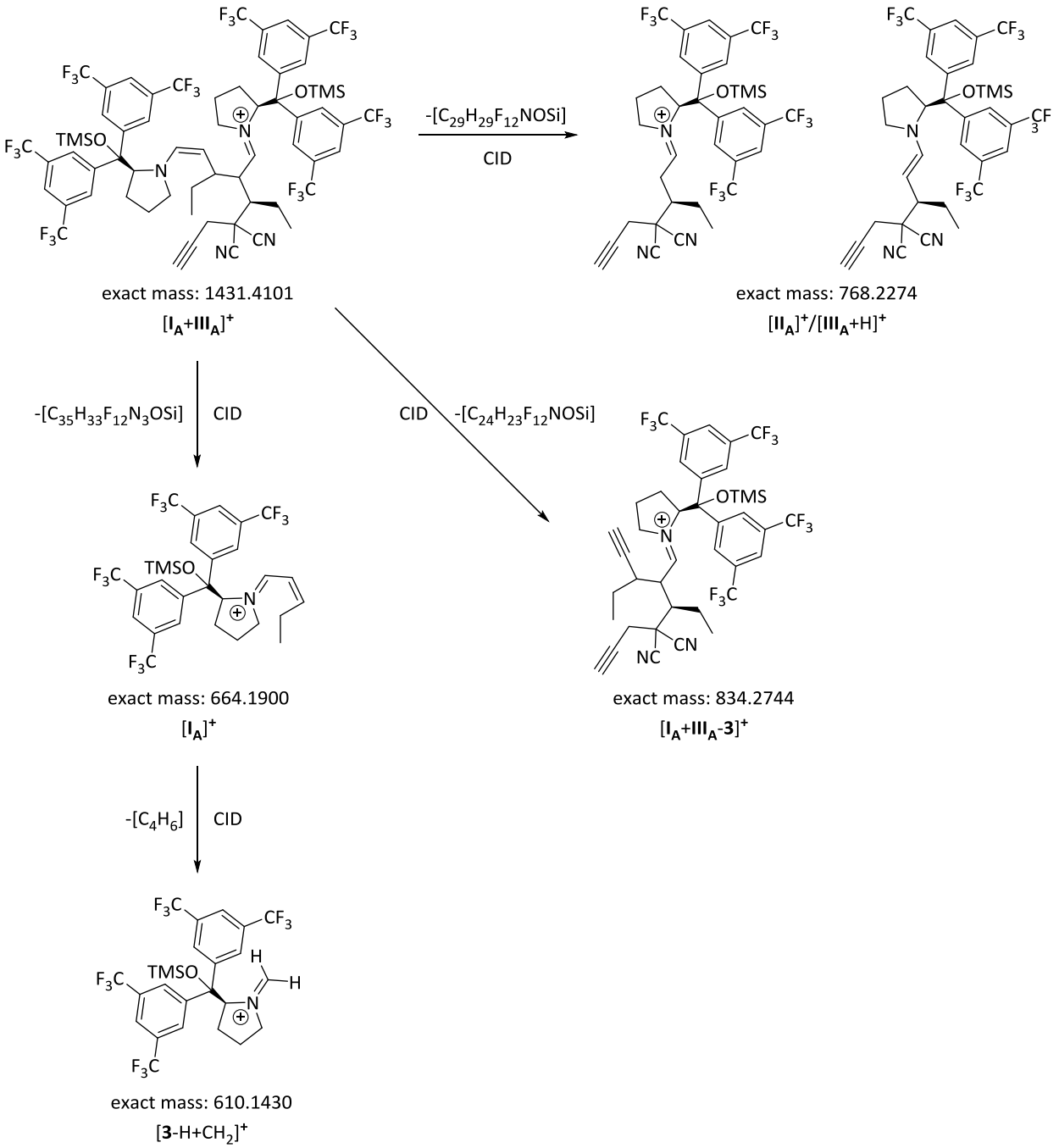

Scheme 3.11. Proposed structural fragmentation scheme of $[\mathbf{I_A}+\mathbf{III_A}]^+$ based on accurate mass.

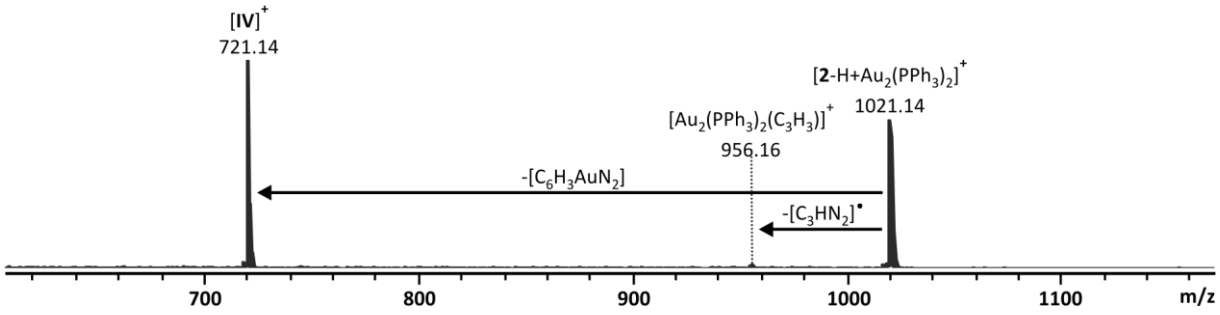

Figure 3.13. ESI(+) CID spectrum of the mass-selected species $[\mathbf{2}\text{-H}+Au_2(PPh_3)_2]^+$ (collision energy 10 eV) recorded with Q/TOF mass spectrometer (a) (chapter 7.2.4).

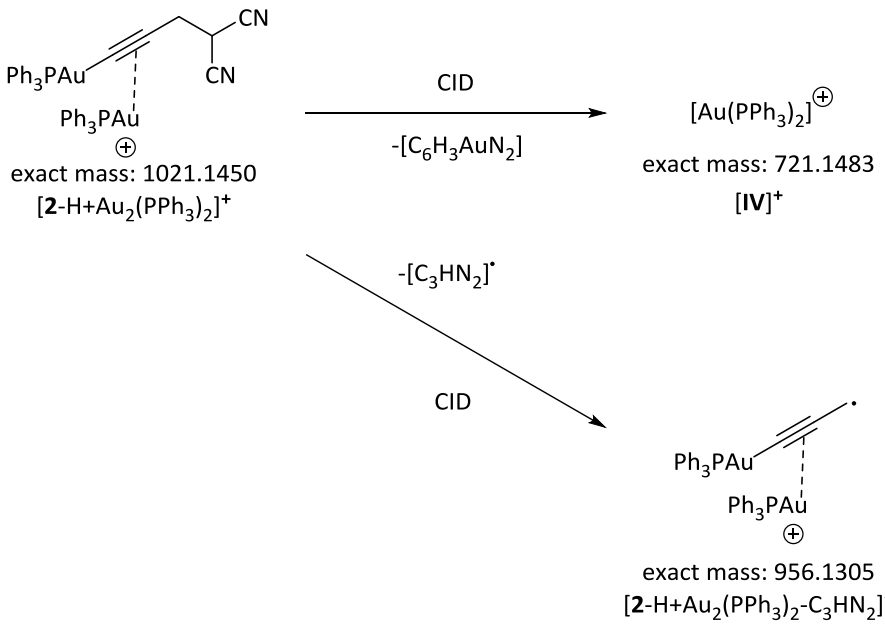

Scheme 3.12. Proposed structure and structural fragmentation scheme for *m/z* 1021 based on accurate mass.

With this information in hand, it was possible to reveal other adduct species that were formed analogically. Altogether, seven different off-cycle species could be identified: $[\mathbf{I'_A}+\mathbf{1_A}]^+$, $[\mathbf{I_A}+\mathbf{1_A}]^+$, $[\mathbf{II'_A}+\mathbf{1_A}]^+$, $[\mathbf{II_A}+\mathbf{1_A}]^+$, $[\mathbf{I'_A}+\mathbf{III_A}]^+$, $[\mathbf{I_A}+\mathbf{III_A}]^+$ and $[\mathbf{2}\text{-H}+Au_2(PPh_3)_2]^+$. An interesting one is species $[\mathbf{2}\text{-H}+Au_2(PPh_3)_2]^+$ with *m/z* 1021. This cation also contains two gold atoms (figure 3.13 and scheme 3.12). It is obtained by deprotoauration of substrate **2**. The existence of $[\mathbf{2}\text{-H}+Au_2(PPh_3)_2]^+$ rose the question of whether the Lewis acidic gold(I) already can bind to the alkyne before the first connection of the two substrates is built by a Michael addition.

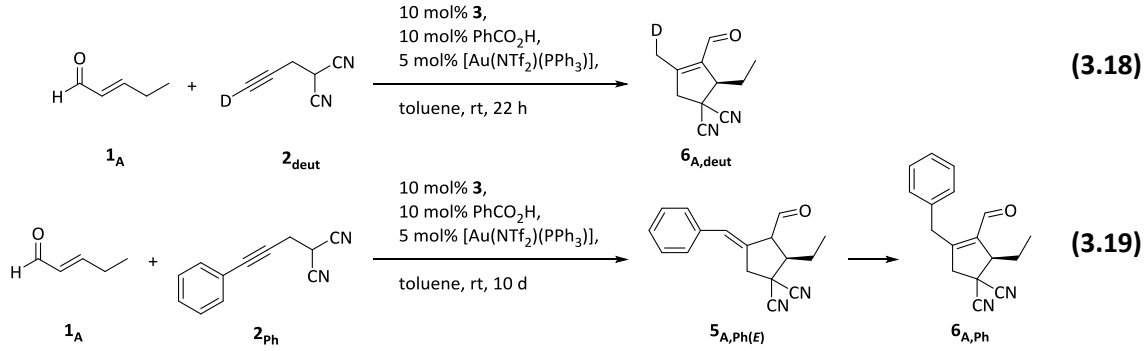

(3.18)

(3.19)

Scheme 3.13. Overall reactions of *trans*-2-pentenal $\mathbf{1_A}$ and substituted alkynes measured *via* ESI-MS and GC-MS prepared according to the group of *Jørgensen*.[224]

Since the CID experiments did not clarify if the covalent bond of the gold-containing species is located at the primary alkyne or not, isotopic labeling was used. Therefore, the primary alkyne of substrate **2** was deuterated (chapter 3.2.1) and the experiment was repeated with deuterated alkyne $\mathbf{2_{deut}}$ (reaction 3.18). The ESI(+) spectrum, recorded after one minute reaction time, is presented in figure 3.14a. All species assigned to contain the alkyne moiety show the expected increase of their individual *m/z* value. In contrast, $[\mathbf{2_{deut}}\text{-D}+Au_2(PPh_3)_2]^+$ (*m/z* 1021) does not include the isotopic label. This reveals that the cation $[\mathbf{2}\text{-H}+Au_2(PPh_3)_2]^+$ is not part of the mechanistic cycle. It also suggests that the C-Au-bond is only formed at the primary alkyne in case of $[\mathbf{2}\text{-H}+Au_2(PPh_3)_2]^+$ (scheme 3.12) but not in case of the cycle (**A**) or (**B**) type species.

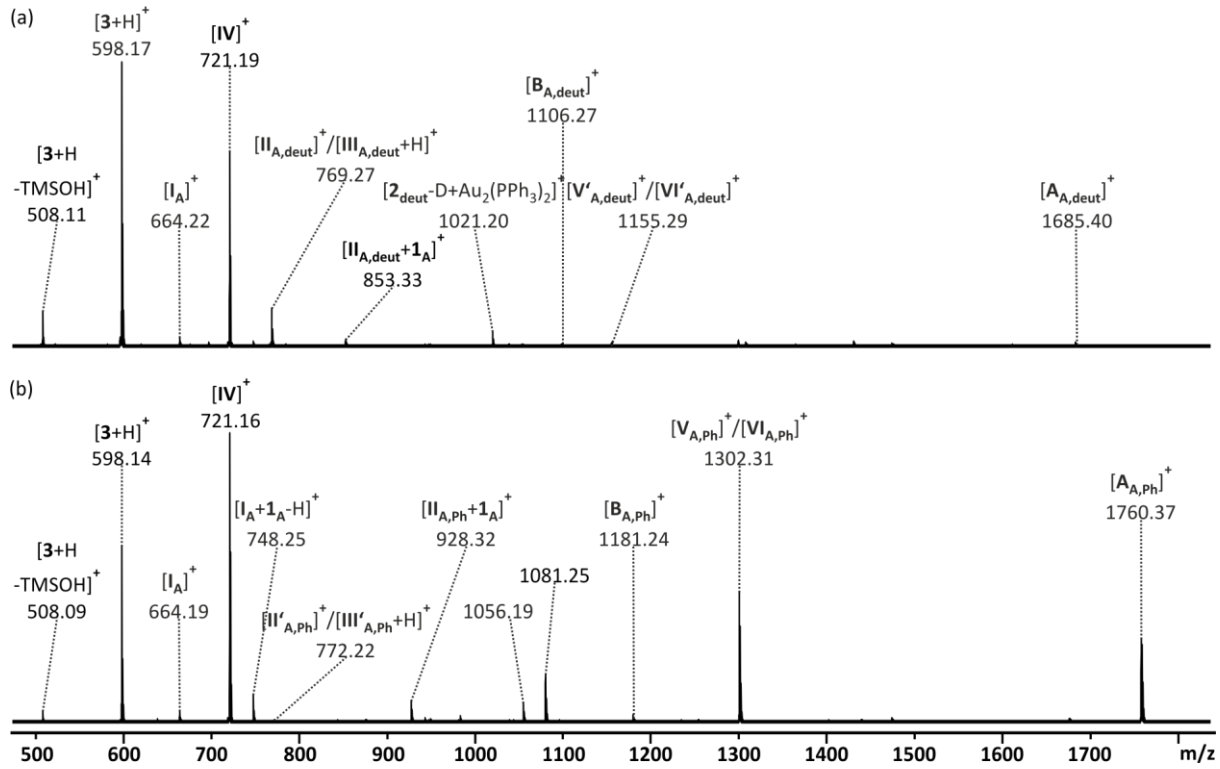

Figure 3.14. ESI(+) mass spectra of the reaction solution of (a) *trans*-2-pentenal $\mathbf{1_A}$ with alkyne $\mathbf{2_{deut}}$ (reaction 3.18) and (b) *trans*-2-pentenal $\mathbf{1_A}$ with alkyne $\mathbf{2_{Ph}}$ (reaction 3.19) in toluene recorded with Q/TOF mass spectrometer (a) (chapter 7.2.4). The samples were taken after one minute reaction time and diluted 1:100 in acetonitrile.

For the off-cycle cation $[\mathbf{2}\text{-H}+Au_2(PPh_3)_2]^+$, the structure suggested is shown in scheme 3.12. *Lu et al.*[49] observed a similar *σ,π*-diaurated molecule during their investigations of an alkyne hydration induced by the same gold catalyst. In their study the *σ,π*-diaurated complex also emerged as a stable off-cycle species formed by the alkyne substrate and the free gold catalyst $[\mathbf{IV}]^+$.

If no primary alkyne was required, this would also allow expansion of the alkyne substrate to not only primary, but also substituted alkynes. To further verify this hypothesis, the aromatic alkyne $\mathbf{2_{Ph}}$ was used (chapter 3.2.1). In this reaction, deprotoauration at the alkyne function is not possible since a phenyl group is present instead. Again, all expected species detected for the standard setup were present and they were shifted by the respective mass difference (Figure 3.14). Surprisingly, the species $[\mathbf{A_{A,Ph}}]^+$ (*m/z* 1760) and $[\mathbf{B_{A,Ph}}]^+$ (*m/z* 1181) show significantly higher intensities compared to the standard and deuterated reaction. It is most likely that the electron rich aromatic ring stabilizes this gold-bond species. An analog to the adduct species $[\mathbf{2}\text{-H}+Au_2(PPh_3)_2]^+$ could not be observed for the phenyl reaction in accordance of the structure proposed above. In summary, a deprotoauration at the primary alkyne can be excluded for the actual reaction mechanism.

Note that the species with *m/z* 1056 and *m/z* 1081 (figure 3.14) as well as *m/z* 1083 (figure 3.7) were also occasionally detected in scans of other setups of the dual activation reaction (examples for *m/z* 1083 in figure 3.22d as well as in figure 3.33a and b). It can be assumed that they belong to the reaction solution and are no simple impurities. Unfortunately, it was not possible to characterize and identify those species by CID. As a consequence, they are not precisely labeled in the spectra.

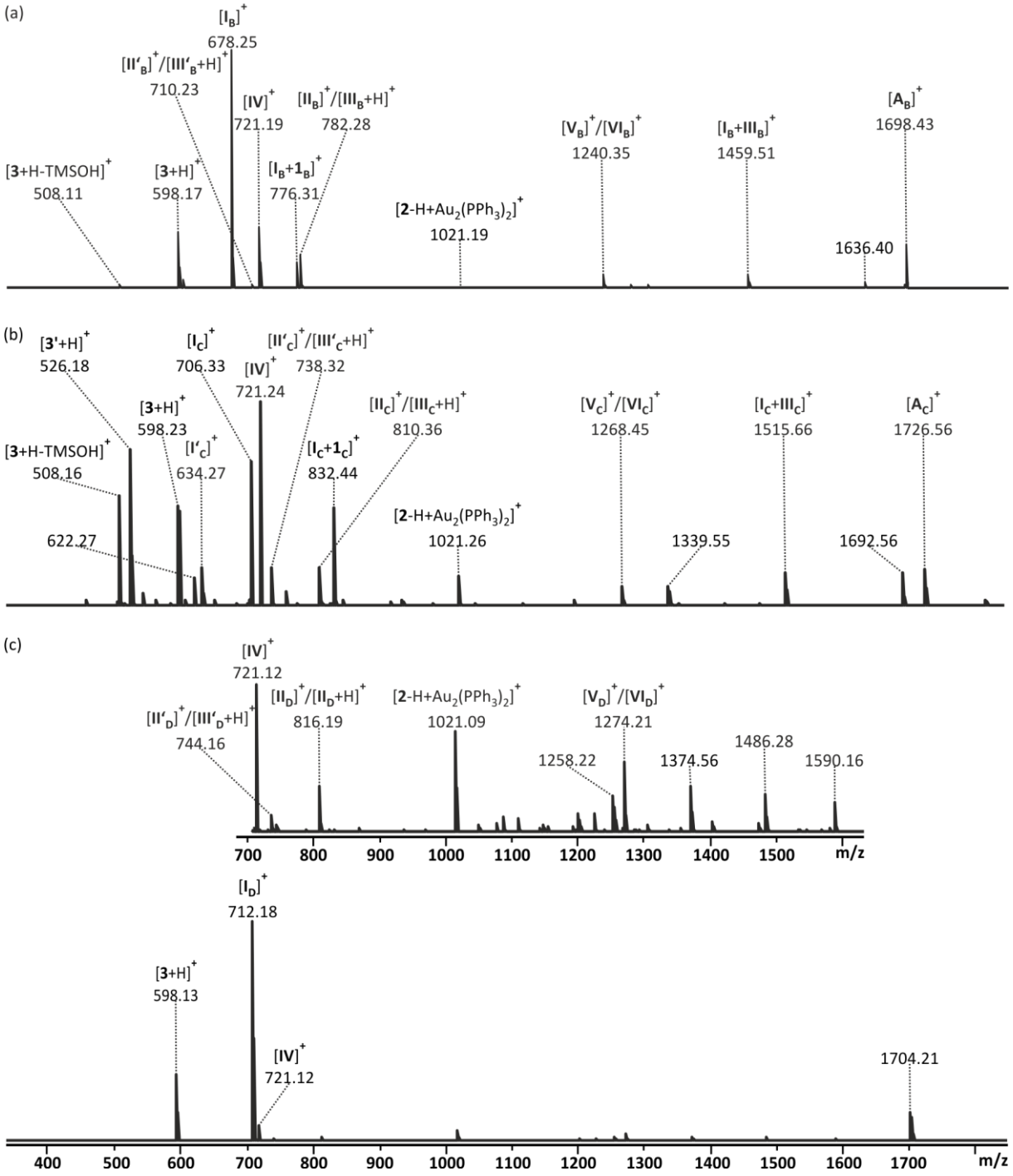

Figure 3.15. ESI(+) mass spectra of the reaction solutions of (a) *trans*-2-hexenal $\mathbf{1_B}$ (reaction 3.15) (b) *trans*-2-octenal $\mathbf{1_C}$ (reaction 3.16) and (c) *trans*-2-cinnamaldehyde $\mathbf{1_D}$ (reaction 3.17) with alkyne **2** in toluene recorded with Q/TOF mass spectrometer (a) (chapter 7.2.4). The samples were taken after one minute reaction time and diluted 1:100 in acetonitrile. For (c) additional tenfold zoom into the spectrum between *m/z* 715 and 1620.

To facilitate and verify the peak interpretation of the reaction of *trans*-2-pentenal $\mathbf{1_A}$, the reactions of other aldehydes ($\mathbf{1_B}$, $\mathbf{1_C}$, $\mathbf{1_D}$, scheme 3.8) were also monitored. Figure 3.15 shows the individual ESI(+) spectra of *trans*-2-hexenal $\mathbf{1_B}$ (figure 3.15a), *trans*-2-cinnamaldehyde $\mathbf{1_C}$ (Figure 3.15b) and *trans*-2-octenal $\mathbf{1_E}$ (figure 3.15c) with alkyne **2**. As for the variation of the alkyne substrate before, the peaks are shifted according to the weight difference of the individual aldehydes to the model system with *trans*-2-pentenal $\mathbf{1_A}$ (compare figure 3.7). In case of *trans*-2-hexenal $\mathbf{1_B}$, the iminium $[\mathbf{I_B}]^+$ (*m/z* 678) emerges as the spectrum's base peak. Signals for two catalysts $[\mathbf{IV}]^+$ (*m/z* 721) and $[\mathbf{3}]^+$ (*m/z* 598) were detectable as well. The base catalyst was observable without the TMSOH group $[\mathbf{3}$+H-TMSOH$]^+$

(*m/z* 508) as well. This typical behavior in solution is consistent with the previous ESI-MS experiments for aldehyde $\mathbf{1_A}$. This is also the case for the loss of the TMS protecting group of iminium/enamine species $[\mathbf{II_B}]^+/[\mathbf{III_B}+H]^+$ (*m/z* 782) which can additionally be seen as $[\mathbf{II'_B}]^+/[\mathbf{III'_B}+H]^+$ (*m/z* 710). Further, some of the adduct molecules were not detectable. In contrast to the iminium/enamine species $[\mathbf{II_B}]^+/[\mathbf{III_B}+H]^+$, adducts could only be found with an intact TMS group. Nevertheless, the detection of $[\mathbf{I_B}+\mathbf{1_B}]^+$ (*m/z* 776) and $[\mathbf{I_B}+\mathbf{III_B}]^+$ (*m/z* 1459) underpin that the formation of unreactive off-cycle adduct molecules is reproducible and does not only occur for *trans*-2-pentenal $\mathbf{1_A}$. The fragmentation pattern observed during the CID experiments (figure 3.12c, fragmentation scheme: appendix, scheme 9.1) also confirmed the first structural suggestion for this kind of molecule. This is all also valid for the off-cycle adduct of alkyne **2** which again underwent a deprotoauration $[\mathbf{2}\text{-H}+Au_2(PPh_3)_2]^+$ (*m/z* 1021). Interestingly, the highly transient species $[\mathbf{B_B}]^+$ (*m/z* 1119) was only detectable in some scans at the noise level. In contrast to this molecule, the (**A**)-type species $[\mathbf{V_B}]^+/[\mathbf{VI_B}]^+$ (*m/z* 1240) and $[\mathbf{A_B}]^+$ (*m/z* 1698) were constantly observable during the reaction.

Since the detection of the desired potential intermediate species appeared more facile in case of the aliphatic aldehydes, the reaction of *trans*-2-octenal $\mathbf{1_E}$ with alkyne **2** (figure 3.15c) was also monitored. A crowded spectrum was the result. The base catalyst **3** and its related iminium/enamines were not only detectable in their original form ($[\mathbf{3}+H]^+$ = *m/z* 598, $[\mathbf{I_C}]^+$ = *m/z* 706 and $[\mathbf{II_C}]^+/[\mathbf{III_C}+H]^+$ = *m/z* 810). Additionally, the typical loss of TMS during the ESI process was observed. This was also the case for catalyst **3**. Therefore, $[\mathbf{3'}+H]^+$ (*m/z* 526) as well as $[\mathbf{3}\text{+H-TMSOH}]^+$ (*m/z* 508), $[\mathbf{I'_C}]^+$ (*m/z* 634) and $[\mathbf{II'_C}]^+/[\mathbf{III'_C}+H]^+$ (*m/z* 738) were detectable as well, confirming the findings for the model system using *trans*-2-pentenal $\mathbf{1_A}$. Additionally, the iminium/enamine species $[\mathbf{V_C}]^+/[\mathbf{VI_C}]^+$ (*m/z* 1268) and the gold adduct $[\mathbf{A_R}]^+$ (*m/z* 1726) were constantly detectable. Only the three adduct species ($[\mathbf{I_C}+\mathbf{1_C}]^+$ = *m/z* 832), $[\mathbf{2}\text{-H}+Au_2(PPh_3)_2]^+$ = *m/z* 1021 and $[\mathbf{I_C}+\mathbf{III_C}]^+$ = *m/z* 1515), which were also observable for *trans*-2-hexenal $\mathbf{1_B}$ ($[\mathbf{I_B}+\mathbf{1_B}]^+$ = *m/z* 776), $[\mathbf{2}\text{-H}+Au_2(PPh_3)_2]^+$ = *m/z* 1021 and $[\mathbf{I_B}+\mathbf{III_B}]^+$ = *m/z* 1459), can be seen in the spectrum.

The reaction of *trans*-2-cinnamaldehyde $\mathbf{1_D}$ only rendered some of the expected species (figure 3.15c). As for the previous reactions, the spectrum is dominated by the iminium species $[\mathbf{I_D}]^+$ (*m/z* 712). In case of the aromatic aldehyde, it appears that this peak possesses such a high intensity that it suppresses the detection of almost every other species. This effect is caused by a high difference in the species' ESI response factor (chapter 2.4). Probably, the iminium species $[\mathbf{I_C}]^+$ is additionally stabilized by the aromatic substituent. At first glance, only the two catalytic units could be identified. Zooming in on the spectrums base line, small peaks of the iminium/enamine species $\mathbf{II_D}^+/\mathbf{III_D}$ became visible in their protected (*m/z* 816) and unprotected form (*m/z* 744). The alkyne-gold adduct $[\mathbf{2}\text{-H}+Au_2(PPh_3)_2]^+$ (*m/z* 1021) became visible as well. Unfortunately, the desired highly transient species were not constantly detectable. Thus, only the (**A**)-type species $[\mathbf{V_D}]^+/[\mathbf{VI_D}]^+$ (*m/z* 1274) is present in the expanded spectrum of figure 3.15c. As presented beforehand for the other two aldehydes' spectra, the detection of the (**B**)-cycle species $[\mathbf{B_R}]^+$ (scheme 3.9d) was only detected in trace amounts in contrast to the (**A**)-type species $[\mathbf{V_R}]^+/[\mathbf{VI_R}]^+$ (scheme 3.9a) and $[\mathbf{A_R}]^+$ (scheme 3.9c). This can either indicate that species $[\mathbf{B_R}]^+$ is too transient due to a very high reactivity of cycle (**B**) or that this is an off-cycle in equilibrium to the more reactive cycle (**A**) that consumes the substrates required for both pathways.

With all this information in hand, structural suggestions can be made for all gold-containing transient species that are shown in scheme 3.9. In general, two classes of species were detected. The coordinative species $[\mathbf{V_A}]^+$ is isomeric to the cyclic molecule $[\mathbf{VI_A}]^+$ (scheme 3.9a). They correspond to the predicted *pre-* and *post*-cyclization cations according to mechanism (**A**) (chapter 3.1, scheme 3.2). An analogous molecule for cycle (**B**) will be presented during the base exchange experiments in chapter 3.6 (possible structures see scheme 3.9b). The second class of detected species is represented by $[\mathbf{A_A}]^+$ and $[\mathbf{B_A}]^+$

(scheme 3.9c and d). They form if the neutral molecules **IX$_A$** and **VIII$_A$** are charged by a second gold(I) cation. It is assumed that the second gold atom attaches to the same carbon atom that is already bound to the first gold atom. The *gem*-diaurated species by [**A$_A$**]$^+$ and [**B$_A$**]$^+$ are very unlikely part of the actual mechanistic cycle. Other experimental studies[27–29,49] found comparable *gem*-diaurated structures that are assumed to be rather a very stable off-cycle resting state of the gold catalyst, while the reactive species are only monoaurated molecules.

Recently, *Roithová* and co-workers[43] presented a study on this phenomenon (chapter 1.1). Investigating a [Au(IPr)(CH_3CN)(BF_4)]-mediated addition of water to alkynes by means of ESI-MS and infrared spectroscopy they found that a neutral monoaurated species is the actual intermediate present in the reaction solution. During the ESI process, it is attached by another gold atom (or a proton). Thereby, the second gold cation binds to the formyl-oxygen that has been the nucleophile in the previous addition. The resulting cation is thus only a gas phase artifact. In contrast to their findings, it can be assumed that the smaller triphenylphosphine ligand used in this study allows the formation of *gem*-diaurated species. This is coherent with the results of *Lu et al.*[49] who showed by means of ESI-MS measurements combined with DFT calculations that the small PPh_3 ligand enables the formation of *gem*-diaurated molecules. Thus, binding to the alkyne or enamine moiety appears very unlikely.

3.4 Overall reaction – GC-MS experiments

As mentioned before, ESI-MS measurements were not suitable to detect neither the substrates nor the products. As a consequence, it was not possible to prove if the deuterated and phenyl-substituted alkyne's reaction leads to the formation of the desired product in an appropriate reaction time with this method. Same is valid for the reaction of the different aldehydes presented before. With parallel GC-MS monitoring, the reactions' progress were examined. As described in chapter 3.2.4, all polar components were separated beforehand by means of a small silica column (0.6 cm diameter, 1 cm height) and diluted in dichloromethane. In general, chromatographic peaks were allocated by their individual EI spectra. In chapter 3.2.4 the retention times of the starting materials and products were determined (table 3.1). This facilitated the assignment of the chromatographic peaks.

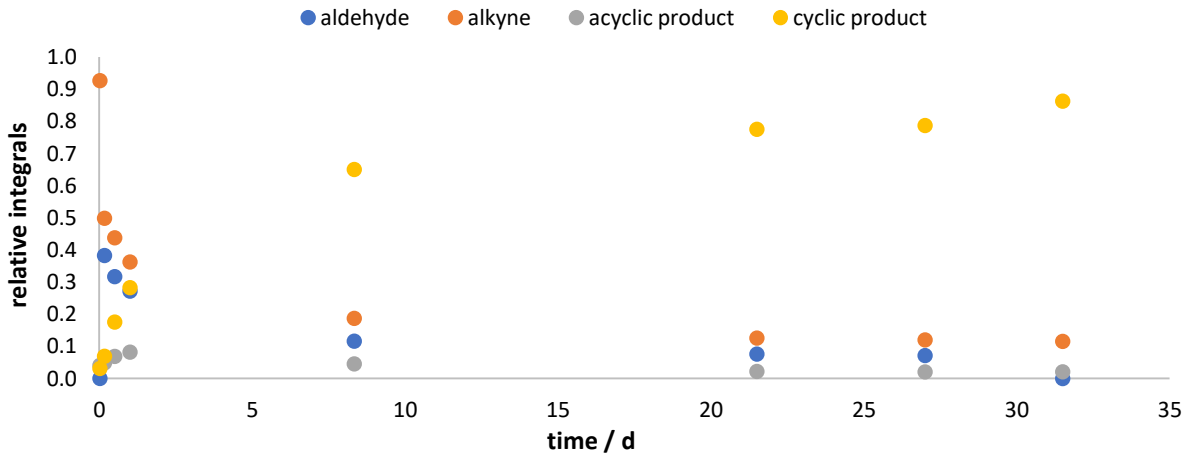

Figure 3.16. Overall reaction of *trans*-2-pentenal **1$_A$** with alkyne **2** (reaction 3.14). The absolute integrals are standardized to the sum of all integrals obtained by GC-MS measurements as function of time during the reaction of *trans*-2-pentenal **1$_A$** with alkyne **2** over 35 hours monitored with GC-MS instrument (b) (chapter 7.2.4).

The temporal evolution of the reaction of *trans*-2-pentenal $\mathbf{1_A}$ with alkyne **2** (reaction 3.14) is depicted in figure 3.16. Each absolute integral was standardized to the sum of all integrals. Thereby, only integrals that were assigned to the starting materials and the products were considered. The predominant peak of toluene (chapter 3.2.2, figure 3.1 and chapter 3.2.4, figure 3.5) was not taken into account for the standardization. As expected, the relative integrals of the starting materials decreased while the one of the Michael product $\mathbf{4_A}$ and the cyclization product $\mathbf{6_A}$ increased. Note that for the first sample after one minute, the amount of *trans*-2-pentenal $\mathbf{1_A}$ was extremely low. This can be attributed to the fact that aldehyde $\mathbf{1_A}$ was added last to start the reaction and was most probably not completely solved within one minute. After 31.5 hours, *trans*-2-pentenal $\mathbf{1_A}$ was not detectable anymore. In contrast, the alkyne **2** was still present in the reaction solution. This is surprising since *trans*-2-pentenal $\mathbf{1_A}$ was applied with 1.3 equivalents compared to the alkyne **2**. The amounts of acyclic Michael product $\mathbf{4_A}$ increased slightly within the first hour. Afterwards, this species was only detectable in traces. In contrast, the relative integral of cyclic product $\mathbf{6_A}$ increased exponentially at the beginning. In general, the behavior of this species resembles a saturation curve that does only reach a conversion of 86% within 31.5 hours reaction time. It is possible that *trans*-2-pentenal $\mathbf{1_A}$ is partially consumed by an unidentified side reaction. This would not only decrease the amounts of aldehyde detected but also explain why the conversion of the reaction is diminished.

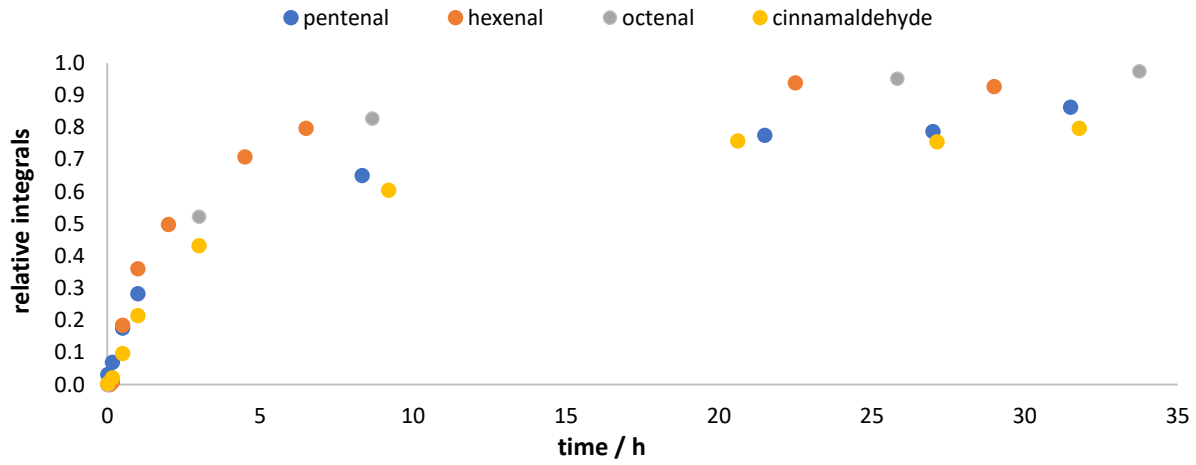

Figure 3.17. Overall reaction of a series of selected aldehydes with alkyne **2** (reaction 3.14-3.17). Integrals of cyclization product $\mathbf{6_R}$ standardized to the sum of all integrals obtained by GC-MS measurements as function of time during the reaction of *trans*-2-pentenal $\mathbf{1_A}$, *trans*-2-hexenal, *trans*-2-octenal $\mathbf{1_C}$ and *trans*-2-cinnamaldehyde $\mathbf{1_D}$ with alkyne **2** over 35 hours. The reaction of *trans*-2-pentenal $\mathbf{1_A}$ was monitored with GC-MS instrument (b). All others were monitored with GC-MS instrument (a) (chapter 7.2.4).

Figure 3.17 and figure 3.18 show the conversion of the individual reactions of alkyne **2** with a series of selected aldehydes. Interestingly, the sterically less demanding *trans*-2-pentenal $\mathbf{1_A}$ reacts slightly slower than the two other aliphatic aldehydes (*trans*-2-hexenal $\mathbf{1_B}$ and *trans*-2-octenal $\mathbf{1_C}$). The reaction of *trans*-2-pentenal $\mathbf{1_A}$ has a comparable rate to the one of the aromatic *trans*-2-cinnamaldehyde $\mathbf{1_D}$. It was surprising that both reactions evolved in an approximately equal amount of time since the group of *Jørgensen*[224] suggested a doubled reaction time (72 hours) for the aromatic aldehydes compared to the aliphatic ones (36 hours). For the model system with *trans*-2-pentenal $\mathbf{1_A}$, the maximal conversion was achieved after more than to two days (55 hours). Therefore, the reaction time should be extended to at least two and a half days (60 hours). This would ensure a gain of product of approximately 7%. With the results of the GC-MS monitoring, the thought of a generally shorter reaction time for aliphatic aldehydes than for aromatic aldehydes has to be reconsidered.

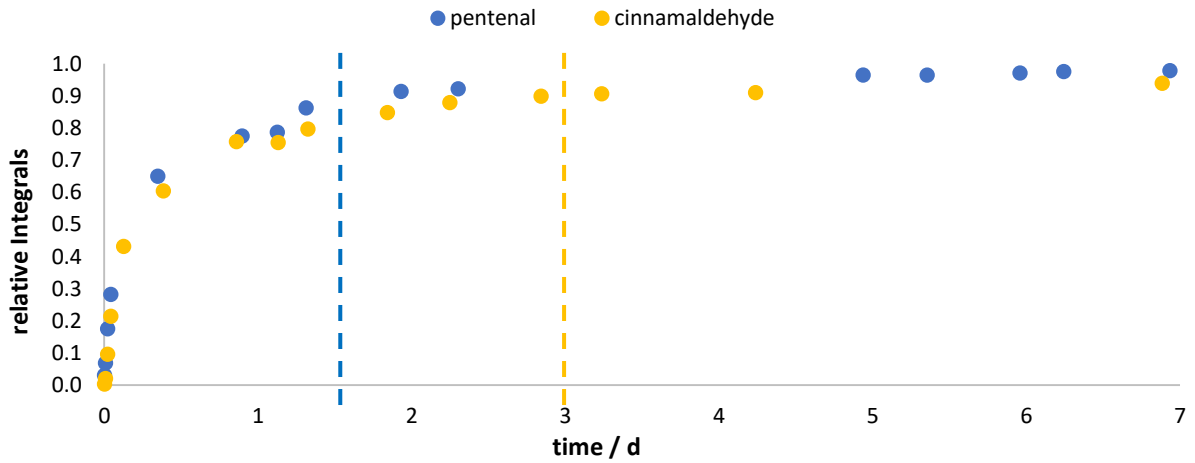

Figure 3.18. Overall reaction of a series of selected aldehydes with alkyne **2** (reaction 3.14 and 3.16). Integrals of cyclization product $\mathbf{6_R}$ standardized to the sum of all integrals obtained by GC-MS measurements as function of time during the reaction of *trans*-2-pentenal $\mathbf{1_A}$ and *trans*-2-cinnamaldehyde $\mathbf{1_D}$ with alkyne **2** over one week. The reaction of *trans*-2-pentenal $\mathbf{1_A}$ was monitored with GC-MS instrument (b). The reaction of *trans*-2-cinnamaldehyde $\mathbf{1_D}$ was monitored with GC-MS instrument (a) (chapter 7.2.4). The blue line is drawn at the suggested reaction time for aliphatic aldehydes (36 hours).[224] The yellow line is drawn at the suggested reaction time for aromatic aldehydes (72 hours).[224]

As expected, the deuterated alkyne increases the reaction time only slightly (figure 3.19). The EI mass spectra recorded during the GC-MS measurements (appendix, figure 9.3) indicate no statistical distribution for the deuterated and non-deuterated cyclization product. As for the synthetic approach (chapter 3.2.2), the isotopic label remained with 56% in the molecules (starting from alkyne $\mathbf{2_{deut}}$ with 94%). Consequentially, this supports the previous suggestion that the deprotoauration does not take place at the primary alkyne since this would decrease the deuteration rate to less than one percent.

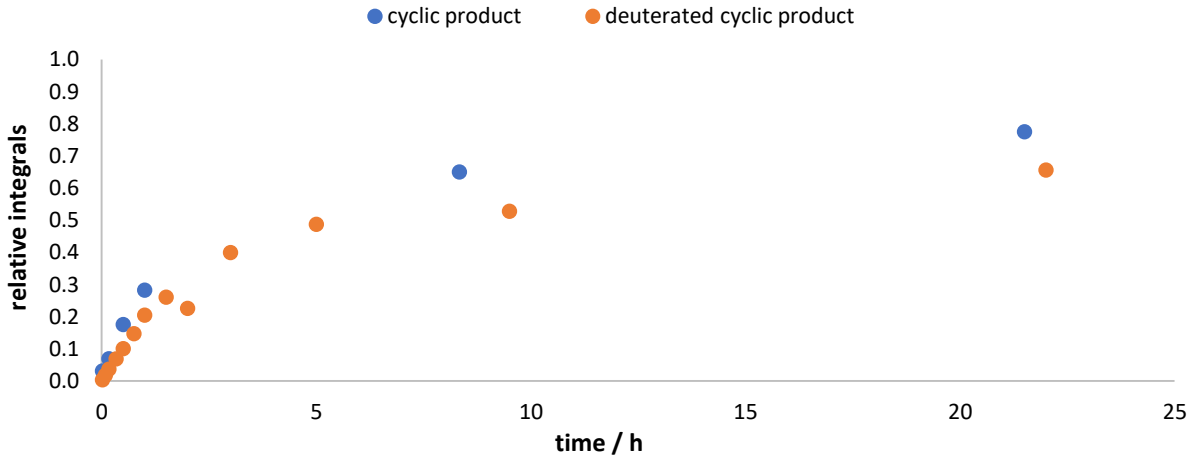

Figure 3.19. Normal overall reaction (reaction 3.14) vs. deuterated overall reaction (reaction 3.18). Integrals of cyclization product $\mathbf{6_R}$ standardized to the sum of all integrals obtained by GC-MS measurements as function of time during the reaction of *trans*-2-pentenal $\mathbf{1_A}$ with alkyne **2** monitored with GC-MS instrument (b) and alkyne $\mathbf{2_{deut}}$ monitored with GC-MS instrument (a) (chapter 7.2.4) over one day.

By means of GC-MS it could be proved that the reaction using phenylated alkyne $\mathbf{2_{Ph}}$ also results in product formation (figure 3.20). This confirmed the synthetic findings that cyclization product $\mathbf{6_{A,Ph}}$ could be isolated with 50% yield after three days (chapter 3.2.3). Due to the phenyl group's high steric demand, the cyclization appears hindered and thus decelerated. Interestingly, it was possible to monitor the usually very fast isomerization process from cyclization product $\mathbf{5_{A,Ph}}$ to cyclopentene

carbaldehyde **6**$_{A,Ph}$. If the alkyne is not substituted, the vinyl product **5** isomerizes spontaneously because of the isomerization product's **6** favorable and larger π-system. If a phenyl group is placed at the alkyne, the aromatic ring most probably stabilizes the first cyclization product **5**$_{A,Ph}$ electronically, retarding the isomerization process. Further, the behavior for *trans*-2-pentenal **1**$_A$ and alkyne **2**$_{Ph}$ is comparable to the reaction of alkyne **2** (figure 3.16). The amounts of aldehyde **1**$_A$ decreased within one and a half days down to the detection limit while the conversion of the alkyne stagnated after four days at 60%. This supports the hypothesis that *trans*-2-pentenal **1**$_A$ is consumed by a side reaction.

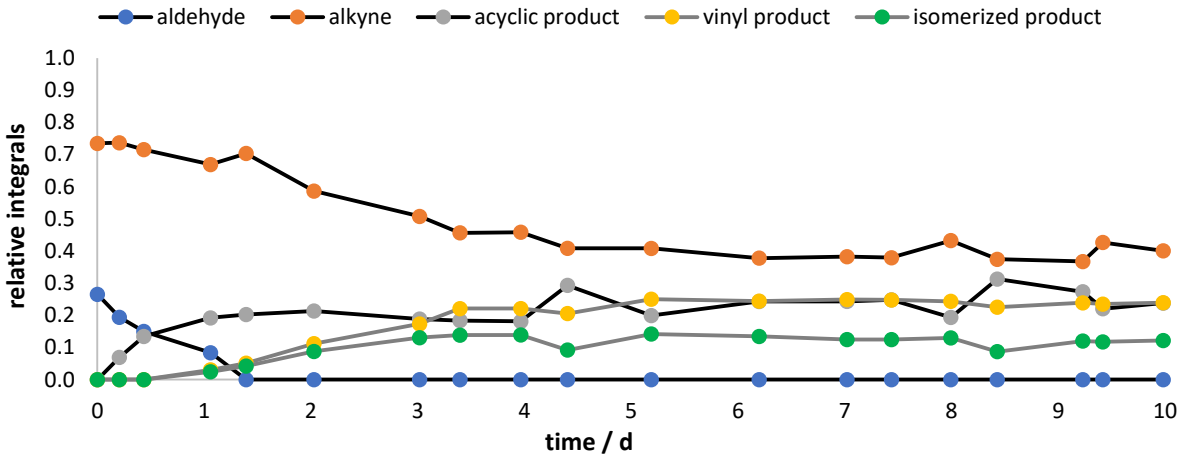

Figure 3.20. Overall reaction of phenyl alkyne **2**$_{Ph}$ (reaction 3.19). Integrals of aldehyde **1**$_A$, alkyne **2**$_{Ph}$, acyclic Michael product **4**$_{A,Ph}$, vinyl cyclization product **5**$_{A,Ph}$ and its isomer **6**$_{A,Ph}$ standardized to the sum of all integrals obtained by GC-MS measurements with GC-MS instrument (a) (chapter 7.2.4) as function of time during the reaction of *trans*-2-pentenal **1**$_A$ with alkyne **2**$_{Ph}$ over ten days.

For a synthetic approach to cyclopentene carbaldehyde **6**$_{A,Ph}$, higher amounts of catalysts and aldehyde are reasonable (reaction 3.20). This does not only accelerate the reaction in general and counters the side reaction suspected for *trans*-2-pentenal **1**$_A$, but also supports the isomerization process as well as the substrates' total conversion. Figure 3.21 shows the temporal evolution of a reaction setup with a doubled amount of all catalyst, additives and *trans*-2-pentenal **1**$_A$ compared to phenylated alkyne **2**$_{Ph}$. This setup leads to a complete conversion of alkyne **2**$_{Ph}$ after ten days. The equilibrium of the two cyclic isomers shifted after three days when aldehyde **1**$_A$ and the acyclic Michael species **4**$_{A,Ph}$ were completely consumed and the conversion of alkyne **2**$_{Ph}$ was at 80%. Then, the vinyl-type isomer **5**$_{A,Ph}$ started to isomerize to the cyclopentene isomer **6**$_{A,Ph}$. As a result, isomerized cyclic product **6**$_{A,Ph}$ can be isolated as the main product after one week.

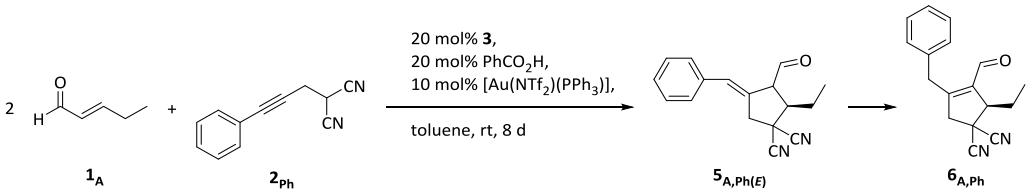

1$_A$ **2**$_{Ph}$ **5**$_{A,Ph(E)}$ **6**$_{A,Ph}$ **(3.20)**

Scheme 3.14. Overall reactions of *trans*-2-pentenal **1**$_A$ and phenylated alkyne **2**$_{Ph}$ measured *via* GC-MS prepared according to the group of *Jørgensen*.[224] Reaction with doubled amount of catalysts, additives and aldehyde **1**$_A$.

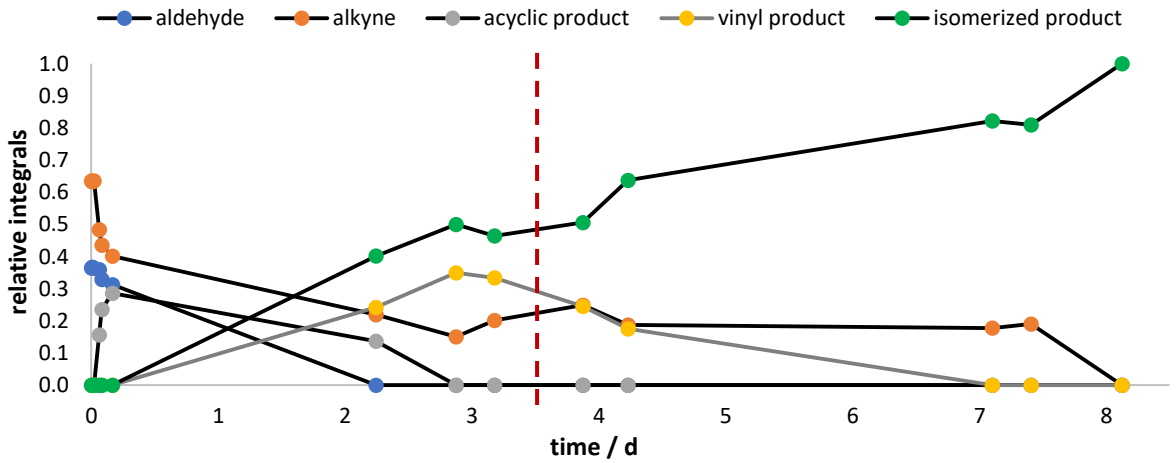

Figure 3.21. Overall reaction of phenyl alkyne $\mathbf{2}_{Ph}$ (reaction 3.20). Integrals of aldehyde $\mathbf{1}_{A}$, alkyne $\mathbf{2}_{Ph}$, acyclic Michael product $\mathbf{4}_{A,Ph}$, vinyl cyclization product $\mathbf{5}_{A,Ph}$ and its isomer $\mathbf{6}_{A,Ph}$ standardized to the sum of all integrals obtained by GC-MS measurements with GC-MS instrument (a) (chapter 7.2.4) as function of time during the reaction of *trans*-2-pentenal $\mathbf{1}_{A}$ with alkyne $\mathbf{2}_{Ph}$ over eight days. Reaction with doubled amounts of catalysts, additives and aldehyde $\mathbf{1}_{A}$. The red line is drawn at a reaction time of three and a half days when both cyclic isomers were present in almost the same amount.

In summary, the reaction monitoring by GC-MS showed that the reaction times vary significantly for every combination of starting materials. A generally shorter reaction time for aliphatic aldehydes compared to aromatic aldehydes, suggested by the group of *Jørgensen*,[224] was debunked. The experiments with deuterated alkyne $\mathbf{2}_{deut}$ and phenyl alkyne $\mathbf{2}_{Ph}$ revealed that the reaction is not limited to primary alkynes. For the reaction of the phenyl-substituted alkyne $\mathbf{2}_{Ph}$, it was additionally possible to detect the vinyl product $\mathbf{5}_{A}$. If the unsubstituted alkyne **2** is applied, this species isomerizes too fast to be observed.

The GC-MS experiments further indicated that the reaction is hindered by consumption of the aldehyde. The side reaction consuming this starting material was not identified. Since this off-cycle reaction is expected to occur in low rate compared to the dual activation reaction, it was not surprising that side products were not detectable during the measurements. Additionally, the detection is suppressed by the high amounts of toluene that dominates all chromatograms (chapter 3.2.2, figure 3.1 and chapter 3.2.4, figure 3.5).

3.5 Stepwise approach

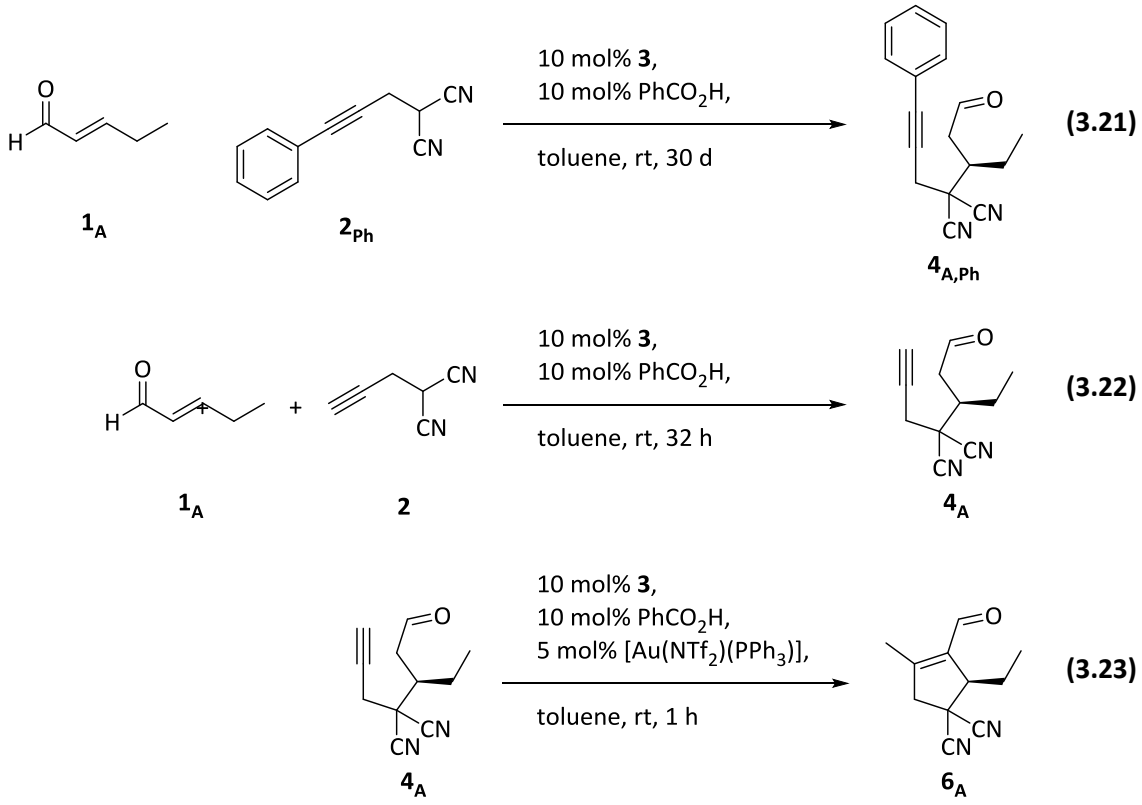

Scheme 3.15. Control reactions for the stepwise approach measured *via* ESI-MS and GC-MS.

To get a more concise understanding of the reaction, it was split into the Michael addition and the 5-*exo*-*dig*-cyclization. The Michael addition was investigated using a setup without the gold catalyst (reaction 3.21 and 3.22). This was expected to stop the reaction after the Michael product **4** was formed. The investigation of the cyclization process required a second setup with Michael product $\mathbf{4_A}$ as starting material (reaction 3.23). The reaction conditions were chosen as for the overall reaction 3.14 before. The group of *Jørgensen*[224] tested these two approaches synthetically. Thereby, they found that the gold catalyst is crucial for the cyclization to occur. However, their experiments indicated that the Michael addition is significantly hindered if performed separately. To examine the mechanistic differences and variations in the reactions' rates, ESI-MS and GC-MS monitoring of both reaction steps was applied. The results of the ESI-MS measurements are presented in the following.

As expected, the Michael addition's ESI(+) spectrum (figure 3.22b) only shows the already known iminium/enamine species $[\mathbf{I_A}]^+$ and $[\mathbf{II_A}]^+/[\mathbf{III_A}+H]^+$, their hydrolysis derivatives ($[\mathbf{I'_A}]^+$ and $[\mathbf{II'_A}]^+/[\mathbf{III'_A}+H]^+$) as well as the free catalyst **3**. The Michael addition of alkyne $\mathbf{2_{Ph}}$ (figure 3.22a) rendered comparable results. However, the iminium/enamine species $[\mathbf{II_A}]^+/[\mathbf{III_A}+H]^+$ (*m*/*z* 844) and $[\mathbf{II'_A}]^+/[\mathbf{III'_A}+H]^+$ (*m*/*z* 772) were detectable with comparably high intensities. This reproducible effect suggests an electronic stabilization of the individual transient species by the phenyl group's lager π-system.

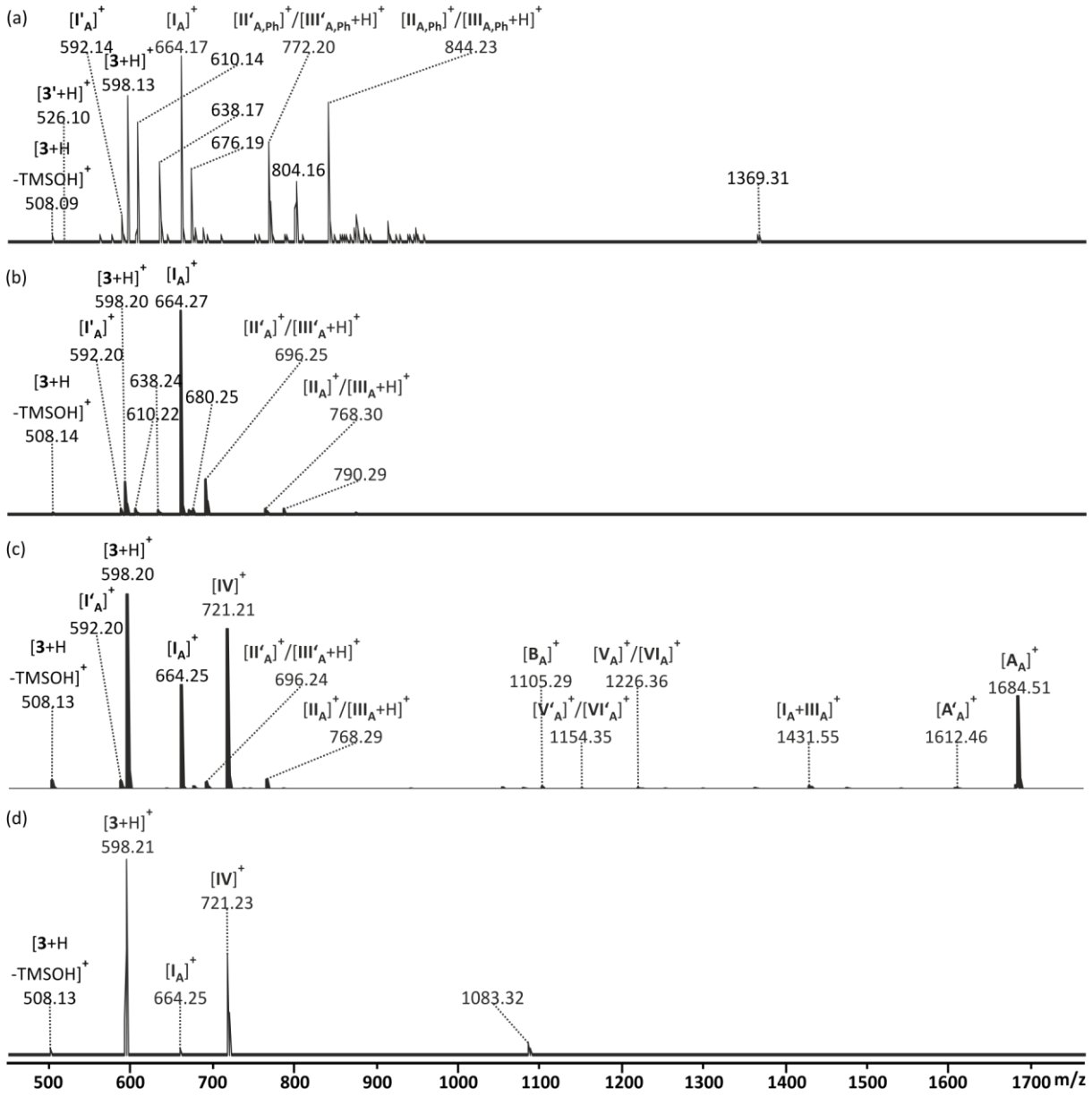

Figure 3.22. ESI(+) mass spectra of the reaction solutions of (a) Michael addition between *trans*-2-pentenal $\mathbf{1_A}$ and phenyl alkyne $\mathbf{2_{Ph}}$ with only the base catalyst **3** (reaction 3.21), (b) Michael addition between *trans*-2-pentenal $\mathbf{1_A}$ and alkyne **2** with only the base catalyst **3** (reaction 3.22), (c) and (d) acyclic Michael product $\mathbf{4_A}$ and to cyclization product $\mathbf{6_A}$ (reaction 3.23) in toluene recorded with Q/TOF mass spectrometer (a) (chapter 7.2.4). The samples for spectrum (a), (b) and (c) were taken after one minute reaction time, the sample for spectrum (d) after one hour reaction time. All were diluted 1:100 in acetonitrile.

In contrast to the Michael addition, the cyclization reaction's ESI(+) spectrum (figure 3.22c) is very similar to the spectrum of the overall reaction (figure 3.7). All species of higher *m/z* values are present. Interestingly, iminium species $[\mathbf{I'_A}]^+$, $[\mathbf{I_A}]^+$ were detected as well as the adduct $[\mathbf{I'_A}+\mathbf{III'_A}]^+$. They are most probably caused by a partial retro Michael addition that can be observed by dissolution of Michael product $\mathbf{4_A}$ and are supported by the relatively high concentration of the acyclic product. This can most likely be attributed to the higher concentration of Michael product $\mathbf{4_A}$ in the reaction solution. Species $[\mathbf{A_A}]^+$ was detectable with high intensity. Since the reaction conditions only varied in the concentration of acyclic product $\mathbf{4_A}$ at the beginning, it can be assumed that no electronic effect as in case of the phenylated reaction contributes to this behavior. As exclusively the species $[\mathbf{A_A}]^+$ is accumulated by this higher concentration, it appears most probable that it is part of the main reaction cycle (chapter 3.8, scheme 3.18, cycle (**A**)). In general, an initial increase of one species' intensity with a

decline after the reaction is finished is expected for species that contribute to the main pathway. In case of the overall reactions (reaction 3.14 to 3.18), all possible reaction intermediates did not vary their intensity significantly during the reaction. In contrast, the monitoring of the stepwise cyclization revealed the accumulated species $[\mathbf{A_A}]^+$ vanishes completely after one hour (figure 3.22d). As discussed in the following, the cyclization process is terminated within this reaction time. This clarifies the reactivity of the intermediates corresponding to $[\mathbf{A_A}]^+$. Thus, the solely gold-tethered cycle (**B**) is definitely demoted to a side pathway.

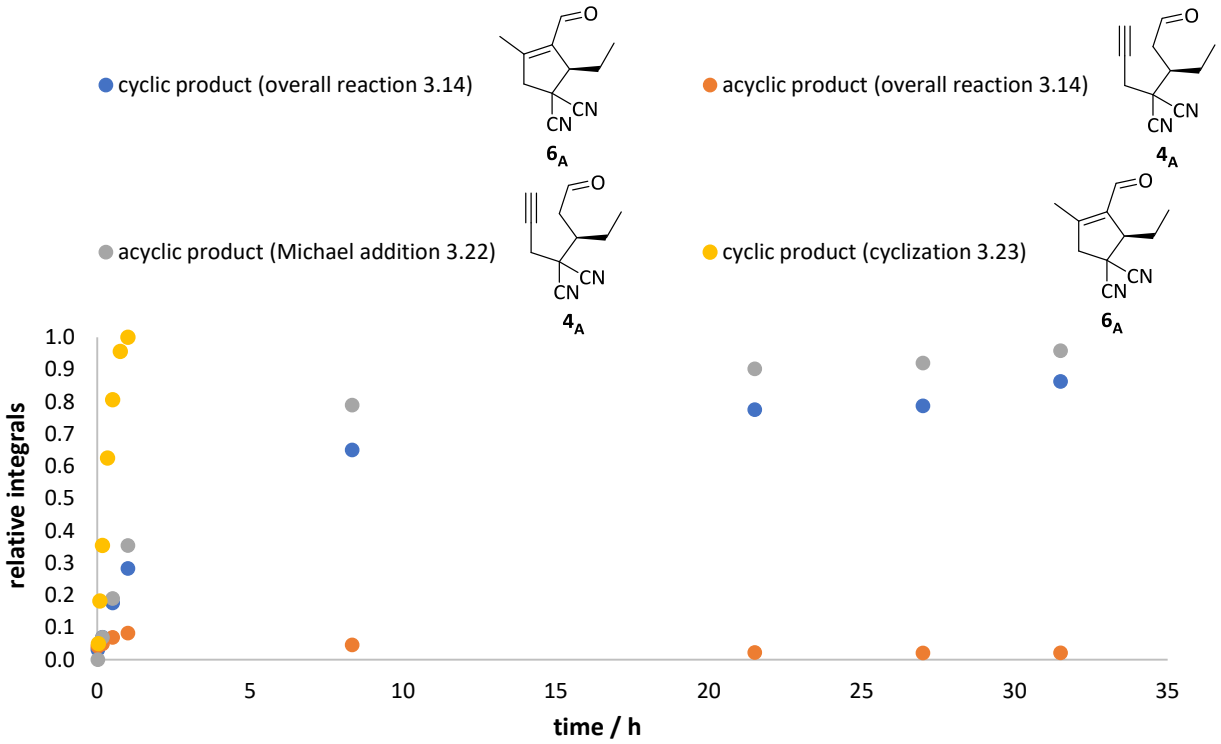

Figure 3.23. Overall reaction (reaction 3.14) vs. Michael addition (reaction 3.22) and 5-*exo*-*dig*-cyclization (reaction 3.23). Integrals of Michael product $\mathbf{4_A}$ and cyclization product $\mathbf{6_A}$ standardized to the sum of all integrals obtained by GC-MS measurements as function of time during the overall reaction of *trans*-2-pentenal $\mathbf{1_A}$ with alkyne **2** to cyclization product $\mathbf{6_A}$, the Michael addition of *trans*-2-pentenal $\mathbf{1_A}$ with alkyne **2** to Michael product $\mathbf{4_A}$ and the cyclization reaction of Michael product $\mathbf{4_A}$ to cyclization product $\mathbf{6_A}$ over 36 hours. The overall reaction (reaction 3.14) and Michael addition (reaction 3.22) were recorded with GC-MS instrument (b). The 5-*exo*-*dig*-cyclization (reaction 3.23) was recorded with GC-MS instrument (a) (chapter 7.2.4).

Intramolecular cyclisation reactions are known to be faster than intermolecular additions.[232] In accordance with this expectation, the GC-MS monitoring shows (figure 3.23) that the intramolecular cyclization proceeds much faster (terminated within one hour) than the Michael addition. One has to take into account that in the normal setup, the Michael product $\mathbf{4_A}$ is removed by the consecutive cyclization. Albeit this influence on the Michael addition step is missing when regarding the reactions separately, the Michael addition's conversion proceeds almost in parallel to the one of the overall reaction. This demonstrates that the reaction's rate is determined by the first step. At this point, it has to be underlined that the cyclization product could not be detected during the Michael reaction's monitoring without the gold catalyst even after one week. In case of the phenyl alkyne $\mathbf{2_{Ph}}$, a Michael addition was monitored even for one month without finding any cyclization product. Thus, the cyclization does not occur without the Lewis acid gold catalyst.

3.6 Base exchange experiments

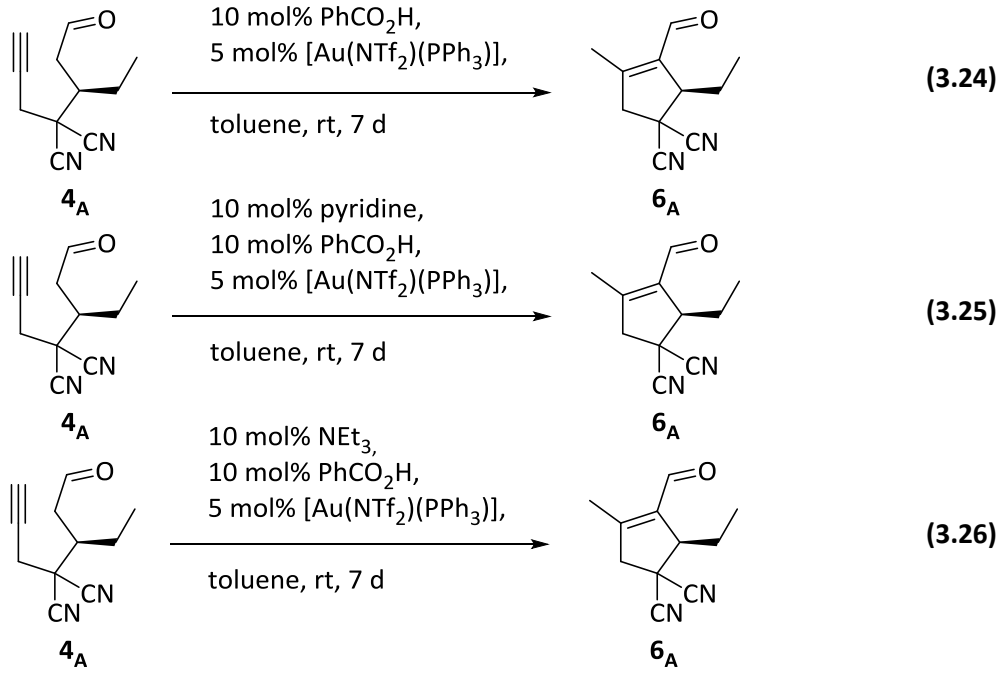

Scheme 3.16. Reactions of the base exchange experiments with acyclic Michael product $\mathbf{4_A}$ measured *via* ESI-MS and GC-MS.

The role of the base **3** during the cyclization process was also addressed in this thesis. *Kirsch* and co-workers[225] suggested that the *L*-proline derivative **3** could solely act as a base in the reaction mixture (chapter 3.1, scheme 3.2, cycle (**B**)). In contrast to the other mechanistic suggestion (cycle (**A**)), which includes iminium/enamine formation, no binding of the amine to the substrate would be required. To shed light on this, the proline derivative **3** was exchanged by the aromatic amine base pyridine (reaction 3.25) as well as the tertiary amine triethylamine (reaction 3.26) for the cyclization of the isolated Michael product $\mathbf{4_A}$. Both bases are not capable of binding to any of the substrates. The product formation was compared to the one of a reaction with solely the gold catalyst present in the reaction mixture (reaction 3.24).

Interestingly, all three reactions showed almost the same peaks in the ESI-MS spectra (figure 3.24). Additionally to the familiar peak of $Au(PPh_3)_2^+$ (*m/z* 721) and the transient digold-containing molecule $[\mathbf{B_A}]^+$ (*m/z* 1105) (chapter 3.3, scheme 3.9d), species $[\mathbf{VIII_A}+H]^+/[\mathbf{X_A}]^+$ (chapter 3.3, scheme 3.9b) with *m/z* 647 could be detected. This very transient species could not be observed in any reaction containing the base catalyst **3**. It can either be assigned to a coordination of the Michael product $\mathbf{4_A}$ to one gold(I) cation with a PPh_3 ligand. Thus, it would be a (**B**)-type analog to coordination species $[\mathbf{V_A}]^+$ (chapter 3.3, scheme 3.9b), named $[\mathbf{X_A}]^+$. Alternatively, it can be of *post*-cyclic form ($[\mathbf{VIII_A}+H]^+$). In this case, it would be an analog to $[\mathbf{VI_A}]^+$ (chapter 3.3, scheme 3.9b). Since CID experiments were not successful, it was not possible to reveal the exact structure of this species. Nevertheless, its detection leads to the conclusion that cyclization product $\mathbf{6_A}$ is formed according to the solely gold-containing mechanisms in these cases (chapter 3.8, scheme 3.18, cycle (**B**)). Interestingly, the detection appeared facilitated when pyridine or triethylamine was added. In contrast, when only the Lewis acid catalyst was present (figure 3.24a) the molecule was not constantly detectable during the reaction. An experiment with the addition of higher amounts of benzoic acid (50 mol%) showed that this species cannot be detected at all in a more acidic milieu (appendix, reaction 9.1, figure 9.7 and 9.8). In general, a less acidic

milieu provides fewer protons, which are required for the release of the cyclization product $\mathbf{5_A}$ and the gold catalyst. As a result, $[\mathbf{VIII_A}+H]^+/[\mathbf{X_A}]^+$ accumulates and can be detected constantly.

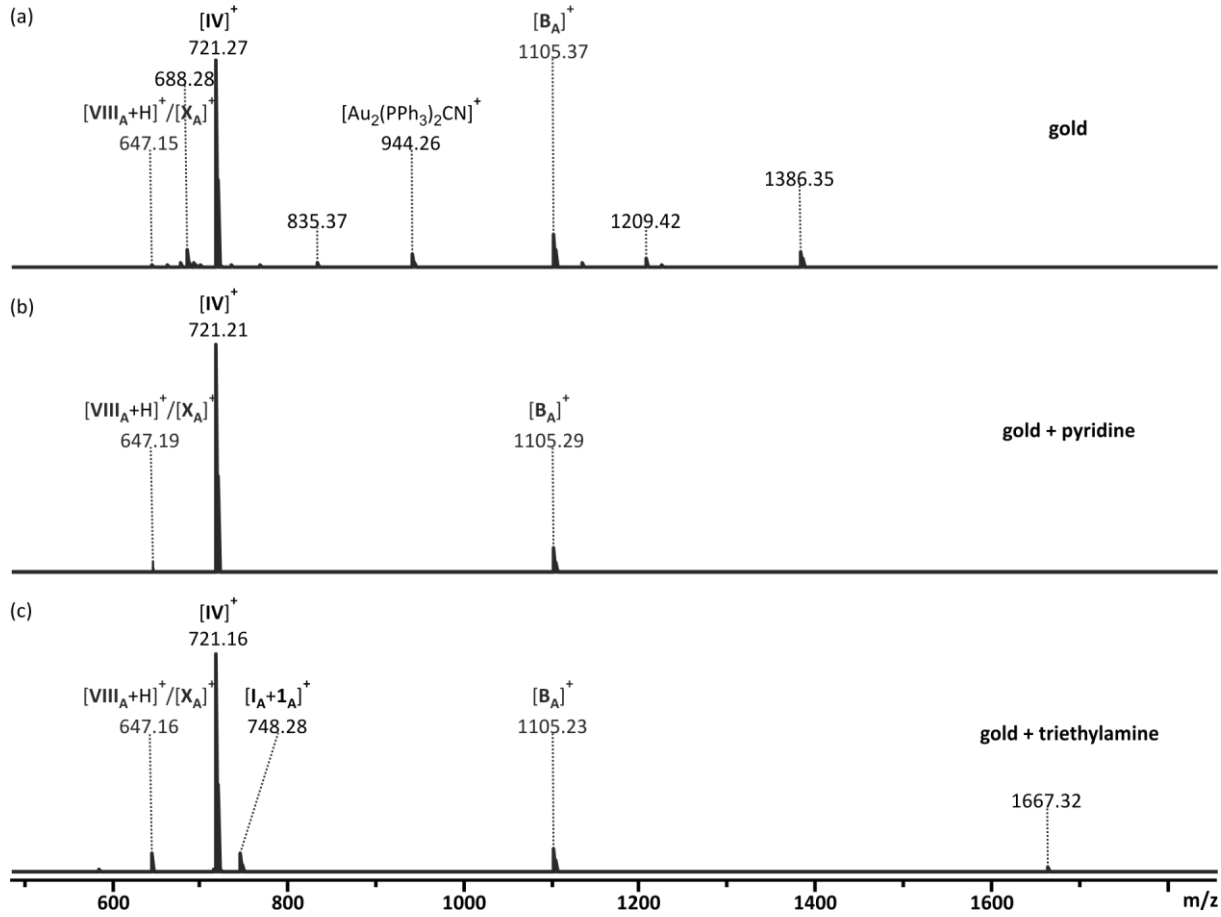

Figure 3.24. ESI(+) mass spectra of the cyclization reaction solution of acyclic Michael product $\mathbf{4_A}$ with (a) solely the gold(I) catalyst present (reaction 3.24), (b) with pyridine as base catalyst (reaction 3.25) and (c) with triethylamine as base catalyst (reaction 3.26) in toluene recorded with Q/TOF mass spectrometer (a) (chapter 7.2.4). The samples were taken after one minute reaction time and diluted 1:100 in acetonitrile.

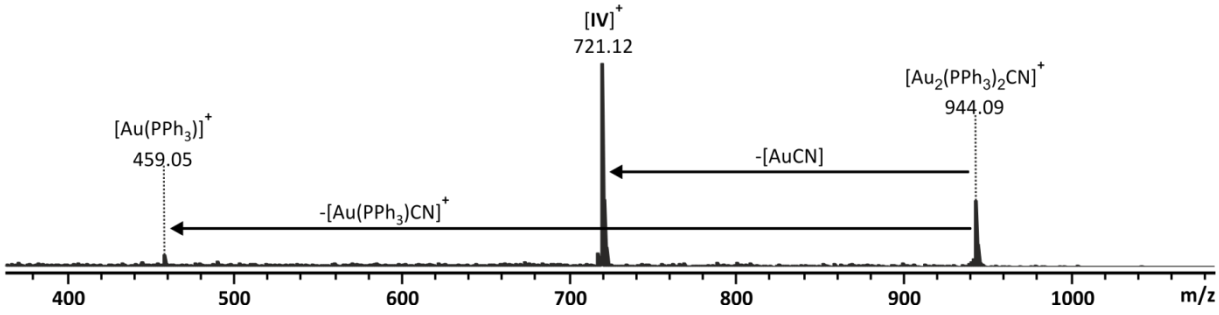

Figure 3.25. ESI(+) CID spectrum of the mass-selected species $[Au_2(PPh_3)_2CN]^+$ (collision energy 30 eV) recorded with Q/TOF mass spectrometer (a) (chapter 7.2.4).

Additionally, species *m/z* 944 was found for the solely gold catalyzed reaction (figure 3.24a). The molecule's structure could be proven by CID experiments (figure 3.25). It is formed by the gold catalyst and a cyano ligand which most probably originates from acetonitrile that is used as solvent. This species was also detectable occasionally during other ESI-MS measurements performed for this study. Another familiar species observed was $[\mathbf{I_A}+\mathbf{1_A}]^+$ (*m/z* 748). This adduct can be seen in the spectrum with triethylamine (figure 3.24c). Since the original starting materials were not used for this setup, the free aldehyde was not expected to be present in the reaction solution. This indicated a partial retro Michael

addition that occurs under the basic conditions with triethylamine. At this point, it has to be pointed out that no ligand-exchange of the free Lewis acid catalyst $[\mathbf{IV}]^+$ with one or two pyridine molecules was observed. This suggests that pyridine does not hinder the gold attachment to the actual substrate by occupation of the gold's ligand sphere and is thus at least as suitable as triethylamine for further experiments.

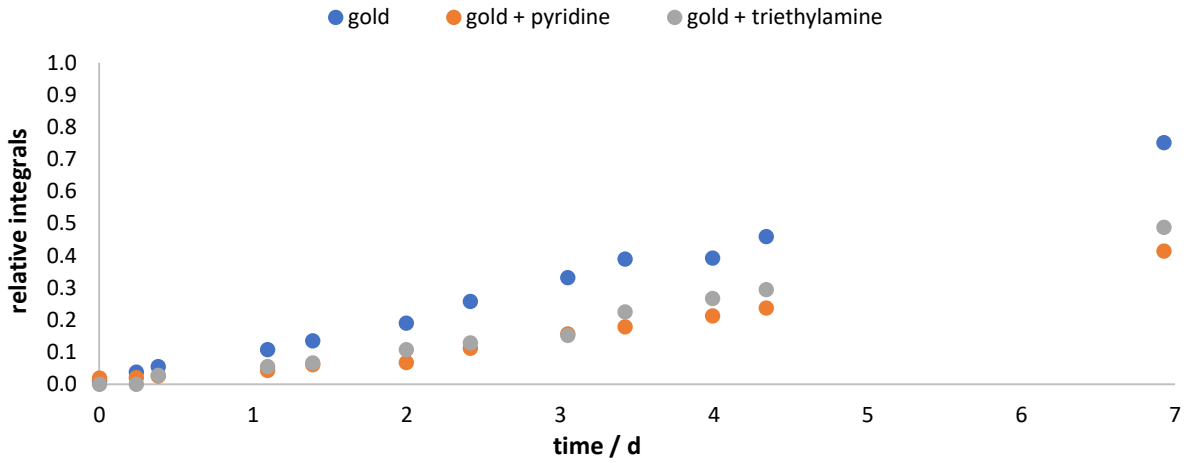

Figure 3.26. Base exchange experiments (reaction 3.24-3.26). Integrals of cyclization product $\mathbf{6_A}$ standardized to the sum of all integrals obtained by GC-MS measurements with GC-MS instrument (a) (chapter 7.2.4) as function of time during the reaction of acyclic product $\mathbf{4_A}$ with solely gold present, with pyridine as base catalyst and with triethylamine as base catalyst over one week.

GC-MS monitoring shown in figure 3.26 revealed that the conversions of all three reactions were very low and extremely slow compared to the usual setup (figure 3.23). Even after hours, the amounts of cyclization product $\mathbf{6_A}$ were barely detectable. Note that the small differences in the rate of reaction 3.25 (pyridine) and 3.26 (triethylamine) were not expected. Since the setups chosen for the GC-MS experiments were very small (0.25 mmol starting material), it was not always technically facile to prepare the reaction solutions in the exact same concentration concerning substrate, catalyst and additives. Nevertheless, both reactions were prepared very cautiously to reduce deviations to a minimum.

These experiments prove that catalyst **3** cannot be exchanged easily without significantly slowing down the reaction. Additionally, they indicate attachment of the secondary amine to the substrates during the cyclization process. As a consequence, pathway (**B**) emerges as a slow side-pathway of the actual cyclization. The accumulation of the highly transient gold species $[\mathbf{B_A}]^+$ observed during the ESI-MS measurements (figure 3.24) also proves that this side-pathway is additionally decelerated by the substitutional bases, although they enabled a glance at the extremely transient species $[\mathbf{X_A}]^+$ that could not be detected before.

3.7 Acid and base influence

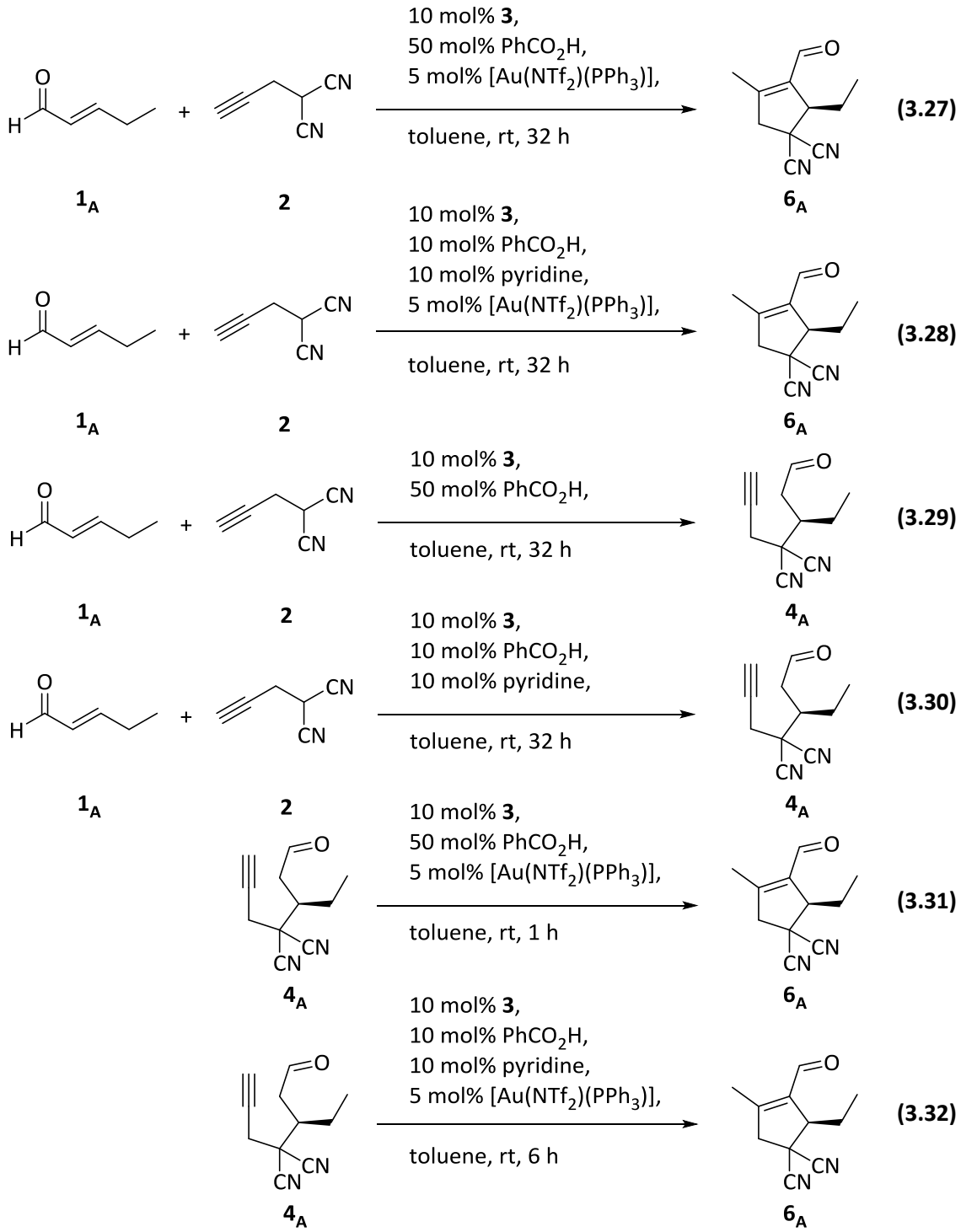

Scheme 3.17. Reactions of the acid and base experiments for the overall reaction, the Michael addition and the cyclization step measured *via* ESI-MS and GC-MS.

Having all these details collected, the role of the benzoic acid was left to be revealed. Therefore, various GC-MS experiments were performed with the overall reaction as well as with the two reaction steps separately. Three setups, which differ in acidity, were used for every part. The 'normal' setups were prepared as suggested by the group of *Jørgensen*,[224] containing 10 mol% of benzoic acid. To the 'base' reactions 10 mol% of pyridine was added, while for the 'acid' setups the amount of benzoic acid was increased to 50 mol%.

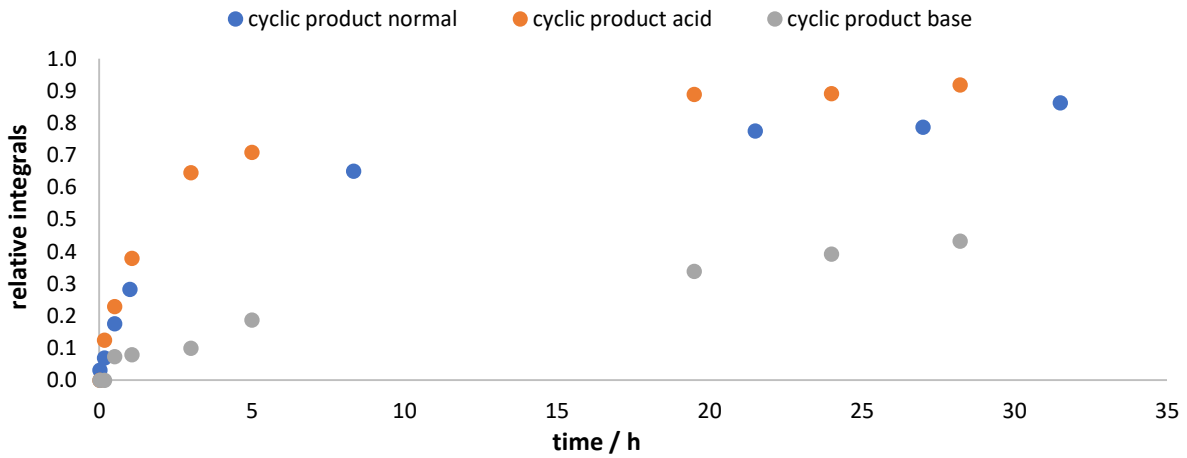

Figure 3.27. Overall reactions (reaction 3.14, 3.27, 3.28) – cyclic products. Integrals of cyclization product $\mathbf{6_A}$ standardized to the sum of all integrals obtained by GC-MS measurements recorded with GC-MS instrument (b) (chapter 7.2.4) as function of time during the normal, acid and base overall reaction of *trans*-2-pentenal $\mathbf{1_A}$ with alkyne **2** over 36 hours.

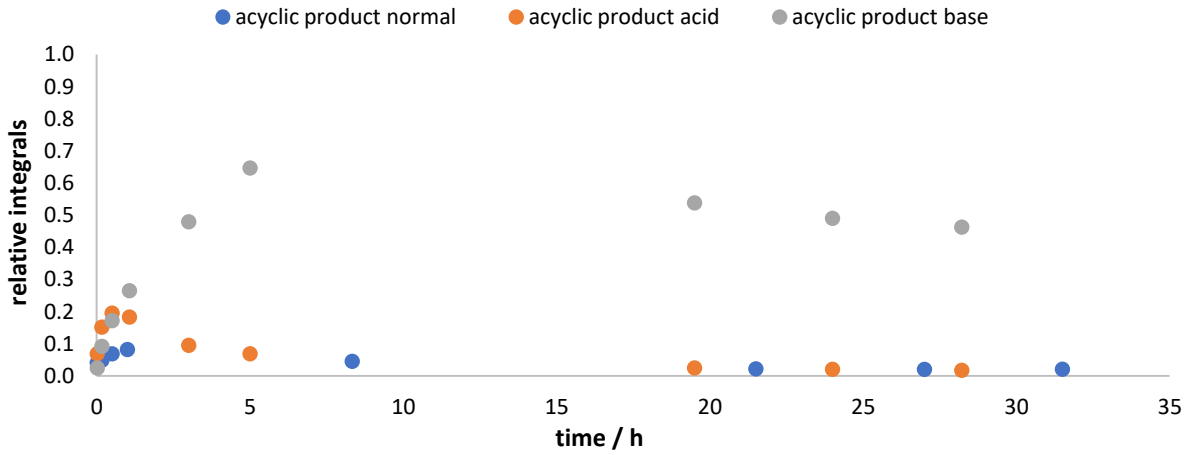

Figure 3.28. Overall reactions (reaction 3.14, 3.27, 3.28) – acyclic products (first step). Integrals of Michael product $\mathbf{4_A}$ standardized to the sum of all integrals obtained by GC-MS measurements recorded with GC-MS instrument (b) (chapter 7.2.4) as function of time during the normal, acid and base overall reaction of *trans*-2-pentenal $\mathbf{1_A}$ with alkyne **2** over 36 hours.

In figure 3.27 all three setups of the overall reaction (reaction 3.14, 3.27 and 3.28) are compared concerning the formation of the cyclic product $\mathbf{6_A}$. It is conspicuous that the larger amount of acid promotes the reaction to cyclization product $\mathbf{6_A}$, while the addition of base causes a slower product formation. Interestingly, the influence of acid and base becomes even more visible, regarding the temporal evolution of the acyclic Michael product $\mathbf{4_A}$. The normal and the acid reaction both show a slight increase of the Michael product $\mathbf{4_A}$ within one hour (figure 3.28). For the base setup, the acyclic product $\mathbf{4_A}$ only reaches its maximum after five hours. Thereby, it reaches a relative integral of 0.65 which is four (normal setup 0.17) and eight times (acid setup 0.08) higher than the maxima of the other two reactions. Additionally, the amount of Michael product $\mathbf{4_A}$ decreases much more slowly compared to the normal and base reactions which show almost no traces of product $\mathbf{4_A}$ after approximately 20 hours. In general, it can be noted that acid promotes the formation of cyclization product $\mathbf{6_A}$, while base hinders its formation, resulting in an accumulation of the acyclic product $\mathbf{4_A}$.

The question that arose after the first acid/base experiments with the overall reaction was how the different setups influence the two reaction steps individually. Therefore, also the normal, base and acid Michael addition (reaction 3.22, 3.29 and 3.30) were monitored separately. Figure 3.29 shows the temporal evolution of the Michael product $\mathbf{4_A}$ for each reaction. While larger amounts of benzoic acid slightly accelerate the reaction, the addition of base decelerates the product formation. Surprisingly, pyridine does not hinder the Michael addition as strongly as it decelerates the overall reaction. Albeit, the Michael addition was revealed to be the rate determining reaction of the two steps.

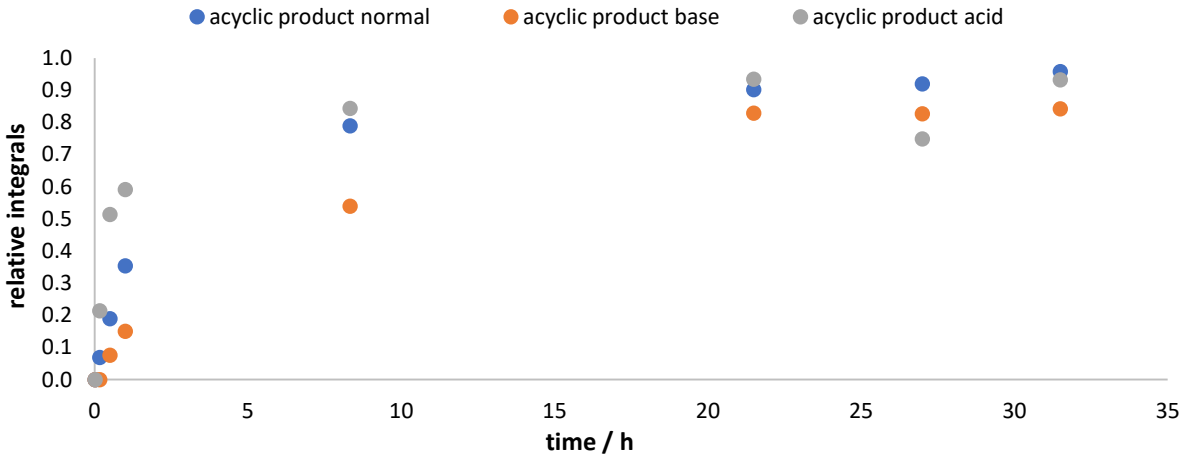

Figure 3.29. Michael additions (reaction 3.22, 3.29, 3.30). Integrals of Michael product $\mathbf{4_A}$ standardized to the sum of all integrals obtained by GC-MS measurements as function of time during the normal, acid and base Michael addition of *trans*-2-pentenal $\mathbf{1_A}$ with alkyne **2** over 36 hours. The normal reaction was recorded with GC-MS instrument (a). The acid and base reactions were recorded with GC-MS instrument (b) (chapter 7.2.4).

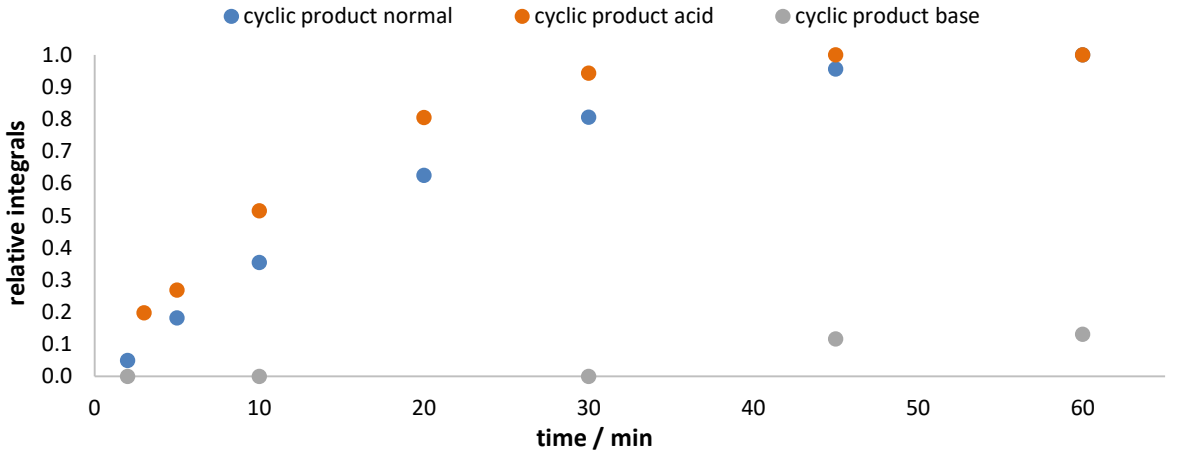

Figure 3.30. Cyclization reactions (reaction 3.23, 3.31, 3.32). Integrals of cyclization product $\mathbf{6_A}$ standardized to the sum of all integrals obtained by GC-MS measurements recorded with GC-MS instrument (a) (chapter 7.2.4) as function of time during the normal, acid and base cyclization of Michael product $\mathbf{4_A}$ over one hour. The first three integrals of the base reaction shown were too small for the device's detection limit.

The previous results of chapter 3.5 (figure 3.23) showed that the Michael addition is much slower than the intramolecular cyclization. Additionally, the overall reaction appears to be significantly stronger hindered by the addition of base than the Michael addition. Further, an accumulation of the Michael product $\mathbf{4_A}$ could be observed for the overall reaction's base setup. This suggests that the influence of acid and base also affects the faster cyclization reaction significantly. To verify this hypothesis, the

normal, base and acid setups were compared for the 5-*exo*-*dig*-cyclization of the isolated Michael product $\mathbf{4_A}$ (reaction 3.23, 3.31 and 3.32). Reaction monitoring with GC-MS over one hour rendered the temporal evolutions presented in figure 3.30. Apparently, an increase of benzoic acid only slightly increases the reaction's rate. Thus, the reaction is terminated within 45 minutes instead of one hour (normal setup). In contrast, the addition of base hinders the cyclization process extremely (appendix, figure 9.9). This confirms the hypothesis that the addition of base does not only decelerate the Michael addition, but also extremely hinders the cyclization process in the following.

By GC-MS reaction monitoring it was shown that benzoic acid plays a determining role for the overall reactions' rate. In general, it can be noted that a higher amount of benzoic acid accelerates the reaction slightly, while the addition of pyridine base hinders the product formation significantly. To obtain a deeper insight into these effects, the two reaction steps were investigated separately. Thereby, it was found that increasing the amount of acid promotes the Michael addition as well as the cyclization step. In contrast, both reactions showed an extremely lowered rate if pyridine was added. Interestingly, the cyclization, typically significantly faster than the prior Michael addition, is more hindered by the addition of base than the first reaction step. Thus, the overall reaction becomes not only significantly slower but also a massive accumulation of the acyclic product $\mathbf{4_A}$ can be noted. Conversely, the increase of the amount of acid diminishes the slight initial accumulation of the acyclic species $\mathbf{4_A}$ compared to the normal setup.

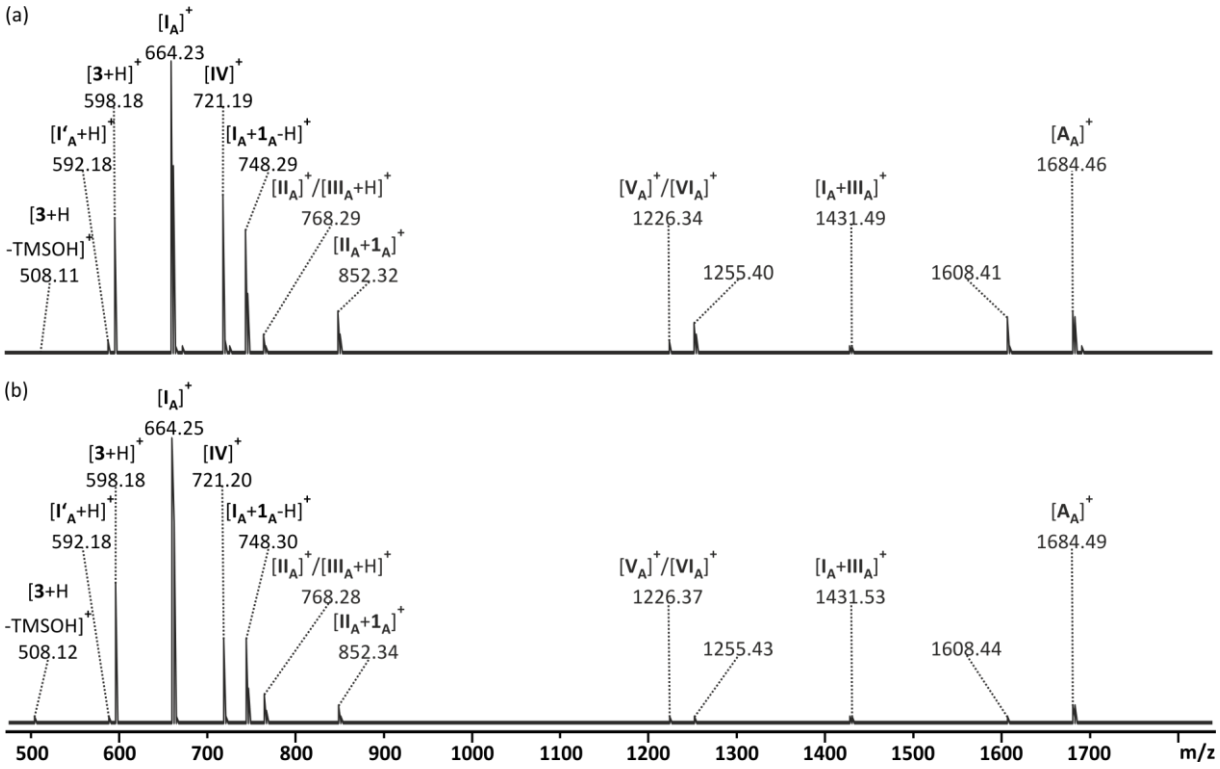

Figure 3.31. ESI(+) mass spectra of the overall reaction's solutions of *trans*-2-pentenal $\mathbf{1_A}$ and alkyne **2** with (a) 50 mol% benzoic acid (reaction 3.27) and (b) 10 mol% pyridine (reaction 3.28) in toluene recorded with Q/TOF mass spectrometer (a) (chapter 7.2.4). The samples were taken after one minute reaction time and diluted 1:100 in acetonitrile.

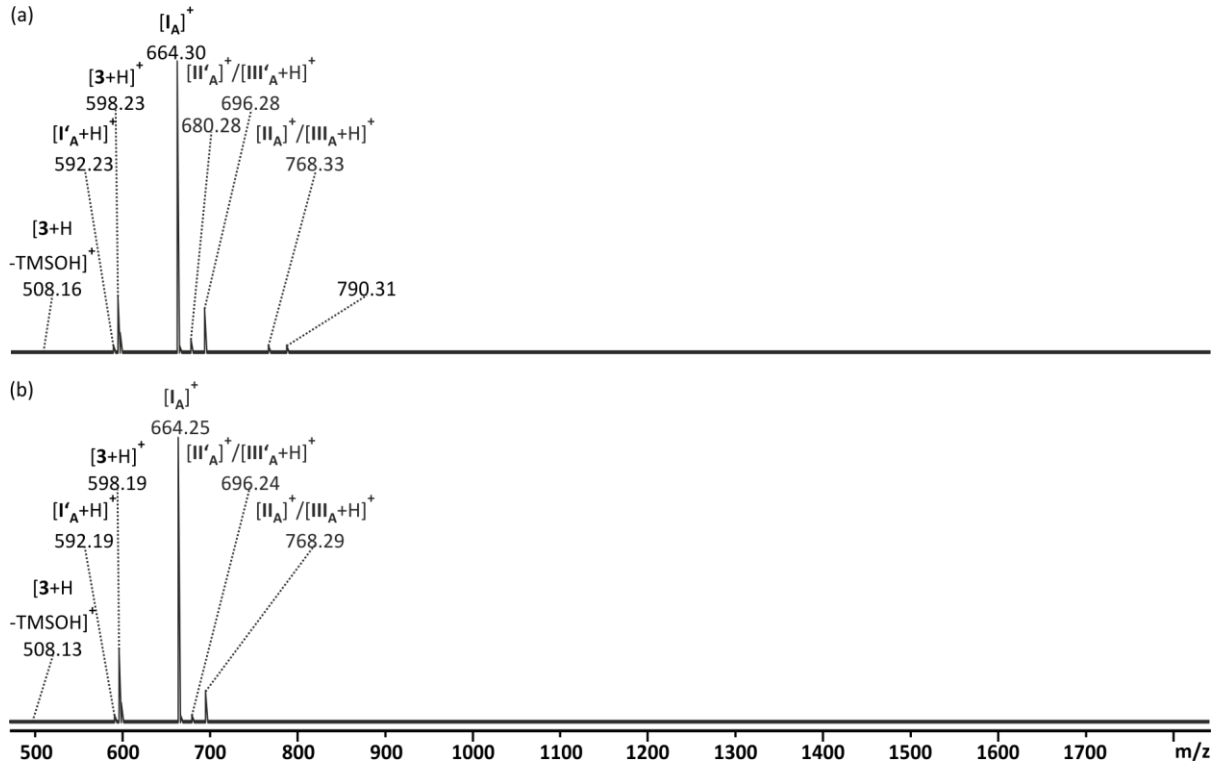

Figure 3.32. ESI(+) mass spectra of the Michael addition's reaction solutions of *trans*-2-pentenal $\mathbf{1_A}$ and alkyne **2** with (a) 50 mol% benzoic acid (reaction 3.29) and (b) 10 mol% pyridine (reaction 3.30) in toluene recorded with Q/TOF mass spectrometer (a) (chapter 7.2.4). The samples were taken after one minute reaction time and diluted 1:100 in acetonitrile.

Additionally, ESI-MS spectra of all base and acid reactions were measured to verify this hypothesis. The spectra of the overall reaction were not affected considerably by the addition of acid and base (figure 3.31). Both spectra show the expected species already found in the normal setup's ESI-MS experiments presented in chapter 3.3 (figure 3.7). Only the off-cycle species $[\mathbf{B_A}]^+$ (*m*/*z* 1105) could not be detected as well as some of the adduct species presented before. $[\mathbf{V_A}]/[\mathbf{VI_A}]^+$ (*m*/*z* 1226), which was uncovered to participate in the actual reaction cycle, could be found as well as the correlated species $[\mathbf{A_A}]^+$ (*m*/*z* 1684). In case of the Michael addition (figure 3.32), no significant deviation from the normal setup presented in figure 3.22 could be observed.

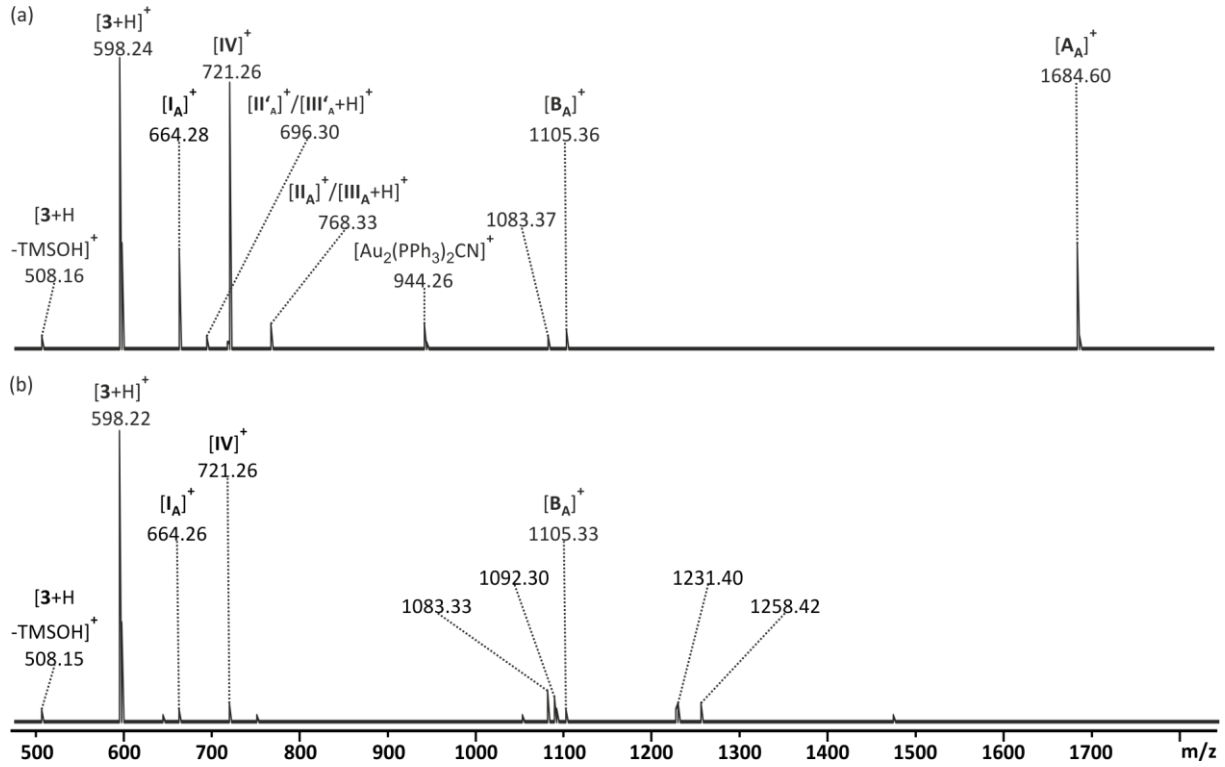

Figure 3.33. ESI(+) mass spectra of the 5-*exo*-*dig*-cyclization's reaction solutions of Michael product $\mathbf{4_A}$ with (a) 50 mol% benzoic acid (reaction 3.31) and (b) 10 mol% pyridine (reaction 3.32) in toluene recorded with Q/TOF mass spectrometer (a) (chapter 7.2.4). The samples were taken after one minute reaction time and diluted 1:100 in acetonitrile.

As for the GC-MS monitoring, it was discovered that the ESI-MS spectra of the cyclization reaction are the most affected by the variation of acid and base. Figure 3.33b shows the ESI(+) spectrum of the base reaction. No species that can be traced back to the actual reaction cycle (**A**) was observed. Only the off-cycle species $[\mathbf{B_A}]^+$ (*m*/*z* 1105) could be found. In contrast, species $[\mathbf{A_A}]^+$ (*m*/*z* 1684) was constantly detectable during the monitoring of the acid reaction (figure 3.33a), indicating that the reaction occurs according to the iminium/enamine cycle (**A**). These findings support the results from the GC-MS monitoring that indicated an insignificant formation of cyclization product $\mathbf{5_A}$ if pyridine was added.

This all leads to the conclusion that in both steps the acid most probably participates in the rate determining step. Since the ESI-MS measurements showed an accumulation of the iminium species $\mathbf{I_A}^+$ in general, it can be assumed that the binding of the alkyne substrate **2** to the iminium species $\mathbf{I_R}^+$ is the rate determining step for the Michael addition. In case of the 5-*exo*-*dig*-cyclization, only the release of the catalysts benefits from a high amount of acid, while the binding of the substrate and the catalysts is expected to be promoted by base. Therefore, the catalysts' release appears to be the cyclization's rate determining step. Since the intermolecular Michael addition is significantly slower than the intramolecular 5-*exo*-*dig*-cyclization, it can be assumed that the overall reaction is determined by the Michael addition's rate determining step.

3.8 Conclusions

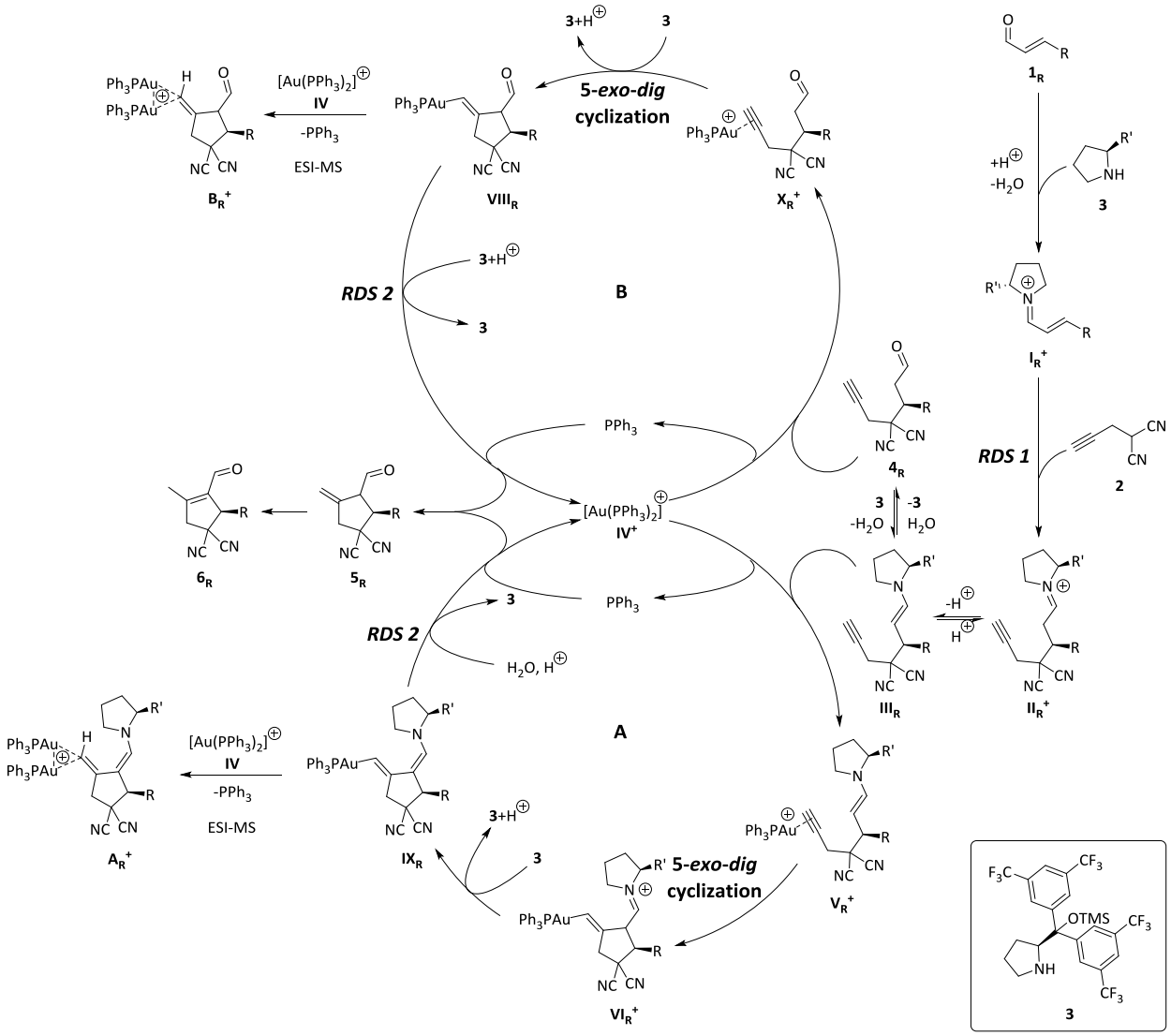

Scheme 3.18. Proposed mechanistic cycles for the dual activation reaction of *α*,*β*-unsaturated aldehydes $\mathbf{1_R}$ with alkyne **2** promoted by Lewis acid and base catalysts correlating to the species detected by ESI-MS. RDS means rate determining step. Catalyst **3** can also be present as **3'** in hydrolyzed form without TMS. In this case the resulting transient species are also without TMS. The species $[\mathbf{II_R}]^+$ and $[\mathbf{III}+H]^+$, $[\mathbf{V_R}]^+$ and $[\mathbf{VI_R}]^+$ and $[\mathbf{IX_R}+H]^+$ as well as the neutral molecules $\mathbf{4_R}$, $\mathbf{5_R}$ and $\mathbf{6_R}$ are isomeric and thus not distinguishable by ESI-MS.

By means of ESI-MS, CID and GC-MS a mechanistic study of a dual activation reaction presented by *Jørgensen* and co-workers[224] was conducted. The reaction is induced by the combination of a Lewis acidic gold(I) catalyst and a basic *L*-proline derivative. All species for the mechanistic cycle (**A**) (scheme 3.18) predicted by the group of *Kirsch*[225] could be detected by ESI-MS. The species were characterized by CID. Thereby, mono- and diaurated species were simultaneously observable. The enamine cycle (**A**) suggested could be complemented, while the species of pathway (**B**) had to be reconsidered (scheme 3.18). Additionally, evidence for (**B**)-type analogs of the coordinative enamine molecule $[\mathbf{V_R}]^+$ have been found. In accordance with the experiments of *Roithová* and co-workers,[43] the diaurated species $[\mathbf{A_R}]^+$ and $[\mathbf{B_R}]^+$ very likely result from the ESI process and are present as monoaurated molecules in the reaction solution. Since a smaller triphenylphosphine ligand was used in this studies, *gem*-diaurated species are most probably detected in the ESI-MS spectra as suggested by *Lu et al.*[49] The active gold(I) catalyst in solution $\mathbf{IV}^+$, proved to be $Au(PPh_3)_2^+$. In order to participate within the

mechanistic cycle of scheme 3.18, this catalyst undergoes a ligand exchange. Thereby, one substrate coordinates to the gold(I) center while one PPh_3 ligand is cleaved off.

In general, the reaction consists of two steps: First a Michael addition and second an intramolecular 5-*exo*-*dig*-cyclization. By exchange of the base from catalyst **3** to pyridine or triethylamine in the second step, it could be revealed that the suggested mechanistic cycle (**B**) is only a side-pathway since covalent binding of the *L*-proline derivative proved to be required. Deprotoauration at the primary alkyne during the reaction was ruled out by the results of the isotopic labeling experiments.

$[\mathbf{V_R}]^+$ and $[\mathbf{VI_R}]^+$ are isomeric transient species that could not be distinguished *via* CID. Therefore, it cannot be specified if only one of the two molecules or both species were detected simultaneously. Since the intramolecular 5-*exo*-*dig*-cyclization proved to be very fast, it can be assumed that the detected molecules are rather of cyclic (*post*-cyclization) character than of acyclic (*pre*-cyclization).

By means of GC-MS it was possible to monitor the reaction's progress. As expected, the Michael addition proved to be the rate determining of the two steps. It is limited by the addition of alkyne **2** to the iminium species $\mathbf{I_R}^+$. Variation of the amounts of benzoic acid as well as the addition of pyridine as base showed that the overall reaction as well as the two individual reaction steps are slightly acid catalyzed and extremely base hindered. These experiments also revealed that the rate determining step of the fast 5-*exo*-*dig*-cyclization is the release of the catalyst. Thereby, the question arose which catalytic unit is cleaved off first. This cannot be determined with the methods used for this study. A cleavage of the base catalyst from $\mathbf{IX_R}$ leads to molecule $\mathbf{VII_R}$, while the release of the Lewis acid from $\mathbf{IX_R}$ gives a cyclic enamine that possesses the same exact mass as the acyclic iminium $\mathbf{II_R}^+$ if detected by ESI-MS. Thus, the resulting ESI-MS peaks would overlap with other species of the mechanistic cycle.

Additional GC-MS studies with phenyl-substituted alkyne $\mathbf{2_{Ph}}$ proved that the reaction is not limited to primary alkynes. To the best of our knowledge this thesis demonstrated the first synthetic approach to the phenyl-substituted Michael product $\mathbf{4_{R,Ph}}$ as well as the cyclic product $\mathbf{5_{R,Ph(\mathit{E})}}$ and isomerization product $\mathbf{6_{R,Ph}}$. Further, the results of the GC-MS monitoring demonstrate that the shorter reaction times *Jørgensen* and co-workers[224] suggested for the aliphatic aldehydes, cannot be applied in general. This has to be optimized for each reaction individually. In case of the phenyl alkyne $\mathbf{2_{Ph}}$, the variation of the reaction time would allow isolation of either both cyclic isomers ($\mathbf{5_{R,Ph(\mathit{E})}}$ and $\mathbf{6_{R,Ph}}$) or solely the cyclopentene isomer $\mathbf{6_{R,Ph}}$ (at least in case of doubled amount of reagents – figure 3.21). This is especially remarkable since the spontaneous isomerization of the vinyl-type isomers $\mathbf{5_R}$ is usually electronically favored and thus extremely fast. Therefore, isolation of these species is typically not possible.

4 Synthetic approach towards an *L*-proline-coupled NHC-gold(I) complex

4.1 Introduction

The investigations on the dual activation reaction of *Jørgensen* and co-workers[224] inspired another project. Instead of two separated catalytic units, the idea of one *L*-proline derived ligand for a monoligated gold(I) catalyst came to mind. Thus, the concept of dual activation would be transferred to a bifunctional catalyst.[98,99,105] As shown in chapter 3, both catalysts are required for the 5-*exo*-*dig*-cyclization reaction. As a consequence, an adjusted design of one catalyst activating both electrophile and nucleophile could possibly enhance the reaction, bringing both catalytic units in close proximity. While the secondary amine could be obtained from *L*-proline, the other part of the molecule was planned to connect to a gold(I) cation and therefore required different properties. Since the final catalyst needed to possess an open binding side, the ligand attachment to the gold(I) cation had to be controlled. With their abilities as *σ*-donors,[53–57] *N*-heterocyclic carbenes appeared to be a reasonable ligand class.

In the following, the synthetic approach towards an *L*-proline-coupled NHC-gold(I) complex is presented and discussed in detail. The complete synthetic sequence is not fully finished so far. Progress and backlash blend most of the time. A conscious decision was made to mention all preparative details within the discussion in order to support future synthetic attempts of other scientists and minimize preventable detours. The approach of an ether bridge with an alkyl chain connecting both units emerged as a reasonable strategy (scheme 4.13). Thereby, the alkyl chain's flexibility promised to enable the required favorable alignment of both catalytic moieties. Unfortunately, the challenging separation of product and side products proved to be major problem as soon as both units were connected. Thus, the subsequent reaction steps were performed with the crude products. Additionally, the connecting S_N2 reaction itself emerged as another problem. The conversion and exact amount of product could not be determined. However, the results of the subsequent deprotection and mesylation as well as the analytic monitoring suggest that this step acts like a bottleneck for the whole reaction sequence. Although this type of reaction had already been applied in a prior synthetic approach of this working group,[86] a slight deviation from the original procedure might have affected the outcome severely. In the original approach, the leaving group was installed at the *L*-proline unit. In contrast, the reaction presented in this thesis used a protected *L*-proline as nucleophile. In doing so, a separation step could be simplified. Nevertheless, the original approach has to be tested in future experiments.

4.2 First synthetic ideas

A simple way to connect an NHC and *L*-proline moiety directly is an ester bridge (figure 4.1).[233] This can be achieved with only a few synthetic steps. Starting from Boc-Hyp-OH (Boc-*L*-hydroxyproline), the required hydroxy group is already installed at the five-membered ring. Further protection of the amine with a Boc (*tert*-butyloxycarbonyl) group was not expected to be a challenge.[86] On the other side of the

molecule a carboxyl function with a linker unit was supposed to be easily connected to an NHC unit by a simple S_N2 reaction.[234–236] This approach was discarded however since comparable S_N2 reactions already proved to be strongly impeded by steric hindrance. Thus, a direct connection was excluded, and a simple alkyl chain was chosen as linker unit in between both fragments.

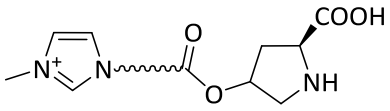

Figure 4.1. NHC and *L*-proline connected by an ester bridge.

The idea was to use a *tert*-butyl ester as protecting group for the proline's carboxylic acid and a Boc protection of the secondary amine. These two protecting groups would allow a global deprotection in the end of the synthetic sequence and they are well established in the syntheses of charge-tagged *L*-proline catalysts that were performed in this working group.[86,237,238] An acidic deprotection also leads to cleavage of the ester bridge. Therefore, another linker between the two moieties had to be found.

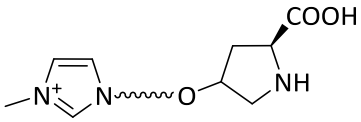

Figure 4.2. NHC and *L*-proline connected by an ether bridge.

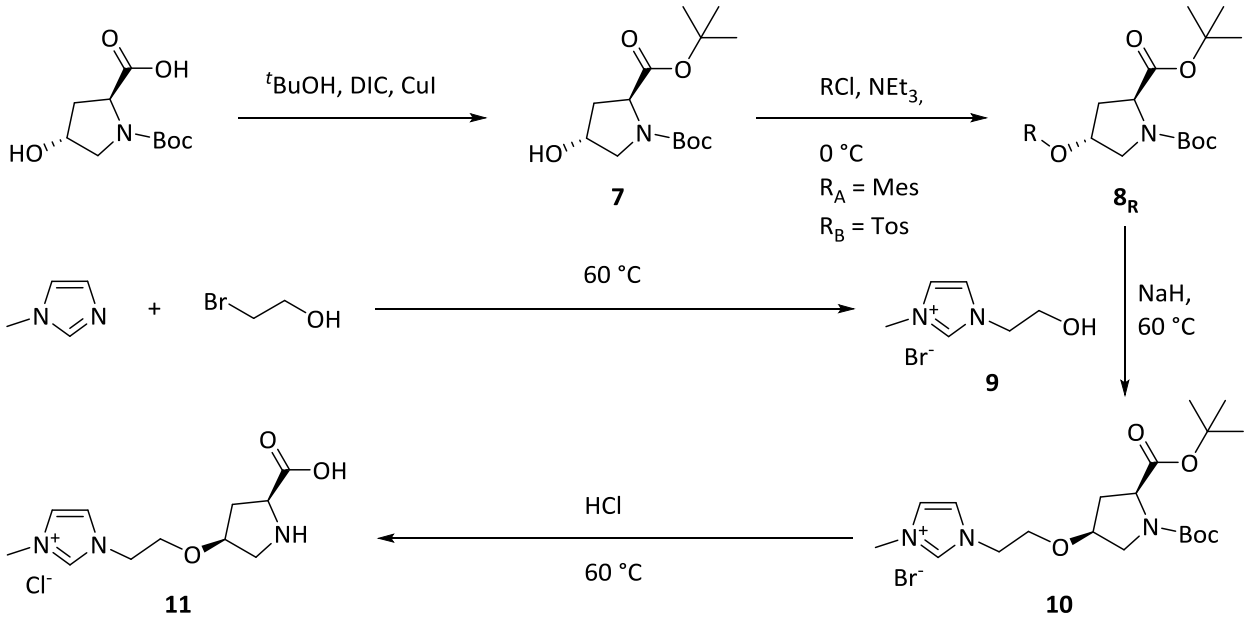

Scheme 4.1. Synthetic plan for an NHC-proline ligand connected imidazolium precursor **11** with C_2 chain as linker.

In contrast to esters, ethers cannot be cleaved that easily under acidic conditions.[239] Thus, an ether bridge had to be installed that was supposed to be stable towards the acidic conditions of the final global deprotection (figure 4.2). Thereby, the shortest reasonable chain length of the aliphatic linker unit is C_2 (ethyl). Boc-Hyp-OH was again chosen as starting material (scheme 4.1). The protection of the secondary amine and the following mesylation and tosylation of the secondary hydroxy group were planned according to the previous work on charge-tagged *L*-proline catalysts conducted in this working group.[86,237,238,240] The second fragment of the molecule was expected to be formed by methyl imidazole (MeIm) and 2-bromoethanol. Previous studies of this working group showed that bromide is a very well suitable leaving group for this type of reaction.[234] During the S_N2 reaction, the mesylate (^{t}Bu-Boc-Hyp-OMes **8_A**) or tosylate (^{t}Bu-Boc-Hyp-OTos **8_B**) was planned to act as a leaving group inverting the

configuration of the side chain. Afterwards, the global deprotection with hydrochloric acid was supposed to give the actual NHC-proline ligand **11** as chloride salt.

4.3 First synthetic approach

Starting with the *L*-proline derivative Boc-Hyp-OH, the first step proved to be more challenging than expected. The esterification was prepared according to *Chabaud et al.*[241] They suggested preparing two individual suspensions: One with the metal catalyst, the carbodiimide and alcohol to perform the alkoxide, the other to dissolve the substrate. Unfortunately, the resulting suspensions could not be transferred completely under inert gas conditions. All transfer tubes (up to a diameter of 2 mm) were blocked by the suspension's solid. Consequently, the transfer was mainly possible for the molecules in solution. Thus, the indissoluble part was lost for the subsequent reaction.

To prevent this loss of starting material, the esterification was performed as one-pot reaction. The first suspension was prepared as before. Then, half of the solvent was added as originally proposed. Afterwards, the substrate was filled in as soon as the solid and the remaining solvent were added. The suspension did not transform into a clear solution. Nevertheless, most of the partially insoluble Boc-Hyp-OH was converted with this protocol. According to the original suggestion, most of the urea side product was filtered off and ^{t}Bu-Boc-Hyp-OH **7** was obtained after column chromatography with a quantitative yield as colorless solid.

This reaction proved to be strongly temperature-dependent. According to the literature, it was performed at room temperature. Depending on the season, the conditions in the lab varied significantly (16-18 °C during winter and 25-32 °C during summer). It was observed that the reaction is more effective in winter time (quantitative) than in summer time (15%). This variation might be caused by the vapor pressure of the volatile solvent dichloromethane. The effect would diminish if the reaction flask was cooled with water (18-22 °C) during summer (67%). In case of lower yields, it was always possible to detect the substrate on TLCs and recover some of it from the column. As a consequence, it can be assumed that the moderate solubility of the substrate is a hint for a comparable moderate solubility of the mesylation product. Thus, the precipitation of the product might be a notable driving force for the whole reaction. This effect might be disturbed if the solubility increases at higher reaction temperatures. Note that for the reaction's work-up the hardly soluble urea side product has to be filtered off. By washing with cooled dichloromethane, most of the solid product that precipitates from the reaction solution is obtained. As the experiments prove, the loss of product by this procedure is insignificant.

The mesylation of the protected *L*-proline derivative ^{t}Bu-Boc-Hyp-OH **7** was performed according the literature.[86] Mesylate ^{t}Bu-Boc-Hyp-OMes $\mathbf{8_A}$ could be obtained with 99% yield as colorless solid. The tosylated proline derivative ^{t}Bu-Boc-Hyp-OTos $\mathbf{8_B}$ was additionally prepared with an analogous method according to *Hack et al.*[242] with a yield of 93%. With this alternative, the challenging S_N2 reaction could be tested with two different substrates.

The preparation of the second fragment was conducted based on the previous work of *Kobialka*[234,236] and *Krause*[234,235] of this working group. After stirring the two liquids for six days the remaining substrates were removed under vacuum at 60 °C. A further recrystallization or column chromatography was not required. Imidazolium **9** (MeIm-C_2-OH) was obtained as colorless solid with 95% yield.

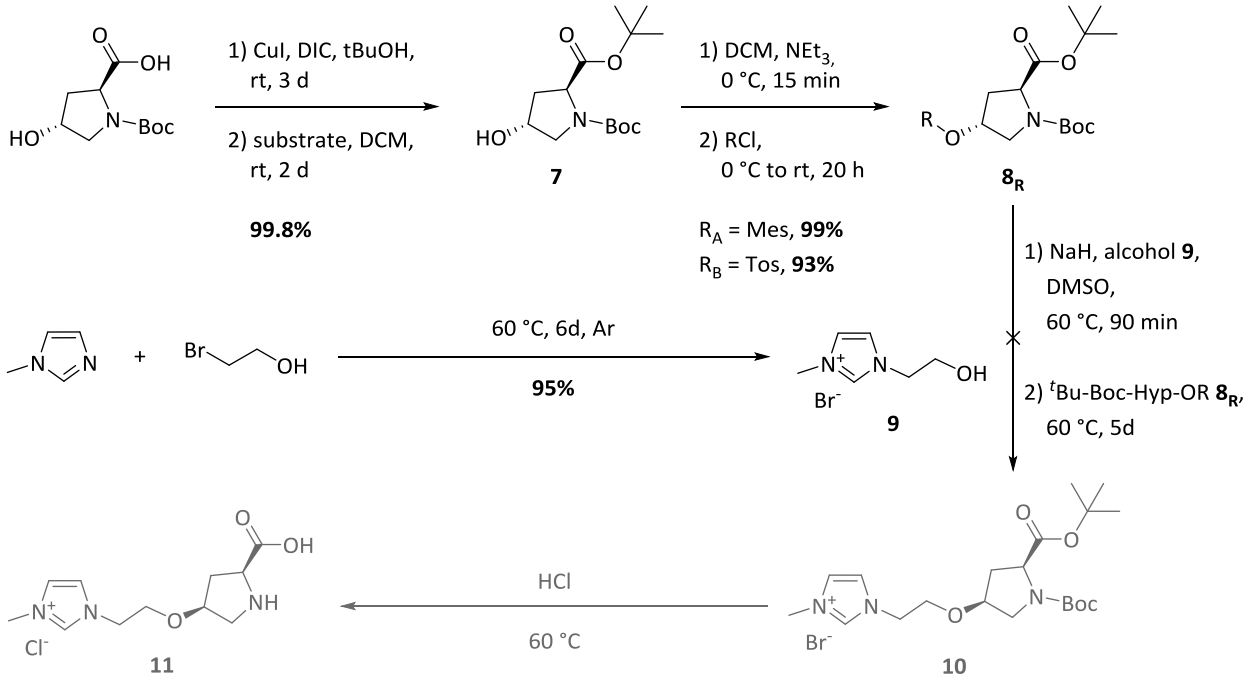

Scheme 4.2. Conducted synthesis of NCH-proline ligand imidazolium precursor with C_2 chain linker.

Unfortunately, the subsequent S_N2 reaction was not successful. The studies on charge-tagged catalysts of this working group had proven that sodium hydride is a suitable base in combination with DMSO (dimethyl sulfoxide) as polar solvent.[86,237,238,240] Previous reactions had shown that sodium hydride was even more effective if used in mineral oil (60 wt%). Like this, the sensitivity against water especially during longer storage is minimized. With all this information in hand, the S_N2 reaction to connect the two fragments appeared promising. Irrespective of the leaving group however, it was observed *via* TLC that a high amount of proline substrate **8$_R$** was not converted. In case of ^{t}Bu-Boc-Hyp-OMes **8$_A$**, the imidazolium substrate MeIm-C_2-OH **9** could also be found. Furthermore, no product could be detected by means of ESI-MS, although the cationic imidazolium product **10** would be easily detectable under these conditions. This led to the conclusion that a new approach had to be found.

4.4 Further synthetic ideas and new synthetic strategy

Since the S_N2 reaction appeared to be the crux of the whole synthesis, new conditions, nucleophiles or leaving groups that enforce this reaction had to be tested. First, the reaction conditions were scrutinized. Therefore, 1-buthanol and 1-octanol were used as test alcohols which were supposed to mimic the linker (scheme 4.3). These nucleophiles were activated with sodium hydride or triethylamine (TEA) in DMSO and NMP (*N*-Methyl-2-pyrrolidon), which proved to facilitate a similar S_N2 reaction conducted before.[240] After five days at 60 °C, only for the setups with the original conditions (NaH and DMSO) the individual product could be detected by ESI-MS (appendix, figure 9.10 and 9.11). The exact conversion was not determined since these test reactions were not worked-up, but only quenched.

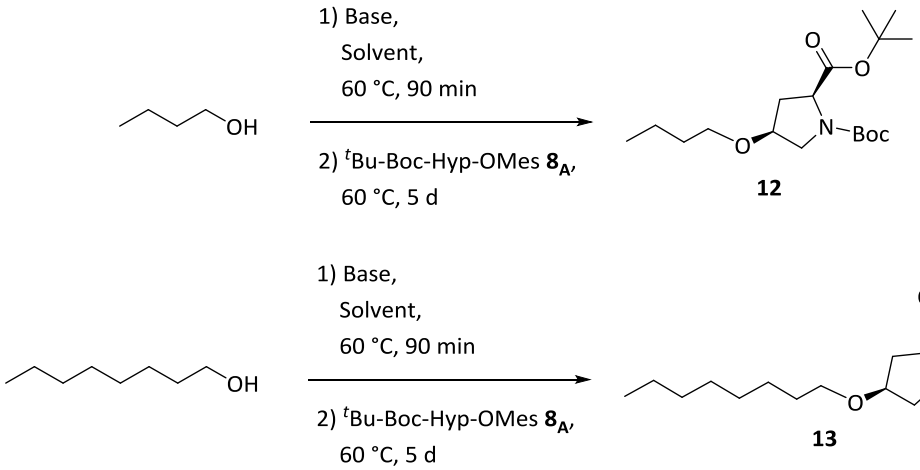

Scheme 4.3. S_N2 test reaction with 1-butanol (top) and 1-octanol (bottom) and ^{t}Bu-Boc-Hyp-OMes $\mathbf{8_A}$ under different reaction conditions. As base NaH or TEA were chosen. The solvents were DMSO or NMP.

As second putative problem, the steric hindrance might be too high in case of a rather short C_2 chain linker. To eliminate this problem, a C_4 chain (butyl) was chosen for further synthetic plans. A single *tert*-butyldimethylsilyl-protected 1,2-butanol (TBSO-C_4-OH) appeared suitable as linker (scheme 4.4). It was tested directly on the mesylated proline ^{t}Bu-Boc-Hyp-OMes $\mathbf{8_A}$ under the usual conditions. Although ESI-MS and APCI-MS showed traces of the product **14**, the TLC showed a vast number of spots. Unfortunately, a preparative TLC did not render the final product. Apparently, some side reactions would take place under these conditions. Thus, a better leaving group might be helpful.

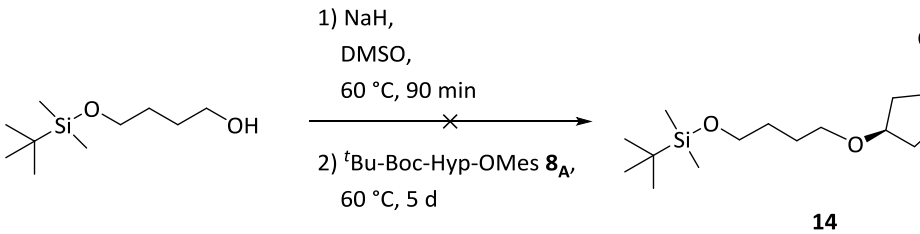

Scheme 4.4. S_N2 test reaction with TBSO-C_4-OH and ^{t}Bu-Boc-Hyp-OMes $\mathbf{8_A}$ analogous to *Willms et al.*[86]

Since work-up of ionic compounds can be challenging in case of column chromatography, it was planned to install the NHC after the demanding S_N2 reaction. For this purpose, the linker's second (protected) alcohol needed to be transferred into a leaving group. As the mesylation could be performed with high yields before (scheme 4.2), this leaving group was also tested for the imidazolium salt formation. 1-Butanol was again chosen as test molecule. During the mesylation according to *Chu et al.*,[243] imidazolium **16** was formed with quantitative yield (scheme 4.5). Monitoring with ^{1}H NMR spectroscopy proved that the reaction is even more efficient than expected and can be stopped after only four days. As a result, mesylate appeared to be a better leaving group than bromide in case of the NHC formation.

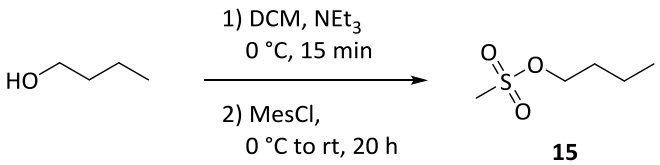

(4.4)

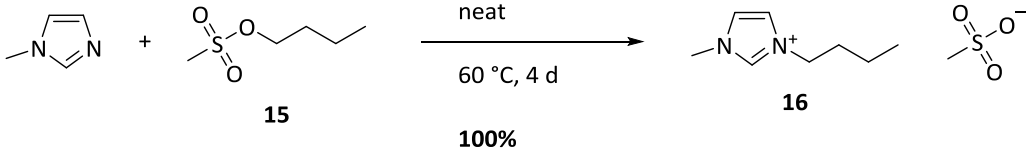

(4.5)

Scheme 4.5. Mesylation of 1-butanol (top) according to *Chu et al.*[243] and test reaction of 1-Bu-OMes **15** and MeIm (bottom).

With this information in hand, the S_N2 reaction of the linker and the proline unit was still to be mastered. There were two possible adjustments: First, a better leaving group was needed and second, proline derivative ^{t}Bu-Boc-Hyp-OH **7** could be used as nucleophile. Thus, bromide was chosen as new leaving group of the linker. The idea was to use a singly brominated aliphatic dialcohol. After protection of the hydroxy function, the substitution reaction could take place. Then, the protected alcohol was expected to be transferred into a mesylate and react with the respective imidazole. That consideration led to test reaction 4.6 shown in scheme 4.6. Unfortunately, no product could be found on the TLC even after seven days.

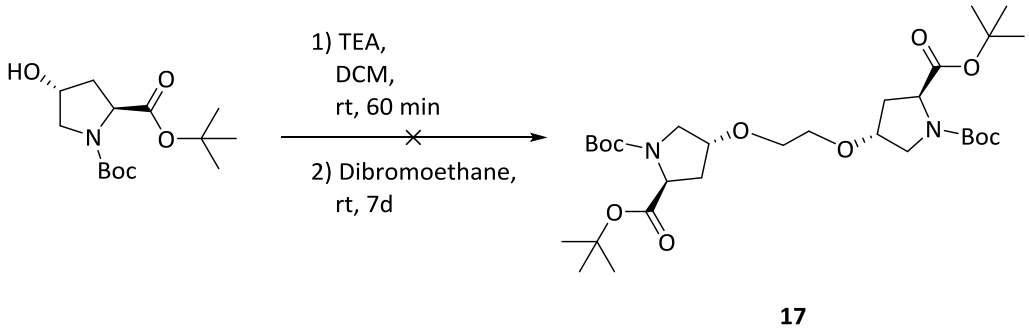

(4.6)

Scheme 4.6. Test reaction of 1,2-dibromoethane and ^{t}Bu-Boc-Hyp-OH.[86,244]

As a consequence, the leaving group's reactivity had to be further increased. Iodine was tested in the next approach. Again, TBSO-C_4-OH was used as starting material (scheme 4.7). In 2018, *Forni et al.*[245] presented a simple iodination of this molecule with excellent yield. The reaction can be performed within one day including work-up. It is particularly efficient since the liquid product does not require purification by column chromatography. A simple filtration is sufficient, although it was not that easy to wash the pure material completely out of the extremely viscous crude. This might have caused a certain loss of product. Thus, TBSO-C_4-I **18** was obtained with 79% yield as a colorless liquid.

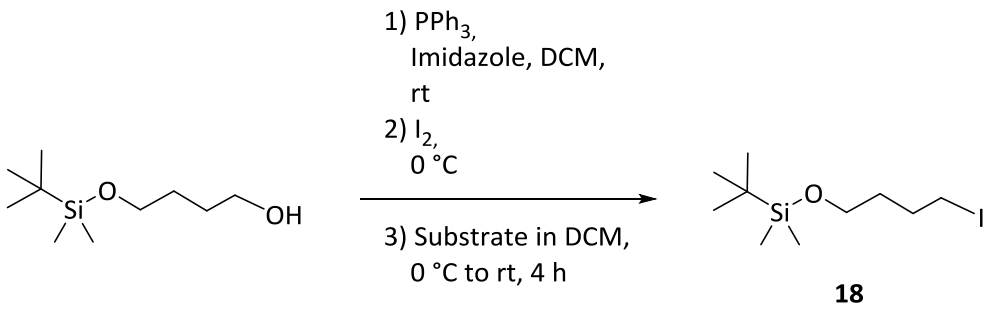

(4.7)

Scheme 4.7. Synthesis of TBSO-C_4-I **18** according to *Forni et al.*[245]

An analogous reaction was tested for ^{t}Bu-Boc-Hyp-OH **7** (scheme 4.8). The same reaction conditions as for the aliphatic silyl ether were applied (reaction 4.7). After stirring the suspension overnight, the TLC showed no traces of the substrate anymore. Instead, a new spot was found suggesting that the reaction was complete. In contrast to the reaction of TBSO-C_4-OH, a solid crude product was obtained that had to be separated by column chromatography. Unfortunately, the purification was not successful so far. As a consequence, this route was postponed. Since the iodine substrate TBSO-C_4-I **18** was already in hands, the sequence with TBSO-C_4-I **18** was investigated first.

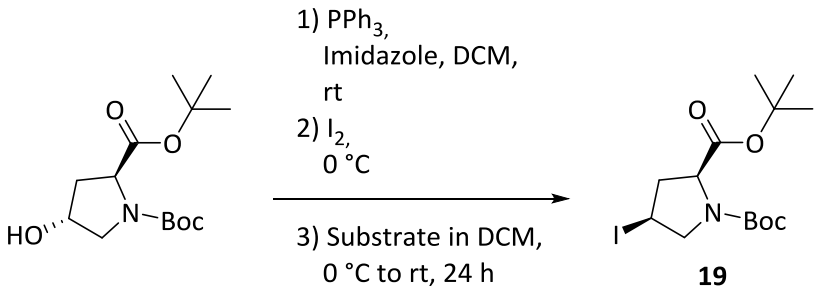

(4.8)

Scheme 4.8. Iodination of ^{t}Bu-Boc-Hyp-OH analogous to *Forni et al.*[245]

The new strategy (scheme 4.9) was planned based on the first approach including the inverted S_N2 reaction with iodine as highly reactive leaving group. Thereafter, the TBS protecting group of **14** was expected to be removed by TBAF (tertra-*n*-butylammonium fluoride), a well-established method in modern total synthesis.[246] This common deprotection had already been performed successfully in presence of Boc groups.[247] Subsequently, the primary alcohol of **20** was supposed to be transferred into a mesylate leaving group, which was expected to react with MeIm to form imidazolium **22**. After the global deprotection, ligand precursor **23** was planned to be used for a complexation with gold(I). It was expected to obtain an open binding side at the gold core by applying the ligand in a 1:1 ratio.

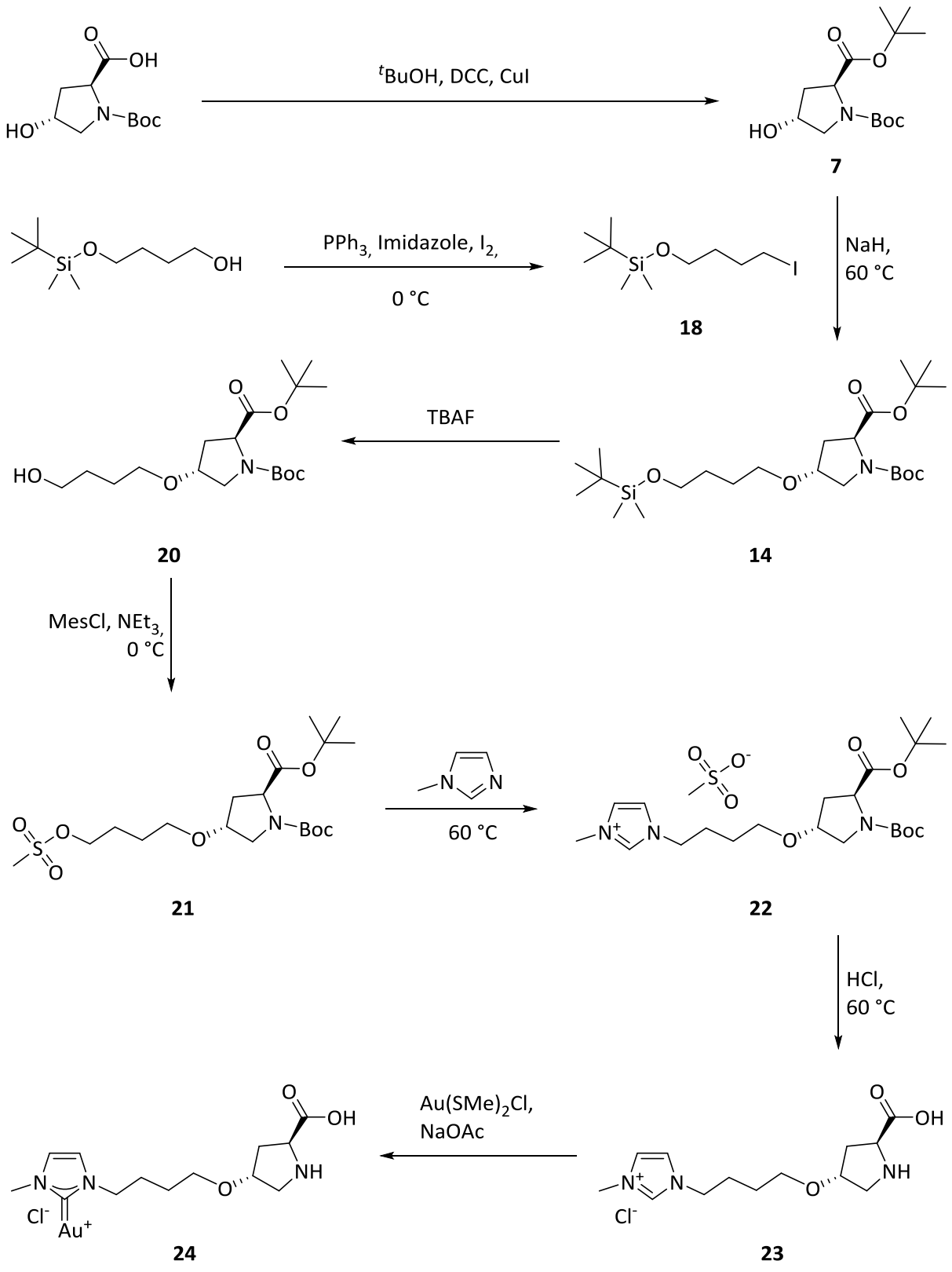

Scheme 4.9. Revised synthetic plan for NCH-proline gold(I) complex with C_4 chain linker.

4.5 Second synthetic approach

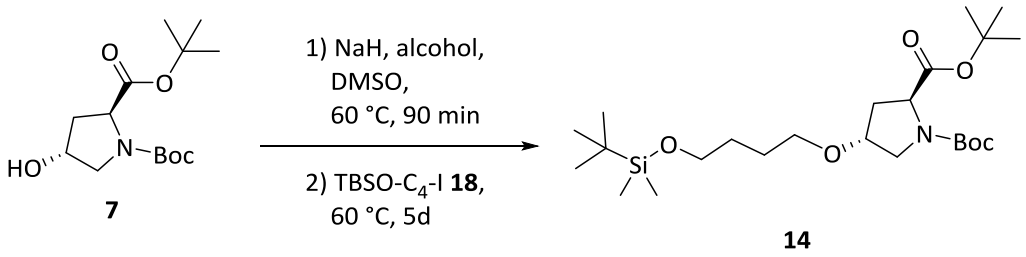

(4.9)

Scheme 4.10. S_N2 reaction with ^{t}Bu-Boc-Hyp-OH **7** and TBSO-C_4-I **18** analogous to *Willms et al.*[86]

The S_N2 step was adopted from the first synthetic approach of chapter 4.3 (scheme 4.2). The resulting ^{t}Bu-Boc-Hyp-OH **7** was activated with sodium hydride in DMSO. Afterwards, the iodine linker (TBSO-C_4-I **18**) was added and after five days, the reaction was quenched. DMSO was removed by distillation and the crude was investigated by ESI-MS. The spectrum is depicted in figure 4.4a and proves that the desired product **14** was formed with a signal for [**14**+Na]$^+$ (*m*/*z* 496). Additionally, the side products **25** and **26** (figure 4.3) with *m*/*z* 440 and with *m*/*z* 626 could be identified. These are caused by a partial cleavage of the ^{t}Bu protecting group (*m*/*z* 440) and a subsequent S_N2 reaction at the free carboxylic acid (*m*/*z* 626). For the free acid **25**, it is also possible that the deprotection takes place during the ESI process. In contrast, the acid's and linker's S_N2 product **26** (*m*/*z* 626) cannot be explained that way. Therefore, it can be assumed that the free acid **25** is also present in solution. A cleavage of the Boc protecting group of the amine was not observed.

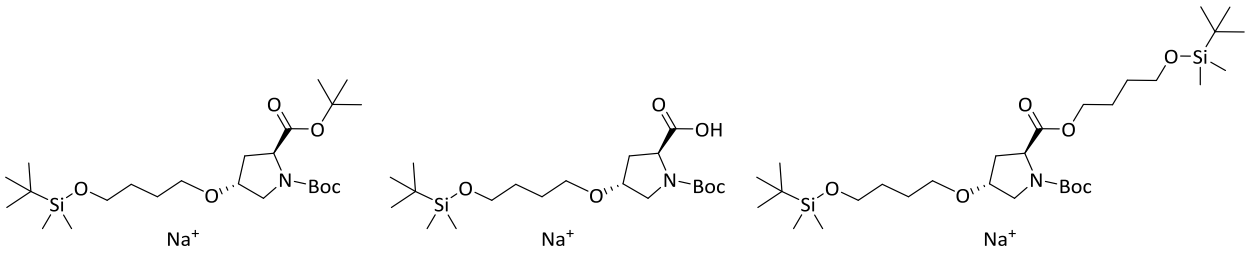

Figure 4.3. Possible species of the S_N2 reaction depicted in scheme 4.10 detected by ESI-MS.

The crude of reaction 4.9 was extracted with dichloromethane. Afterwards, an ESI-MS sample was taken. The spectrum of the combined organic layers looked exactly as the one measured for the crude (figure 4.4b). Since less crude product than expected was obtained, the aqueous phase was also investigated *via* ESI-MS. The spectrum shown in figure 4.4d proves that the product as well as the two side products were not transferred completely during the first extraction. As a consequence, a second extraction with dichloromethane was conducted and the organic and aqueous layers were again analyzed by ESI-MS. In the second combined organic layers (figure 4.4c) mainly the free acid side product **25** (*m*/*z* 440) and only small traces of the product **14** and the double S_N2 side product **26** (*m*/*z* 626) could be found. Additionally, only a barely measureable amount of substance was obtained this time. Furthermore, the spectrum of the second aqueous layer (figure 4.4e) still shows the same pattern of signals as the first aqueous phase, only with decreased base peak (*m*/*z* 440). Thus, only a simple extraction was used for further reactions. Purification by column chromatography did not provide any of the desired substance. Since further purification by column chromatography was planned after the mesylation step, the S_N2 reaction's crude was used for the following synthetic step. The

additional mesylate groups were expected to facilitate a separation due to the increased difference in polarity between all three molecules.

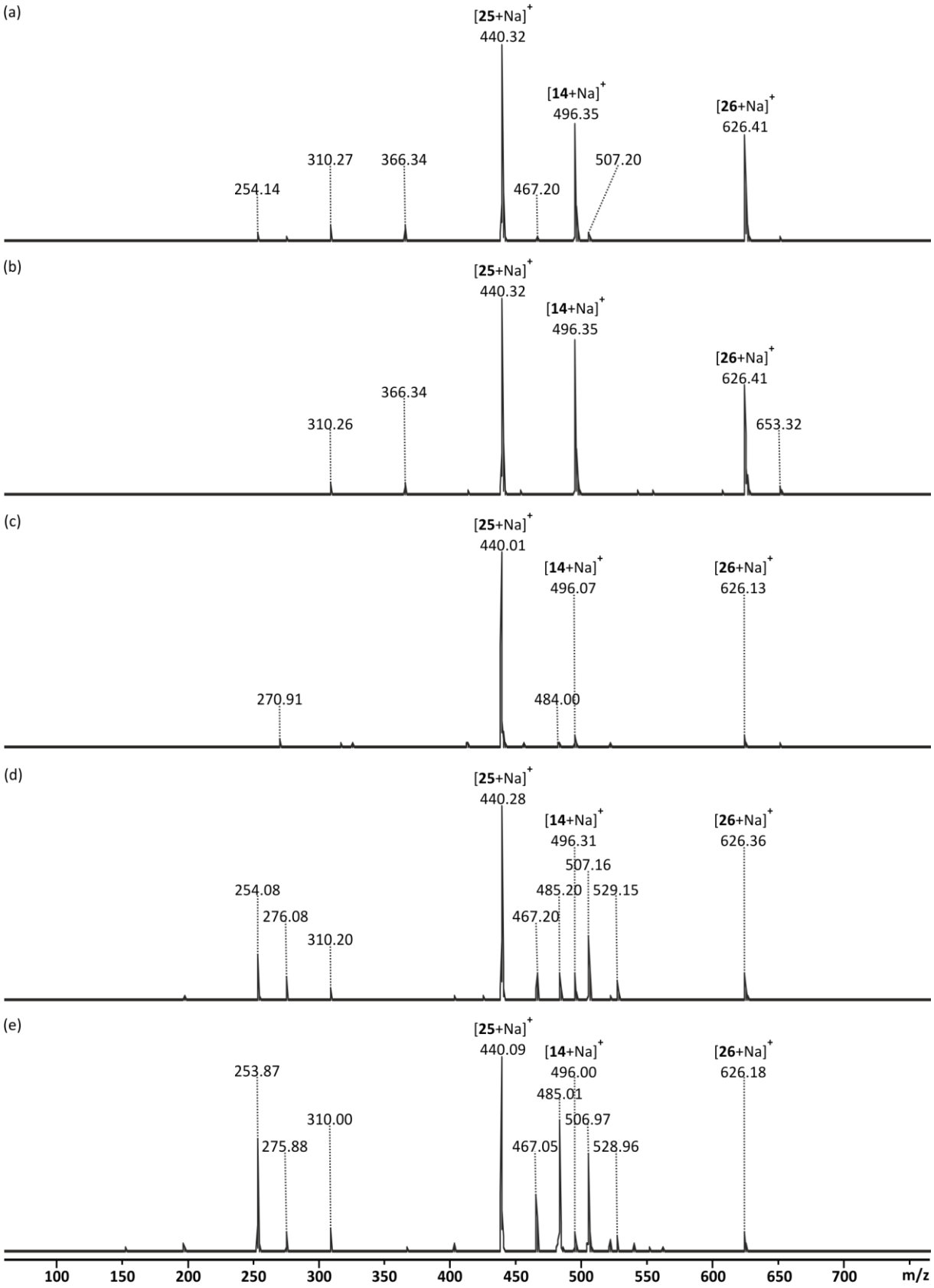

Figure 4.4. ESI(+) mass spectra of the S_N2 reaction 4.9 from acetonitrile recorded with ESI-MS instrument (b) (chapter 7.2.4). (a) ESI(+) mass spectrum of the crude after distillation. (b) ESI(+) mass spectrum of the first combined organic layers. (c) ESI(+) mass spectrum of the second combined organic layers. (d) ESI(+) mass spectrum of the first aqueous layer (e) ESI(+) mass spectrum of the second aqueous layer.

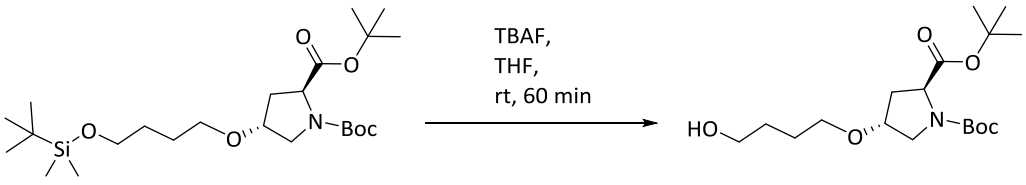

(4.10)

14 **20**

Scheme 4.11. TBAF deprotection of ^{t}Bu-Boc-Hyp-C_4-OTBS **20** analogous to *Jin et al.*[247]

The consecutive TBAF deprotection (reaction 4.10) was conducted according to *Jin et al.*[247] After the reaction was finished, the TBAF salt was removed by extraction with ethyl acetate. The ESI-MS spectrum of the crude is shown in figure 4.6a. Unfortunately, the spectrum is dominated by corresponding $[TBA]^+$ cation with *m*/*z* 242. This behavior does not correlate necessarily with a high concentration of TBAF in solution. Due to the already cationic form, the *tert*-butyl ammonium cation (TBA^+) can be detected easily with ESI-MS and thereby suppresses potential signals of other species (ESI response – chapter 2.4). Therefore, a ^{1}H NMR spectrum was measured (appendix, figure 9.12). Unfortunately, this quantitative method confirmed that a high amount of TBAF contaminated the crude product. Thus, a separation with a very small silica column of only about 2 cm height was tried. The orange crude was applied on dry silica (crude : silica 1 :10). Then, the organic components were washed down with ethyl acetate until the silica was almost colorless (crude : ethyl acetate 1 mg : 0.25 mL). Figure 4.6b shows that additional organic components besides TBA^+ ($[TBA]^+$ = *m*/*z* 242 and $[2TBA+Cl]^+$ = *m*/*z* 519) could be detected after this step. As a result, product **20** was detectable as $[\mathbf{20}+Na]^+$ (*m*/*z* 382) as well as the two deprotected side products of the free acid **27** ($[\mathbf{27}+Na]^+$ = *m*/*z* 326) and the double S_N2 side reaction **28** ($[\mathbf{28}+Na]^+$ = *m*/*z* 398) (figure 4.5). It was not surprising to observe **27** and **28**, since the side products of the previous S_N2 reaction were not removed. In general, no silyl protected alcohols were found neither for the product nor in case of the side products. Since the detectability of both functional groups is not expected to differ significantly in ESI-MS, the deprotection can be assumed to be a quantitative reaction.

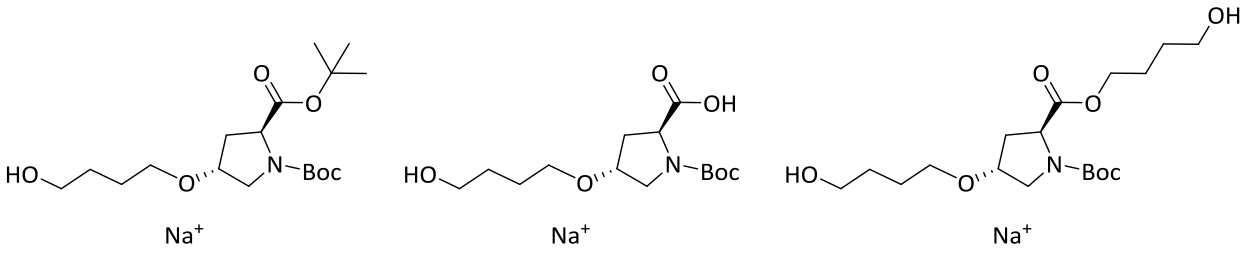

Figure 4.5. Possible species of the deprotection reaction with TBAF depicted in scheme 4.13 detected by ESI-MS.

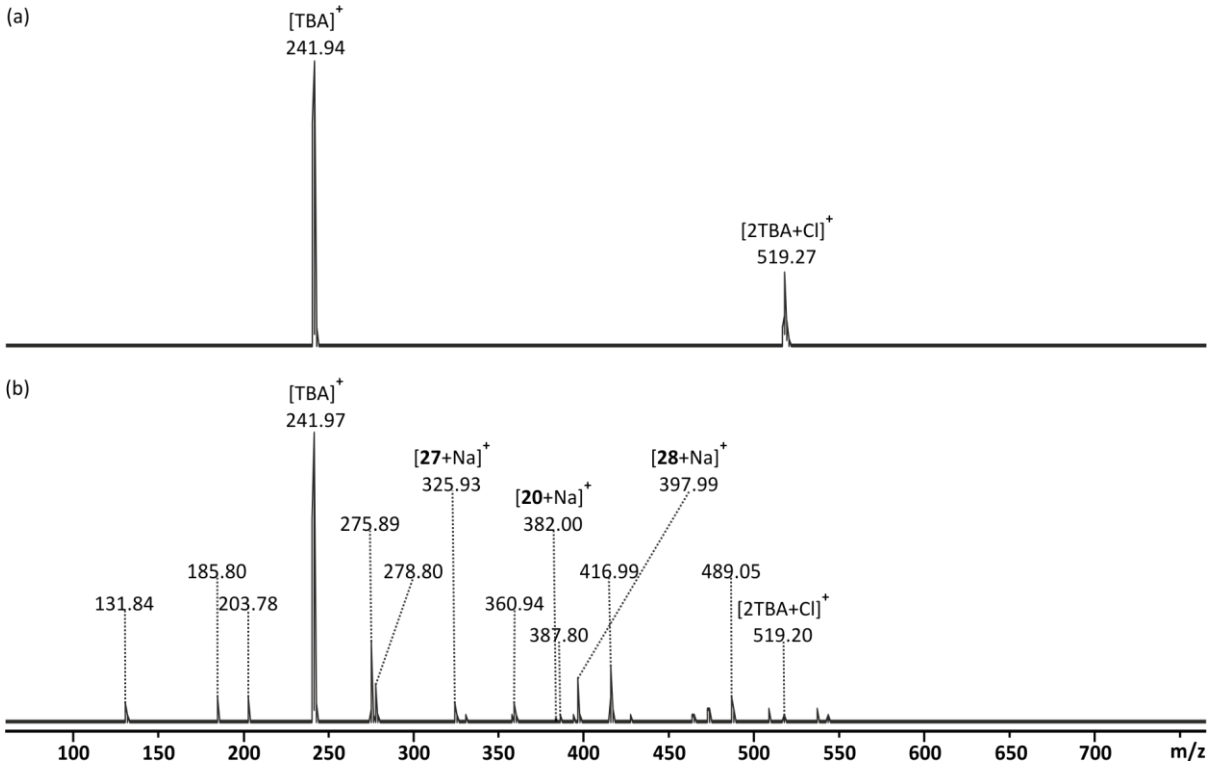

Figure 4.6. ESI(+) mass spectra of the deprotection reaction 4.10 with TBAF from acetonitrile recorded with ESI-MS instrument (b) (chapter 7.2.4). (a) ESI(+)-MS spectrum of the crude after extraction. (b) ESI(+)-MS spectrum of the crude after filtration over silica.

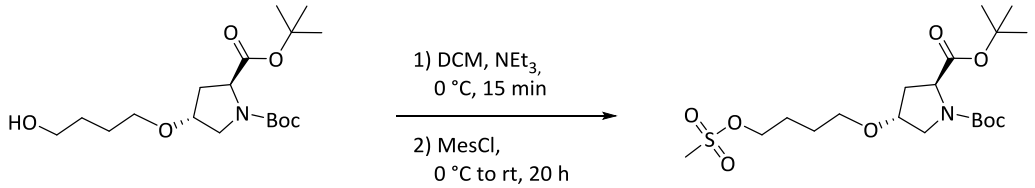

20 **21**

< 5%
over three steps

(4.11)

Scheme 4.12. Mesylation of ^{t}Bu-Boc-Hyp-C_4-OH **21** analogous to *Willms et al.*[86]

The partially purified crude of reaction 4.10 was used in the following to aim for the mesylation (reaction 4.11). The conditions were adopted from the first synthetic route (chapter 4.3).[86] After the reaction was quenched and extracted with dichloromethane, about ten different spots appeared on the crude TLC plate. At least five of them merged into each other hinting that the subsequent separation would be demanding. In parallel, a crude sample was measured by means of ESI-MS to determine if the product was formed at all. In figure 4.8, the target molecule **21** can be found with small intensity ([**21**+Na]$^+$ = *m*/*z* 460). Again, two side products could be assigned (figure 4.7). Interestingly, the acid was not only mesylated at the primary alcohol. It contained an additional mesylate which most probably resulted from an exchange of the acid's proton ([**29**+Na]$^+$ = *m*/*z* 482). A single mesylated compound originating from the acid could not be found. In case of the double linker side product only a double mesylated compound ([**30**+Na]$^+$ = *m*/*z* 554) was detected. Unfortunately, TBAF was still present as [TBA]$^+$ which proves the cation's easy detectability by ESI-MS.

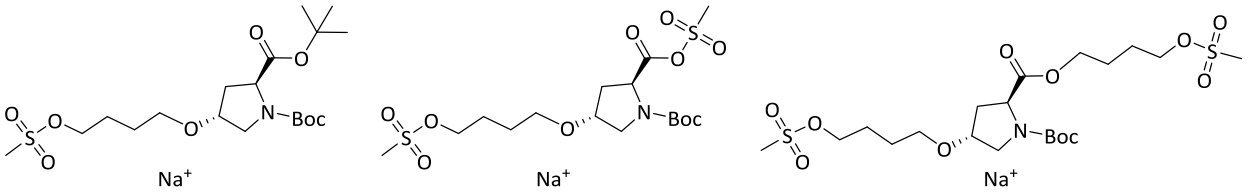

[**21**+Na]$^+$
exact mass: 460.1976

[**29**+Na]$^+$
exact mass: 482.554

[**30**+Na]$^+$
exact mass: 554.1700

Figure 4.7. Possible species of the mesylation depicted in scheme 4.13 detected by ESI-MS.

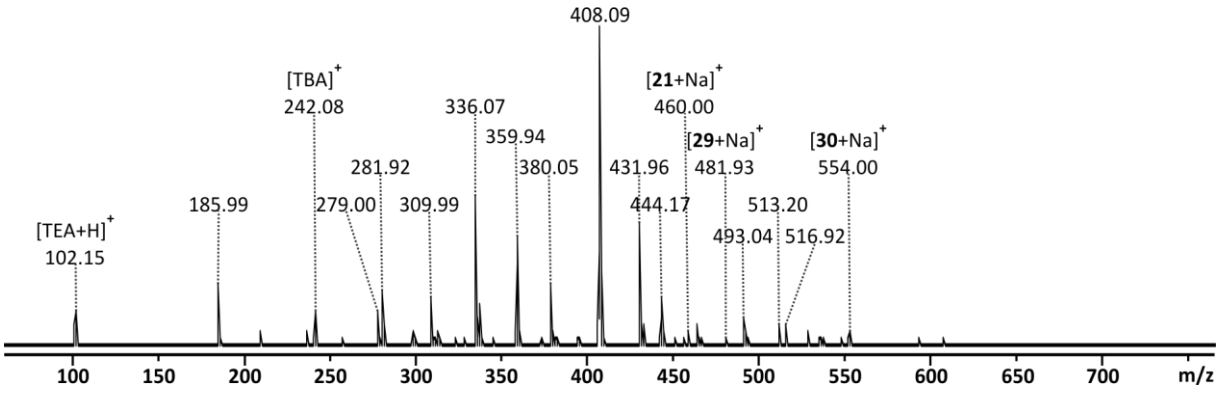

Figure 4.8. ESI(+) mass spectrum of the mesylation 4.11 from acetonitrile recorded with ESI-MS instrument (b) (chapter 7.2.4).

The separation by column chromatography was not successful. An overview of all eluent mixtures and additives tested can be found in the appendix (table 9.2). Each separation approach was monitored by ESI-MS. Small samples were taken from every fraction. Mesylation product **21** could be obtained as colorless liquid with 5% yield over three steps, but it was not enough to be characterized by NMR spectroscopy. The separated material was investigated by ESI-MS (figure 4.9). This revealed that the molecule had the right accurate mass, but it was still contaminated with unknown impurities. Neither the two side products **29** and **30** nor TBAF nor triethylamine were detected. As a result, the separation from the knwon impurities was successful.

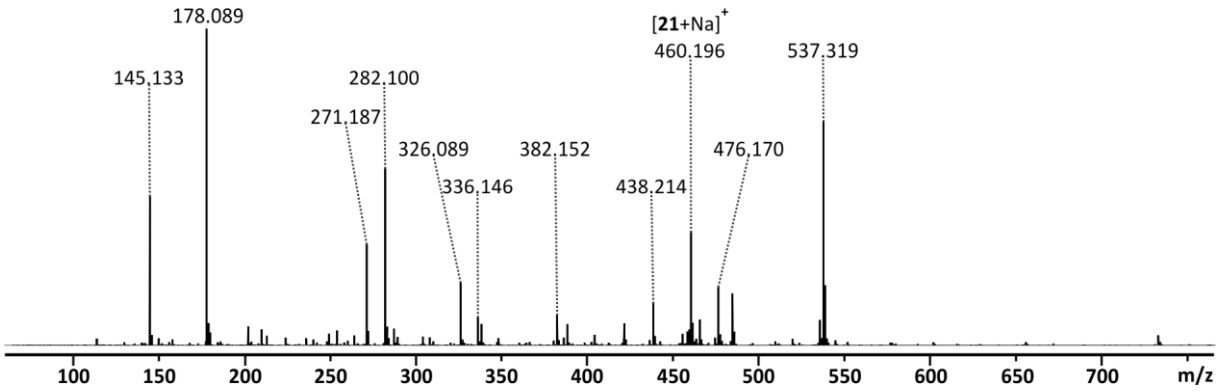

Figure 4.9. ESI(+) mass spectrum of the isolated mesylation product **21** after column chromatography (reaction 4.11) from acetonitrile. The spectrum was recorded with the high-resolution instrument (c) (chapter 7.2.4).

4.6 Conclusions and outlook

The first synthetic approach, using the proline moiety as electrophile did not lead to the desired product (scheme 4.2) since the connection of both fragments was not successful. It might have been impeded by steric hindrance resulting from a small aliphatic linker chain. Therefore, a C_4-chain instead of a C_2-chain was used to connect both units afterwards. Additionally, the fragments' electronic demand was inverted using ^{t}Bu-Boc-Hyp-OH **7** as nucleophile. Scheme 4.13 shows all synthetic steps that could be conducted for the second synthetic approach. The first step was the protection of Boc-Hyp-OH's acid moiety, which had been performed for approach one with almost quantitative yield. The second fragment required for the desired ligand was the aliphatic linker unit. Iodine was introduced as leaving group. Thereby, TBSO-C_4-I **18** was obtained with 79% yield. To combine the proline section with the linker unit, an S_N2 reaction with sodium hydride was performed. Even though ^{t}Bu-Boc-Hyp-O-C_4-OTBS **14** was detectable *via* mass spectrometry, it could not be isolated since it decomposed on the column. Thus, the extraction's crude product was used for the following TBAF deprotection of the silyl ether. According to the ESI-MS spectra, the deprotection was quantitative. No species with silyl ether were observed. Unfortunately, TBAF proved to stick to the substance even after the mesylation step. A separation by column chromatography rendered the desired product **21** with 5% yield over three steps. However, ESI-MS spectra showed that mesylation product **21** was still not completely pure, but the two side products **29** and **30**, which were not separable after the substitution step, could be removed at this point of the synthesis. With ^{t}Bu-Boc-Hyp-O-C_4-OMes **21** in hand, the final synthetic steps can now be conducted to obtain the *L*-proline-tethered NHC ligand precursor **23** and in the end the desired gold(I) complex **24**.

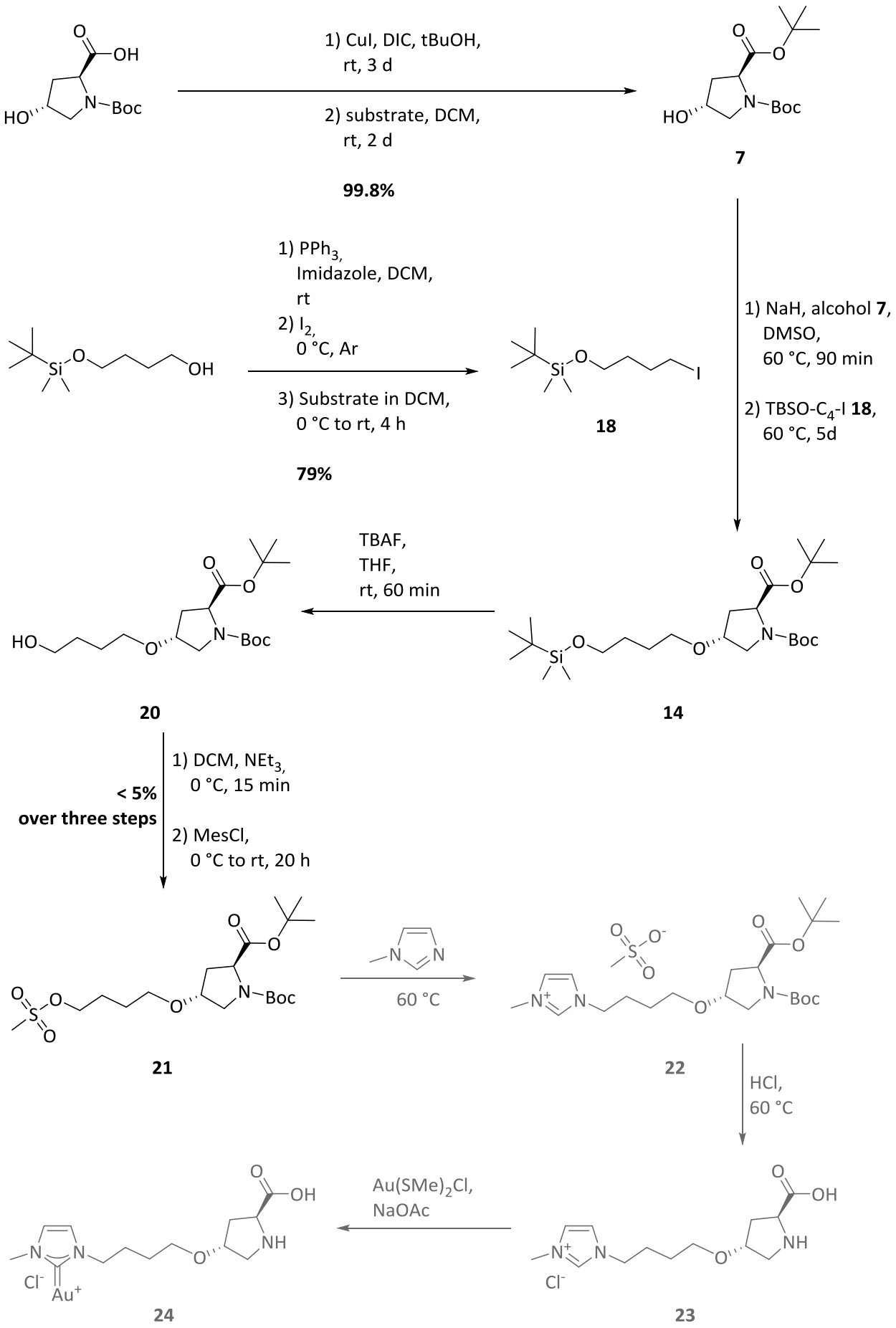

Scheme 4.13. Conducted synthesis of NCH-proline gold(I) complex with C_4 chain linker.

Apparently, the S_N2 reaction is the crux of the whole synthesis. This step already proved to be challenging in previous synthetic studies.[238,240] The side products observed indicate that the reactivity of the linker unit with iodine as leaving group is sufficient. A different protecting group for the acid might prevent the unwanted deprotection and additional substitution at this moiety. To the best of our knowledge, a deprotection of the *tert*-butyl ester under the basic substitution conditions was not observed in any of the related synthetic studies.[238,240] If this problem already existed during other S_N2 reactions, it might be an explanation for other difficult substitutions with comparable substrates.[238,240] Test reactions of a similar synthesis proved that a methyl ester can only be hardly removed at the sequence's end. It might also be interesting to follow the route introduced by scheme 4.8 with the iodine attached to the proline derivative instead. If the nucleophile is prepared at the aliphatic linker first (scheme 4.14), it might be possible that the excellent iodine leaving group enables a spontaneous reaction that is much more favored than any reaction at the (protected) acid. Thus, ^{t}Bu-Boc-Hyp-O-C_4-OTBS **14** would be obtained in higher yield and with less side products like **25** and **26**.

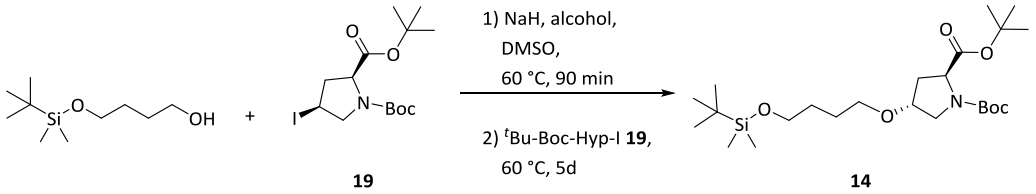

(4.12)

Scheme 4.14. Synthetic suggestion for an alternative S_N2 reaction with TBSO-C_4-OH and ^{t}Bu-Boc-Hyp-I **19**.

After the successful synthesis of the desired *L*-proline-tethered NHC ligand precursor **23**, a complexation with gold(I) will be conducted. Thereby, the first step is the formation of a stable complex with two *L*-proline-tethered NHC ligands **23**. If crystallization was possible, this would enable single crystal X-ray diffraction measurements and facilitate the characterization of the ligand as well as the active catalyst. The catalyst itself is expected to form by applying it in a 1:1 ratio. Like that, a gold(I) complex with one *L*-proline-tethered NHC ligand **23** and a free binding side can be formed. With this in hand, it would be very interesting to apply this bifunctional catalyst on the reaction of *Jørgensen* and co-workers[224] presented before (chapter 3). This could deliver new mechanistic insights into this intriguing reaction.

5 Kinetic investigations of a domino cyclization with oxidative coupling catalyzed by aurochloric acid

5.1 Introduction

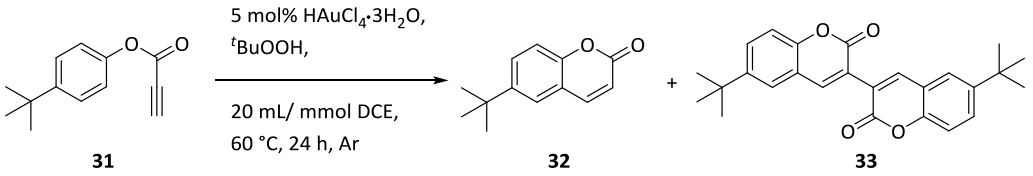

(5.1)

Scheme 5.1. Domino cyclisation and oxidative coupling of *tert*-butyl-arylpropiolic ester **31** according to *Wegner et al.*[13]

The third part of this thesis focuses on the investigations of the domino cyclization presented by *Wegner et al.*[13] (scheme 5.1). Mechanistic studies of this reaction *via* ESI-MS have already been conducted by *Krause*,[235] a former member of this working group. *Krause*[235] succeeded in identifying most of the species predicted by *Wegner et al.*[13] and was able to shed light on the individual species' structure and ligand sphere by means of ESI-MS (scheme 5.2). However, the studies of this interesting C-C coupling had not been completed so far. Thus, the aim of this thesis was to reveal the reaction's kinetic behavior.

For this purpose, a quantitative detection of substrate **31**, monomer **32** and dimer **33** was required. ESI-MS is not suitable for this task, but was conducted in parallel to prove comparability to the work of *Krause*.[235] As mentioned before (chapter 2.4), the ESI response complicates quantification of the individual species detected. Therefore, the domino cyclization was first monitored by means of GC-MS. Unfortunately, dimer **33** was not detectable with this technique. Most probably, the molecule is too large to pass the device's column. As a consequence, another quantitative method had to be found. ^{1}H NMR and UHPLC- (*ultra high performance liquid chromatography*)[248] coupled UV/Vis spectroscopy appeared to be very promising. However, NMR spectroscopy requires deuterated solvents. Thus, either the reaction had to be performed in deuterated dichloroethane in order to monitor the conversion continuously or the reaction had to be worked up for every single measurement. In the second case, a quantitative measurement is performed with a crude product worked up after a specific reaction time. In contrast to NMR spectroscopy, a direct reaction monitoring was excluded for UHPLC-coupled UV/Vis spectroscopy since the reaction conditions of inert gas and heating cannot be provided by this technique. As a consequence, this method requires work-up for every sample.

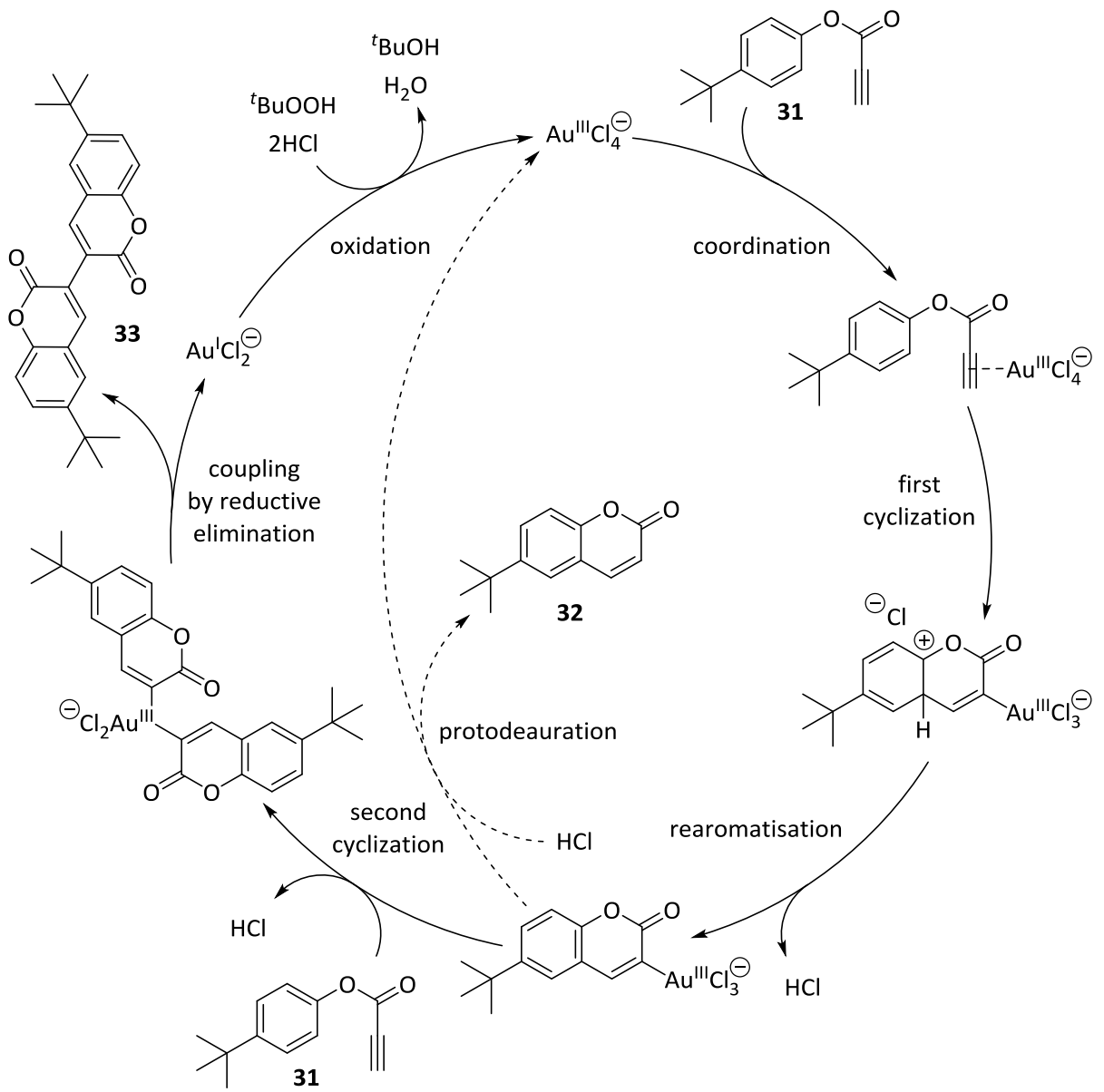

Scheme 5.2. Mechanistic cycle of the domino cyclization with oxidative coupling catalyzed by aurochloric acid by *Wegner et al.*[13] proposed by *Krause*[235] based on ESI-MS experiments.

To monitor the crude directly, the separation by UHPLC *a priori* is indispensable to determine the exact amount of every component. This common separation technique uses columns of coated silica to enable reversed phase operation.[126] Usually, the coat consists of siloxanes with distinct alkyl or aryl end groups.[126] These functional groups are responsible for the interaction with the analyte.[126] In case of reversed-phase columns, long alkyl chains bind stronger to low-polarity molecules, while highly polar substances or ionic materials can pass by.[126] As a result, rather polar solvents like acetonitrile or water are very common.[126] The chromatographic resolution can be further increased if the solvent mixture is applied in a gradient, increasing the concentration of the organic solvent.[126]

By detection *via* UV/Vis spectroscopy afterwards, the exact composition of the reaction solution can be determined. This spectroscopic technique uses light in the ultraviolet, visible and near-infrared region to induce electron transitions in the analyte.[212] Based on the *Beer-Lambert law*,[249] the resulting absorbance of a solution is directly proportional to the concentration of the absorbing species and the path length of the light.[212] Since the measurements are conducted at constant path length, the absorbance can be used to determine the concentration of the analyte.[212] In general, molecules will

exhibit absorption when the radiation causes an electronic transition.[212] Thus, this process is accompanied with an electronic transition induced by the energy of the light. Thereby, the electrons can be promoted either from a *σ*-bonding or an *n*-non-bonding to a *σ**-anti-bonding molecular orbital or from an *n*-non-bonding or a *π*-bonding to a *π*-*anti-bonding molecular orbital.[212] Since the transition to a *σ**-anti-bonding molecular orbital requires comparably much energy, it occurs in the region of ultraviolet light.[212] In contrast, the less energetic transition to a *π*-*anti-bonding molecular orbital usually is observed at lower wavelengths.[212] In case of the reaction by *Wegner et al.*,[13] all three components of interest possess a large aromatic system and thus are well suitable for detection with UV/Vis spectroscopy.[212] However, the absorbance also depends on the solvent used for the experiments.[212] Therefore, an individual calibration is required in order to calculate exact amounts of substance from an absorbance spectrum.

5.2 Quantitative ^{1}H NMR experiments

Unfortunately, deuterated dichloroethane was not available as solvent for the ^{1}H NMR experiments. Thus, a direct monitoring *via* ^{1}H NMR of the reaction was not possible. Therefore, several series of individual micro setups for reaction 5.1 were prepared. They were quenched after an exactly measured reaction time by the addition of thiosulfate solution and the aqueous phases were extracted according to the work-up of *Wegner et al.*[13] The extractions' crudes were dissolved in deuterated solvents and crude ^{1}H NMR spectra were measured. To obtain an overview of the reaction's kinetic behavior, the different micro reactions were stopped after different reaction times. Thereby, every single experiment of a series was conducted in parallel to the other experiments of this study to gain maximal comparability.

To distinguish between substrate **31**, monomer **32** and dimer **33**, the three individual and discrete signals had to be found in the ^{1}H NMR spectrum before the actual study could be conducted. Figure 5.1 shows an example for a ^{1}H NMR spectrum of a typical crude product measured in deuterated dichloromethane. All species can be seen simultaneously. Substrate **31** is the only molecule with a primary alkyne. This functional group can be detected at 3.16 ppm. Further, monomer **32** and dimer **33** differ by the *α*-carbonyl proton that is lost during the coupling process. Therefore, the doublet at 6.37 ppm can be attributed to the monomer **32**. In the low field, a signal can be found that is generated by dimer **33**'s sp^2-hybridized *β*-carbonyl proton of the heterocycle. One has to be careful that the integral of the signal at 8.51 ppm had to be doubled for calculations since the signal describes two symmetric protons in dimer **33**.

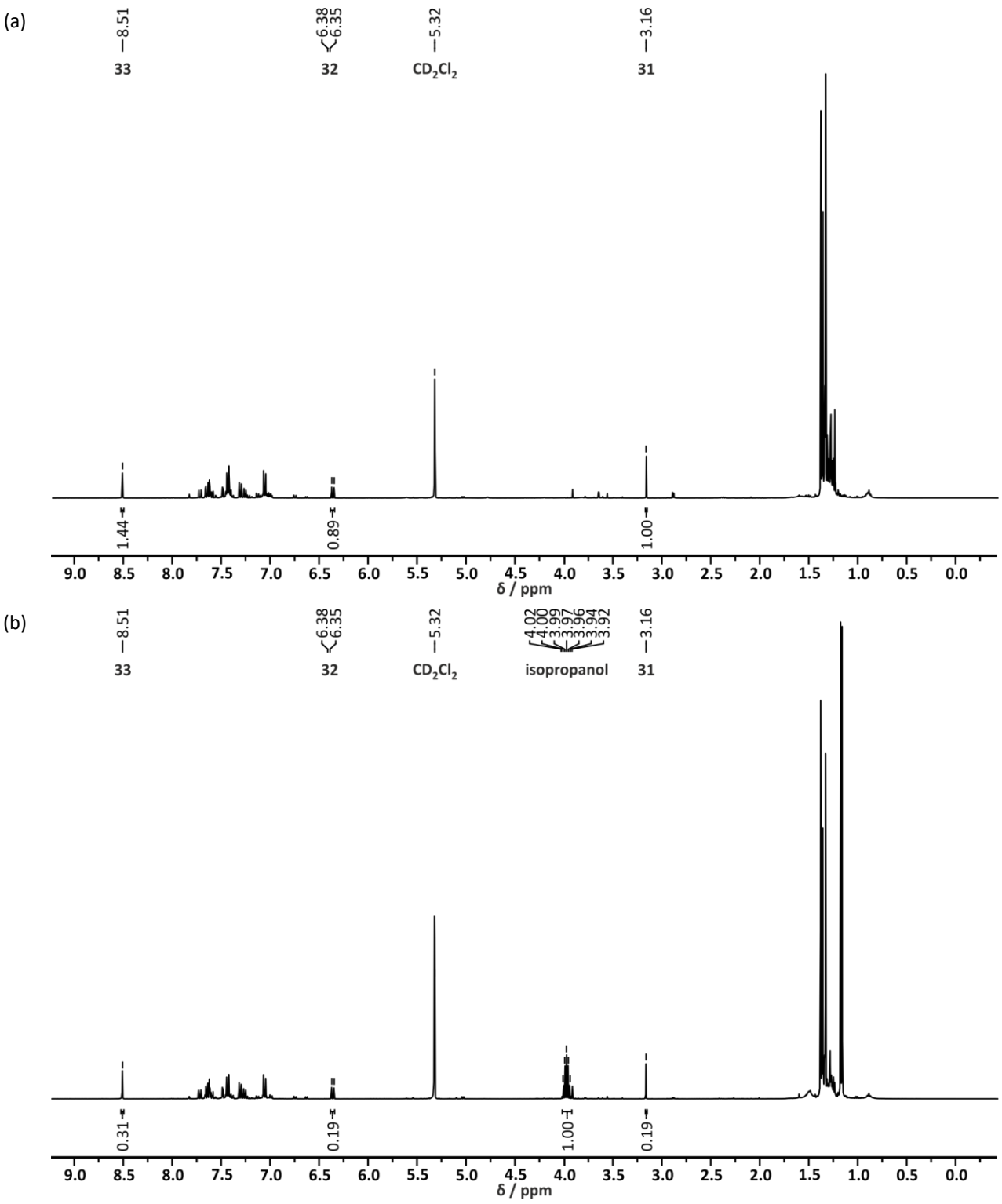

Figure 5.1. ^{1}H NMR spectra of the crude product of reaction 5.1 (a) after a reaction time of three hours measured in CD_2Cl_2 and (b) after a reaction time of five hours measured in CD_2Cl_2 with isopropanol as internal standard. The spectra were recorded with NMR instrument (a) (chapter 7.2.3).

Since this is a time-dependent study, all integrals were plotted as standardized values ($I_{st,\mathbf{i}}$) against time. This means that the integral values ($I_{rel,\mathbf{i}}$) of the individual species ($\boldsymbol{i}$) detected in the same spectrum were standardized to the sum of all integrals of all depicted species (figure 5.2). For this purpose, they were divided by the proton-weighted sum of the integrals of all species measured at the specific time. Arbitrarily, ester **31**'s proton at 6.41 ppm was chosen as reference. Thus, this signal was set to one. That

enabled calculations using absolute numbers which extremely facilitate the comparison of the individual studies.

$$I_{st,\mathbf{i}} = \frac{I_{rel,\mathbf{i}}}{I_{rel,\mathbf{31}}+I_{rel,\mathbf{32}}+2I_{rel,\mathbf{33}}}$$

Figure 5.2. Equation used to standardize the individual integrals to the sum of all integrals.

Since individual setups had to be prepared for every point of reaction time, disproportional losses of substances that occurred during the individual work-ups cannot be excluded. As a consequence, small deviations in the integral values that distort the overall kinetics were expected. Based on the work of *Krause*,[235] a variation of the reaction temperature and the catalyst loading was tried first to examine how accurate the integrals could be determined. Surprisingly, the studies showed no slope for every single graph with deuterated chloroform as NMR solvent.[250] This led to the conclusion that either a problem of solubility had occurred or reaction 5.1 had already been completed within the first measurements after ten minutes even though *Wegner et al.*[13] suggested a reaction time of one day. As a result, different promising NMR solvents (benzene-d_6, DCM-d_2 and THF-d_8) were tested.

(a)

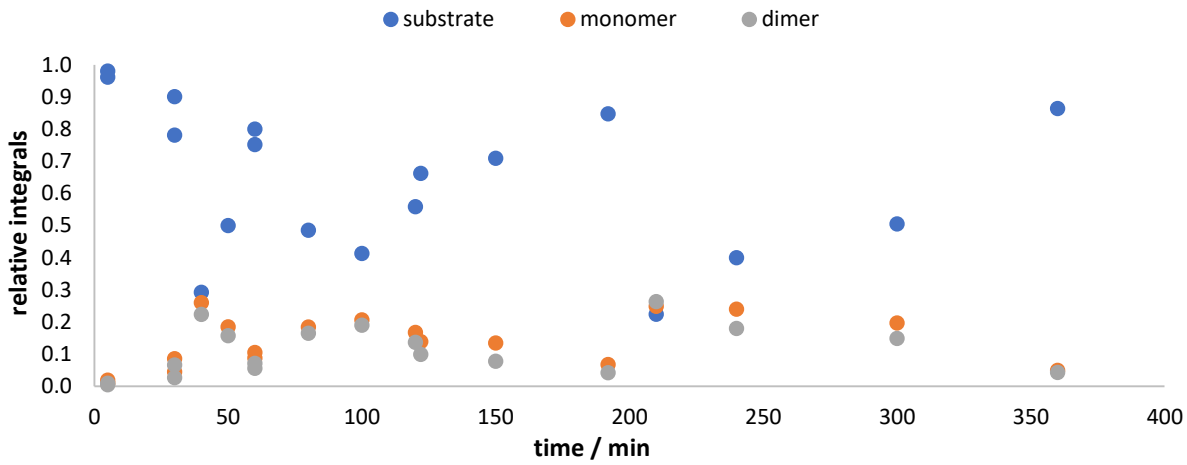

(b)

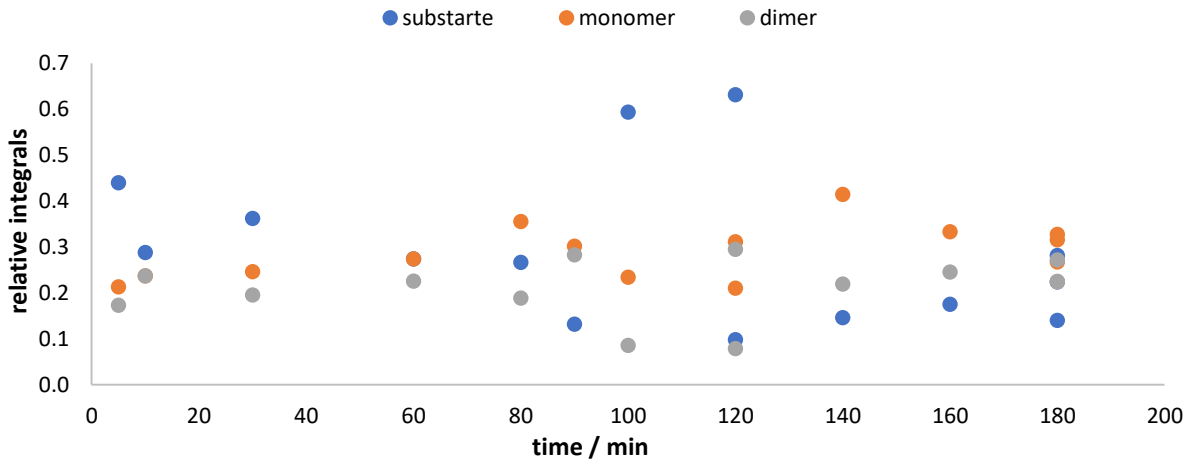

Figure 5.3. Temporal evolution of reaction 5.1 recorded with ^{1}H NMR spectroscopy from crude products of individual solutions with a concentration of about **10 mg/mL** in (a) dichloromethane-d_2 and (b) dichloromethane-d_2 with isopropanol as standard. All integrals were standardized to the sum of all integrals except for (b). In this case, all integrals were standardized to an exact amount of isopropanol that was added to the NMR solvent. The spectra were recorded with NMR instrument (a) (chapter 7.2.3).

The results of the studies with dichloromethane-d_2 are shown in figure 5.3. As in the studies with deuterated chloroform conducted before,[250] the individual crude products were dissolved completely

in deuterated dichloromethane. The integrals were standardized to the sum of all integrals as described before (figure 5.3a). The measurements showed no reasonable evolution of the product integrals. The signals of the substrate **31** varied even more dramatically. Thus, the experiments were repeated and a ^{1}H NMR solution with an internal standard was prepared. For this purpose, isopropanol was added in a known concentration to the deuterated dichloromethane. The same stock solution was used for every ^{1}H NMR experiment and again dissolved the crude products completely. This time, ester **31**'s integral was not chosen as standard, but the additive's was used instead. Unfortunately, this did not change the outcome. As visible in figure 5.3b the amount of monomer **32** and dimer **33** does not increase and the substrate **31**'s signals vary again vastly.

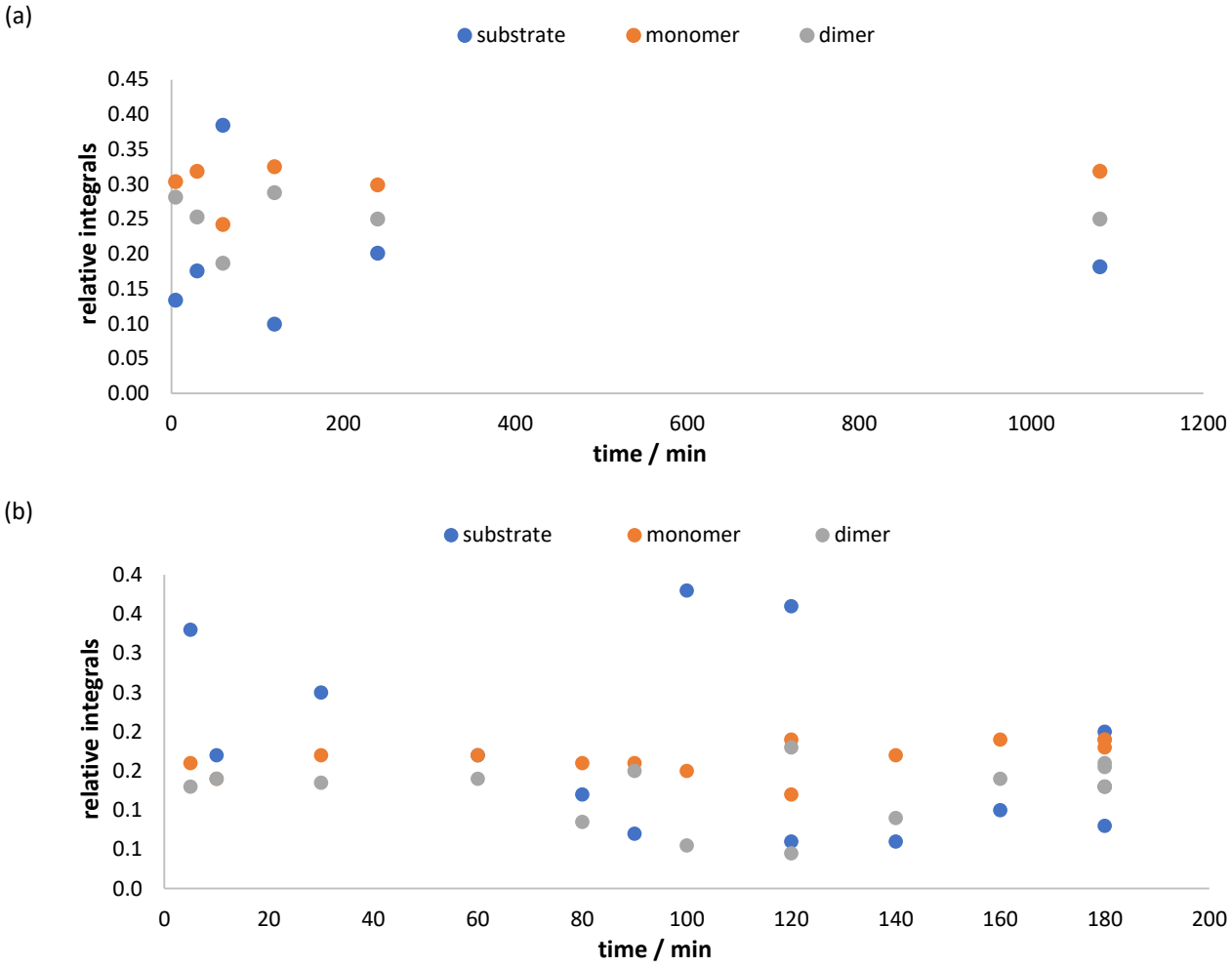

Figure 5.4. Temporal evolution of reaction 5.1 recorded with ^{1}H NMR spectroscopy from crude products of individual solutions with a concentration of **1 mg/mL** in (a) dichloromethane-d_2 and (b) dichloromethane-d_2 with isopropanol as standard. All integrals were standardized to the sum of all integrals except for (b). In this case, all integrals were standardized to an exact amount of isopropanol that was added to the NMR solvent. The spectra were recorded with NMR instrument (a) (chapter 7.2.3).

The question arose of whether there was still a problem of solubility in case of dichloromethane-d_2. So far, the individual crude products were dissolved completely (10 mg/mL). For the next series, the concentration was lowered for all ^{1}H NMR solutions to 1 mg/mL. In this experimental series, a sufficient amount of the crude products remained after the first NMR measurements to dissolve another sample with 1 mg/mL in the isopropanol stock solution used before. This was expected to finally render a temporal evolution of all three components. Figure 5.4 proves that both attempts did not solve the problem. In case of the isopropanol solutions, a partial evolution of the two products can be observed, but substrate **31** showed again a significant variation. In general, the preparation of the solutions with

exact concentration proved to be challenging. This caused a high risk of variation especially with the low concentrations samples that were hardly detectable. Thus, this approach was discarded and the original standardization process with the sum of all integrals based on ester's **31** proton was used again.

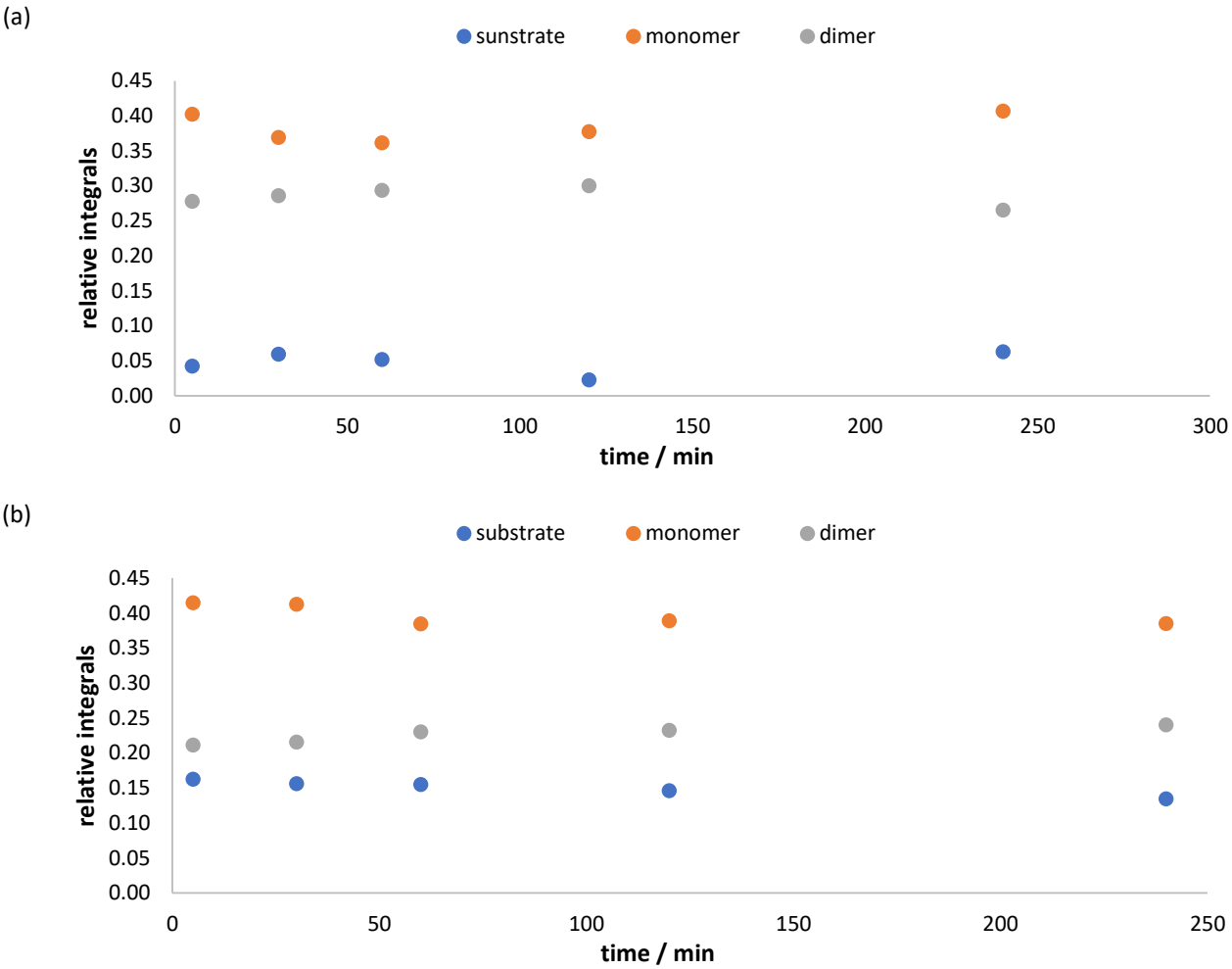

Figure 5.5. Temporal evolution of reaction 5.1 recorded with ^{1}H NMR spectroscopy from crude products of individual solutions with a concentration of 1 mg/mL in (a) benzene-d_6 and (b) THF-d_8. All integrals were standardized to the sum of all integrals detected. The spectra were recorded with NMR instrument (a) (chapter 7.2.3).

The solubility experiments showed that also benzene-d_6 and THF-d_8 were very promising. Thus, the experiments were repeated. Therefore, the individual crude products were dissolved in benzene-d_6 as well as THF-d_8 with a concentration of 1 mg/mL. With these solvents and the low ^{1}H NMR concentration a comparable behavior of all three components can be seen in figure 5.4. Unfortunately, no significant decline or increase of any species can be found. By means of a laser pointer it became visible that no deuterated solvent used so far had dissolved the crude completely (10 mg/mL). Additionally, the low concentration samples of dichloromethane-d_2 and benzene-d_6 showed small residue particles present in the solutions. As a consequence, every solution turned out to be a suspension due to the low solubility of the products. Only in case of THF-d_8 no particles could be seen with the naked eye. But since the results obtained using this solvent were similar to the ones in benzene-d_6, they indicated the existence of a similar problem for the THF-d_8 experiments. Further decreasing of the ^{1}H NMR concentration appeared not very reasonable since the integrals were already hardly distinguishable from the chemical noise.

This was additionally confirmed when measurements in the reaction's solvent dichloroethane (non-deuterated) were conducted. The predominant solvent signal was suppressed to enable the detection of the three components. Again, it was not possible to depict a temporal evolution. Thus, no further attempts of reaction monitoring *via* NMR spectroscopy were made.

5.3 Quantitative UHPLC-UV/Vis experiments

With UHPLC-coupled UV/Vis spectroscopy, a lower detection limit compared to NMR spectroscopy was expected. Figure 5.6 shows a chromatogram of a randomly mixed sample of the substrate **31** and the purified products **32** and **33**. Combining all three reaction components, a suitable method that allows detection of all three species simultaneously could be established. This was required since crude products of individual setups of reaction 5.1 were measured again.

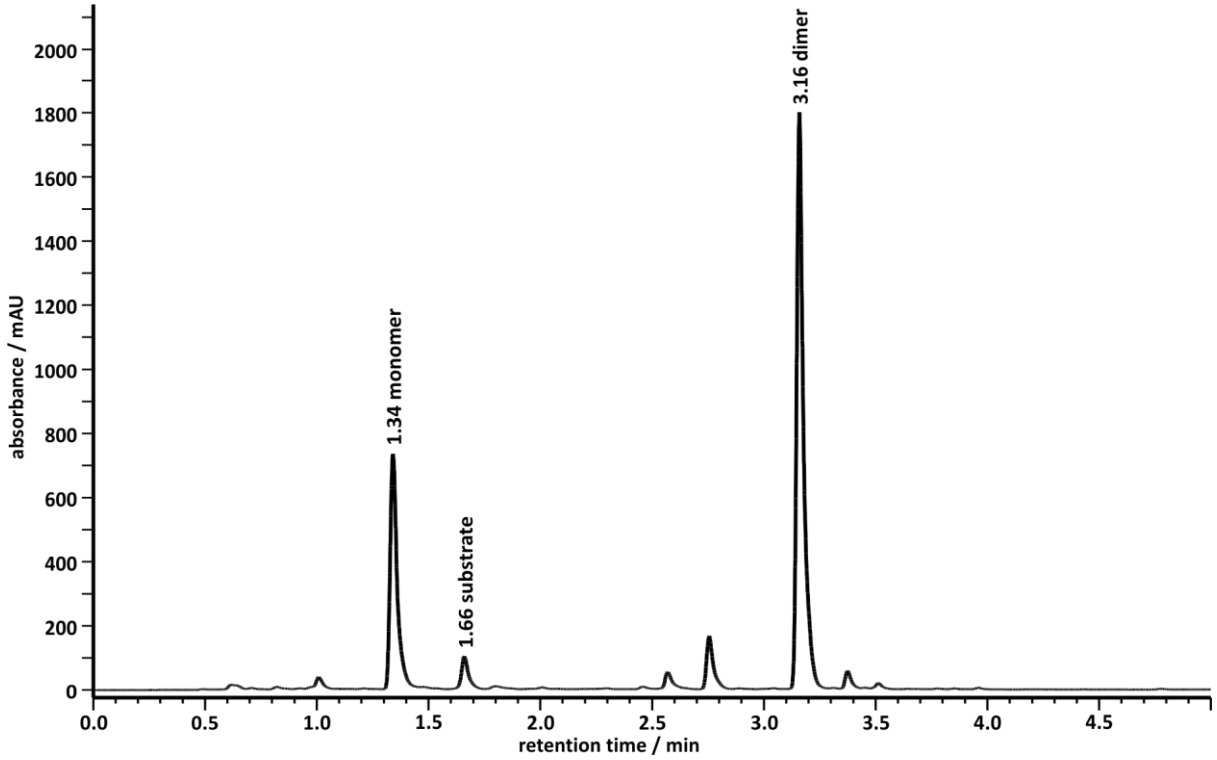

Figure 5.6. Chromatogram of a mixture of substrate **31**, monomer **32** and dimer **33** recorded with UHPLC-UV/Vis spectroscopy (chapter 7.2.5). The sample was mixed randomly to establish a suitable detection method that allows detection of all three components simultaneously.

To determine the amount of the three species correctly at a certain reaction time, the absorption of each individual component had to be calibrated first. For this purpose, a stock solution was prepared in THF with known concentration for every single pure component. Thereby, concentrations of similar magnitude as the one expected for the study's reaction setups were chosen. The concentrations of all solutions used for the calibration measurements can be found in table 5.1. Afterwards, a dilution series was created with all components in known concentrations. The lowest concentration was 21.9 µg/mL, the highest 175.2 µg/mL. A comparable system was expected for the actual samples from the individual reaction setups. Five dilution steps were chosen and a sample of 2 µL for the UHPLC was taken for every dilution step. This allowed the creation of a calibration curve for every component and further assignment to a UV/Vis signal of substrate **31**, monomer **32** and dimer **33**. The calibration

measurements were repeated three times to ensure an accurate assignment of the individual absorbance to an exact amount of substance. The variation was insignificant (appendix, figure 9.13). With this suitable concentration, area the actual samples could be investigated in the following.

Table 5.1. Concentrations of the stock solutions and individual as well as summed concentration for the calibration dilution series for substrate **31**, monomer **32** and dimer **33** recorded with UHPLC-UV/Vis spectroscopy.

dilution	substrate 31 / µg/mL	monomer 32 / µg/mL	dimer 33 / µg/mL	sum of all components / µg/mL
stock solutions	309.0	352.1	434.0	1095.1
dilution step 1	49.4	56.3	69.4	175.2
dilution step 2	24.7	28.2	34.7	87.6
dilution step 3	18.5	21.1	26.0	65.7
dilution step 4	12.4	14.1	17.4	43.8
dilution step 5	6.2	7.0	8.7	21.9

As for the NMR studies, crude products of individual setups of reaction 5.1 were measured. All setups were of approximately same size. The crude products were dissolved in exact amounts of THF (approximate concentration 0.25 to 0.5 mg/mL). The masses obtained were standardized to the amount of starting material used for the individual setup.

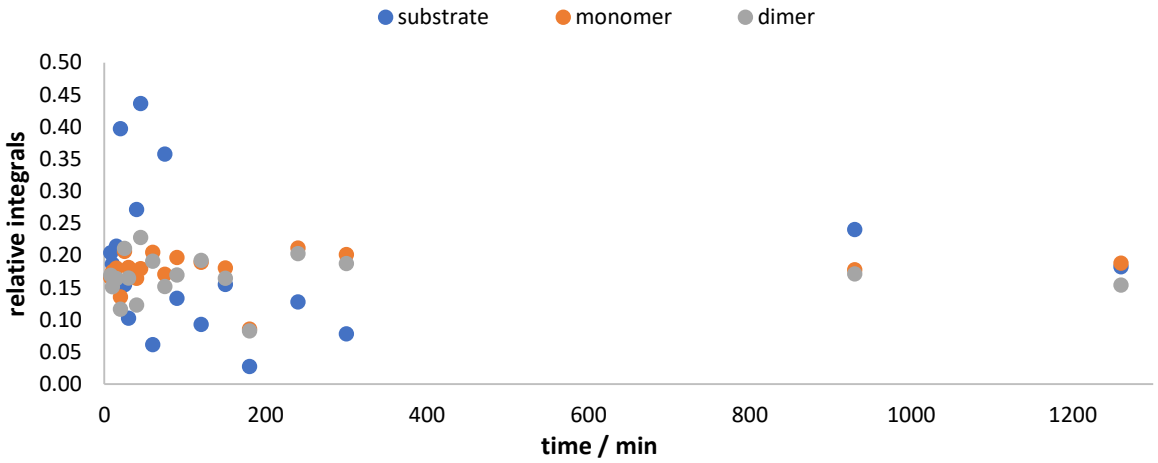

Figure 5.7. Temporal evolution of reaction 5.1 recorded with UHPLC-UV/Vis spectroscopy from crude products of individual solutions.

Unfortunately, the UHPLC-coupled UV/Vis measurements of reaction 5.1 rendered comparable results as the ^{1}H NMR studies of chapter 5.3 before (figure 5.7). No clear time dependent evolution could be discovered. In contrast, the two products **32** and **33** showed almost no change of concentration although the concentrations of the crude product samples were very low. This led to the conclusion that this was no effect of bad solubility. If the reaction was terminated within less than ten minutes, the concentration of all species during the UV/Vis and the ^{1}H NMR experiments would stay constant afterwards.

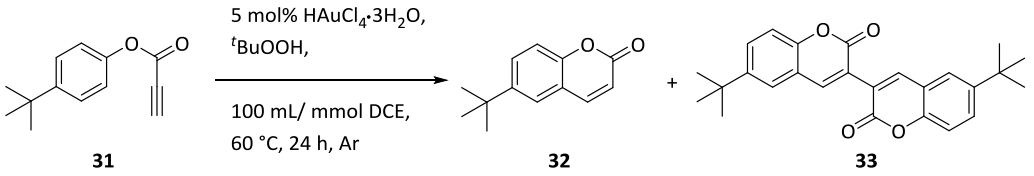

(5.2)

Scheme 5.3. Domino cyclisation and oxidative coupling of *tert*-butyl-arylpropiolic ester **32** performed in a fivefold amount of solvent according to *Wegner et al.*[13]

To slow down the reaction, reaction solutions were prepared with a fivefold amount of solvent (reaction 5.2). Figure 5.8 shows the results of the UHPLC-coupled UV/Vis measurements of reaction 5.2. A decrease of substrate **31** with simultaneous increase of the two products **32** and **33** can be observed. This proves that reaction 5.1 could not be monitored neither by ^{1}H NMR nor by UHPLC-coupled UV/Vis spectroscopy, since it was terminated within minutes.

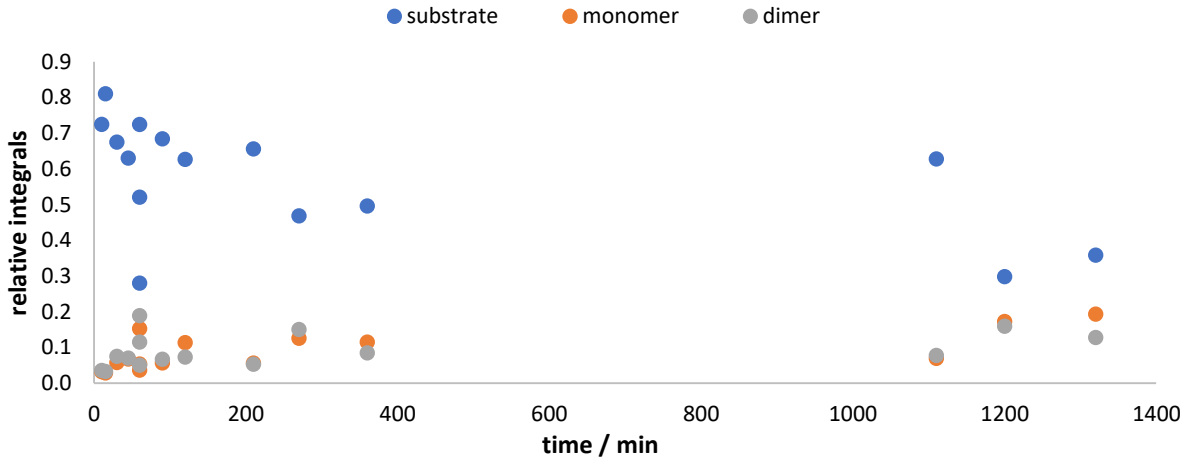

Figure 5.8. Temporal evolution of reaction 5.2 recorded with UHPLC-UV/Vis spectroscopy from crude products of individual solutions.

5.4 Conclusions

The domino cyclization and oxidative coupling reaction induced by aurochloric acid (reaction 5.1) that was reported by *Wegner et al.*[13] was investigated. In contrast to *Krause*,[235] who used ESI-MS only, a kinetic study by means of ^{1}H NMR and UHPLC-coupled UV/Vis spectroscopy was aimed at this thesis. To ensure comparability to the work of the predecessor, ESI-MS experiments of every reaction were conducted in parallel. As observed in previous studies of this working group[250] no significant deviation from *Krause's*[235] ESI-MS measurements could be found. Thus, we are positive that our results are applicable to the prior investigations and complete the comprehensive overview of the reaction. After various NMR and UHPLC-coupled UV/Vis studies, it can be assumed that the small deviations of the ESI-MS peaks, interpreted as temporal evolutions, were only insignificant variations of the concentration or detectability in solution. In case of the substrate **32** and the two products **32** and **33**, we are certain that these hardly soluble components could not have been dissolved completely. As a consequence, a temporal evolution could not have been observed by *Krause's*[235] ESI-MS measurements.

By lowering the reaction's concentration (reaction 5.2) monitoring of a temporal evolution of all three components became possible *via* UHPLC-coupled UV/Vis spectroscopy (figure 5.8). This proved that the

original reaction 5.1 was too fast for our and *Krause's*[235] techniques to be investigated. It was possible to reveal that the reaction is terminated within minutes. Thus, stirring for 24 hours as suggested by *Wegner et al.*[13] is not required. The results of the diluted reaction setups also suggest that the low solubility might be a key driving force for the reaction's conversion taking the products out of the overall equilibrium in solution.

6 Conclusions of this thesis

In the first part of this thesis mechanistic studies of an intermolecular cyclization reaction induced by a dual catalyst system were presented. By means of ESI-MS, it was possible to detect many species directly from the reaction solution. Additionally, all reaction setups were monitored by GC-MS to obtain a temporal evolution of all substrates and products. This all enabled an insight into the reaction's mechanism and allowed complementation of the suggested mechanistic cycles. For a more concise understanding, both reaction steps (Michael addition and 5-*exo*-*dig*-cyclization) were investigated separately. It was revealed that the 5-*exo*-*dig*-cyclization reaction only occurs with reasonable conversion if the pyrrolidine catalyst forms an enamine species before the gold(I) catalyst induces the cyclization process. By variation of the free protons in the reaction solution, the two rate determining steps of the Michael addition and the cyclization were uncovered to be acid-assisted. Further, the application of a deuterated and a substituted alkyne demonstrated that the reaction is not limited to primary alkynes. Additionally, the GC-MS experiments revealed that the reaction times suggested have to be reconsidered.

The second part focused on the first synthetic approaches towards a new NHC-*L*-proline catalyst. It was possible to improve the reaction conditions of the first steps towards the *L*-proline fragment and obtain the product in almost quantitative yield. The imidazolium fragment was also obtained in good yield. However, the connection between both fragments proved to be challenging. Based on many synthetic experiments, a new sequence was proposed that includes new reactions as well as optimized ones.

In the third part of this thesis a kinetic study of a domino cyclization with oxidative coupling induced by aurochloric acid was presented. Thereby, reaction monitoring with quantitative UHPLC-coupled UV/Vis spectroscopy revealed that the reaction occurs within minutes instead of several hours. Thus, the reaction had to be slowed down by dilution to be monitored.

7 Experimental section

7.1 General indications

If not mentioned otherwise, all reactions were performed under normal atmosphere. Treatment under inert gas is indicated if required for the individual reaction. The terms ‘Schlenk conditions’, ‘under argon’ or ‘under inert gas’ imply that the reactions were performed in evacuated Schlenk flasks which were baked out and subsequently filled with argon gas. This is especially recommended for substances that are air and/or water sensitive. In these cases, the solvents were dried by activated molecular sieve and stored under argon.

All solvents were removed under reduced pressure using a rotary evaporator with a diaphragm pump. Any deviations from this procedure are marked. All chemicals which are commercially available were used without any further purification. Absolute solvents were obtained by drying and distilling using the standard methodology[251] if not received as such.

7.2 Instruments, methods and chemicals

7.2.1 Thin-layer chromatography

TLC plates:	Aluminum sheets with silica gel 60 F_{254}, MERCK
Detection:	Fluorescent light λ = 245 nm and λ = 366 nm
Stain solution:	1.5 g $KMnO_4$, 10 g K_2CO_3 and 1.25 mL 10% NaOH in 200 mL water

7.2.2 Column chromatography

Stationary phase:	Silica gel 60; 40–63 µm; MERCK;
	Celite®, Sigma-Aldrich
Columns:	1.5–12 cm diameter with frit

7.2.3 NMR spectroscopy

^{1}H and ^{13}C NMR: a) Bruker Advance I 400 MHz, Bruker,

Equipped with a RT 5 mm BBO 400 BB-H with z-gradient and ATM probe head and a BACS 60 autosampler,

^{1}H 400 MHz, ^{13}C 100 MHz;

b) Bruker Advance I 500 MHz (Oxford Magnet), Bruker,

Equipped with a RT 5 mm BBFO 500 BBF-H with z-gradient and ATM probe head and a SampleXpress 60 autosampler,

^{1}H 500 MHz, ^{13}C 125 MHz;

c) Bruker Advance I HD Ascend 700 MHz, Bruker,

Equipped with a He-CP 700 QCI H-P/C/N with z-gradient probe head and a SampleJet 24 autosampler,

^{1}H 700 MHz, ^{13}C 175 MHz.

Reference [ppm]: Benzene-d_6 (^{1}H: 7.16, ^{13}C: 128.06);

Chloroform-d_1 (^{1}H: 7.26; ^{13}C: 77.16);

Dichloromethane-d_2 (^{1}H: 5.32, ^{13}C: 53.84);

Dimethylsulfoxide-d_6 (^{1}H: 2.50; ^{13}C: 39.52);

Tetrahydrofurane-d_8 (^{1}H: 1.72, 3.58, ^{13}C: 25.31, 67.21)

All chemical shifts of the individual cores are reported relatively to the residual non-deuterated solvent signals listed above. The signal assignment of the ^{1}H and ^{13}C NMR spectra was also confirmed with COSY, HSQC and HMBC NMR experiments that are not mentioned separately.

7.2.4 Mass spectrometry

Devices

ESI-MS: a) micrOTOF-Q, quadrupole time-of-flight mass spectrometer, Bruker Daltonik,

Equipped with an Apollo ESI source and an Agilent series 1200 autosampler with a Knauer Azura degasser,

Or syringe pumps from Cole Parmer or KD Scientific used with gastight glass syringes from Hamilton;

b) HCT ultra PTM, high capacity ion trap ultra posttranslational modification discovery system, Bruker Daltonik,

Equipped with an Apollo ESI source and an Agilent series 1200 autosampler with a Knauer Azura degasser,

Or syringe pumps from Cole Parmer or KD Scientific used with gastight glass syringes from Hamilton;

c) LTQ Orbitrap XL, Thermo Fisher Scientific,

Equipped with an ESI/APCI ION Max source and an Dionex UltiMate 3000 autosampler with a Dionex UlitMate 3000 pump,

Syringe pump integrated by Thermo Fisher Scientific used with gastight glass syringes from Hamilton,

To prevent corrosion, experiments with aurochloric acid were conducted with an ESI needle and capillaries made of inert fused silica instead of stainless steel.

For all ESI mass spectrometers, nitrogen was used as spraying and nebulizing gas. Peeks were assigned based on selected representative experiments with careful mass calibration. Tubes with an inside diameter of 0.13 mm were used for the connection of the devices. If a syringe pump was used, the analyte solutions were passed into the spectrometer at a flow of 0.3 mL/h. If an autosampler was used, a flow of 0.05 mL/min was applied.

GC-MS (EI):

a) Gas chromatograph GC-2010 Plus, Shimadzu,

Quadrupole mass analyzer and autospample integrated by Shimadzu,

Equipped with a Zebron ZB-5MSI column (30 m length, 0.250 mm inside diameter, 0.25 µm film, 5% Phenylpolysiloxan, 95% Dimethylpolysiloxan)

b) Agilent Technologies 7890B GC system, Agilent Technologies,

Equipped with an Agilent Technologies Accurate-Mass Q-TOF GC/MS, quadrupole time-of-flight spectrometer and an Agilent Technologies series 7693 autosampler,

Further equipped with an Agilent Technologies HP-5MS UI (30 m length, 0.250 mm inside diameter, 0.50 µm film, 5% diphenylpolysiloxan, 95% dimethylpolysiloxan).

Parameters for the ESI-MS experiments

a) Parameters for the micrOTOF-Q commercial quadrupole time-of-flight mass spectrometer equipped with an Apollo ESI source and an Agilent series 1200 autosampler with a Knauer Azura degasser for positive-mode measurements.

micrOTOF-Q	**minimum value**		**maximum value**	**unit**
end plate offset	-550	-	-450	V
capillary voltage	-5000	-	-4000	V
nebulizer gas	2.0	-	4.5	bar
drying gas	1.0	-	5.0	L/min
drying temperature	120	-	250	°C
collision energy	0.0	-	8.0	eV
collision RF	60.0	-	1230.0	Vpp
transfer time	90.0	-	150.0	µs
pre-pulse storage	5.0	-	18.0	µs
funnel 1 RF	80.0	-	300.0	Vpp
funnel 2 RF	90.0	-	400.0	Vpp
hexapole RF	70.0	-	400.0	Vpp
ISCID energy	0.0	-	0.0	eV
quadrupole ion energy	4.0	-	7.0	eV
minimum detection	21	-	300	*m*/*z*
maximum detection	950	-	6000	*m*/*z*

b) Parameters for the HCT ultra PTM commercial high capacity ion trap mass spectrometer equipped with an Apollo ESI source and an Agilent series 1200 autosampler with a Knauer Azura degasser for positive-mode measurements.

HCT ultra PTM	minimum value		maximum value	unit
end plate offset	-500	-	-500	V
capillary voltage	-4000	-	-4000	V
nebulizer gas	15.0	-	15.0	psi
drying gas	3.0	-	10.0	L/min
drying temperature	250	-	300	°C
skimmer	40.0	-	40.0	V
capillary exit	95.5	-	109.0	V
trap dive	24.6	-	77.3	
Oct 1 DC	8.00	-	8.00	V
Oct 2 DC	1.70	-	2.48	V
Oct RF	103.0	-	200.0	Vpp
lens 1	-5.0	-	-5.0	V
lens 2	-60.0	-	-60.0	V
minimum detection	50	-	120	*m/z*
maximum detection	2000	-	2800	*m/z*

7.2.5 UHPLC-coupled UV/Vis

All experiments were conducted with a Platinblue series device from Knauer Wissenschaftliche Geräte GmbH equipped with an autosampler AS-1 and a UV/Vis photodiode array detector PDA-1 at 210 nm. An Erosphere II 100-2 C18 reversed phase column was used for the separation at 25 °C. 2 µL of the individual sample were injected. A gradient of 70% acetonitrile and 30% water to 100% acetonitrile was used with a flow of 0.5 mL/min.

7.2.6 Chemicals

chemical	manufacturer	purity
(*S*)-*α*,*α*-bis[3,5-bis(trifluoromethyl)phenyl]-2-pyrrolidinemethanol	Aldrich	97%
[bis(trifluoromethanesulfonyl)imidate](triphenylphosphine) gold(I) in toluene	Aldrich	2:1 adduct
1,2-dibromoethane*	Merck	>99%
1,2-dichloroethane	Riedel-de Haën	>99%
1-butanol	Alfa Aesar	99%
1-methyl imidazole	Alfa Aesar	99%
1-octanol	Aldrich	99%
2-bromoethanol	Aldrich	99%
4-(dimethylamino)cinnamaldehyde (DMAC)	Sigma	>98%
4-(*tert*-butyldimethylsilyl)oxy-1-butanol (TBSO-C_4-OH)	Sigma-Aldrich	97%
4-dimethylaminopyridine (DMAP)	Aldrich	>99%
acetonitrile	VWR	≥99.9%
benzoic acid	Sigma-Aldrich	>99.9%
copper(I) chloride	Merck	99%
deuterated benzene (C_6D_6)	deuteron	99.8%
deuterated chloroform ($CDCl_3$)	deuteron	99.8%
deuterated dimethylsulfoxide (DMSO-d_6) over molecular sieve	VWR	99.80%
deuterated methanol (methanol-d_4)*	deutero	99.8%
deuterated tetrahydrofurane (THF-d_8)	deutero	99.8%
dimethylsulfoxide (DMSO)	Riedel-de Haën	>99.9%
gold(III) chloride trihydrate	Alfa Aesar	>99.99%
imidazole	Alfa Aesar	99%
iodine	KMF	99.5%
magnesium sulfate	Riedel-de Haën	>99.0%
malononitrile	Aldrich	99%
methansulfonyl chloride	Aldrich	>99.7%
N,*N'*-diisopropylcarbodiimide (DIC)	Iris Biotech	99%
N-boc-4-*trans*-hydroxy-*L*-proline (Boc-Hyp-OH)	Alfa Aesar	97%
N-boc-4-*trans*-hydroxy-*L*-proline methyl ester (Boc-Hyp-OMe)	Aldrich	>99%
N-methyl-2-pyrrolidon (NMP)*	Aldrich	99.5%
propargyl bromide solution in toluene*	Aldrich	80 wt%
sodium hydride (in mineral oil)	Aldrich	60 wt%
sodium hydrogencarbonate	FMF	≥99.9%
tert-butanol	Alfa Aesar	>99%
tert-butyl hydroperoxide in decane	Aldrich	5.5 M
tertra-n-butylammonium fluoride (TBAF) in THF*	Sigma-Aldrich	1 M

chemical	manufacturer	purity
tetra-butylammonium bromide (TBAB)	Janssen	99%
tetrahydrofurane (THF)	VWR	100.0%
toluene	VWR	≥99.9%
tosyl chloride	Sigma	98%
trans-2-cinnamaldehyde	Aldrich	>99%
trans-2-hexenal	Aldrich	98%
trans-2-octenal	Aldrich	>95%
trans-2-pentenal	Sigma-Aldrich	>95%
triethylamine	Merck	>99.5%
triphenylphosphine	Sigma-Aldrich	99%

*Bottle sealed with septum. If required, used for inert gas reactions without any prior treatment.

7.3 Experimental procedures for the synthesis

Prop-2-ynylmalononitrile **2** was prepared according to known procedure which was slightly modified. *Díez-Barra et al.*[229] presented a solvent-free setup with a phase transfer catalyst. Propargyl bromide could not be obtained in a pure form. Only solutions were accessible. Thus, an 80 wt% solution in toluene from Aldrich was used.

Malononitrile (4778.5 mg, 72.23 mmol, 4.03 eq) was melted at 60 °C. Sodium hydrogencarbonate (6013.2 mg, 71.58 mmol, 3.99 eq) and tetrabutylammonium bromide (604.8 mg, 0.0018 mmol, 0.10 eq) were added and the mixture was stirred at 60 °C for 40 minutes. Propargyl bromide in toluene (2.00 mL, 17.96 mmol, 1.00 eq) was added to the orange suspension. The reaction mixture turned red and was stirred at 60 °C for 22 hours. The red-brown reaction mixture was quenched by addition of water (40 mL). The suspension was diluted in dichloromethane (40 mL). After phase separation, the aqueous phase was extracted three times with dichloromethane (3x 40 mL). The combined organic layers were dried over magnesium sulfate and the volatile components were removed under reduced pressure. The crude product was purified by column chromatography (SiO_2, cyclohexane/ethyl acetate 4:1) to yield **2** as yellow oil (6723.5 mg, 37%). The spectroscopic data confirm the responded ones.[229]

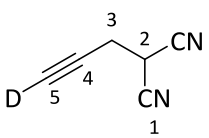

2_{deut}

2-D-prop-2-ynylmalononitrile **2_{deut}**. Alkyne **2** (1041.2 mg, 10.00 mmol, 1.00 eq) was dissolved in toluene (8 mL). Diaion WA30 free base (1520.0 mg, 152 mg/mmol) and deuterium oxide (40 mL) were added to the yellow solution. The reaction mixture was stirred for 21 hours at 50 °C. The base's beads turned from colorless to red within minutes. Then the base was filtered off. The aqueous phase was extracted with (non-deuterated) ethyl acetate (3x 30 mL). The combined organic layers were dried over magnesium sulfate and the volatile components were removed under reduced pressure. The amount of deuterated product was determined by GC-coupled EI-MS measurements in dichloromethane. **2_{deut}** was obtained as dark-brown oil (836.3 mg, 80%, 94% deuterated). ^{1}H NMR (700 MHz, $CDCl_3$, 298 K, δ in ppm): 3.93 (t, 1H, H-2, $^3J_{2,3}$ = 6.8 Hz), 2.96 (d, 2H, H-3, $^3J_{2,3}$ = 6.8 Hz). ^{13}C NMR (175 MHz, $CDCl_3$, 298 K, δ in

ppm): 111.4 (C-1), 75.0 (C-4), 74.6* (C-5), 23.1 (C-3), 22.1 (C-2). EI-MS *m/z*: $[M]^{+\cdot}$, calc. for $[C_6H_3DN_2]^{+\cdot}$ 105.04, found 105.15 (appendix, figure 9.2).

*The second signal at 74.6 ppm is a triplet due to the deuterium bound to this carbon atom.

2-Phenyl-prop-2-ynylmalononitrile **2$_{Ph}$** was prepared according to known procedure.[231]

Cyclopentene carbaldehydes **6$_A$**, **6$_B$**, **6$_C$** and **6$_E$** were prepared according to known procedure.[224]

*Due to purification problems, the exact amount of **6$_E$** could not be determined. Cyclopentene carbaldehydes **6$_E$** was obtained as yellow oil (12%). Since the amount of product were too little for an ^{1}H NMR characterization, the molecule was confirmed by mass spectrometry. EI-MS *m/z*: $[M]^{+\cdot}$, calc. for $[C_{17}H_{17}N_3O]^{+\cdot}$ 279.14, found 279.30. ESI-MS(+) *m/z*: $[M+H]^+$, calc. for $[C_{17}H_{17}N_3O+H]^+$ 280.14, found 280.18.

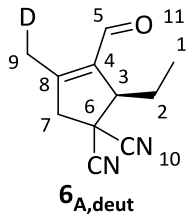

6$_{A,deut}$

Cyclopentene carbaldehyde **6$_{A,deut}$** was prepared in accordance with the procedure of *Jensen et al.*[224] The deuteration rate was determined by GC-coupled EI-MS. (31%, 56% deuterated). ^{1}H NMR (500 MHz, $CDCl_3$, 298 K, δ in ppm): 9.98 (s, 1H, H-5), 3.62-3.59 (m, 1H, H-3), 3.37-3.18 (m, 2H, H-7), 2.23-2.19 (m, 2H, H-9), 2.06 (dqd, 1H, H-2a, $^2J_{2a,2b}$ = 15.1 Hz, $^3J_{1,2a}$ = 7.5 Hz, $^3J_{2a,3}$ = 4.6 Hz), 1.81 (dqd, 1H, H-2b, $^2J_{2a,2b}$ = 15.1 Hz, $^3J_{1,2b}$ = $^3J_{2b,3}$ = 7.5 Hz). ^{13}C NMR (125 MHz, $CDCl_3$, 298 K, δ in ppm): 186.3 (C-5), 154.7 (C-8), 137.2 (C-4), 116.7 (C-10a), 114.1 (C-10b), 55.1 (C-3), 49.8 (C-7), 36.0 (C-6), 23.7 (C-2), 14.1 (C-9), 13.9* (C-9), 11.2 (C-1). EI-MS *m/z*: $[M]^{+\cdot}$, calc. for $[C_{11}H_{11}DN_2O]^{+\cdot}$ 189.10, found 189.20 (appendix, figure 9.3).

*The second signal at 13.9 ppm is induced by the deuteration of the methyl group. This signal is a triplet.

Vinyl product **5$_{A,Ph}$** and cyclopentene carbaldehyde **6$_{A,Ph}$** were prepared in accordance with the procedure of *Jensen et al.*[224] Alkyne **2$_{Ph}$** (225.6 mg, 1.25 mmol, 1.00 eq), base catalyst **3** (77.0 mg, 0.13 mmol, 0.10 eq), [Bis(trifluoromethanesulfonyl)imidate](triphenylphosphine)gold(I) in toluene (49.09 mg, 0.03 mmol, 0.03 eq) and benzoic acid (15.7 mg, 0.13 mmol, 0.10 eq) were dissolved in toluene (2.5 mL). *trans*-2-Pentenal **1$_A$** (0.17 mL, 1.63 mmol, 1.30 eq) was added to start the reaction. The yellow solution turned red within hours and was stirred for four days. The mixture was separated by a preparative TLC (SiO_2, cyclohexane/ethyl acetate/methanol 8:1:1).*

*Due to purification problems, the exact amount of both products could not be determined. Cyclopentene carbaldehyde **6$_{A,Ph}$** was obtained as colorless oil (28.8 mg, 9%). Both substances were detected by GC-coupled EI-MS. For **6$_{A,Ph}$** EI-MS *m/z*: $[M]^{+\cdot}$, calc. for $[C_{17}H_{16}N_2O]^{+\cdot}$ 264.13, found 264.20 (chapter 3.2.2, figure 3.2a). For **5$_{A,Ph(E)}$** EI-MS *m/z*: $[M]^{+\cdot}$, calc. for $[C_{17}H_{16}N_2O]^{+\cdot}$ 264.13, found 264.20 (chapter 3.2.2, figure 3.2b).

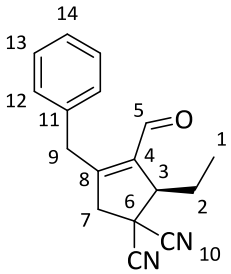

6$_{A,Ph}$

Cyclopentene carbaldehyde **6$_{A,Ph}$** was also investigated by NMR spectroscopy. ^{1}H NMR (500 MHz, $CDCl_3$, 298 K, δ in ppm): 10.14 (s, 1H, H-5), 7.37 (dd, 2H, H-13, $^{3}J_{13,14}$ = 7.3 Hz, $^{3}J_{12,13}$ = 7.1 Hz), 7.32 (t, 1H, H-14, $^{3}J_{13,14}$ = 7.3 Hz), 7.16 (d, 2H, H-12, $^{3}J_{12,13}$ = 7.1 Hz), 3.97 (S, 2H, H-9), 3.67 (dd, 1H, H-3, $^{3}J_{2b,3}$ = 6.2 Hz, $^{3}J_{2a,3}$ = 4.7 Hz), 3.20 (d, 1H, H-7a, $^{2}J_{7a,7b}$ = 18.2 Hz), 3.13 (d, 1H, H-7b, $^{3}J_{7a,7b}$ = 18.2 Hz), 2.07 (dqd, 1H, H-2a, $^{2}J_{2a,2b}$ = 15.0 Hz, $^{3}J_{1,2a}$ = 7.5 Hz, $^{3}J_{2a,3}$ = 4.7 Hz), 1.86 (dqd, 1H, H-2b, $^{2}J_{2a,2b}$ = 15.0 Hz, $^{3}J_{1,2b}$ = 7.5 Hz, $^{3}J_{2b,3}$ = 6.2 Hz), 1.04 (t, 3H, H-1, $^{3}J_{1,2}$ = 7.5 Hz). ^{13}C NMR (125 MHz, $CDCl_3$, 298 K, δ in ppm): 186.2 (C-5), 156.6 (C-4), 137.8 (C-8), 135.0 (C-11), 129.5 (C-13), 128.6 (C-12), 127.9 (C-14), 116.5 (C-10a), 113.9 (C-10b).

Michael product **4$_A$** was prepared according to known procedure[224] which was slightly modified. Alkyne **2** (260.0 mg, 2.50 mmol, 1.00 eq), base catalyst **3** (154.1 mg, 0.25 mmol, 0.10 eq) and benzoic acid (30.5 mg, 0.25 mmol, 0.10 eq) were dissolved in toluene (5 mL). *trans*-2-Pentenal **1$_A$** (0.34 mL, 3.25 mmol, 1.30 eq) was added to start the reaction. The yellow solution was stirred for 22 hours. The mixture was purified by column chromatography (SiO_2, cyclohexane/ethyl acetate 4:1) to give the product as yellow oil (392.6 mg, 83%). The spectroscopic data confirm the responding ones.[224]

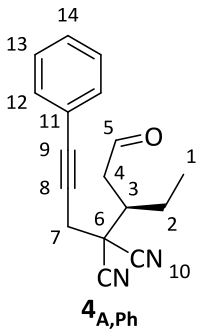

4$_{A,Ph}$

Michael product **4$_{A,Ph}$**. Alkyne **2$_{Ph}$** (45.0 mg, 2.50 mmol, 1.00 eq), base catalyst **3** (15.7 mg, 0.03 mmol, 0.10 eq) and benzoic acid (3.8 mg, 0.03 mmol, 0.10 eq) were dissolved in toluene (0.5 mL). *trans*-2-Pentenal **1$_A$** (0.03 mL, 0.32 mmol, 1.30 eq) was added to start the reaction. The yellow solution was stirred for 22 hours. The mixture was purified by column chromatography (SiO_2, cyclohexane/dichloromethane 2:1) to give the product as yellow oil (33.2 mg, 50%). ^{1}H NMR (700 MHz, $CDCl_3$, 298 K, δ in ppm): 9.86 (dd, 1H, H-5, $^{3}J_{4b,5}$ = 0.9 Hz, $^{3}J_{4a,5}$ = 0.7 Hz), 7.49-7.47 (m, 2H, H-12), 7.44-7.40 (m, 1H, H-13), 7.37-7.32 (m, 2H, H-14), 3.17 (d, 1H, H-7a, $^{2}J_{7a,7b}$ = 17.0 Hz), 3.14 (d, 1H, H-7b, $^{2}J_{7a,7b}$ = 17.0 Hz), 2.93-2.92 (m, 1H, H-3), 2.92 (ddd, 1H, H-4a, $^{2}J_{4a,4b}$ = 18.5 Hz, $^{3}J_{4a,3}$ = 4.4 Hz, $^{3}J_{4a,5}$ = 0.7 Hz), 2. 78 (ddd, 1H, H-4b, $^{2}J_{4a,4b}$ = 18.5 Hz, $^{3}J_{4b,3}$ = 6.4 Hz, $^{3}J_{4b,5}$ = 0.9 Hz), 1.94-1.90 (m, 1H, H-2a), 1.62-1.56 (m, 1H, H-2b), 1.04 (t, 3H, H-1, $^{3}J_{1,2}$ = 7.4 Hz). ^{13}C NMR (175 MHz, $CDCl_3$, 298 K, δ in ppm): 197.7 (C-5), 132.1 (C-12), 129.3 (C-14), 128.5 (C-13), 121.7 (C-11), 114.5 (C-10a), 114.4 (C-10b), 87.5 (C-9), 79.4 (C-8), 44.7 (C-4), 42.3 (C-6), 38.9 (C-3), 28.1 (C-7), 24.8 (C-2), 11.6 (C-1). EI-MS *m/z*: $[M]^{+\cdot}$, calc. for $[C_{17}H_{16}N_2O]^{+\cdot}$ 264.13, found 264.20 (chapter 3.2.2, figure 3.2c).

^{t}Bu-Boc-Hyp-OH **7** was prepared according to known procedure[86,241] which was slightly modified. Copper(I) chloride (148.6 mg, 1.50 mmol, 0.10 eq) and diisopropyl carbodiamide (14.0 mL, 90.41 mmol, 6.03 eq) were filled in a Schlenk flask under argon. *Tert*-butanol was heated to 30 °C for melting and added (10.0 mL, 104.56 mmol, 6.97 eq). The yellow-green suspension was stirred for three days at room temperature.* Then Boc-Hyp-OH (3458.1 mg, 14.98 mmol, 1.00 eq) and dry dichloromethane (60 mL) were added. The reaction mixture was stirred for two days at room temperature.* The white solid was filtered over Celite and washed with ice-cooled dichloromethane (100 mL). The volatile components were removed under reduced pressure. The green crude was purified by column chromatography (SiO_2, cyclohexane/ethyl acetate 1:1) to give the product as colorless solid (4301.0 mg, 99.8%).* The spectroscopic data confirm the responded ones.[86]

*The room temperature varied dependent on the season. The yields obtained were highly temperature-dependent. Winter: 16-18 °C, 99.8% yield. Summer: 25-32 °C, 15% yield. Summer with cooled Schlenk flask: 18-22 °C, 67% yield.

^{t}Bu-Boc-Hyp-OMes $\mathbf{8_A}$[86] and ^{t}Bu-Boc-Hyp-OTos $\mathbf{8_B}$[242] were prepared according to literature.

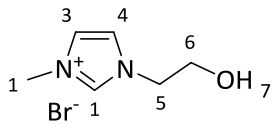

9

MeIm-C_2-OH **9**. 1-Methyl imidazole (0.79 mL, 9.96 mmol, 1.00 eq) and 2-bromoethanol (0.71 mL, 10.02 mmol, 1.01 eq) were filled in a two-neck flask with a condenser under argon. The reaction mixture was stirred for six days at 60 °C. The remaining volatile substrates were removed under reduced pressure at 60 °C. The product was obtained as colorless solid (1946.7 mg, 95%). ^{1}H NMR (500 MHz, DMSO-d_6, 298 K, δ in ppm): 9.11-9.09 (m, 1H, H-2), 7.73-7.72 (m, 1H, H-3), 7.70-7.69 (m, 1H, H-4), 5.16 (t, 1H, H-7, $^{3}J_{6,7}$ = 5.2 Hz), 4.21 (2H, H-5. $^{3}J_{5,6}$ = 4.9 Hz), 3.86 (s, 3H, H-1), 3.72 (dt, 2H, H-6, $^{3}J_{6,7}$ = 5.2 Hz, $^{3}J_{5,6}$ = 4.9 Hz). ^{13}C NMR (125 MHz, DMSO-d_6, 298 K, δ in ppm): 136.8 (C-2), 123.9 (C-3), 122.7 (C-4), 59.3 (C-6), 51.6 (C-5), 35.6 (C-1). HR ESI-MS *m/z*: $[M+Na]^{+\cdot}$, calc. for $[C_6H_{11}N_2O]^{+\cdot}$ 127.0866, found 127.0863.

C_4-OMes **15**[243] was prepared according to literature.

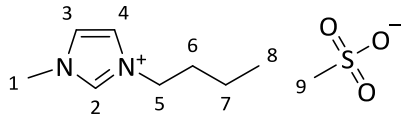

16

MeIm-C_4-OMes **16**. 1-Methyl imidazole (0.76 mL, 2.00 mmol, 1.00 eq) and C_4-OMes **15** (0.28 mL, 2.00 mmol, 1.00 eq) were filled in a two-neck flask with a condenser under argon. The reaction mixture was stirred for four days at 60 °C. ^{1}H NMR and ^{13}C NMR showed no evidence of the substrates anymore. Further work-up was not required. ^{1}H NMR (700 MHz, $CDCl_3$, 298 K, δ in ppm): 9.89 (dd, 1H, H-2, $^{3}J_{2,3}$ = $^{4}J_{2,4}$ = 1.8 Hz), 7.43 (dd, 1H, H-3, $^{3}J_{2,3}$ = $^{3}J_{3,4}$ = 1.8 Hz), 7.32 (dd, 1H, H-4, $^{3}J_{3,4}$ = $^{4}J_{2,4}$ = 1.8 Hz), 4.24 (t, 2H, H-5, $^{3}J_{5,6}$ = 7.4 Hz), 4.02 (s, 3H, H-1), 2.76 (s, 3H, H-9), 1.84 (tt, 2H, H-6, $^{3}J_{5,6}$ = $^{3}J_{6,7}$ = 7.4 Hz), 1.34 (tq, 2H, H-7, $^{3}J_{6,7}$ = $^{3}J_{7,8}$ = 7.4 Hz), 0.93 (t, 3H, H-8, $^{3}J_{7,8}$ = 7.4 Hz). ^{13}C NMR (175 MHz, $CDCl_3$, 298 K, δ in ppm): 138.3 (C-2), 123.6 (C-3), 121.9 (C-4), 49.8 (C-5), 39.8 (C-9), 36.1 (C-1), 32.2 (C-6), 19.5 (C-7), 13.5 (C-8). ESI-MS(+) *m/z*: $[M]^{+}$, calc. for $[C_8H_{15}N_2]^{+}$ 139.12, found 139.24.

TBSO-C_4-I **18**[245] was prepared according to literature.

^{t}Bu-Boc-Hyp-O-C_4-OTBS **14**. Sodium hydride (240.1 mg, 6.00 mmol, 2.00 eq) was filled in a two-neck flask with a condenser under argon and dissolved in dry dimethylsulfoxide (30 mL) at 60 °C. ^{t}Bu-Boc-Hyp-OH **7** (862.1 mg, 3.00 mmol, 1.00 eq) was added and the mixture was stirred for 90 minutes at 60 °C. Then TBSO-C_4-I **18** (0.78 mL, 3.00 mmol, 1.00 eq) was added and the orange reaction mixture was stirred for five days at 60 °C. It turned red and was quenched by addition of water (30 mL). Water was removed under reduced pressure. Dimethylsulfoxide was removed by vacuum distillation at 60 °C. Thereafter, water (30 mL) was added again. The aqueous phase was extracted with dichloromethane (3x 30 mL). The combined organic layers were dried over magnesium sulfate and the volatile components were removed under reduced pressure. The crude (817.9 mg) was used as obtained. The formation of the product was confirmed by ESI-MS measurements. ESI-MS(+) *m/z*: $[M+Na]^{+}$, calc. for $[C_{24}H_{47}NNaO_6Si]^{+}$ 496.31, found 496.35 (figure 4.4a).

^{t}Bu-Boc-Hyp-O-C_4-OH **20**. ^{t}Bu-Boc-Hyp-O-C_4-OTBS **14** (crude, 200.2 mg, 0.42 mmol, 1.00 eq) was dissolved in tetrahydrofurane. A 1M *tertra*-n-butylammonium fluoride solution in tetrahydrofurane was added (2.11 mL, 2.11 mmol, 5.00 eq). The reaction mixture turned red immediately. It was stirred for one hour. Then it was washed with water (20 mL) and saturated sodium chloride solution (15 mL). The aqueous phase was extracted with ethyl acetate (3x 40 mL). The combined organic layers were dried over magnesium sulfate and the volatile components were removed under reduced pressure. For filtration, the extraction crude (324.1 mg) was applied on dry silica (3.24 g, 2 cm height) and washed down with ethyl acetate (65 mL). The crude (95.3 mg) was used as obtained. The formation of the product was confirmed by ESI-MS measurements. ESI-MS(+) *m*/*z*: $[M+Na]^+$, calc. for $[C_{18}H_{33}NNaO_6]^+$ 282.22, found 282.00 (figure 4.6b).

^{t}Bu-Boc-Hyp-O-C_4-OMes **21**. ^{t}Bu-Boc-Hyp-O-C_4-OH **20** (crude, 95.3 mg, 0.27 mmol, 1.00 eq), was dissolved in dichloromethane (1.2 mL). Cooled with ice, triethylamine (0.15 mL, 0.66 mmol, 2.50 eq) was added slowly. After 15 minutes methanesulfonyl chloride (0.04 mL, 0.53 mmol, 2.00 eq) was added slowly. The reaction was stirred overnight. Thereby, the ice bath was not renewed and the temperature reached room temperature. The reaction was quenched by the addition of saturated sodium carbonate solution (2 mL). The aqueous phase was extracted with dichloromethane (3x 5 mL). The combined organic layers were dried over magnesium sulfate and the volatile components were removed under reduced pressure. The crude was purified by column chromatography (SiO_2, cyclohexane/ethyl acetate 49:1 + 5% methanol) to give the product as colorless solid (11.7 mg, 10%). The formation of the product was confirmed by ESI-MS measurements. ESI-MS(+) *m*/*z*: $[M+Na]^+$, calc. for $[C_{19}H_{35}NNaO_8S]^+$ 460.20, found 460.20 (figure 4.9).*

*The spectrometric data show that the product is still contaminated with unidentified species. The expected yield is less than 5%.

4-*tert*-Butylphenyl propiolate **32** was prepared according to the literature.[13]

7.4 Experimental procedures for the ESI-MS and GC-coupled EI-MS experiments of chapter 3 and 4

For the ESI-MS measurements, small samples of 50 µL were taken time-dependently and directly from the reaction solutions, diluted with 5.0 mL acetonitrile and fed into the spectrometer in timely manner. For the GC monitoring, samples of 50 µL were taken time-dependently and directly from the solution. The polar components were filtered off by a small silica column (0.6 cm diameter) of about 1 cm height and dichloromethane (1.0-1.5 mL). Then the sample was fed into the device in timely manner.

7.4.1 For chapter 3.3, 3.4 and 3.7

Procedure A

The overall reactions (reaction 3.14, 3.15, 3.16, 3.17, 3.18 and 3.19) were performed according to *Jensen et al.*[224] The alkyne (0.250 mmol, 1.00 eq), base catalyst **3** (15.4 mg, 0.025 mmol, 0.10 eq), [Bis(trifluoromethanesulfonyl)imidate](triphenylphosphine)gold(I) in toluene (9.8 mg, 0.006 mmol, 0.03 eq) and benzoic acid (3.1 mg, 0.025 mmol, 0.10 eq) were dissolved in 0.5 mL toluene. In case of reaction 3.20, the original ratios of all reactants were doubled compared to alkyne $\mathbf{2_{Ph}}$. The aldehyde (0.325 mmol, 1.30 eq) was added to start the reaction.

7.4.2 For chapter 3.5

Procedure B

The Michael additions (reaction 3.21 and 3.32) were performed according to *Jensen et al.*[224] with slight modification. The alkyne (0.250 mmol, 1.00 eq), base catalyst **3** (15.4 mg, 0.025 mmol, 0.10 eq) and benzoic acid (3.1 mg, 0.025 mmol, 0.10 eq) were dissolved in 0.5 mL toluene. *trans*-2-Pentenal $\mathbf{1_A}$ (0.033 mL, 0.325 mmol, 1.30 eq) was added to start the reaction.

Procedure C

The 5-*exo*-*dig*-cyclizations (reaction 3.23) were performed according to *Jensen et al.*[224] Michael product $\mathbf{4_A}$ (47.1 mg, 0.250 mml, 1.00 eq), base catalyst **3** (15.4 mg, 0.025 mmol, 0.10 eq), [Bis(trifluoro-methanesulfonyl)imidate](triphenylphosphine)gold(I) in toluene (9.8 mg, 0.006 mmol, 0.03 eq) and benzoic acid (3.1 mg, 0.025 mmol, 0.10 eq) were dissolved in 0.5 mL toluene to start the reaction.

7.4.3 For chapter 3.6

Procedure D

For the base exchange experiments (reaction 3.24, 3.25 and 3.26), cyclization reactions were prepared analogous to the usual procedure C with slight modification. Michael product $\mathbf{4_A}$, the [Bis(trifluoromethanesulfonyl)imidate] (triphenylphosphine)gold(I) in toluene (49.09 mg, 0.03 mmol, 0.03 eq) and benzoic acid (3.1 mg, 0.025 mmol, 0.10 eq) were dissolved in toluene to start the reaction. In case of reaction 3.25 pyridine (0.002 mL, 0.025 mmol, 0.10 eq) in case of reaction 3.26 triethylamine (0.003 mL, 0.025 mmol, 0.10 eq) was added. Small samples of 50 µL were taken time-dependently, diluted with 5.0 mL acetonitrile and fed into the spectrometer in timely manner.

7.4.4 For chapter 3.7

Procedure E

For the 'acid' (reaction 3.27, 3.29, 3.31 and 9.1) and 'base' reactions (reaction 3.28, 3.30 and 3.32), 10 mol% (0.10 eq) pyridine or instead of 10 mol% 50 mol% (0.50 eq) benzoic acid were added to the individual setup that was performed according to another procedure of ours.

7.4.5 For chapter 4.4

^{t}Bu-Boc-Hyp-O-C_4 **12** and ^{t}Bu-Boc-Hyp-O-C_8 **13**. Base (0.40 mmol, 2.00 eq) was filled in a two-neck flask with a condenser under argon and dissolved in dry solvent (2 mL) at 60 °C. Alcohol (0.20 mmol, 1.00 eq) was added and the mixture was stirred for 90 minutes at 60 °C. Then ^{t}Bu-Boc-Hyp-OMes $\mathbf{8_A}$ (73.1 mg, 0.20 mmol, 1.00 eq) was added and the orange reaction mixture was stirred for five days at 60 °C. It was quenched by addition of water (2 mL). Water was removed under reduced pressure. Dimethylsulfoxide was removed by vacuum distillation at 60 °C. A small sample was taken from the crude, dissolved in 0.5 mL acetonitrile and fed into the device.

Base was either sodium hydride in mineral oil or triethylamine. Solvent was either DMSO or NMP. Alcohol was either 1-butanol or 1-octanol.

^{t}Bu-Boc-Hyp-O-C_4-OTBS **14**. Sodium hydride (40.06 mg, 1.02 mmol, 2.03 eq) was filled in a two-neck flask with a condenser under argon and dissolved in dry dimethylsulfoxide (5 mL) at 60 °C. TBSO-C_4-OH (0.15 mL, 0.50 mmol, 1.00 eq) was added and the mixture was stirred for 90 minutes at 60 °C. Then ^{t}Bu-Boc-Hyp-OMes (182.8 mg, 0.50 mmol, 1.00 eq) was added and the orange reaction mixture was stirred for five days at 60 °C. It was quenched by addition of water (2 mL). Water was removed under reduced pressure. Dimethylsulfoxide was removed by vacuum distillation at 60 °C. A small sample was taken from the crude, dissolved in 0.5 mL acetonitrile and fed into the device.

7.5 Experimental procedures for the quantitative ^{1}H NMR and UHPLC-coupled UV/Vis experiments of chapter 5

The highly hygroscopic aurochloric acid was weighed into a baked out two-neck flask in a glove box under argon. The flask was sealed with two septa and transferred quickly under a continuous flow of argon to a condenser that was baked out and sealed before. The reaction was performed according to *Wegner et al.*[13]

4-*tert*-butylphenyl propiolate (10.12 mg, 0.500 mmol, 1.00 eq) was added to aurochloric acid trihydrate (1.00 mg, 0.025 mmol, 0.05 eq) in dry dichloroethane (1 mL) in a two-neck flask with a condenser under argon. The mixture was stirred at 60 °C for an exact amount of time.* The reaction was quenched by addition of 10 wt% aqueous thiosulfate solution (1 mL). The mixture was washed with water (5 mL) and diluted in dichloromethane (5 mL). After phase separation, the aqueous phase was extracted with

dichloromethane (3x 5 mL) and the combined organic layers were dried over magnesium sulfate. The volatile components were removed under reduced pressure.

*The individual reaction setups were stirred for different time periods. The shortest was five minutes, the longest 18 hours.

7.5.1 For chapter 5.2

Procedure F

For the ^{1}H NMR measurements with 10 mg/mL, a stock solution of isopropanol standard and dichloromethane-d_2 was prepared by adding 0.004 mL isopropanol to 1 mL dichloromethane-d_2. This ratio was chosen to ensure a comparable magnitude of protons for the isopropanol standard and the crude product's components. For the 10 mg/mL measurements the crude was dissolved completely in dichloromethane-d_2 or dichloromethane-d_2 with isopropanol to give a 10 mg/mL NMR sample. (400.1 MHz, 298 K, δ in ppm in DCM-d_2): substrate **31** 3.06 ppm, monomer **32** 6.40 ppm, dimer **33** 8.62 ppm. The ratios of the individual components were determined as described before.

Procedure G

For the ^{1}H NMR measurements with 1 mg/mL, a stock solution of isopropanol as internal standard and dichloromethane-d_2 was prepared by adding 0.004 mL isopropanol to 1 mL dichloromethane-d_2. This ratio was chosen to ensure a comparable magnitude of protons for the isopropanol standard and the crude product's components. For the 1 mg/mL measurements the crude product was completely dissolved in tetrahydrofurane. The concentration of the crude was exactly 0.5 mg/mL to ensure complete solvation. 1.000 mL of the solution was transferred into a flask. The solvent was removed under reduced pressure. Then the crude was redissolved in deuterated solvent (0.5 mL) to give a 1 mg/mL NMR sample. (400.1 MHz, 298 K, δ in ppm in DCM-d_2): Substrate **31** 3.06 ppm, monomer **32** 6.40 ppm, dimer **33** 8.62 ppm. The ratios of the individual components were determined as described before. (400.1 MHz, 298 K, δ in ppm in benzene-d_6): Substrate **31** 1.99 ppm, monomer **32** 5.96 ppm, dimer **33** 8.63 ppm. The ratios of the individual components were determined as described before. (400.1 MHz, 298 K, δ in ppm in THF-d_8): Substrate **31** 3.84 ppm, monomer **32** 6.31 ppm, dimer **33** 8.63 ppm. The ratios of the individual components were determined as described before.

7.5.2 For chapter 5.3

Procedure H

For the UHPLC coupled UV/Vis experiments of reaction 5.1 (normal setup), 4-*tert*-butylphenyl propiolate **31** (0.26 mg, 0.013 mmol, 1.00 eq) was added to aurochloric acid trihydrate (5.00 mg, 0.013 mmol, 0.05 eq) in dry dichloroethane (5 mL) in a two-neck flask with a condensor under argon. The mixture was stirred at 60 °C for an exact amount of time.* The reaction was quenched by addition of 10 wt% aqueous thiosulfate solution (5 mL). The mixture was washed with water (5 mL) and diluted in dichloromethane (8 mL). After phase separation, the aqueous phase was extracted with

dichloromethane (3x 8 mL) and the combined organic layers were dried over magnesium sulfate. The volatile components were removed under reduced pressure. The crude product was completely dissolved in exact 5 mL tetrahydrofurane. The solution was tempered to 20 °C and 2 µL were fed into the UHPLC device.

*The individual reaction setups were stirred for different time periods. The shortest was eight minutes, the longest 21 hours.

Procedure I

For the UHPLC-coupled UV/Vis experiments of reaction 5.2 (diluted setup), 4-*tert*-butylphenyl propiolate **31** (0.26 mg, 0.013 mmol, 1.00 eq) was added to aurochloric acid trihydrate (5.00 mg, 0.013 mmol, 0.05 eq) in dry dichloroethane (25 mL) in a two-neck flask with a condensor under argon. The mixture was stirred at 60 °C for an exact amount of time.* The reaction was quenched by addition of 10 wt% aqueous thiosulfate solution (15 mL). The mixture was washed with water (15 mL). After phase separation, the aqueous phase was extracted with dichloromethane (3x 25 mL) and the combined organic layers were dried over magnesium sulfate. The volatile components were removed under reduced pressure. The crude product was completely dissolved in exact 5 mL tetrahydrofurane. The solution was tempered to 20 °C and 2 µL were fed into the UHPLC device.

*The individual reaction setups were stirred for different time periods. Shortest was ten minutes, longest 22 hours.

8 Literature

[1] A. S. K. Hashmi, *Gold Bull.* **2004**, *37*, 51.

[2] A. S. K. Hashmi, *Angew. Chem. Int. Ed.* **2005**, *44*, 6990.

[3] B. Hammer, J. K. Norskov, *Nature* **1995**, *376*, 238.

[4] T. Ishida, T. Murayama, A. Taketoshi, M. Haruta, *Chem. Rev.* **2020**, *120*, 464.

[5] G. J. Hutchings, *J. Catal.* **1985**, *96*, 292.

[6] B. Nkosi, N. J. Coville, G. J. Hutchings, *J. Chem. Soc., Chem. Commun.* **1988**, 71.

[7] G. Malta, S. A. Kondrat, S. J. Freakley, C. J. Davies, L. Lu, S. Dawson, A. Thetford, E. K. Gibson, D. J. Morgan, W. Jones et al., *Science* **2017**, *355*, 1399.

[8] M. Haruta, T. Kobayashi, H. Sano, N. Yamada, *Chem. Lett.* **1987**, *16*, 405.

[9] M. Haruta, *J. Catal.* **1989**, *115*, 301.

[10] X. Zhao, M. Rudolph, A. S. K. Hashmi, *Chem. Commun.* **2019**, *55*, 12127.

[11] A. S. K. Hashmi, T. M. Frost, J. W. Bats, *J. Am. Chem. Soc.* **2000**, *122*, 11553.

[12] G. C. Bond, *Gold Bull.* **2016**, *49*, 53.

[13] H. A. Wegner, S. Ahles, M. Neuburger, *Chem. Eur. J.* **2008**, *14*, 11310.

[14] a) S. Kramer, *Synthesis* **2020**, *52*, 2017; b) A. Nijamudheen, A. Datta, *Chem. Eur. J.* **2020**, *26*, 1442.

[15] a) S. Bhunia, P. Ghosh, S. R. Patra, *Adv. Synth. Catal.* **2020**, *362*, 3664; b) M. Rigoulet, O. Du Thillaye Boullay, A. Amgoune, D. Bourissou, *Angew. Chem. Int. Ed.* **2020**, *59*, 16625; c) J. L. Mascareñas, I. Varela, F. López, *Acc. Chem. Res.* **2019**, *52*, 465.

[16] M. Lein, M. Rudolph, S. K. Hashmi, P. Schwerdtfeger, *Organometallics* **2010**, *29*, 2206.

[17] C. M. Hendrich, K. Sekine, T. Koshikawa, K. Tanaka, A. S. K. Hashmi, *Chem. Rev.* **2021**, *121*, 9113.

[18] A. Fürstner, P. W. Davies, *Angew. Chem. Int. Ed.* **2007**, *46*, 3410.

[19] H. A. Wegner, M. Auzias, *Angew. Chem. Int. Ed.* **2011**, *50*, 8236.

[20] Michalak, Kośnik, *Catalysts* **2019**, *9*, 890.

[21] a) J. M. Alonso, M. P. Muñoz, *Org. Lett.* **2019**, *21*, 7639; b) R. Casado, M. Contel, M. Laguna, P. Romero, S. Sanz, *J. Am. Chem. Soc.* **2003**, *125*, 11925; c) L. Nunes Dos Santos Comprido, J. E. M. N. Klein, G. Knizia, J. Kästner, A. S. K. Hashmi, *Chem. Eur. J.* **2017**, *23*, 10901; d) R. L. Reyes, T. Iwai, M. Sawamura, *Chem. Rev.* **2021**, *121*, 8926.

[22] P. H.-Y. Cheong, P. Morganelli, M. R. Luzung, K. N. Houk, F. D. Toste, *J. Am. Chem. Soc.* **2008**, *130*, 4517.

[23] A. Gómez-Suárez, S. P. Nolan, *Angew. Chem. Int. Ed.* **2012**, *51*, 8156.

[24] a) V. G. Andrianov, Y. T. Struchkov, E. R. Rossinskaja, *J. Chem. Soc., Chem. Commun.* **1973**, 338; b) A. N. Nesmeyanov, E. G. Perevalova, K. I. Grandberg, D. A. Lemenovskii, T. V. Baukova, O. B. Afanassova, *J. Organomet. Chem.* **1974**, *65*, 131.

[25] A. S. K. Hashmi, I. Braun, M. Rudolph, F. Rominger, *Organometallics* **2012**, *31*, 644.

[26] L. Ye, Y. Wang, D. H. Aue, L. Zhang, *J. Am. Chem. Soc.* **2012**, *134*, 31.

[27] T. J. Brown, D. Weber, M. R. Gagné, R. A. Widenhoefer, *J. Am. Chem. Soc.* **2012**, *134*, 9134.

[28] M. Hansmann, M. Rudolph, F. Rominger, A. S. K. Hashmi, *Angew. Chem. Int. Ed.* **2013**, *52*, 2593.

[29] J. Preindl, K. Jouvin, D. Laurich, G. Seidel, A. Fürstner, *Chem. Eur. J.* **2016**, *22*, 237.

[30] Y. Tang, J. Li, Y. Zhu, Y. Li, B. Yu, *J. Am. Chem. Soc.* **2013**, *135*, 18396.

[31] Bayrakdar, Tahani A. C. A., T. Scattolin, X. Ma, S. P. Nolan, *Chem. Soc. Rev.* **2020**, *49*, 7044.

[32] G. Seidel, C. W. Lehmann, A. Fürstner, *Angew. Chem. Int. Ed.* **2010**, *49*, 8466.

[33] K. A. Porter, A. Schier, H. Schmidbaur, *Organometallics* **2003**, *22*, 4922.

[34] D. Weber, M. A. Tarselli, M. R. Gagné, *Angew. Chem. Int. Ed.* **2009**, *48*, 5733.

[35] D. Weber, M. R. Gagné, *Chem. Sci.* **2013**, *47*, 335.

[36] A. Zhdanko, M. E. Maier, *Chem. Eur. J.* **2014**, *20*, 1918.

[37] A. S. K. Hashmi, M. Wieteck, I. Braun, M. Rudolph, F. Rominger, *Angew. Chem. Int. Ed.* **2012**, *51*, 10633.

[38] a) A. S. K. Hashmi, M. Wieteck, I. Braun, P. Nösel, L. Jongbloed, M. Rudolph, F. Rominger, *Adv. Synth. Catal.* **2012**, *354*, 555; b) M. H. Larsen, K. N. Houk, A. S. K. Hashmi, *J. Am. Chem. Soc.* **2015**, *137*, 10668.

[39] A. S. K. Hashmi, I. Braun, P. Nösel, J. Schädlich, M. Wieteck, M. Rudolph, F. Rominger, *Angew. Chem. Int. Ed.* **2012**, *51*, 4456.

[40] L. Jašíková, M. Anania, S. Hybelbauerová, J. Roithová, *J. Am. Chem. Soc.* **2015**, *137*, 13647.

[41] J. Roithová, Š. Janková, L. Jašíková, J. Váňa, S. Hybelbauerová, *Angew. Chem. Int. Ed.* **2012**, *51*, 8378.

[42] Q. Zhao, D. F. León Rayo, D. Campeau, M. Daenen, F. Gagosz, *Angew. Chem. Int. Ed.* **2018**, *57*, 13603.

[43] M. Anania, L. Jašíková, J. Zelenka, E. Shcherbachenko, J. Jašík, J. Roithová, *Chem. Sci.* **2019**, *11*, 980.

[44] A. Zhdanko, M. E. Maier, *Organometallics* **2013**, *32*, 2000.

[45] L. M. Aleese, A. Simon, T. B. McMahon, J.-M. Ortega, D. Scuderi, J. Lemaire, P. Maître, *Int. J. Mass Spectrom.* **2006**, *249-250*, 14.

[46] a) H.-B. Oh, C. Lin, H. Y. Hwang, H. Zhai, K. Breuker, V. Zabrouskov, B. K. Carpenter, F. W. McLafferty, *J. Am. Chem. Soc.* **2005**, *127*, 4076; b) J. R. Eyler, *Mass Spectrom. Rev.* **2009**, *28*, 448.

[47] J. Roithová, *Chem. Soc. Rev.* **2012**, *41*, 547.

[48] a) M. Anania, L. Jašíková, J. Jašík, J. Roithová, *Org. Biomol. Chem.* **2017**, *15*, 7841; b) J. Schulz, J. Jašík, A. Gray, J. Roithová, *Chem. Eur. J.* **2016**, *22*, 9827.

[49] M. Lu, Y. Su, P. Zhao, X. Ye, Y. Cai, X. Shi, E. Masson, F. Li, J. L. Campbell, H. Chen, *Chem. Eur. J.* **2018**, *24*, 2144.

[50] A. J. Arduengo, R. L. Harlow, M. Kline, *J. Am. Chem. Soc.* **1991**, *113*, 361.

[51] a) S. K. Schneider, W. A. Herrmann, E. Herdtweck, *Z. Anorg. Allg. Chem.* **2003**, *629*, 2363; b) C. Nieto-Oberhuber, S. López, A. M. Echavarren, *J. Am. Chem. Soc.* **2005**, *127*, 6178; c) M. M. Díaz-Requejo, P. J. Pérez, *J. Organomet. Chem.* **2005**, *690*, 5441; d) P. de Frémont, N. M. Scott, E. D. Stevens, S. P. Nolan, *Organometallics* **2005**, *24*, 2411.

[52] a) J.-J. Jiang, M.-K. Wong, *Chemistry, an Asian journal* **2021**, *16*, 364; b) J.-Q. Zhang, Y. Liu, X.-W. Wang, L. Zhang, *Organometallics* **2019**, *38*, 3931.

[53] F. Glorius, *N-Heterocyclic Carbenes in Transition Metal Catalysis*, Springer, Berlin, Heidelberg, **2007**.

[54] F. E. Hahn, M. C. Jahnke, *Angew. Chem. Int. Ed.* **2008**, *47*, 3122.

[55] M. Melaimi, M. Soleilhavoup, G. Bertrand, *Angew. Chem. Int. Ed.* **2010**, *49*, 8810.

[56] T. Dröge, F. Glorius, *Angew. Chem. Int. Ed.* **2010**, *49*, 6940.

[57] N. Marion, S. P. Nolan, *Chem. Soc. Rev.* **2008**, *37*, 1776.

[58] a) A. S. K. Hashmi, G. J. Hutchings, *Angew. Chem. Int. Ed.* **2006**, *45*, 7896; b) A. S. K. Hashmi, *Chem. Rev.* **2007**, *107*, 3180.

[59] a) M. C. Gimeno, A. Laguna, *Chem. Rev.* **1997**, *97*, 511; b) D. J. Gorin, F. D. Toste, *Nature* **2007**, *446*, 395; c) A. S. K. Hashmi, *Angew. Chem. Int. Ed.* **2010**, *49*, 5232.

[60] M. H. Aukland, B. List, *Pure Appl. Chem.* **2021**, *93*, 1371.

[61] B. List, R. A. Lerner, C. F. Barbas, *J. Am. Chem. Soc.* **2000**, *122*, 2395.

[62] K. A. Ahrendt, C. J. Borths, D. W. C. MacMillan, *J. Am. Chem. Soc.* **2000**, *122*, 4243.

[63] T. Akiyama, I. Ojima (Eds.) *Catalytic asymmetric synthesis*, Wiley, Hoboken, **2022**.

[64] The Nobel Prize in Chemistry 2021, *https://www.nobelprize.org/prizes/chemistry/2021/summary/*, accessed 2022-07-13.

[65] S. Bertelsen, K. A. Jørgensen, *Chem. Soc. Rev.* **2009**, *38*, 2178.

[66] a) D. Krištofíková, V. Modrocká, M. Mečiarová, R. Šebesta, *ChemSusChem* **2020**, *13*, 2828; b) Y.-B. Wang, B. Tan, *Acc. Chem. Res.* **2018**, *51*, 534.
[67] a) Z. G. Hajos, D. R. Parrish, *J. Org. Chem.* **1974**, *39*, 1615; b) U. Eder, G. Sauer, R. Wiechert, *Angew. Chem. Int. Ed.* **1971**, *10*, 496.
[68] F. Giacalone, M. Gruttadauria, P. Agrigento, R. Noto, *Chem. Soc. Rev.* **2012**, *41*, 2406.
[69] D. W. C. MacMillan, *Nature* **2008**, *455*, 304.
[70] T. Govender, P. I. Arvidsson, G. E. M. Maguire, H. G. Kruger, T. Naicker, *Chem. Rev.* **2016**, *116*, 9375.
[71] V. Oliveira, M. Cardoso, L. Forezi, *Catalysts* **2018**, *8*, 605.
[72] I. R. Shaikh, *J. Catal.* **2014**, *2014*, 1.
[73] G. Anilkumar, S. Saranya, *Green Organic Reactions*, Springer, Singapore, **2021**.
[74] P. I. Dalko, L. Moisan, *Angew. Chem. Int. Ed.* **2004**, *43*, 5138.
[75] F. An, B. Maji, E. Min, A. R. Ofial, H. Mayr, *J. Am. Chem. Soc.* **2020**, *142*, 1526.
[76] a) B. S. Vachan, M. Karuppasamy, P. Vinoth, S. Vivek Kumar, S. Perumal, V. Sridharan, J. C. Menéndez, *Adv. Synth. Catal.* **2020**, *362*, 87; b) D. G. Valapil, M. Kadagathur, N. Shankaraiah, *Eur. J. Org. Chem.* **2021**, *2021*, 5288.
[77] Y.-Q. Zou, F. M. Hörmann, T. Bach, *Chem. Soc. Rev.* **2018**, *47*, 278.
[78] S. Mukherjee, J. W. Yang, S. Hoffmann, B. List, *Chem. Rev.* **2007**, *107*, 5471.
[79] K. N. Houk, P. H.-Y. Cheong, *Nature* **2008**, *455*, 309.
[80] P. Dinér, A. Kjaersgaard, M. A. Lie, K. A. Jørgensen, *Chem. Eur. J.* **2008**, *14*, 122.
[81] J. Franzén, M. Marigo, D. Fielenbach, T. C. Wabnitz, A. Kjaersgaard, K. A. Jørgensen, *J. Am. Chem. Soc.* **2005**, *127*, 18296.
[82] D. Seebach, A. K. Beck, D. M. Badine, M. Limbach, A. Eschenmoser, A. M. Treasurywala, R. Hobi, W. Prikoszovich, B. Linder, *Helv. Chim. Acta* **2007**, *90*, 425.
[83] a) D. G. Blackmond, A. Moran, M. Hughes, A. Armstrong, *J. Am. Chem. Soc.* **2010**, *132*, 7598; b) N. Zotova, A. Franzke, A. Armstrong, D. G. Blackmond, *J. Am. Chem. Soc.* **2007**, *129*, 15100.
[84] a) M. B. Schmid, K. Zeitler, R. M. Gschwind, *Angew. Chem. Int. Ed.* **2010**, *49*, 4997; b) M. H. Haindl, J. Hioe, R. M. Gschwind, *J. Am. Chem. Soc.* **2015**, *137*, 12835.
[85] a) D. A. Bock, C. W. Lehmann, B. List, *Proc. Natl. Acad. Sci. U.S.A.* **2010**, *107*, 20636; b) T. Kanzian, S. Lakhdar, H. Mayr, *Angew. Chem. Int. Ed.* **2010**, *49*, 9526; c) A. K. Sharma, R. B. Sunoj, *Chem. Commun.* **2011**, *47*, 5759.
[86] J. A. Willms, R. Beel, M. L. Schmidt, C. Mundt, M. Engeser, *Beilstein J. Org. Chem.* **2014**, *10*, 2027.
[87] M. A. Ashley, J. S. Hirschi, J. A. Izzo, M. J. Vetticatt, *J. Am. Chem. Soc.* **2016**, *138*, 1756.
[88] J. A. Willms, J. Vidic, J. Barthelmes, V. Steinmetz, T. Bredow, P. Maître, M. Engeser, *Phys. Chem. Chem. Phys.* **2019**, *21*, 2578.
[89] L.-J. Yu, M. T. Blyth, M. L. Coote, *Top. Catal.* **2022**, *65*, 354.
[90] P. Dinér, M. Nielsen, M. Marigo, K. A. Jørgensen, *Angew. Chem. Int. Ed.* **2007**, *46*, 1983.
[91] D. Seebach, U. Grošelj, D. M. Badine, W. B. Schweizer, A. K. Beck, *Helv. Chim. Acta* **2008**, *91*, 1999.
[92] S. Bertelsen, M. Marigo, S. Brandes, P. Dinér, K. A. Jørgensen, *J. Am. Chem. Soc.* **2006**, *128*, 12973.
[93] L. Klier, F. Tur, P. H. Poulsen, K. A. Jørgensen, *Chem. Soc. Rev.* **2017**, *46*, 1080.
[94] S. Lakhdar, T. Tokuyasu, H. Mayr, *Angew. Chem. Int. Ed.* **2008**, *47*, 8723.
[95] S. Lakhdar, B. Maji, H. Mayr, *Angew. Chem. Int. Ed.* **2012**, *51*, 5739.
[96] H. Mayr, S. Lakhdar, B. Maji, A. R. Ofial, *Beilstein J. Org. Chem.* **2012**, *8*, 1458.
[97] a) M. Marigo, T. C. Wabnitz, D. Fielenbach, K. A. Jørgensen, *Angew. Chem. Int. Ed.* **2005**, *44*, 794; b) Y. Hayashi, H. Gotoh, T. Hayashi, M. Shoji, *Angew. Chem. Int. Ed.* **2005**, *44*, 4212.
[98] A. E. Allen, D. W. C. MacMillan, *Chem. Sci.* **2012**, *2012*, 633.
[99] U. B. Kim, J. Da Jung, H. J. Jeon, K. Rathwell, S. Lee, *Chem. Rev.* **2020**, *120*, 13382.

[100] R. A. Sheldon, *Chem. Soc. Rev.* **2012**, *41*, 1437.
[101] D.-F. Chen, L.-Z. Gong, *J. Am. Chem. Soc.* **2022**, *144*, 2415.
[102] B. Kim, Y. Kim, S. Y. Lee, *J. Am. Chem. Soc.* **2021**, *143*, 73.
[103] C. D.-T. Nielsen, J. D. Linfoot, A. F. Williams, A. C. Spivey, *Org. Biomol. Chem.* **2022**, *20*, 2764.
[104] A. Sinibaldi, V. Nori, A. Baschieri, F. Fini, A. Arcadi, A. Carlone, *Catalysts* **2019**, *9*, 928.
[105] V. Venugopalan Nair, D. Arunprasath, S. Pandidurai, G. Sekar, *Eur. J. Org. Chem.* **2022**, *2022*, e202200244.
[106] a) J. M. Lee, Y. Na, H. Han, S. Chang, *Chem. Soc. Rev.* **2004**, *33*, 302; b) N. T. Patil, V. S. Shinde, B. Gajula, *Org. Biomol. Chem.* **2012**, *10*, 211.
[107] T. B. Drew, J. W. Hoopes, T. Vermeulen (Eds.) *Advances in Chemical Engineering*, *Volume 5*, Academic Press, New York, **1964**.
[108] a) P. A. Dub, J. C. Gordon, *ACS Catal.* **2017**, *7*, 6635; b) L.-Q. Lu, X.-L. An, J.-R. Chen, W.-J. Xiao, *Synlett* **2012**, *23*, 490; c) J. Pan, X. L. Tian, S. Zaman, Z. Dong, H. Liu, H. S. Park, B. Y. Xia, *Batteries & Supercaps* **2019**, *2*, 336; d) B. Ramasamy, P. Ghosh, *Eur. J. Inorg. Chem.* **2016**, *2016*, 1448; e) A. M. Robinson, J. E. Hensley, J. W. Medlin, *ACS Catal.* **2016**, *6*, 5026; f) M. Shibasaki, M. Kanai, S. Matsunaga, N. Kumagai, *Acc. Chem. Res.* **2009**, *42*, 1117.
[109] K. Itoh, S. Kanemasa, *J. Am. Chem. Soc.* **2002**, *124*, 13394.
[110] a) F. Chen, X. Feng, B. Qin, G. Zhang, Y. Jiang, *Org. Lett.* **2003**, *5*, 949; b) Z. Chen, Q.-Q. Yang, W. Du, Y.-C. Chen, *Tetrahedron* **2022**, *2*, 100017; c) H. Noda, K. Motokura, W.-J. Chun, A. Miyaji, S. Yamaguchi, T. Baba, *Catal. Sci. Technol.* **2015**, *5*, 2714; d) Z.-X. Wang, Z. Zhou, W. Xiao, Q. Ouyang, W. Du, Y.-C. Chen, *Chem. Eur. J.* **2017**, *23*, 10678.
[111] a) P. Bellotti, M. Koy, C. Gutheil, S. Heuvel, F. Glorius, *Chem. Sci.* **2020**, *12*, 1810; b) Y. Huang, A. M. Walji, C. H. Larsen, D. W. C. MacMillan, *J. Am. Chem. Soc.* **2005**, *127*, 15051; c) D. Moock, T. Wagener, T. Hu, T. Gallagher, F. Glorius, *Angew. Chem. Int. Ed.* **2021**, *60*, 13677.
[112] a) C. Arroniz, G. Chaubet, E. A. Anderson, *ACS Catal.* **2018**, *8*, 8290; b) C. Chapman, C. Frost, *Synthesis* **2007**, *2007*, 1; c) C.-Y. Tan, H. Lu, J.-L. Zhang, J.-Y. Liu, P.-F. Xu, *J. Org. Chem.* **2020**, *85*, 594.
[113] a) L. T. Ball, T. J. A. Corrie, A. J. Cresswell, G. C. Lloyd-Jones, *ACS Catal.* **2020**, *10*, 10420; b) P. Qian, H. Guan, Y.-E. Wang, Q. Lu, F. Zhang, D. Xiong, P. J. Walsh, J. Mao, *Nat Commun.* **2021**, *12*, 6613.
[114] R. Peters, *Cooperative Catalysis*. *Designing Efficient Catalysts for Synthesis*, Wiley-VCH, Weinheim, **2015**.
[115] S. Krautwald, D. Sarlah, M. A. Schafroth, E. M. Carreira, *Science* **2013**, *340*, 1065.
[116] S. M. Inamdar, V. S. Shinde, N. T. Patil, *Org. Biomol. Chem.* **2015**, *13*, 8116.
[117] a) N. Butt, G. Yang, W. Zhang, *Chem. Rec.* **2016**, *16*, 2683; b) Y. Deng, S. Kumar, H. Wang, *Chem. Commun.* **2014**, *50*, 4272.
[118] Z. Shao, H. Zhang, *Chem. Soc. Rev.* **2009**, *38*, 2745.
[119] S. Krautwald, E. M. Carreira, *J. Am. Chem. Soc.* **2017**, *139*, 5627.
[120] B. S. Donslund, T. K. Johansen, P. H. Poulsen, K. S. Halskov, K. A. Jørgensen, *Angew. Chem. Int. Ed.* **2015**, *54*, 13860.
[121] J. J. Thomson, *Philos. Mag.* **1911**, *21*, 225.
[122] A. O. Nier, *Int. J. Mass Spectrom.* **1990**, *100*, 1.
[123] A. J. Dempster, *Phys. Rev.* **1918**, *11*, 316.
[124] W. Bleakney, *Phys. Rev.* **1929**, *34*, 157.
[125] A. O. NIER, *Rev. Sci. Inst.* **1947**, *18*, 398.
[126] J. H. Gross, *Mass Spectrometry*, Springer International Publishing, Chambridge, **2017**.
[127] W. Paul, M. Raether, *Z. Phys.* **1955**, *140*, 262.
[128] W. Paul, H. Steinwedel, *Z. Naturforsch. A* **1953**, *8*, 448.

[129] W. Paul, *Angew. Chem. Int. Ed.* **1990**, *29*, 739.
[130] W. E. Stephens, *Phys. Rev.* **1946**, *69*, 691.
[131] Q. Hu, R. J. Noll, H. Li, A. Makarov, M. Hardman, R. Graham Cooks, *J. Mass Spectrom.* **2005**, *40*, 430.
[132] A. Makarov, *Anal. Chem.* **2000**, *72*, 1156.
[133] H. Mirzaei, M. Carrasco, *Modern Proteomics – Sample Preparation, Analysis and Practical Applications*, Springer International Publishing, Cham, **2016**.
[134] P. S. H. Wong, R. G. Cooks, *Curr. Sep.* **1997**, *16*, 85.
[135] M. Karas, U. Bahr, *Trends Anal. Chem.* **1990**, *9*, 321.
[136] H. R. Morris, T. Paxton, A. Dell, J. Langhorne, M. Berg, R. S. Bordoli, J. Hoyes, R. H. Bateman, *Rapid Commun. Mass Spectrom.* **1996**, *10*, 889.
[137] T. D. Märk, *Electron Impact Ionization*, Springer Wien, Vienna, **1985**.
[138] F. H. Field, *Electron Impact Phenomena*. *And the Properties of Gaseous Ions*, Elsevier Science, Burlington, **1957**.
[139] K. Habfast, *Massenspektrometrische Funktionselemente: Ionenquellen*, Wiley-VCH, Weinheim, **1968**.
[140] W. C. Wiley, I. H. McLaren, *Rev. Sci. Inst.* **1955**, *26*, 1150.
[141] a) W. Foci, *Int. J. Mass Spectrom.* **1969**, *3*, 285; b) O. A. Schaeffer, *Rev. Sci. Inst.* **1954**, *25*, 660.
[142] M. Karni, A. Mandelbaum, *Org. Mass Spectrom.* **1980**, *15*, 53.
[143] K. Wolkenstein, J. H. Gross, T. Oeser, H. F. Schöler, *Tetrahedron Lett.* **2002**, *43*, 1653.
[144] T. D. Märk, *Int. J. Mass Spectrom.* **1982**, *45*, 125.
[145] H. M. Rosenstock, *Int. J. Mass Spectrom.* **1976**, *20*, 139.
[146] NIST Chemistry WebBook, *http://webbook.nist.gov/*, accessed 2022-07-13.
[147] R. E. Honig, *J. Chem. Phys.* **1948**, *16*, 105.
[148] W. Lotz, *Z. Physik* **1967**, *206*, 205.
[149] a) R. Kondrat, *Int. J. Mass Spectrom.* **2001**, *212*, 89; b) F. W. McLafferty, *Int. J. Mass Spectrom.* **2001**, *212*, 81; c) J. D. Williams, D. J. Burinsky, *Int. J. Mass Spectrom.* **2001**, *212*, 111.
[150] R. S. Gohlke, *Anal. Chem.* **1959**, *31*, 535.
[151] A.T. James, A. J. P. Martin, *Biochem. J.* **1952**, *50*, 679.
[152] R. S. Gohlke, F. W. McLafferty, *J. Am. Soc. Mass Spectrom.* **1993**, *4*, 367.
[153] H.-J. Hübschmann, *Handbook of GC-MS*. *Fundamentals and applications*, Wiley-VCH, Weinheim, **2015**.
[154] K. D. Bartle, P. Myers, *Trends Anal. Chem.* **2002**, *21*, 547.
[155] W. H. McFadden, *J. Chromatogr. Sci.* **1979**, *17*, 2.
[156] a) C. Zhu, X. Pan, G. Li, C. Li, D. Wu, J. Tang, Y. Huang, L. Zou, L. Laghi, *Int. J. Mol. Sci.* **2022**, *23*, 11544; b) P. Lorenz, M. Bunse, I. Klaiber, J. Conrad, T. Laumann-Lipp, F. C. Stintzing, D. R. Kammerer, *Chem. Biodivers.* **2020**, *17*, e2000485.
[157] Z. Zhang, H. Chen, K. K. Chan, T. Budd, R. Ganapathi, *J. Chromatogr. B* **1999**, *728*, 85.
[158] M. Becker, F. Liebner, T. Rosenau, A. Potthast, *Talanta* **2013**, *115*, 642.
[159] N. W. Kwiecien, D. J. Bailey, M. J. P. Rush, J. S. Cole, A. Ulbrich, A. S. Hebert, M. S. Westphall, J. J. Coon, *Anal. Chem.* **2015**, *87*, 8328.
[160] G. van Erven, R. de Visser, D. W. H. Merkx, W. Strolenberg, P. de Gijsel, H. Gruppen, M. A. Kabel, *Anal. Chem.* **2017**, *89*, 10907.
[161] M. Dole, R. L. Hines, L. L. Mack, R. C. Mobley, L. D. Ferguson, M. B. Alice, *Macromolecules* **1968**, *1*, 96.

[162] a) H. P. Nguyen, K. A. Schug, *J. Sep. Sci.* **2008**, *31*, 1465; b) F. Rosu, S. Pirotte, E. de Pauw, V. Gabelica, *Int. J. Mass Spectrom.* **2006**, *253*, 156; c) M. Tsednee, Y.-C. Huang, Y.-R. Chen, K.-C. Yeh, *Sci. Rep.* **2016**, *6*, 26785.
[163] J. B. Fenn, *Angew. Chem. Int. Ed.* **2003**, *42*, 3871.
[164] P. Kebarle, U. H. Verkerk, *Mass Spectrom. Rev.* **2009**, *28*, 898.
[165] J. B. Fenn, M. Mann, C. K. Meng, S. F. Wong, C. M. Whitehouse, *Science* **1989**, *246*, 64.
[166] a) G. K. Poon, G. M. F. Bisset, P. Mistry, *J. Am. Soc. Mass Spectrom.* **1993**, *4*, 588; b) J. C. Traeger, *Int. J. Mass Spectrom.* **2000**, *200*, 387.
[167] a) Y. Cai, R. B. Cole, *Anal. Chem.* **2002**, *74*, 985; b) R. B. Cole, J. Zhu, *Rapid Commun. Mass Spectrom.* **1999**, *13*, 607; c) H. Wang, M. Cao, T. Li, L. Yang, Z. Duan, X. Zhou, G. Du, *Polymers* **2018**, *10*, 602; d) J. Zhu, R. B. Cole, *J. Am. Soc. Mass Spectrom.* **2000**, *11*, 932.
[168] D. Schröder, *Acc. Chem. Res.* **2012**, *45*, 1521.
[169] J. Zeleny, *Phys. Rev.* **1917**, *10*, 1.
[170] G. I. Taylor, *Proc. R. Soc. Lond. A* **1964**, *280*, 383.
[171] J. Gieniec, L. L. Mack, K. Nakamae, C. Gupta, V. Kumar, M. Dole, *Biomed. Mass Spectrom.* **1984**, *11*, 259.
[172] M. Yamashita, J. B. Fenn, *J. Phys. Chem.* **1984**, *88*, 4671.
[173] M. L. Alexandrov, L. N. Gall, N. V. Krasnov, V. I. Nikolaev, V. A. Pavlenko, V. A. Shkurov, *Rapid Commun. Mass Spectrom.* **2008**, *22*, 267.
[174] Y. A. Zolotov in *Russian Contributions to Analytical Chemistry*, Springer, Cham, **2018**, pp. 25–46.
[175] The Nobel Prize in Chemistry 2002, *https://www.nobelprize.org/prizes/chemistry/2002/summary/*, accessed 2022-07-26.
[176] A. P. Bruins, *Mass Spectrom. Rev.* **1991**, *10*, 53.
[177] P. Kebarle, L. Tang, *Anal. Chem.* **1993**, *65*, 972A-986A.
[178] A. P. Bruins, T. R. Covey, J. D. Henion, *Anal. Chem.* **1987**, *59*, 2642.
[179] T. R. Covey, R. F. Bonner, B. I. Shushan, J. Henion, *Rapid Commun. Mass Spectrom.* **1988**, *2*, 249.
[180] T. R. Covey, A. P. Bruins, J. D. Henion, *Biomedical Mass Spectrometry* **1988**, *23*, 178.
[181] M. G. Ikonomou, A. T. Blades, P. Kebarle, *Anal. Chem.* **1991**, *63*, 1989.
[182] J. Abian, *Biomedical Mass Spectrometry* **1999**, *34*, 157.
[183] S. A. Schaffer, K. Tang, G. A. Anderson, D. C. Prior, H. R. Udseth, R. D. Smith, *Rapid Commun. Mass Spectrom.* **1997**, *11*, 1813.
[184] S. A. Shaffer, D. C. Prior, G. A. Anderson, H. R. Udseth, R. D. Smith, *Anal. Chem.* **1998**, *70*, 4111.
[185] T. Kim, A. V. Tolmachev, R. Harkewicz, D. C. Prior, G. Anderson, H. R. Udseth, R. D. Smith, *Anal. Chem.* **2000**, *72*, 2247.
[186] Y. M. Ibrahim, M. E. Belov, A. V. Liyu, R. D. Smith, *Anal. Chem.* **2008**, *80*, 5367.
[187] Y. Ibrahim, M. E. Belov, A. V. Tolmachev, D. C. Prior, R. D. Smith, *Anal. Chem.* **2007**, *79*, 7845.
[188] M. S. Wilm, M. Mann, *Int. J. Mass Spectrom.* **1994**, *136*, 167.
[189] R. B. Cole, *J. Mass Spectrom.* **2000**, *35*, 763.
[190] L. Rayleigh, *Philos. Mag.* **1882**, *14*, 184.
[191] A. Gomez, K. Tang, *Phys. Fluids* **1994**, *6*, 404.
[192] L. L. Mack, P. Kralik, A. Rheude, M. Dole, *J. Chem. Phys.* **1970**, *52*, 4977.
[193] a) J. V. Iribarne, *J. Chem. Phys.* **1976**, *64*, 2287; b) B. A. Thomson, J. V. Iribarne, *J. Chem. Phys.* **1979**, *71*, 4451.
[194] M. Labowsky, J. B. Fenn, J. La Fernandez de Mora, *Anal. Chim. Acta* **2000**, *406*, 105.
[195] J. B. Fenn, *J. Am. Soc. Mass Spectrom.* **1993**, *4*, 524.
[196] J. B. Fenn, J. Rosell, C. K. Meng, *J. Am. Soc. Mass Spectrom.* **1997**, *8*, 1147.
[197] P. Liigand, J. Liigand, K. Kaupmees, A. Kruve, *Anal. Chim. Acta* **2021**, *1152*, 238117.

[198] N. B. Cech, C. G. Enke, *Mass Spectrom. Rev.* **2001**, *20*, 362.
[199] G. J. van Berkel, J. M. Quirke, R. A. Tigani, A. S. Dilley, T. R. Covey, *Anal. Chem.* **1998**, *70*, 1544.
[200] J. M. E. Quirke, C. L. Adams, G. J. van Berkel, *Anal. Chem.* **1994**, *66*, 1302.
[201] a) M. Oss, A. Kruve, K. Herodes, I. Leito, *Anal. Chem.* **2010**, *82*, 2865; b) K. R. Chalcraft, R. Lee, C. Mills, P. Britz-McKibbin, *Anal. Chem.* **2009**, *81*, 2506; c) A. Kruve, *Biomed. Mass Spectrom.* **2016**, *51*, 596; d) M. Ojakivi, J. Liigand, A. Kruve, *ChemistrySelect* **2018**, *3*, 335; e) J. Liigand, A. Kruve, P. Liigand, A. Laaniste, M. Girod, R. Antoine, I. Leito, *J. Am. Soc. Mass Spectrom.* **2015**, *26*, 1923.
[202] C. Marquez, J. O. Metzger, *Chem. Commun.* **2006**, *0*, 1539.
[203] M. N. Eberlin, *Eur. J. Mass Spectrom.* **2007**, *13*, 19.
[204] A. Teichert, A. Pfaltz, *Angew. Chem. Int. Ed.* **2008**, *47*, 3360.
[205] J. Zelenka, J. Roithová, *ChemBioChem* **2020**, *21*, 2232.
[206] a) V. Carrasco-Sanchez, M. J. Simirgiotis, L. S. Santos, *Molecules* **2009**, *14*, 3989; b) G. Guillena, M. C. Del Hita, C. Nájera, S. F. Viózquez, *J. Org. Chem.* **2008**, *73*, 5933; c) J. J. Haven, J. Vandenbergh, T. Junkers, *Chem. Commun.* **2015**, *51*, 4611; d) C. Hinderling, C. Adlhart, P. Chen, *Angew. Chem. Int. Ed.* **1998**, *37*, 2685; e) P. S. D. Robinson, G. N. Khairallah, G. Da Silva, H. Lioe, R. A. J. O'Hair, *Angew. Chem. Int. Ed.* **2012**, *51*, 3812.
[207] L. P. E. Yunker, R. L. Stoddard, J. S. McIndoe, *Biomed. Mass Spectrom.* **2014**, *49*, 1.
[208] K. L. Vikse, M. P. Woods, J. S. McIndoe, *Organometallics* **2010**, *29*, 6615.
[209] G. T. Thomas, S. Donnecke, I. C. Chagunda, J. S. McIndoe, *Chemistry Methods* **2022**, *2*.
[210] J. Luo, A. G. Oliver, J. S. McIndoe, *Dalton trans.* **2013**, *42*, 11312.
[211] a) C. Adlhart, P. Chen, *Helv. Chim. Acta* **2000**, *83*, 2192; b) F. F. D. Oliveira, M. R. dos Santos, P. M. Lalli, E. M. Schmidt, P. Bakuzis, A. A. M. Lapis, A. L. Monteiro, M. N. Eberlin, B. A. D. Neto, *J. Org. Chem.* **2011**, *76*, 10140.
[212] G. Verma, M. Mishra, *World J. Pharm. Res.* **2018**, *7*, 1170.
[213] A. Schnell, J. A. Willms, S. Nozinovic, M. Engeser, *Beilstein J. Org. Chem.* **2019**, *15*, 30.
[214] F. W. McLafferty, *Science* **1981**, *214*, 280.
[215] a) S. Crotti, M. Menicatti, M. Pallecchi, G. Bartolucci, *Mass Spectrom. Rev.* **2021**, e21757; b) Z. Gao, Y. He, Q. He, W. Wei, Y. Luo, Z. Ma, W. Chen, F. Chu, S. Zhang, Y. Liu et al., *Talanta* **2022**, *249*, 123674; c) Y. Huang, E. D. Dodds, *Anal. Chem.* **2015**, *87*, 5664; d) P. Waridel, J.-L. Wolfender, K. Ndjoko, K. R. Hobby, H. J. Major, K. Hostettmann, *J. Chromatogr. A* **2001**, *926*, 29.
[216] J. V. Johnson, R. A. Yost, P. E. Kelley, D. C. Bradford, *Anal. Chem.* **1990**, *62*, 2162.
[217] G. L. Glish, *Analyst* **1994**, *119*, 533.
[218] K. Levsen, H. Schwarz, *Angew. Chem. Int. Ed.* **1976**, *15*, 509.
[219] Y. O. Tsybin, M. Witt, G. Baykut, F. Kjeldsen, P. Håkansson, *Rapid Commun. Mass Spectrom.* **2003**, *17*, 1759.
[220] a) K. F. Haselmann, B. A. Budnik, F. Kjeldsen, M. L. Nielsen, J. V. Olsen, R. A. Zubarev, *Eur. J. Mass Spectrom.* **2002**, *8*, 117; b) B. A. Budnik, K. F. Haselmann, R. A. Zubarev, *Chem. Phys. Lett.* **2001**, *342*, 299; c) F. Kjeldsen, O. A. Silivra, I. A. Ivonin, K. F. Haselmann, M. Gorshkov, R. A. Zubarev, *Chem. Eur. J.* **2005**, *11*, 1803; d) I. Anusiewicz, M. Jasionowski, P. Skurski, J. Simons, *J. Phys. Chem.* **2005**, *109*, 11332.
[221] R. C. Dunbar, *Mass Spectrom. Rev.* **2004**, *23*, 127.
[222] F. W. McLafferty, P. F. Bente, R. Kornfeld, S.-C. Tsai, I. Howe, *J. Am. Chem. Soc.* **1973**, *95*, 2120.
[223] R. Guevremont, R. K. Boyd, *Rapid Commun. Mass Spectrom.* **1988**, *2*, 1.
[224] K. L. Jensen, P. T. Franke, C. Arróniz, S. Kobbelgaard, K. A. Jørgensen, *Chem. Eur. J.* **2010**, *16*, 1750.
[225] J. T. Binder, B. Crone, T. T. Haug, H. Menz, S. F. Kirsch, *Org. Lett.* **2008**, *10*, 1025.
[226] K. L. Jensen, G. Dickmeiss, H. Jiang, L. Albrecht, K. A. Jørgensen, *Acc. Chem. Res.* **2012**, *45*, 248.
[227] P. Melchiorre, K. A. Jørgensen, *J. Org. Chem.* **2003**, *68*, 4151.

[228] M. Nielsen, D. Worgull, T. Zweifel, B. Gschwend, S. Bertelsen, K. A. Jørgensen, *Chem. Commun.* **2011**, *47*, 632.
[229] E. Díez-Barra, A. de La Hoz, A. Moreno, P. Sánchez-Verdú, *J. Chem. Soc.* **1991**, 2589.
[230] T. Yamada, K. Park, Y. Monguchi, Y. Sawama, H. Sajiki, *RSC Adv.* **2015**, *5*, 92954.
[231] R. Schiller, M. Pour, H. Fáková, J. Kunes, I. Císarová, *J. Org. Chem.* **2004**, *69*, 6761.
[232] a) H. Morawetz in *Macromolecular Microsymposia-XII and XIII* (Ed.: B. Sedlácek), Elsevier Science, Burlington, **1974**, pp. 267–277; b) A. J. Kirby in *Advances in Physical Organic Chemistry* (Eds.: V. Gold, D. Bethell), Academic Press, **1980**, pp. 183–278.
[233] B. Neises, W. Steglich, *Angew. Chem. Int. Ed.* **1978**, *17*, 522.
[234] S. Kobialka, C. Müller-Tautges, M. T. S. Schmidt, G. Schnakenburg, O. Hollóczki, B. Kirchner, M. Engeser, *Inorg. Chem.* **2015**, *54*, 6100.
[235] M. T. S. Krause, *Dissertation*, Rheinische Friedrich-Wilhelms-Universität, Bonn, **2020**.
[236] S. Kobialka, *Dissertation*, Rheinische Friedrich-Wilhelms-Universität, Bonn, **2015**.
[237] R. Beel, *Diplomarbeit*, Rheinische Friedrich-Wilhelms-Universität, Bonn, **2010**.
[238] C. Mundt, *Diplomarbeit*, Rheinische Friedrich-Wilhelms-Universität, Bonn, **2012**.
[239] B. C. Ranu, S. Bhar, *Org. Prep. Proced. Int.* **1996**, *28*, 371.
[240] K. H. Schuppener, *Bachelorarbeit*, Rheinische Friedrich-Wilhelms-Universität, Bonn, **2016**.
[241] P. Chabaud, G. Pèpe, J. Courcambeck, M. Camplo, *Tetrahedron* **2005**, *61*, 3725.
[242] V. Hack, C. Reuter, R. Opitz, P. Schmieder, M. Beyermann, J.-M. Neudörfl, R. Kühne, H.-G. Schmalz, *Angew. Chem. Int. Ed.* **2013**, *52*, 9539.
[243] Y.-H. Chu, M.-F. Cheng, Y.-H. Chiang, *Sci. Rep.* **2020**, *10*, 18247.
[244] L. Dinkelborg, M. Berndt, M. Friebe, H. Schmitt-Willich, D. Suelzle, N. Koglin, *Synthesis of 18F-labelled L-glutamic acid derivatives for use in treatment of neoplasms*, Patent Number WO2009141091, Bayer Schering Pharma Aktiengesellschaft, Germany, **2009**.
[245] J. A. Forni, L. F. T. Novaes, R. Galaverna, J. C. Pastre, *Catal. Today* **2018**, *308*, 86.
[246] a) Y. Deng, Y. Zou, C.-P. H. Yang, K. N. Houk, A. B. Smith, *J. Org. Chem.* **2021**, *86*, 13583; b) Y. Kaburagi, Y. Kishi, *Org. Lett.* **2007**, *9*, 723; c) I. Paterson, R. D. M. Davies, R. Marquez, *Angew. Chem. Int. Ed.* **2001**, *40*, 603; d) J. Revol-Cavalier, V. Bultel-Poncé, A. Guy, T. Durand, C. Oger, J.-M. Galano, *Org. Lett.* **2020**, *22*, 7455; e) T. Xie, C. Zheng, K. Chen, H. He, S. Gao, *Angew. Chem. Int. Ed.* **2020**, *132*, 4360.
[247] W. Jin, J. D. Trzupek, T. J. Rayl, M. A. Broward, G. A. Vielhauer, S. J. Weir, I. Hwang, D. L. Boger, *J. Am. Chem. Soc.* **2007**, *129*, 15391.
[248] M. W. Dong, K. Zhang, *Trends Anal. Chem.* **2014**, *63*, 21.
[249] D. F. Swinehart, *J. Chem. Educ.* **1962**, *39*, 333.
[250] K. H. Schuppener, *Master Thesis*, Rheinische Friedrich-Wilhelms-Universität, Bonn, **2018**.
[251] W. L. F. Armarego, *Purification of laboratory chemicals*, Butterworth-Heinemann, Kidlington, Oxford, Cambridge, **2017**.

9 Appendix

9.1 List of abbreviations – General abbreviations

δ	chemical shift
λ	wavelength
A	analyte
Ar	argon
BIRD	blackbody infrared radiative dissociation
Boc	*tert*-butyloxycarbonyl
Boc-Hyp-OH	*N*-Boc-4-*trans*-hydroxy-*L*-proline
Boc-Hyp-OMe	*N*-Boc-4-*trans*-hydroxy-*L*-proline methyl ester
CID	collision-induced dissociation
CRM	charged residue model
d_i	deuterated protons (NMR)
DC	direct current
DCE	dichloroethane
DCM	dichloromethane
DEPT	distortionless enhancement by polarization transfer
DFT	density functional theory
DIC	*N,N'*-diisopropylcarbodiimide
DMAC	4(dimethylamino)cinnamaldehyde
DMAP	4-dimethylaminopyridine
DMSO	dimethylsulfoxide
EDD	electron detachment dissociation
EI	electron ionisation
Elec	electrophile
eq	equivalents
ESI	electrospray ionisation
ESI(+)	electrospray ionisation in positive mode
et al.	and others ('*et alii*')
et seq.	and following ('*et sequentes*')
ETD	electron transfer dissociation
GC	gas chromatography
HCT	high capacity ion trap
HOMO	highest occupied molecular orbital
HR	High resolution
I_{rel}	relative integral
I_{st}	standardised integral
IEM	ion evaporation model
IR	infrared
IRMPD	infrared multiphoton dissociation
IT	iron trap
L	ligand
LTQ	linear trap quadrupole
LUMO	lowest unoccupied molecular orbital
M	molar
m/z	mass-to-charge ratio
MeIm	1-Methyl imidazole
Mes	mesylate
mol%	mole percent
MS	mass spectrometry
MS/MS or MS^2	tandem mass spectrometry
MS^n	multi stage mass spectrometry
NHC	*N*-hetreocyicloc carbene
NMP	*N*-methyl-2-pyrrolidon
NMR	nuclear magnetic resonance
Nuc	nucleophile

pH	negative decadic logarithm of the proton concentration
pK_A	negative decadic logarithm of the acid constant
ppm	parts per million
PTM	posttranslational modification
Q	quadrupole
Q/TOF	quadrupole time-of-flight
R	resolution
RDS	rate-determining step
RF	radio frequency
rt	room temperature
SOMO	singly occupied molecular orbital
TBAB	*tetra*-butylammonium bromide
TBS	*tert*-butyldimethylsilyl
TEA	triethylamine
THF	tetrahydrofurane
TLC	thin-layer chromatography
TMS	trimethylsilyl
TOF	time-of-flight
Tos	tosylate
UHPLC	ultra high performance liquid chromatography
UV/Vis	ultraviolet and visible light
wt%	weight percent

9.2 List of substances

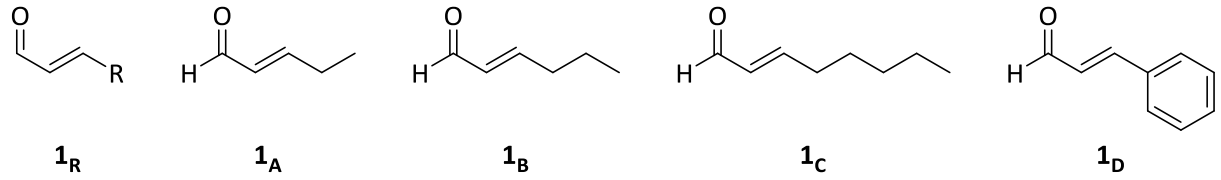

1_R **1_A** **1_B** **1_C** **1_D**

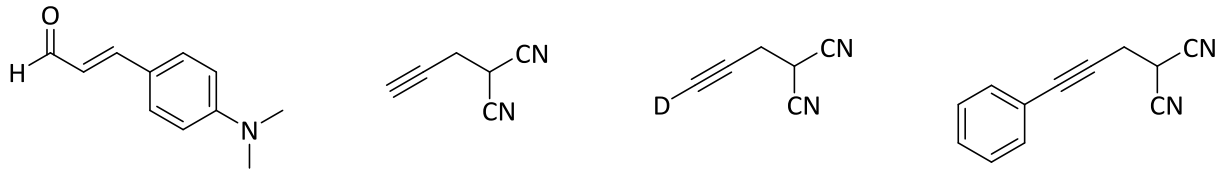

1_E **2** **2_{deut}** **2_{Ph}**

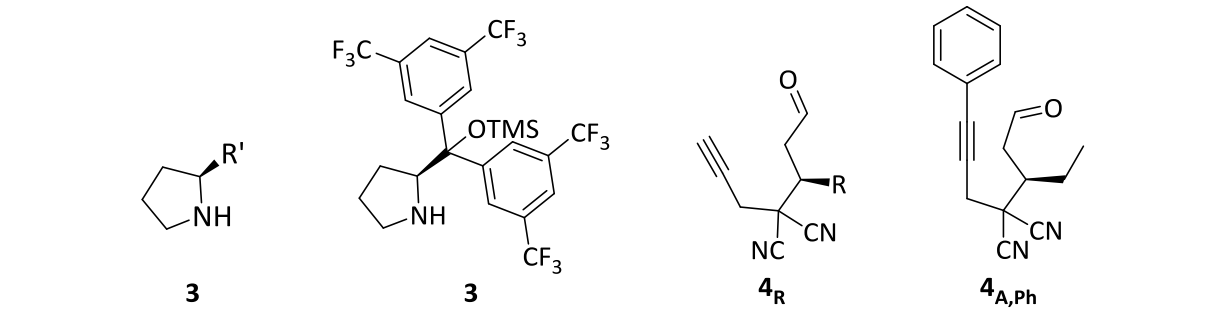

3 **3** **4_R** **$4_{A,Ph}$**

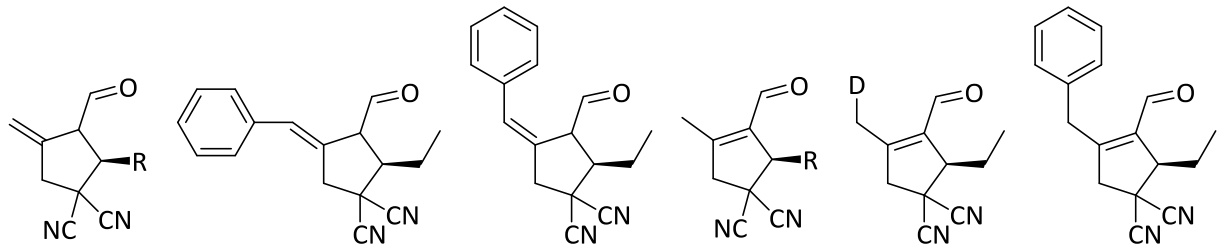

5_R **$5_{A,Ph(E)}$** **$5_{A,Ph(Z)}$** **6_R** **$6_{A,deut}$** **$6_{A,Ph}$**

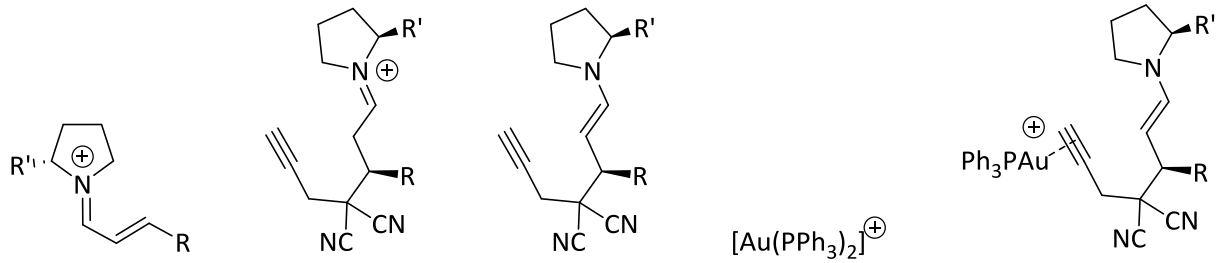

I_R **II_R^+** **III_R** **IV^+** **V_R^+**

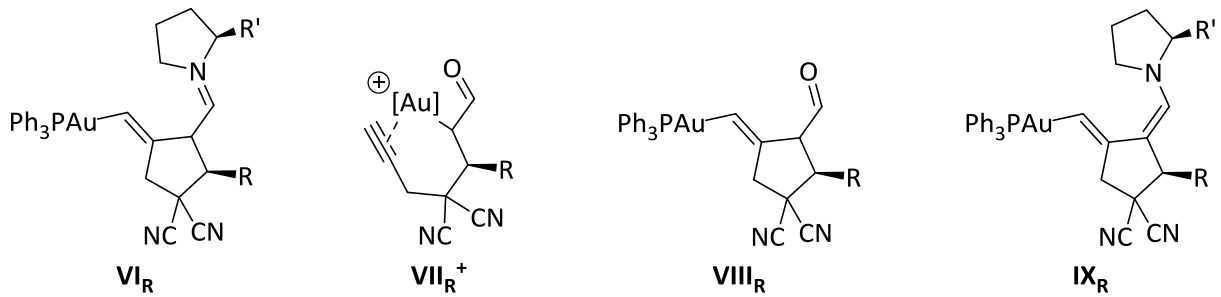

VI_R **VII_R^+** **$VIII_R$** **IX_R**

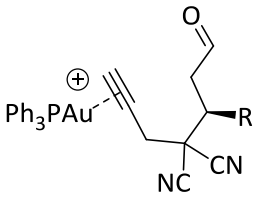

X_R^+

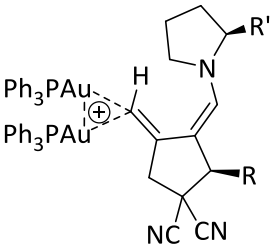

A_R^+

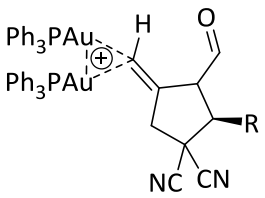

B_R^+

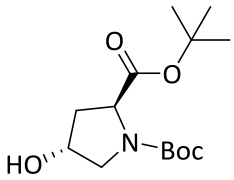

7

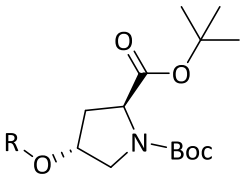

8_R

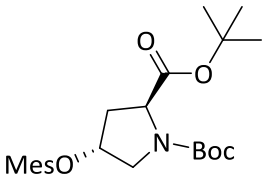

8_A

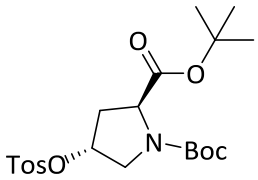

8_B

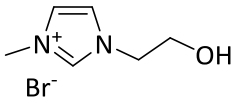

9

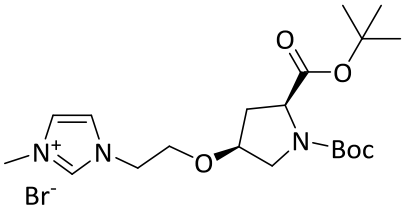

10

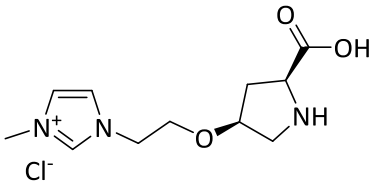

11

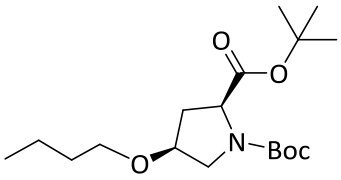

12

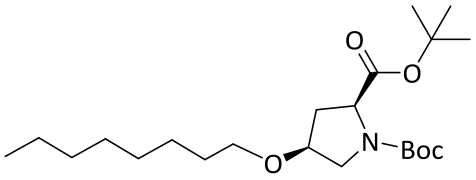

13

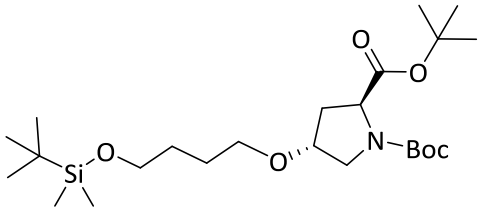

14

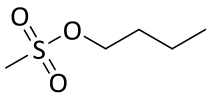

15

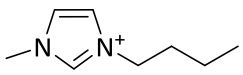

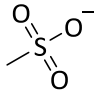

16

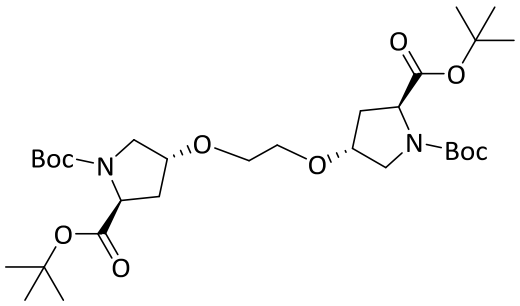

17

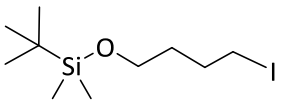

18

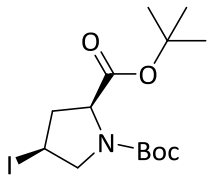

19

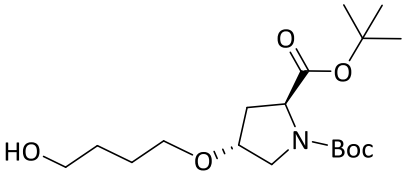

20

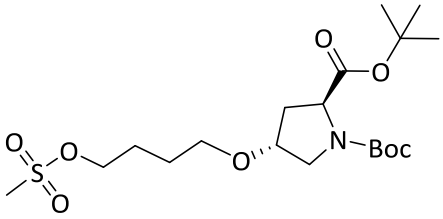

21

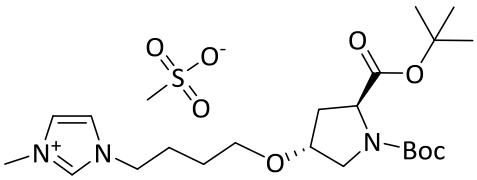

22

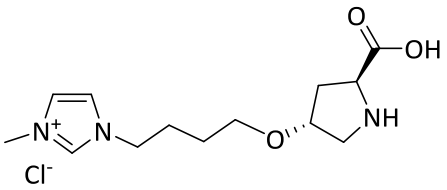

23

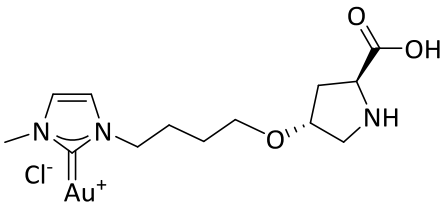

24

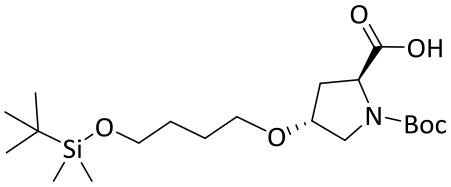

25

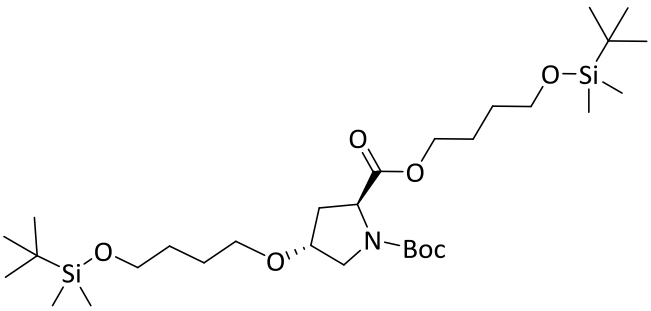

26

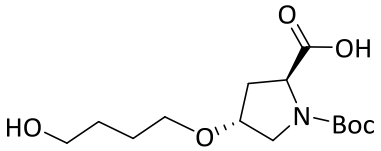

27

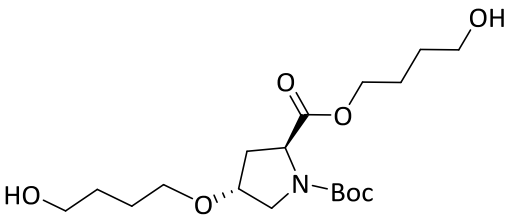

28

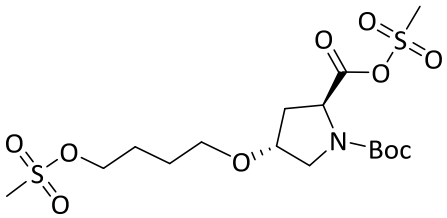

29

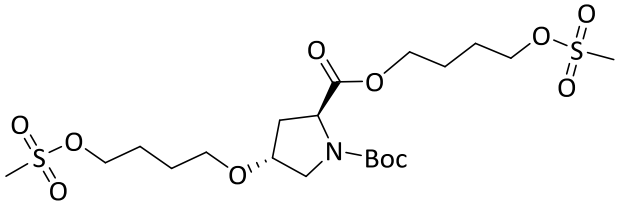

30

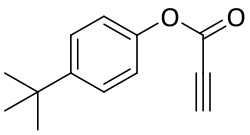

31

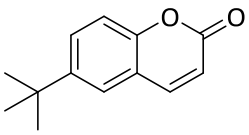

32

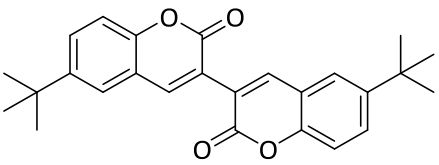

33

9.3 Additional spectra, tables and fragmentation schemes

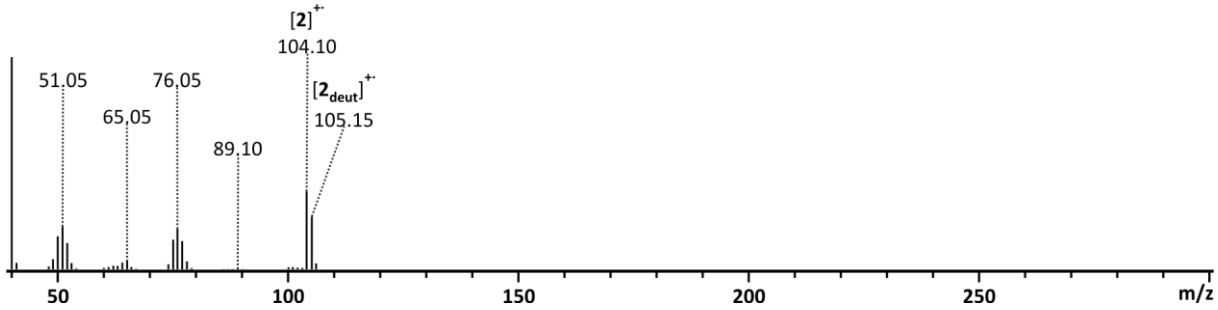

Figure 9.1. EI mass spectrum of deuterated alkyne $\mathbf{2}_{deut}$ formed according to reaction 3.2 at room temperature recorded with GC-MS instrument (a) (chapter 7.2.4). The deuteration rate was determined by the ratio of the deuterated to the non-deuterated peak to 41%.

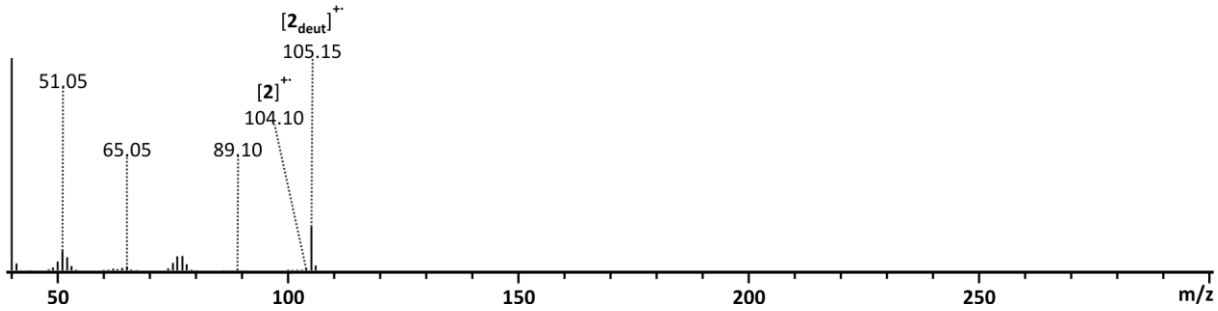

Figure 9.2. EI mass spectrum of deuterated alkyne $\mathbf{2}_{deut}$ formed according to reaction 3.3 at 50 °C recorded with GC-MS instrument (a) (chapter 7.2.4). The deuteration rate was determined by the ratio of the deuterated to the non-deuterated peak to 94%.

Table 9.1. Comparison of the reactions 3.5 to 3.13 to the literature.[224] *56% Deuteration determined by EI-MS (appendix, figure 9.1, 9.2 and 9.3).**4-(Dimethylamino)-cinnamaldehyde $\mathbf{1_E}$. ***Yield could not be determined due to purification problems.

aldehyde	alkyne	product	yield	yield literature
trans-2-pentenal $\mathbf{1_A}$	**2**	$\mathbf{4_A}$	83%	-
trans-2-pentenal $\mathbf{1_A}$	**2**	$\mathbf{6_A}$	39%	88%
trans-2-pentenal $\mathbf{1_A}$	$\mathbf{2_{deut}}$	$\mathbf{6_{A,deut}}$	31%*	-
trans-2-pentenal $\mathbf{1_A}$	$\mathbf{2_{Ph}}$	$\mathbf{4_{A,Ph}}$	-**	-
trans-2-pentenal $\mathbf{1_A}$	$\mathbf{2_{Ph}}$	$\mathbf{6_{A,Ph}}$	-**	-
		$\mathbf{5_{A,Ph(\mathit{E})}}$	-**	-
trans-2-hexenal $\mathbf{1_B}$	**2**	$\mathbf{6_B}$	53%	89%
trans-2-cinnamaldehyde $\mathbf{1_D}$	**2**	$\mathbf{6_D}$	16%	80%
DMAC** $\mathbf{1_E}$	**2**	$\mathbf{6_E}$	-***	-

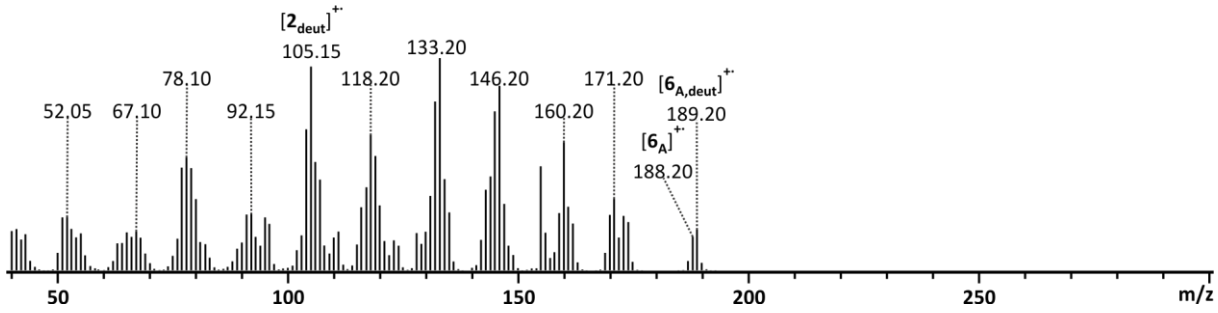

Figure 9.3. EI mass spectrum of deuterated cyclopente carbaldehyde $\mathbf{6_{A,deut}}$ formed according to reaction 3.9 recorded with GC-MS instrument (a) (chapter 7.2.4). The deuteration rate was determined by the ratio of the deuterated to the non-deuterated peak to 56%.

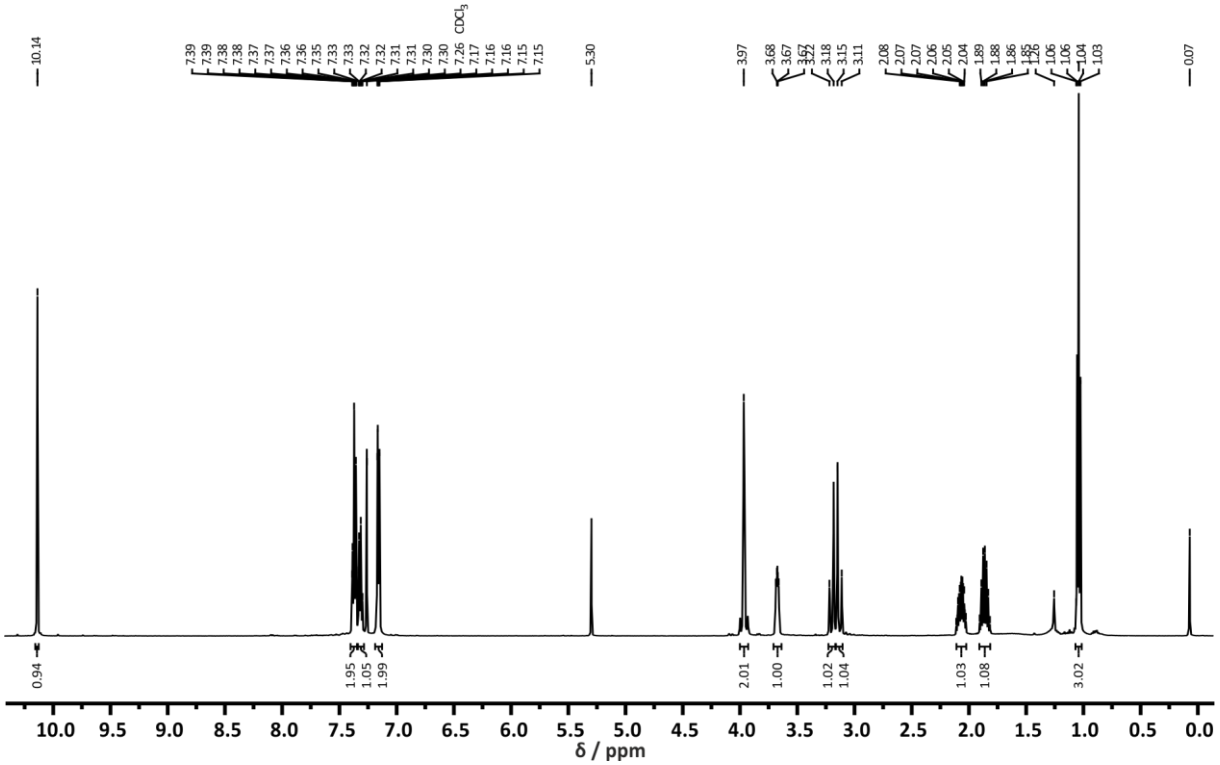

Figure 9.4. ^{1}H NMR spectrum of the isolated cyclopentene carbaldehyde **$6_{A,Ph}$** in $CDCl_3$ recorded with NMR instrument (c) (chapter 7.2.3).

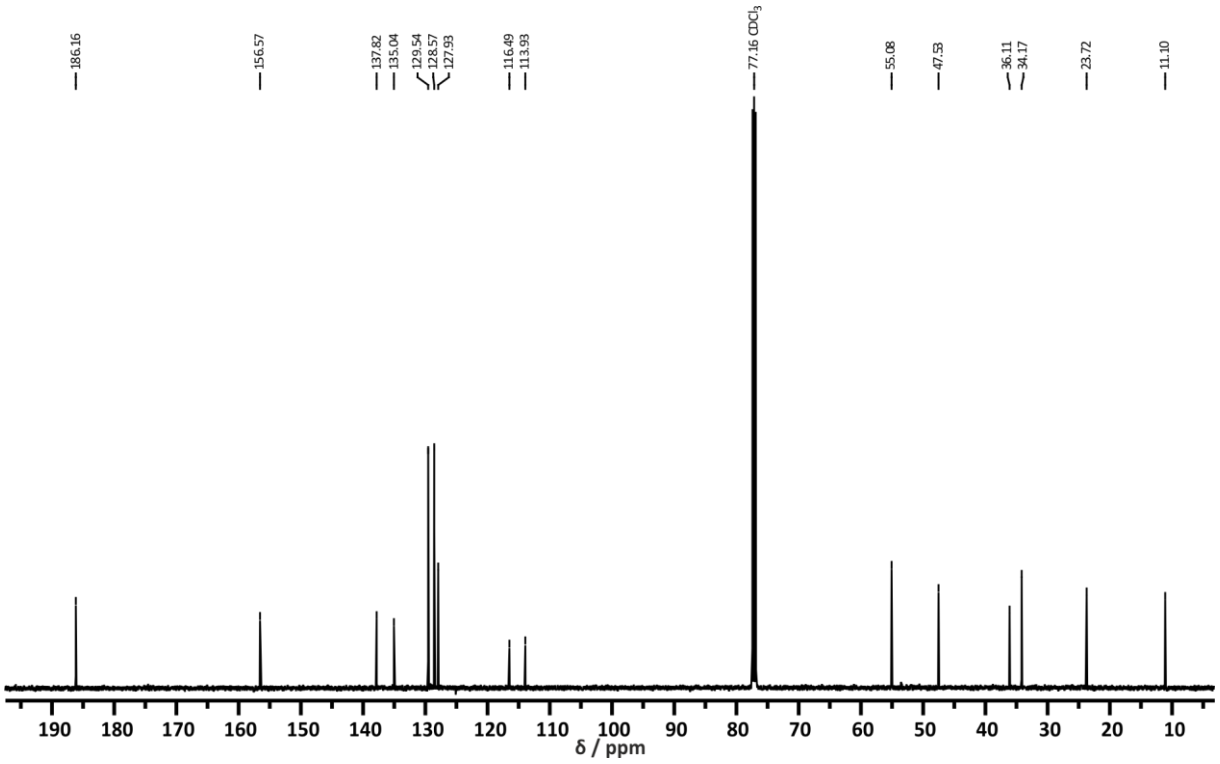

Figure 9.5. ^{13}C NMR spectrum of the isolated cyclopentene carbaldehyde **$6_{A,Ph}$** in $CDCl_3$ recorded with NMR instrument (c) (chapter 7.2.3).

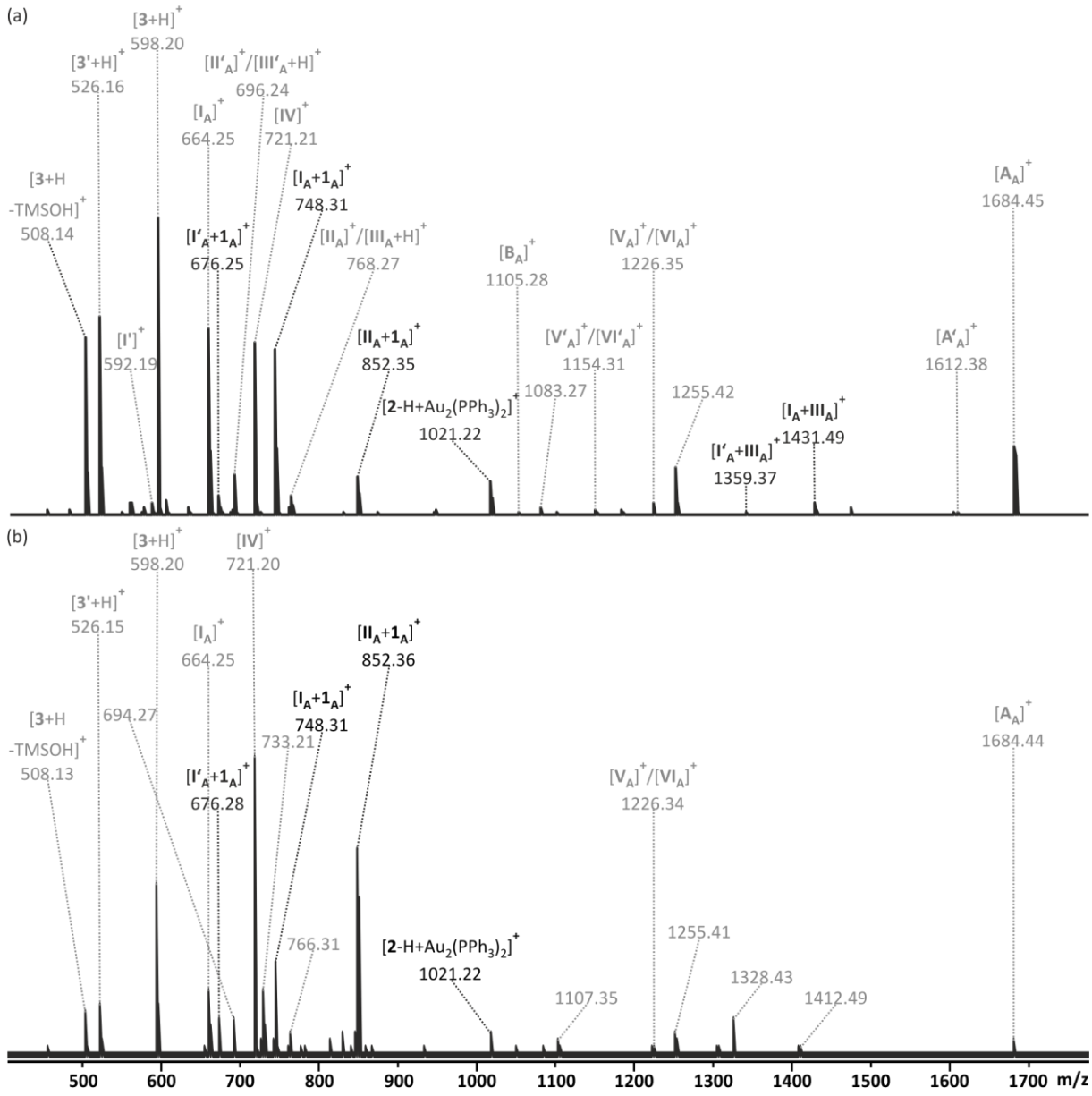

Figure 9.6. ESI(+) mass spectrum of the reaction solution of *trans*-2-pentenal $\mathbf{1_A}$ and alkyne **2** in toluene (reaction 3.14) recorded with Q/TOF mass spectrometer (a) (chapter 7.2.4). The sample for spectrum (a) was taken after one minute, the sample for spectrum (b) after two days reaction time. Both were diluted 1:100 in acetonitrile. Since the loss of TMSOH is mainly attributed to the ESI conditions (chapter 3.3), the ratio of the peak intensities of the free base catalyst $[\mathbf{3}+H]^+$ (*m*/*z* 598) and its form without TMSOH (*m*/*z* 508) can be used as reference to estimate the variation of the adduct species' intensities marked in black.

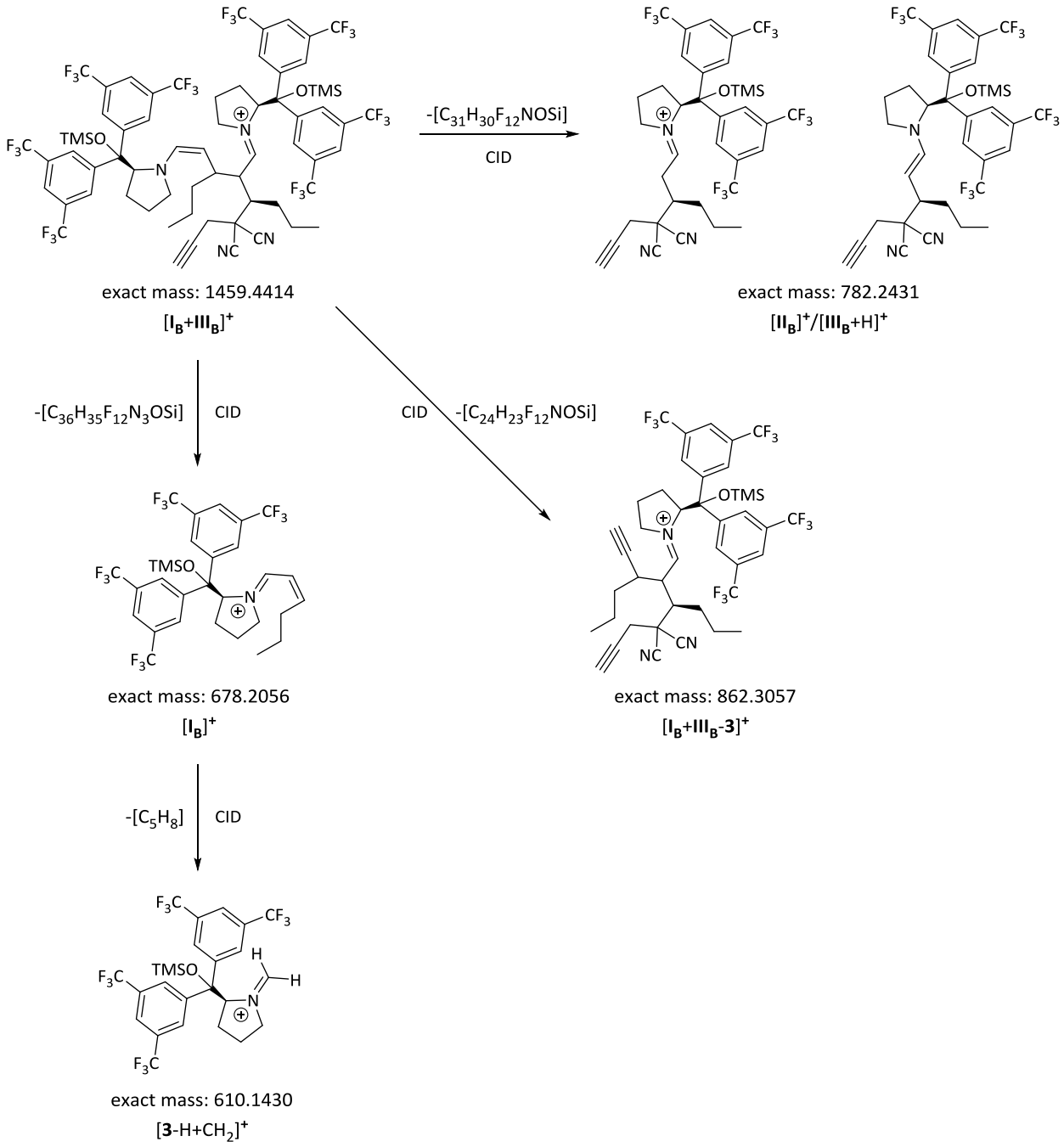

Scheme 9.1. Proposed fragmentation scheme of $[\mathbf{I_B}+\mathbf{III_B}]^+$ based on accurate mass.

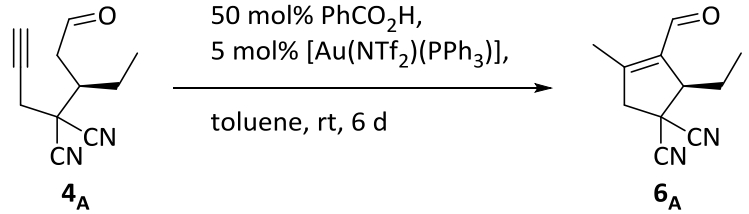

$\mathbf{4_A}$ $\mathbf{6_A}$ **(9.1)**

Scheme 9.2. Additional acid setup for the base exchange experiments . Reaction of acyclic Michael product $\mathbf{4_A}$ with solely gold and 50 mol% benzoic acid measured via mass spectrometry.

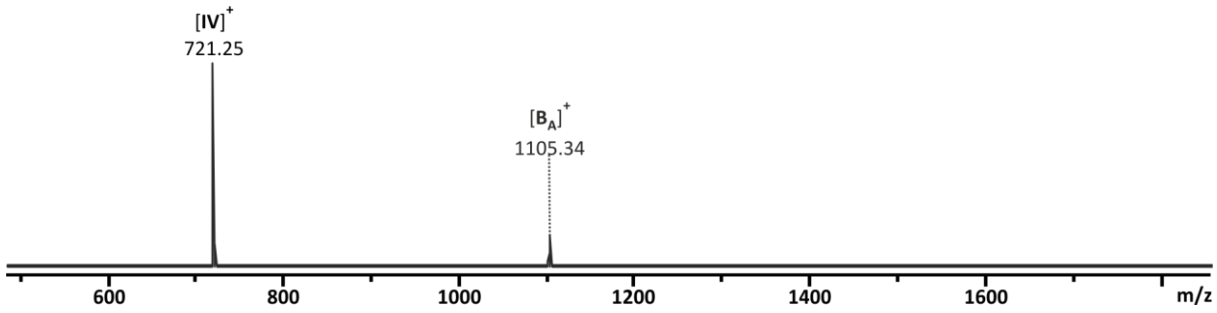

Figure 9.7. ESI(+)-mass spectrum of the cyclization reaction of acyclic Michael product $\mathbf{4_A}$ with solely gold present and with 50 mol% benzoic acid (reaction 9.1) in toluene recorded with Q/TOF mass spectrometer (a) (chapter 7.2.4). The sample was taken after one minute reaction time and diluted 1:100 in acetonitrile.

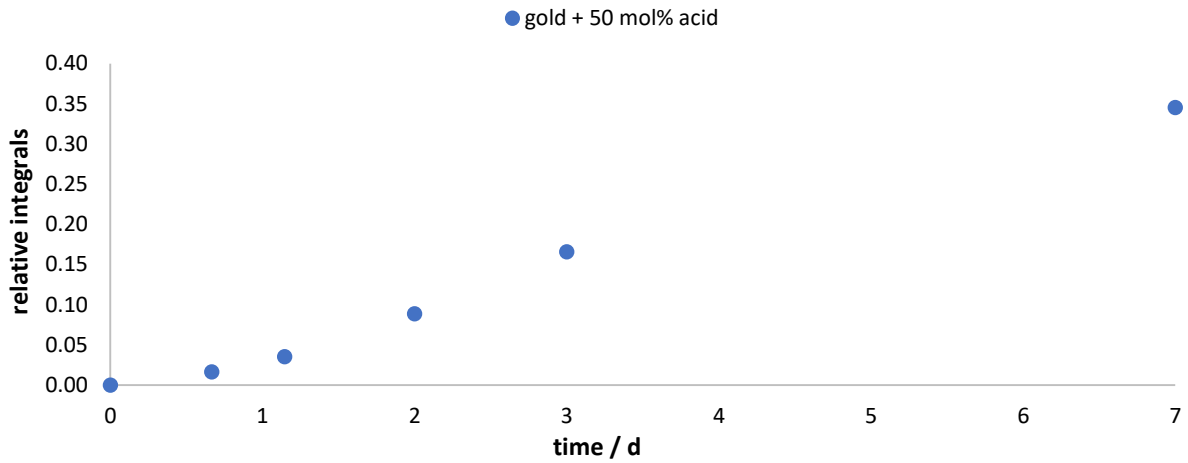

Figure 9.8. Additional acid setup for the base exchange experiments (reaction 9.1). Integrals of cyclization product $\mathbf{6_A}$ standardized to the sum of all integrals obtained by GC-MS measurements monitored with GC-MS instrument (a) (chapter 7.2.4) as function of time during the reaction of acyclic product $\mathbf{4_A}$ with solely gold and 50 mol% benzoic acid over one week.

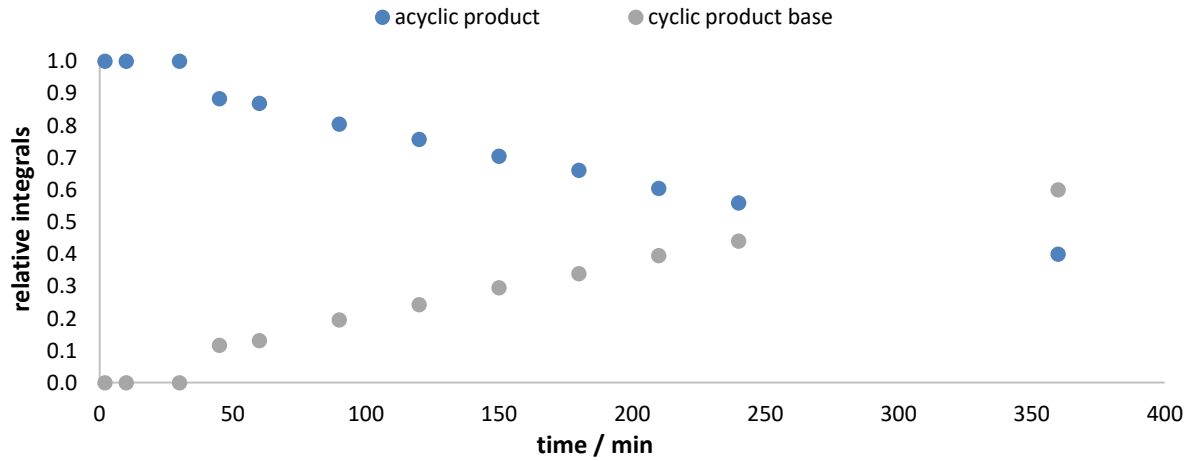

Figure 9.9. Long term base cyclization (reaction 3.32). Integrals of cyclization product $\mathbf{6_A}$ standardized to the sum of all integrals obtained by GC-MS measurements monitored with GC-MS instrument (b) (chapter 7.2.4) as function of time during the base cyclization of Michael product $\mathbf{4_A}$ over six hours. The first three integrals of the base reaction shown were too small for the device's detection limit.

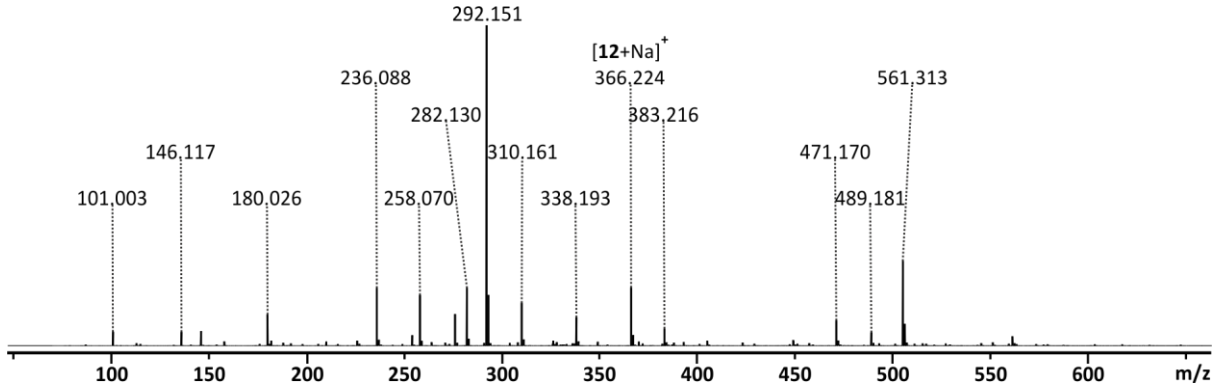

Figure 9.10. ESI(+)-mass spectrum of the crude product of test reaction 4.1 with 1-butanol under the original S_N2 conditions from acetonitrile. The spectrum was recorded with the high-resolution ESI-MS instrument (c) (chapter 7.2.4).

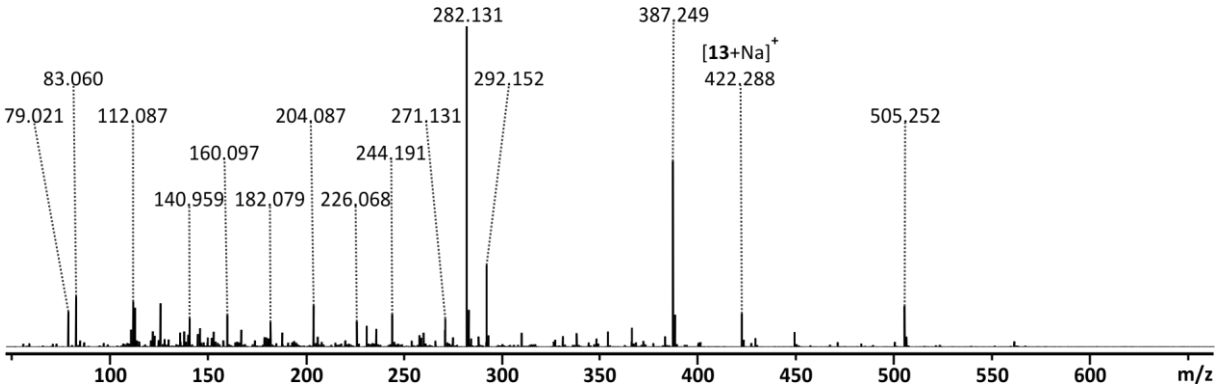

Figure 9.11. ESI(+)-mass spectrum of the crude product of test reaction 4.2 with 1-octanol under the original S_N2 conditions from acetonitrile. The spectrum was recorded with the high-resolution ESI-MS instrument (c) (chapter 7.2.4).

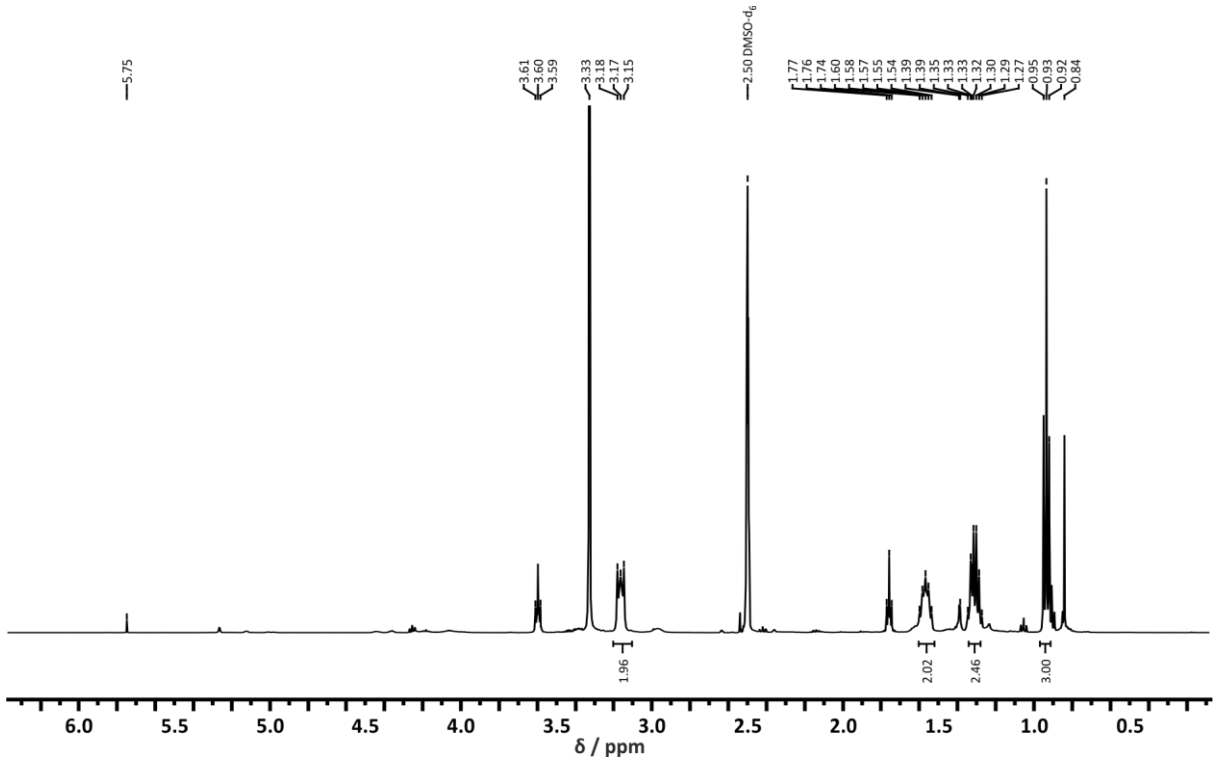

Figure 9.12. ^{1}H NMR spectrum of the deprotection reaction with TBAF depicted in scheme 4.13 in DMSO-d_6 recorded with NMR instrument (b) (chapter 7.2.3). ^{1}H NMR spectrum of the crude after extraction. All integrals marked can be attributed to TBAF. The signal at 3.33 ppm originates from water.

Table 9.2. Eluent mixtures tested for the separation of reaction 4.11 with their volume ratio.

attempt	cyclohexane	ethyl acetate	additive	separation	comment
a	1	1	-	-	for TLCs
b	2	1	-	only *m/z* 460 from *m/z* 540	first Column
c	9	1	-	first spot sticks	too slow
d	6	1	-	first spot sticks	too slow
e	6	1	5% TEA	first spot sticks	TLCs tricky to dye
f	9	1	5% MeOH	first spot sticks less	
g	19	1	5% MeOH	first spot sticks less	
h	49	1	5% MeOH	first spot sticks less	best result (ESI-MS)
i	99	1	5% MeOH	first spot sticks less	

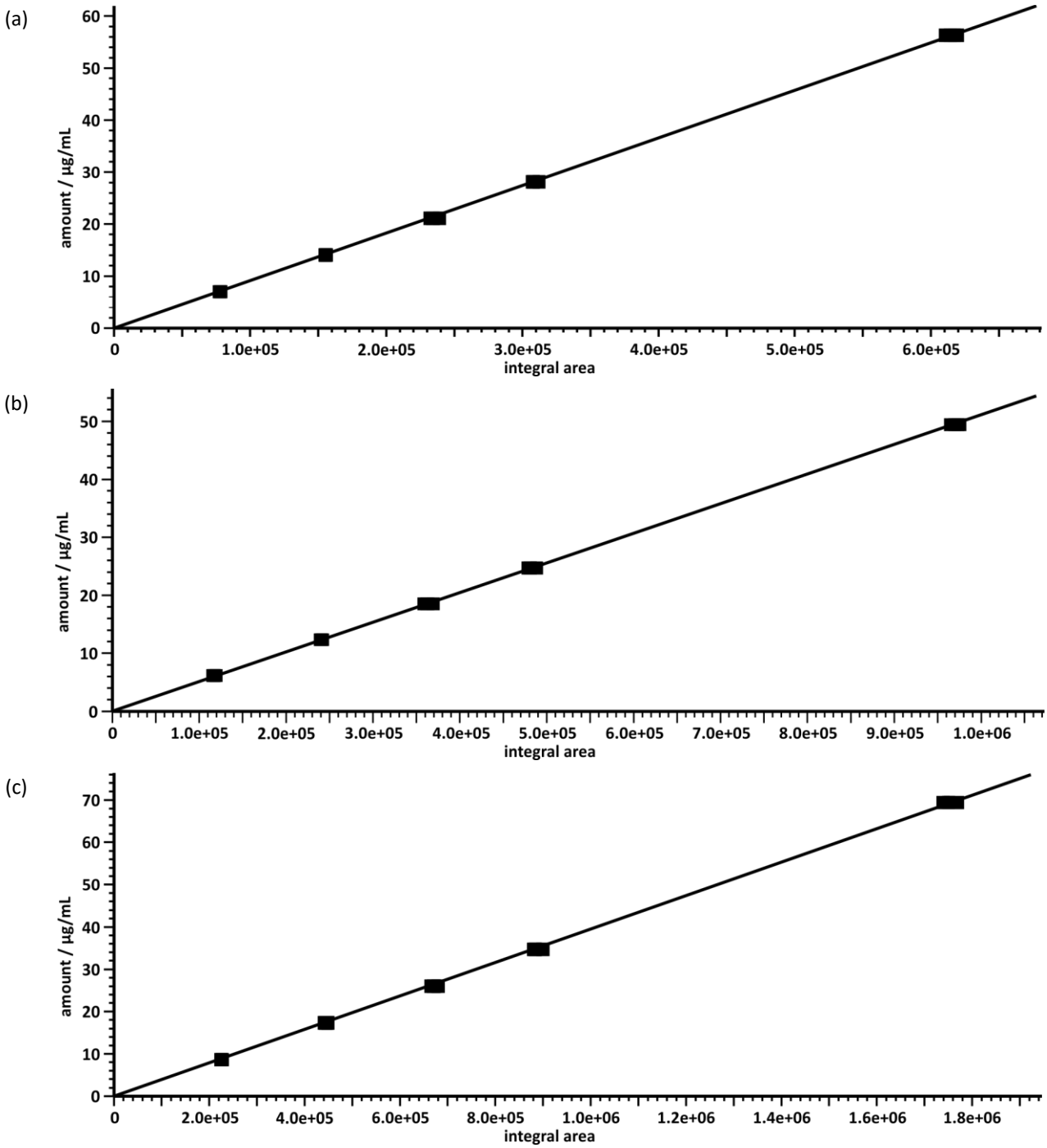

Figure 9.13. Calibration curves of (a) substrate **31**, (b) monomer **32** and (c) dimer **33** recorded with UHPLC-UV/Vis spectroscopy. The individual amount in µg/mL is assigned to the integral area.

9.4 Data tables of all graphs

Table 9.3. Values of the temporal evolution of the overall reaction of *trans*-2-pentenal **1_A** with alkyne **2** (reaction 3.14, figure 3.16, 3.17, 3.18, 3.19, 3.23, 3.27 and 3.25) recorded with GC-MS instrument (b) (chapter 7.2.4).

reaction time			absolute integrals				relative integrals			
time / min	time / h	time / d	aldehyde **1_A**	alkyne **2**	acyclic product **4_A**	cyclic product **6_A**	aldehyde **1_A**	alkyne **2**	acyclic product **4_A**	cyclic product **6_A**
1	0.02	0.00	47234046010	2118686152	94306220	72117901	0.00	0.93	0.04	0.03
10	0.17	0.01	38869051374	1163097660	114373686	161981666	0.38	0.50	0.05	0.07
30	0.50	0.02	32037151435	719794284	113537553	289111343	0.32	0.44	0.07	0.18
60	1.00	0.04	34266341290	795598289	180726765	620517210	0.27	0.36	0.08	0.28
500	8.33	0.35	20458137483	253304374	61808967	879099755	0.12	0.19	0.05	0.65
1290	21.50	0.90	26446425593	215447841	38044308	1325184351	0.08	0.13	0.02	0.78
1620	27.00	1.13	25490321999	208230292	35926616	1361694518	0.07	0.12	0.02	0.79
1890	31.50	1.31	22512635197	167572537	30582693	1248530191	0.00	0.12	0.02	0.86
2780	46.33	1.93	14313312100	54140292	289293	579143673	0.00	0.09	0.00	0.91
3315	55.25	2.30	16453121449	59904530	0	710740463	0.00	0.08	0.00	0.92
7110	118.50	4.94	14345539146	41786828	0	1154693807	0.00	0.03	0.00	0.97
7710	128.50	5.35	11919781122	34776672	0	956333494	0.00	0.04	0.00	0.96
8580	143.00	5.96	16002765388	45805157	0	1553289022	0.00	0.03	0.00	0.97
8990	149.83	6.24	14968789069	46455694	0	1880585926	0.00	0.02	0.00	0.98
9985	166.42	6.93	16317175019	54498442	0	2512071147	0.00	0.02	0.00	0.98

Table 9.4. Values of the temporal evolution of the overall reaction of *trans*-2-hexenal **1_B** with alkyne **2** (reaction 3.15, figure 3.17 and 3.18) recorded with GC-MS instrument (a) (chapter 7.2.4).

reaction time			absolute integrals				relative integrals			
time / min	time / h	time / d	aldehyde **1_A**	alkyne **2**	acyclic product **4_A**	cyclic product **6_A**	aldehyde **1_A**	alkyne **2**	acyclic product **4_A**	cyclic product **6_A**
1	0.02	0.00	2.70	2.21	0.00	0.00	0.55	0.45	0.00	0.00
5	0.08	0.00	2.70	2.18	0.00	0.00	0.55	0.45	0.00	0.00
10	0.17	0.01	2.70	2.18	0.00	0.04	0.55	0.44	0.00	0.01
30	0.50	0.02	2.22	1.84	0.00	0.92	0.45	0.37	0.00	0.18
60	1.00	0.04	1.70	1.57	0.19	1.95	0.31	0.29	0.04	0.36
120	2.00	0.08	1.18	1.35	0.00	2.51	0.23	0.27	0.00	0.50
270	4.50	0.19	0.57	1.02	0.07	4.03	0.10	0.18	0.01	0.71
390	6.50	0.27	0.43	0.75	0.00	4.64	0.07	0.13	0.00	0.80
1350	22.50	0.94	0.00	0.42	0.00	6.42	0.00	0.06	0.00	0.94
1740	29.00	1.21	0.00	0.50	0.00	6.35	0.00	0.07	0.00	0.93

Table 9.5. Values of the temporal evolution of the overall reaction of *trans*-2-cinnamaldehyde **1_C** with alkyne **2** (reaction 3.16, figure 3.17 and 3.18) recorded with GC-MS instrument (a) (chapter 7.2.4).

reaction time			absolute integrals				relative integrals			
time / min	time / h	time / d	aldehyde **1_A**	alkyne **2**	acyclic product **4_A**	cyclic product **6_A**	aldehyde **1_A**	alkyne **2**	acyclic product **4_A**	cyclic product **6_A**
1	0.02	0.00	21.17	8.24	0.87	0.12	0.70	0.27	0.03	0.00
10	0.17	0.01	22.79	8.76	2.05	0.73	0.66	0.26	0.06	0.02
30	0.50	0.02	19.08	7.16	2.90	3.12	0.59	0.22	0.09	0.10
60	1.00	0.04	19.03	7.20	4.95	8.53	0.48	0.18	0.12	0.21
180	3.00	0.13	10.88	4.71	4.27	15.11	0.31	0.13	0.12	0.43
552	9.20	0.38	7.26	3.35	2.66	20.30	0.22	0.10	0.08	0.60
1237	20.62	0.86	4.46	2.25	1.84	26.78	0.13	0.06	0.05	0.76
1628	27.13	1.13	3.74	2.03	2.19	24.55	0.12	0.06	0.07	0.76
1907	31.78	1.32	3.10	1.84	1.47	25.19	0.10	0.06	0.05	0.80
2652	44.20	1.84	3.34	1.95	1.71	39.16	0.07	0.04	0.04	0.85
3237	53.95	2.25	2.23	1.54	1.22	36.37	0.05	0.04	0.03	0.88
4092	68.20	2.84	1.80	1.29	1.07	37.14	0.04	0.03	0.03	0.90
4660	77.67	3.24	1.49	1.07	1.01	34.69	0.04	0.03	0.03	0.91
6102	101.70	4.24	1.47	1.12	1.46	41.14	0.03	0.02	0.03	0.91
9913	165.22	6.88	0.51	1.46	0.46	37.68	0.01	0.04	0.01	0.94
10500	175.00	7.29	0.91	0.82	1.07	54.88	0.02	0.01	0.02	0.95
11340	189.00	7.88	0.60	0.65	0.66	54.87	0.01	0.01	0.01	0.97

Table 9.6. Values of the temporal evolution of the overall reaction of *trans*-2-octenal $\mathbf{1_E}$ with alkyne **2** (reaction 3.17, figure 3.17 and 3.18) recorded with GC-MS instrument (a) (chapter 7.2.4).

reaction time			absolute integrals				relative integrals			
time / min	time / h	time / d	aldehyde $\mathbf{1_A}$	alkyne **2**	acyclic product $\mathbf{4_A}$	cyclic product $\mathbf{6_A}$	aldehyde $\mathbf{1_A}$	alkyne **2**	acyclic product $\mathbf{4_A}$	cyclic product $\mathbf{6_A}$
1	0.02	0.00	19.04	7.53	0.00	0.00	0.72	0.28	0.00	0.00
180	3.00	0.13	6.75	3.11	1.61	12.54	0.28	0.13	0.07	0.52
520	8.67	0.36	1.75	1.22	0.39	16.12	0.09	0.06	0.02	0.83
1550	25.83	1.08	0.31	0.76	0.13	23.53	0.01	0.03	0.01	0.95
2025	33.75	1.41	0.00	0.67	0.00	25.58	0.00	0.03	0.00	0.97
2805	46.75	1.95	0.00	0.65	0.00	30.73	0.00	0.02	0.00	0.98
3460	57.67	2.40	0.00	0.00	0.00	26.59	0.00	0.00	0.00	1.00
4395	73.25	3.05	0.00	0.00	0.00	28.03	0.00	0.00	0.00	1.00
4960	82.67	3.44	0.00	0.00	0.00	27.57	0.00	0.00	0.00	1.00
5670	94.50	3.94	0.00	0.00	0.00	18.05	0.00	0.00	0.00	1.00
6230	103.83	4.33	0.00	0.00	0.00	23.27	0.00	0.00	0.00	1.00
9995	166.58	6.94	0.00	0.24	0.00	39.59	0.00	0.01	0.00	0.99

Table 9.7. Values of the temporal evolution of the overall reaction of *trans*-2-pentenal $\mathbf{1_A}$ with deuterated alkyne $\mathbf{2_{deut}}$ (reaction 3.18, figure 3.19) recorded with GC-MS instrument (a) (chapter 7.2.4).

reaction time			absolute integrals				relative integrals			
time / min	time / h	time / d	aldehyde $\mathbf{1_A}$	alkyne **2**	acyclic product $\mathbf{4_A}$	cyclic product $\mathbf{6_A}$	aldehyde $\mathbf{1_A}$	alkyne **2**	acyclic product $\mathbf{4_A}$	cyclic product $\mathbf{6_A}$
1	0.02	0.00	4.23	3.22	0.04	0.03	0.56	0.43	0.01	0.00
5	0.08	0.00	5.06	3.45	0.10	0.16	0.58	0.39	0.01	0.02
10	0.17	0.01	4.79	3.33	0.18	0.32	0.56	0.39	0.02	0.04
20	0.33	0.01	4.15	2.89	0.24	0.54	0.53	0.37	0.03	0.07
30	0.50	0.02	4.06	2.77	0.30	0.80	0.51	0.35	0.04	0.10
45	0.75	0.03	3.77	2.65	0.29	1.16	0.48	0.34	0.04	0.15
60	1.00	0.04	3.81	2.73	0.32	1.77	0.44	0.32	0.04	0.21
90	1.50	0.06	3.08	2.16	0.28	1.95	0.41	0.29	0.04	0.26
120	2.00	0.08	2.25	1.70	0.19	1.21	0.42	0.32	0.04	0.23
180	3.00	0.13	2.46	1.73	0.24	2.95	0.33	0.23	0.03	0.40
300	5.00	0.21	2.39	1.70	0.25	4.13	0.28	0.20	0.03	0.49
570	9.50	0.40	2.32	1.70	0.17	4.69	0.26	0.19	0.02	0.53
1320	22.00	0.92	1.72	1.27	0.00	5.71	0.20	0.15	0.00	0.66
5760	96.00	4.00	1.19	0.93	0.00	8.50	0.11	0.09	0.00	0.80

Table 9.8. Values of the temporal evolution of the overall reaction of *trans*-2-pentenal $\mathbf{1_A}$ with phenyl alkyne $\mathbf{2_{Ph}}$ (reaction 3.19, figure 3.20) recorded with GC-MS instrument (a) (chapter 7.2.4).

reaction time			absolute integrals					relative integrals				
time / min	time / h	time / d	aldehyde $\mathbf{1_A}$	alkyne $\mathbf{2_{Ph}}$	acyclic product $\mathbf{4_{A,Ph}}$	vinyl product $\mathbf{5_{A,Ph}}$	cyclic product $\mathbf{6_{A,Ph}}$	aldehyde $\mathbf{1_A}$	alkyne $\mathbf{2_{Ph}}$	acyclic product $\mathbf{4_{A,Ph}}$	vinyl product $\mathbf{5_{A,Ph}}$	cyclic product $\mathbf{6_{A,Ph}}$
1	0.02	0.00	6.74	18.66	0.00	0.00	0.00	0.27	0.73	0.00	0.00	0.00
297	4.95	0.21	3.16	12.00	1.13	0.00	0.00	0.19	0.74	0.07	0.00	0.00
627	10.45	0.44	2.49	11.87	2.23	0.00	0.00	0.15	0.72	0.13	0.00	0.00
1527	25.45	1.06	1.67	13.34	3.83	0.61	0.49	0.08	0.67	0.19	0.03	0.02
2007	33.45	1.39	0.00	6.98	2.01	0.51	0.42	0.00	0.70	0.20	0.05	0.04
2922	48.70	2.03	0.00	7.22	2.63	1.38	1.08	0.00	0.59	0.21	0.11	0.09
4347	72.45	3.02	0.00	10.93	4.06	3.73	2.81	0.00	0.51	0.19	0.17	0.13
4892	81.53	3.40	0.00	5.54	2.23	2.68	1.68	0.00	0.46	0.18	0.22	0.14
5712	95.20	3.97	0.00	11.47	4.53	5.53	3.48	0.00	0.46	0.18	0.22	0.14
6342	105.70	4.40	0.00	9.65	6.93	4.86	2.18	0.00	0.41	0.29	0.21	0.09
7472	124.53	5.19	0.00	6.49	3.17	3.98	2.26	0.00	0.41	0.20	0.25	0.14
8927	148.78	6.20	0.00	6.92	4.45	4.47	2.46	0.00	0.38	0.24	0.24	0.13
10112	168.53	7.02	0.00	7.57	4.82	4.93	2.47	0.00	0.38	0.24	0.25	0.12
10712	178.53	7.44	0.00	7.39	4.84	4.83	2.43	0.00	0.38	0.25	0.25	0.12
11512	191.87	7.99	0.00	10.19	4.56	5.74	3.06	0.00	0.43	0.19	0.24	0.13
12138	202.30	8.43	0.00	6.77	5.66	4.08	1.58	0.00	0.37	0.31	0.23	0.09
13292	221.53	9.23	0.00	6.78	5.05	4.41	2.22	0.00	0.37	0.27	0.24	0.12
13562	226.03	9.42	0.00	10.46	5.41	5.76	2.88	0.00	0.43	0.22	0.24	0.12
14377	239.62	9.98	0.00	8.82	5.24	5.27	2.68	0.00	0.40	0.24	0.24	0.12

Table 9.9. Values of the temporal evolution of the overall reaction of *trans*-2-pentenal $\mathbf{1_A}$ with phenyl alkyne $\mathbf{2_{Ph}}$ (reaction 3.20, figure 3.21) recorded with GC-MS instrument (a) (chapter 7.2.4).

reaction time			absolute integrals					relative integrals				
time / min	time / h	time / d	aldehyde $\mathbf{1_A}$	alkyne $\mathbf{2_{Ph}}$	acyclic product $\mathbf{4_{A,Ph}}$	vinyl product $\mathbf{5_{A,Ph}}$	cyclic product $\mathbf{6_{A,Ph}}$	aldehyde $\mathbf{1_A}$	alkyne $\mathbf{2_{Ph}}$	acyclic product $\mathbf{4_{A,Ph}}$	vinyl product $\mathbf{5_{A,Ph}}$	cyclic product $\mathbf{6_{A,Ph}}$
1	0.02	0.00	4.20	7.32	0.00	0.00	0.00	0.36	0.64	0.00	0.00	0.00
10	0.17	0.01	4.34	7.48	0.00	0.00	0.00	0.37	0.63	0.00	0.00	0.00
30	0.50	0.02	3.95	6.89	0.00	0.00	0.00	0.36	0.64	0.00	0.00	0.00
90	1.50	0.06	3.33	4.48	1.45	0.00	0.00	0.36	0.48	0.16	0.00	0.00
120	2.00	0.08	2.53	3.35	1.81	0.00	0.00	0.33	0.44	0.24	0.00	0.00
240	4.00	0.17	2.46	3.16	2.25	0.00	0.00	0.31	0.40	0.29	0.00	0.00
3231	53.85	2.24	0.00	0.93	0.58	1.02	1.70	0.00	0.22	0.14	0.24	0.40
4140	69.00	2.88	0.00	0.77	0.00	1.78	2.54	0.00	0.15	0.00	0.35	0.50
4577	76.28	3.18	0.00	1.07	0.00	1.78	2.47	0.00	0.20	0.00	0.33	0.46
5580	93.00	3.88	0.00	0.78	0.00	0.77	1.59	0.00	0.25	0.00	0.25	0.51
6092	101.53	4.23	0.00	0.56	0.00	0.52	1.89	0.00	0.19	0.00	0.18	0.64
10227	170.45	7.10	0.00	0.66	0.00	0.00	3.07	0.00	0.18	0.00	0.00	0.82
10667	177.78	7.41	0.00	0.61	0.00	0.00	2.58	0.00	0.19	0.00	0.00	0.81
11700	195.00	8.13	0.00	0.00	0.00	0.00	2.49	0.00	0.00	0.00	0.00	1.00

Table 9.10. Values of the temporal evolution of the Michael addition of *trans*-2-pentenal **1_A** with alkyne **2** (reaction 3.22, figure 3.23 and 3.29) recorded with GC-MS instrument (b) (chapter 7.2.4).

reaction time			absolute integrals				relative integrals			
time / min	time / h	time / d	aldehyde **1_A**	alkyne **2**	acyclic product **4_A**	cyclic product **6_A**	aldehyde **1_A**	alkyne **2**	acyclic product **4_A**	cyclic product **6_A**
1	0.02	0.00	90721275	195846559	0		0.32	0.68	0.00	
10	0.17	0.01	347636820	390501436	54835085		0.44	0.49	0.07	
30	0.50	0.02	50595745	173992120	52578421		0.18	0.63	0.19	
60	1.00	0.04	28332758	145495232	95258274		0.11	0.54	0.35	
500	8.33	0.35	29134131	74862431	389890185		0.06	0.15	0.79	
1290	21.50	0.90	33053148	35910822	634656438		0.05	0.05	0.90	
1620	27.00	1.13	18519750	23777983	486187318		0.04	0.04	0.92	
1890	31.50	1.31	0	28818467	660673831		0.00	0.04	0.96	
2780	46.33	1.93	0	173573359	495852811		0.00	0.26	0.74	
3315	55.25	2.30	0	164044186	464475700		0.00	0.26	0.74	
7110	118.50	4.94	0	232317257	729484703		0.00	0.24	0.76	
7710	128.50	5.35	0	167237578	556695029		0.00	0.23	0.77	
8580	143.00	5.96	0	191222600	813753981		0.00	0.19	0.81	
8990	149.83	6.24	0	188836352	904684797		0.00	0.17	0.83	
9985	166.42	6.93	0	207609310	873321992		0.00	0.19	0.81	

Table 9.11. Values of the temporal evolution of the cyclization reaction of Michael product **4_A** (reaction 3.23, figure 3.23 and 3.30) recorded with GC-MS instrument (a) (chapter 7.2.4).

reaction time			absolute integrals				relative integrals			
time / min	time / h	time / d	aldehyde **1_A**	alkyne **2**	acyclic product **4_A**	cyclic product **6_A**	aldehyde **1_A**	alkyne **2**	acyclic product **4_A**	cyclic product **6_A**
2	0.03	0.00			4.98	0.26			0.95	0.05
5	0.08	0.00			5.89	1.31			0.82	0.18
10	0.17	0.01			5.03	2.76			0.65	0.35
20	0.33	0.01			3.02	5.04			0.37	0.63
30	0.50	0.02			1.64	6.82			0.19	0.81
45	0.75	0.03			0.45	9.78			0.04	0.96
60	1.00	0.04			0.00	10.25			0.00	1.00

Table 9.12. Values of the temporal evolution of the cyclization reaction of Michael product $\mathbf{4_A}$ with solely the gold catalyst present in solution (reaction 3.24, figure 3.26) recorded with GC-MS instrument (a) (chapter 7.2.4).

Reaction Time			Absolute Integrals				Relative Integrals			
Time / min	Time / h	Time / d	Aldehyde $\mathbf{1_A}$	Alkyne **2**	Acyclic Product $\mathbf{4_A}$	Cyclic Product $\mathbf{6_A}$	Aldehyde $\mathbf{1_A}$	Alkyne **2**	Acyclic Product $\mathbf{4_A}$	Cyclic Product $\mathbf{6_A}$
1	0.02	0.00			4.85	0.05			0.99	0.01
346	5.77	0.24			4.31	0.17			0.96	0.04
551	9.18	0.38			3.60	0.21			0.94	0.06
1576	26.27	1.09			3.39	0.41			0.89	0.11
1999	33.32	1.39			3.71	0.58			0.86	0.14
2876	47.93	2.00			2.51	0.59			0.81	0.19
3476	57.93	2.41			2.39	0.83			0.74	0.26
4389	73.15	3.05			2.78	1.38			0.67	0.33
4926	82.10	3.42			2.90	1.85			0.61	0.39
5746	95.77	3.99			2.77	1.79			0.61	0.39
6249	104.15	4.34			2.20	1.87			0.54	0.46
9976	166.27	6.93			1.14	3.45			0.25	0.75

Table 9.13. Values of the temporal evolution of the cyclization reaction of Michael product $\mathbf{4_A}$ with solely the gold catalyst and pyridine (reaction 3.25, figure 3.26) recorded with GC-MS instrument (a) (chapter 7.2.4).

reaction time			absolute integrals				relative integrals			
time / min	time / h	time / d	aldehyde $\mathbf{1_A}$	alkyne **2**	acyclic product $\mathbf{4_A}$	cyclic product $\mathbf{6_A}$	aldehyde $\mathbf{1_A}$	alkyne **2**	acyclic product $\mathbf{4_A}$	cyclic product $\mathbf{6_A}$
1	0.02	0.00			4.02	0.08			0.98	0.02
346	5.77	0.24			4.71	0.10			0.98	0.02
551	9.18	0.38			4.93	0.13			0.97	0.03
1576	26.27	1.09			5.10	0.23			0.96	0.04
1999	33.32	1.39			5.85	0.38			0.94	0.06
2876	47.93	2.00			1.10	0.08			0.93	0.07
3476	57.93	2.41			3.88	0.49			0.89	0.11
4389	73.15	3.05			3.71	0.69			0.84	0.16
4926	82.10	3.42			4.18	0.91			0.82	0.18
5746	95.77	3.99			4.59	1.24			0.79	0.21
6249	104.15	4.34			5.08	1.58			0.76	0.24
9976	166.27	6.93			4.79	3.39			0.59	0.41

Table 9.14. Values of the temporal evolution of the cyclization reaction of Michael product **4_A** with solely the gold catalyst and triethylamine (reaction 3.26, figure 3.26) recorded with GC-MS instrument (a) (chapter 7.2.4).

reaction time			absolute integrals				relative integrals			
time / min	time / h	time / d	aldehyde **1_A**	alkyne **2**	acyclic product **4_A**	cyclic product **6_A**	aldehyde **1_A**	alkyne **2**	acyclic product **4_A**	cyclic product **6_A**
1	0.02	0.00			1.48	0.00			1.00	0.00
346	5.77	0.24			3.85	0.00			1.00	0.00
551	9.18	0.38			4.17	0.12			0.97	0.03
1576	26.27	1.09			6.34	0.37			0.94	0.06
1999	33.32	1.39			5.20	0.37			0.93	0.07
2876	47.93	2.00			4.72	0.57			0.89	0.11
3476	57.93	2.41			4.26	0.63			0.87	0.13
4389	73.15	3.05			2.73	0.49			0.85	0.15
4926	82.10	3.42			4.30	1.25			0.77	0.23
5746	95.77	3.99			3.90	1.42			0.73	0.27
6249	104.15	4.34			2.85	1.19			0.71	0.29
9976	166.27	6.93			2.82	2.69			0.51	0.49

Table 9.15. Values of the temporal evolution of cyclization reaction of Michael product **4_A** with solely the gold catalyst and 50 mol% benzoic acid (reaction 9.1, figure 9.8) recorded with GC-MS instrument (a) (chapter 7.2.4).

reaction time			absolute integrals				relative integrals			
time / min	time / h	time / d	aldehyde **1_A**	alkyne **2**	acyclic product **4_A**	cyclic product **6_A**	aldehyde **1_A**	alkyne **2**	acyclic product **4_A**	cyclic product **6_A**
1	0.02	0.00			2.77	0.00			1.00	0.00
960	16.00	0.67			2.99	0.05			0.98	0.02
1650	27.50	1.15			6.00	0.22			0.96	0.04
2880	48.00	2.00			2.67	0.26			0.91	0.09
4320	72.00	3.00			1.66	0.33			0.83	0.17
10080	168.00	7.00			0.91	0.48			0.65	0.35

Table 9.16. Values of the temporal evolution of the overall reaction with base of *trans*-2-pentenal **1_A** with alkyne **2** (reaction 3.27, figure 3.27 and 3.28) recorded with GC-MS instrument (b) (chapter 7.2.4).

reaction time			absolute integrals				relative integrals			
time / min	time / h	time / d	aldehyde **1_A**	alkyne **2**	acyclic product **4_A**	cyclic product **6_A**	aldehyde **1_A**	alkyne **2**	acyclic product **4_A**	cyclic product **6_A**
1	0.02	0.00	169249755	233554611	10263856	0	0.41	0.57	0.02	0.00
10	0.17	0.01	97832160	124632680	22617334	0	0.40	0.51	0.09	0.00
30	0.50	0.02	79106353	99062235	40667356	17386323	0.33	0.42	0.17	0.07
64	1.07	0.04	82798417	111908667	78857191	23649326	0.28	0.38	0.27	0.08
180	3.00	0.13	69300425	86383798	177504309	36901768	0.19	0.23	0.48	0.10
300	5.00	0.21	28980302	835373	116383835	33717606	0.16	0.00	0.65	0.19
1170	19.50	0.81	78602572	479155691	2447126781	1539810941	0.02	0.11	0.54	0.34
1440	24.00	1.00	18700280	386219161	1697325929	1358377042	0.01	0.11	0.49	0.39
1693	28.22	1.18	15161088	385894100	1784197011	1667365646	0.00	0.10	0.46	0.43
2610	43.50	1.81	11739059	295844139	2039535359	2942293958	0.00	0.06	0.39	0.56
3220	53.67	2.24	9302303	273925083	1213826443	2562684369	0.00	0.07	0.30	0.63

Table 9.17. Values of the temporal evolution of the overall reaction with acid of *trans*-2-pentenal **1_A** with alkyne **2** (reaction 3.28, figure 3.27 and 3.28) recorded with GC-MS instrument (b) (chapter 7.2.4).

reaction time			absolute integrals				relative integrals			
time / min	time / h	time / d	aldehyde **1_A**	alkyne **2**	acyclic product **4_A**	cyclic product **6_A**	aldehyde **1_A**	alkyne **2**	acyclic product **4_A**	cyclic product **6_A**
1	0.02	0.00	110207046	182798458	21796978	0	0.35	0.58	0.07	0.00
10	0.17	0.01	74585922	133046533	43670288	35850884	0.26	0.46	0.15	0.12
30	0.50	0.02	121014325	159272541	95373652	111757704	0.25	0.33	0.20	0.23
64	1.07	0.04	82630437	98727903	76032251	157293153	0.20	0.24	0.18	0.38
180	3.00	0.13	53755409	64604025	43654047	295148380	0.12	0.14	0.10	0.65
300	5.00	0.21	52658506	80226973	41461015	424621375	0.09	0.13	0.07	0.71
1170	19.50	0.81	3515948	447334120	131871537	4673504920	0.00	0.09	0.03	0.89
1440	24.00	1.00	518039	365256102	87288856	3724942766	0.00	0.09	0.02	0.89
1693	28.22	1.18	701487	457533009	128470530	6618184001	0.00	0.06	0.02	0.92
2610	43.50	1.81	1141647	278229141	72166880	5123732154	0.00	0.05	0.01	0.94
3220	53.67	2.24	1281857	273419223	65443940	6628770678	0.00	0.04	0.01	0.95

Table 9.18. Values of the temporal evolution of the Michael addition with base of *trans*-2-pentenal **1_A** with alkyne **2** (reaction 3.29, figure 3.29) recorded with GC-MS instrument (b) (chapter 7.2.4).

reaction time			absolute integrals				relative integrals			
time / min	time / h	time / d	aldehyde **1_A**	alkyne **2**	acyclic product **4_A**	cyclic product **6_A**	aldehyde **1_A**	alkyne **2**	acyclic product **4_A**	cyclic product **6_A**
1	0.02	0.00	18896464	176903581	0		0.10	0.90	0.00	
10	0.17	0.01	33274662	193989221	0		0.15	0.85	0.00	
30	0.50	0.02	139843685	254720480	32502204		0.33	0.60	0.08	
60	1.00	0.04	87282985	198489938	50633746		0.26	0.59	0.15	
500	8.33	0.35	67332538	105018582	201967560		0.18	0.28	0.54	
1290	21.50	0.90	18166970	61533852	386137453		0.04	0.13	0.83	
1620	27.00	1.13	22913766	54960704	372176308		0.05	0.12	0.83	
1890	31.50	1.31	28541730	69923450	526333553		0.05	0.11	0.84	
2780	46.33	1.93	7096458	129396784	276245126		0.02	0.31	0.67	
3315	55.25	2.30	6938276	193510705	343192626		0.01	0.36	0.63	
7110	118.50	4.94	0	205457578	481884069		0.00	0.30	0.70	
7710	128.50	5.35	0	279607419	654906590		0.00	0.30	0.70	
8580	143.00	5.96	0	220292877	567396866		0.00	0.28	0.72	
8990	149.83	6.24	0	248225338	618936262		0.00	0.29	0.71	
9985	166.42	6.93	0	343409124	1064754772		0.00	0.24	0.76	

Table 9.19. Values of the temporal evolution of the Michael addition with acid of *trans*-2-pentenal **1_A** with alkyne **2** (reaction 3.30, figure 3.29) recorded with GC-MS instrument (b) (chapter 7.2.4).

reaction time			absolute integrals				relative integrals			
time / min	time / h	time / d	aldehyde **1_A**	alkyne **2**	acyclic product **4_A**	cyclic product **6_A**	aldehyde **1_A**	alkyne **2**	acyclic product **4_A**	cyclic product **6_A**
1	0.02	0.00	69951067	2174200410	0		0.03	0.97	0.00	
10	0.17	0.01	125142950	153243962	75892086		0.35	0.43	0.21	
30	0.50	0.02	38549438	5500326934	5853907803		0.00	0.48	0.51	
60	1.00	0.04	81937833	109363580	276763211		0.18	0.23	0.59	
500	8.33	0.35	35387906	52768240	475813336		0.06	0.09	0.84	
1290	21.50	0.90	7945048	40475039	691458687		0.01	0.05	0.93	
1620	27.00	1.13	33105755	3816445221	11475532162		0.00	0.25	0.75	
1890	31.50	1.31	23369739	36788605	830875938		0.03	0.04	0.93	
2780	46.33	1.93	0	259405061	2480631296		0.00	0.09	0.91	
3315	55.25	2.30	0	216042759	2518948403		0.00	0.08	0.92	
7110	118.50	4.94	0	181903027	2091575250		0.00	0.08	0.92	
7710	128.50	5.35	0	226139575	2467280734		0.00	0.08	0.92	
8580	143.00	5.96	0	242574778	2876085928		0.00	0.08	0.92	
8990	149.83	6.24	0	240688336	3429491013		0.00	0.07	0.93	
9985	166.42	6.93	0	254834427	3096535369		0.00	0.08	0.92	

Table 9.20. Values of the temporal evolution of the cyclization reaction with base of Michael product **4_A** (reaction 3.31, figure 3.30 and 9.9) recorded with GC-MS instrument (a) (chapter 7.2.4).

reaction time			absolute integrals				relative integrals			
time / min	time / h	time / d	aldehyde **1_A**	alkyne **2**	acyclic product **4_A**	cyclic product **6_A**	aldehyde **1_A**	alkyne **2**	acyclic product **4_A**	cyclic product **6_A**
2	0.03	0.00			1.81	0.00			1.00	0.00
10	0.17	0.01			5.47	0.00			1.00	0.00
30	0.50	0.02			4.82	0.00			1.00	0.00
45	0.75	0.03			5.46	0.72			0.88	0.12
60	1.00	0.04			4.51	0.68			0.87	0.13
90	1.50	0.06			5.02	1.22			0.80	0.20
120	2.00	0.08			4.30	1.38			0.76	0.24
150	2.50	0.10			4.34	1.82			0.70	0.30
180	3.00	0.13			4.09	2.10			0.66	0.34
210	3.50	0.15			3.99	2.61			0.60	0.40
240	4.00	0.17			3.53	2.78			0.56	0.44
360	6.00	0.25			2.72	4.08			0.40	0.60

Table 9.21. Values of the temporal evolution of the cyclization reaction with acid of Michael product **4_A** (reaction 3.32, figure 3.30) recorded with GC-MS instrument (a) (chapter 7.2.4).

reaction time			absolute integrals				relative integrals			
time / min	time / h	time / d	aldehyde **1_A**	alkyne **2**	acyclic product **4_A**	cyclic product **6_A**	aldehyde **1_A**	alkyne **2**	acyclic product **4_A**	cyclic product **6_A**
3	0.05	0.00			2.11	0.52			0.80	0.20
5	0.08	0.00			3.57	1.31			0.73	0.27
10	0.17	0.01			3.07	3.26			0.48	0.52
20	0.33	0.01			1.28	5.29			0.19	0.81
30	0.50	0.02			0.47	7.79			0.06	0.94
45	0.75	0.03			0.00	10.01			0.00	1.00
60	1.00	0.04			0.00	10.37			0.00	1.00
75	1.25	0.05			0.00	8.88			0.00	1.00
90	1.50	0.06			0.00	9.70			0.00	1.00
105	1.75	0.07			0.00	10.90			0.00	1.00
120	2.00	0.08			0.00	9.52			0.00	1.00

Table 9.22. Values of the temporal evolution of the domino cyclization of ester **31** (reaction 5.1, figure 5.3a) recorded with ^{1}H NMR spectroscopy in dichloromethane-d_2 with 10 mg/mL. The spectra were recorded with NMR instrument (a) (chapter 7.2.3).

	absolute integrals (substrate **31** as reference)			relative integrals		
time / min	substrate **31**	monomer **32**	dimer **33**	substrate **31**	monomer **32**	dimer **33**
5	1.00	0.02	0.01	0.96	0.02	0.01
5	1.00	0.01	0.01	0.98	0.01	0.00
30	1.00	0.05	0.03	0.90	0.05	0.03
30	1.00	0.11	0.09	0.78	0.09	0.07
40	1.00	0.11	0.07	0.80	0.09	0.06
50	1.00	0.30	0.25	0.56	0.17	0.14
60	1.00	0.39	0.30	0.51	0.20	0.15
60	1.00	0.76	0.54	0.35	0.27	0.19
80	1.00	0.06	0.05	0.86	0.05	0.04
100	1.00	0.17	0.15	0.68	0.12	0.10
120	1.00	0.14	0.10	0.75	0.11	0.07
122	1.00	0.08	0.05	0.85	0.07	0.04
150	2.00	0.41	0.27	0.68	0.14	0.09
192	1.00	0.21	0.15	0.66	0.14	0.10
210	3.00	0.24	0.20	0.83	0.07	0.05
240	4.00	0.23	0.20	0.86	0.05	0.04
300	1.00	0.89	0.77	0.29	0.26	0.22
360	1.00	0.37	0.32	0.50	0.19	0.16
1343	1.00	0.38	0.34	0.49	0.18	0.17
1440	1.00	0.50	0.46	0.41	0.21	0.19
1740	1.00	0.19	0.11	0.71	0.13	0.08
2902	1.00	1.11	1.18	0.22	0.25	0.26
4320	1.00	0.60	0.45	0.40	0.24	0.18

Table 9.23. Values of the temporal evolution of the domino cyclization of ester **31** (reaction 5.1, figure 5.3b) recorded with ^{1}H NMR spectroscopy in dichloromethane-d_2 with 10 mg/mL and isopropanol as internal standard. The spectra were recorded with NMR instrument (a) (chapter 7.2.3).

	absolute integrals (substrate **31** as reference)			relative integrals		
time / min	substrate **31**	monomer **32**	dimer **33**	substrate **31**	monomer **32**	dimer **33**
5	0.33	0.16	0.13			
10	0.17	0.14	0.14			
30	0.25	0.17	0.14			
60	0.17	0.17	0.14			
80	0.12	0.16	0.09			
90	0.07	0.16	0.15			
100	0.38	0.15	0.06			
120	0.06	0.19	0.18			
120	0.36	0.12	0.05			
140	0.06	0.17	0.09			
160	0.10	0.19	0.14			
180	0.20	0.19	0.16			
180	0.13	0.19	0.13			
180	0.08	0.18	0.16			

Table 9.24. Values of the temporal evolution of the domino cyclization of ester **31** (reaction 5.1, figure 5.4) recorded with ^{1}H NMR spectroscopy in dichloromethane-d_2 with 1 mg/mL and isopropanol as internal standard. The spectra were recorded with NMR instrument (a) (chapter 7.2.3).

	absolute integrals (substrate **31** as reference)			relative integrals		
time / min	substrate **31**	monomer **32**	dimer **33**	substrate **31**	monomer **32**	dimer **33**
5	0.03	0.08	0.07	0.13	0.30	0.28
30	0.06	0.11	0.09	0.18	0.32	0.25
60	0.17	0.11	0.08	0.38	0.24	0.19
120	0.04	0.13	0.12	0.10	0.33	0.29
240	0.08	0.12	0.10	0.20	0.30	0.25
1080	0.06	0.10	0.08	0.18	0.32	0.25

Table 9.25. Values of the temporal evolution of the domino cyclization of ester **31** (reaction 5.1, figure 5.5a) recorded with ^{1}H NMR spectroscopy in benzene-d_6 with 1 mg/mL. The spectra were recorded with NMR instrument (a) (chapter 7.2.3).

	absolute integrals (substrate **31** as reference)			relative integrals		
time / min	substrate **31**	monomer **32**	dimer **33**	substrate **31**	monomer **32**	dimer **33**
5	1.00	9.50	6.56	0.04	0.40	0.28
30	1.00	6.21	4.81	0.06	0.37	0.29
60	1.00	6.97	5.66	0.05	0.36	0.29
120	1.00	16.60	13.20	0.02	0.38	0.30
240	1.00	3.66	2.34	0.11	0.39	0.25

Table 9.26. Values of the temporal evolution of the domino cyclization of ester **31** (reaction 5.1, figure 5.5b) recorded with ^{1}H NMR spectroscopy in THF-d_8 with 1 mg/mL. The spectra were recorded with NMR instrument (a) (chapter 7.2.3).

	absolute integrals (substrate **31** as reference)			relative integrals		
time / min	substrate **31**	monomer **32**	dimer **33**	substrate **31**	monomer **32**	dimer **33**
5	1.00	1.83	1.47	0.17	0.32	0.25
30	1.00	2.22	1.80	0.15	0.32	0.26
60	1.00	1.62	1.24	0.20	0.32	0.24
120	1.00	2.18	1.78	0.15	0.32	0.26
240	1.00	2.12	1.41	0.17	0.36	0.24
1080	1.00	2.27	1.94	0.14	0.32	0.27

Table 9.27. Values of the calibration curves of figure 9.13 recorded with UHPLC-UV/Vis spectroscopy.

ester **31**	regression y = 9.15E-05x+0.00			goodness of r^2 0.999923	
	level 1	level 2	level 3	level 4	level 5
amount	7.04	14.08	21.13	28.17	56.34
area	77717.5	155128	233854	308098	614145
RF	9.06E-05	9.07E-05	9.04E-05	9.14E-05	9.17E-05
rep 1 RF	9.06E-05	9.10E-05	9.11E-05	9.17E-05	9.23E-05
rep 2 RF	9.12E-05	9.06E-05	9.01E-05	9.15E-05	9.10E-05
rep 3 RF	8.96E-05	9.03E-05	8.84E-05	9.03E-05	9.13E-05

monomer **32**	regression y = 5.11E-05x+0.00			goodness of r^2 0.999920	
	level 1	level 2	level 3	level 4	level 5
amount	6.18	12.36	18.54	24.72	49.44
area	116583	240075	361615	480798	969187
RF	5.30E-05	5.15E-05	5.13E-05	5.42E-05	5.10E-05
rep 1 RF	5.36E-05	5.17E-05	5.17E-05	5.17E-05	5.12E-05
rep 2 RF	5.27E-05	5.14E-05	5.10E-05	5.13E-05	5.07E-05
rep 3 RF	5.18E-05	5.11E-05	5.02E-05	5.06E-05	5.08E-05

dimer **33**	regression y = 3.95E-05x+0.00			goodness of r^2 0.999836	
	level 1	level 2	level 3	level 4	level 5
amount	8.68	17.36	26.04	34.72	69.44
area	224592	443712	669483	883826	1750212
RF	3.86E-05	3.91E-05	3.89E-05	3.93E-05	3.97E-05
rep 1 RF	3.88E-05	3.94E-05	3.92E-05	3.95E-05	3.99E-05
rep 2 RF	3.86E-05	3.89E-05	3.87E-05	3.94E-05	3.92E-05
rep 3 RF	3.82E-05	3.87E-05	3.83E-05	3.86E-05	3.96E-05

Table 9.28. Values of the temporal evolution of the domino cyclization of ester **31** (reaction 5.1, figure 5.7) recorded with UHPLC-UV/Vis spectroscopy. All signals were standardized to the amount of substrate **32** used for the individual setup.

substrate **31**	reference		measurements			average		standardized
time / min	$m_{31,Start}$ / mg	$n_{31,Start}$ / mol	$m_{31,1}$ / mg	$m_{31,2}$ / mg	$m_{31,3}$ / mg	$\bar{m}_{31}$ / mg	$\bar{n}_{31}$ / mol	$\frac{\bar{n}_{31}}{n_{31,Start}}$
8	41.44	0.20	7.27	9.10	9.02	8.46	0.04	0.20
10	42.77	0.21	8.05	7.93	7.98	7.99	0.04	0.19
15	52.48	0.26	11.34	11.16	11.27	11.26	0.06	0.21
20	51.76	0.26	20.18	20.88	20.61	20.56	0.10	0.40
25	67.06	0.33	10.23	10.33	10.51	10.36	0.05	0.15
30	38.56	0.19	3.86	3.96	4.04	3.95	0.02	0.10
40	39.46	0.20	10.66	10.59	10.89	10.71	0.05	0.27
45	58.14	0.29	15.22	45.56	15.32	25.37	0.13	0.44
60	65.07	0.32	4.07	3.96	3.95	3.99	0.02	0.06
75	44.11	0.22	15.49	15.67	16.17	15.78	0.08	0.36
90	50.89	0.25	6.73	6.79	6.85	6.79	0.03	0.13
120	81.50	0.40	7.53	7.48	7.68	7.56	0.04	0.09
150	51.51	0.25	8.02	7.90	8.03	7.98	0.04	0.15
180	55.73	0.28	1.40	1.60	1.58	1.53	0.01	0.03
240	41.64	0.21	5.25	5.37	5.34	5.32	0.03	0.13
300	58.75	0.29	4.55	4.54	4.68	4.59	0.02	0.08
930	29.36	0.15	7.05	6.99	7.13	7.06	0.03	0.24
1260	31.66	0.16	5.72	5.72	5.89	5.78	0.03	0.18

monomer **32**	reference		measurements			average		standardized
time / min	$m_{31,Start}$ / mg	$n_{31,Start}$ / mol	$m_{32,1}$ / mg	$m_{32,2}$ / mg	$m_{32,3}$ / mg	$\bar{m}_{32}$ / mg	$\bar{n}_{32}$ / mol	$\frac{\bar{n}_{32}}{n_{31,Start}}$
8	41.44	0.20	6.21	7.17	7.21	6.86	0.03	0.17
10	42.77	0.21	7.40	7.50	7.52	7.47	0.04	0.17
15	52.48	0.26	9.42	9.38	9.59	9.46	0.05	0.18
20	51.76	0.26	6.88	7.11	7.06	7.02	0.03	0.14
25	67.06	0.33	13.73	13.84	13.95	13.84	0.07	0.21
30	38.56	0.19	6.93	6.97	7.08	6.99	0.03	0.18
40	39.46	0.20	6.45	6.41	6.62	6.49	0.03	0.16
45	58.14	0.29	10.23	10.62	10.46	10.44	0.05	0.18
60	65.07	0.32	13.11	13.51	13.39	13.34	0.07	0.20
75	44.11	0.22	7.41	7.56	7.63	7.53	0.04	0.17
90	50.89	0.25	9.97	9.92	10.17	10.02	0.05	0.20
120	81.50	0.40	15.49	15.36	15.46	15.44	0.08	0.19
150	51.51	0.25	9.27	9.22	9.42	9.30	0.05	0.18
180	55.73	0.28	4.72	4.77	4.81	4.77	0.02	0.09
240	41.64	0.21	8.70	8.93	8.80	8.81	0.04	0.21
300	58.75	0.29	11.65	11.77	12.09	11.84	0.06	0.20
930	29.36	0.15	5.25	5.19	5.22	5.22	0.03	0.18
1260	31.66	0.16	5.85	6.03	5.98	5.95	0.03	0.19

dimer **33**	reference		measurements			average		standardized
time / min	$m_{31,Start}$ / mg	$n_{31,Start}$ / mol	$m_{33,1}$ / mg	$m_{33,2}$ / mg	$m_{33,3}$ / mg	$\overline{m}_{33}$ / mg	$\overline{n}_{33}$ / mol	$\frac{\overline{n}_{33}}{n_{31,Start}}$
8	41.44	0.20	12.59	14.61	14.66	13.95	0.03	0.17
10	42.77	0.21	12.82	12.85	13.00	12.89	0.03	0.15
15	52.48	0.26	16.99	16.99	17.47	17.15	0.04	0.16
20	51.76	0.26	11.87	12.17	11.96	12.00	0.03	0.12
25	67.06	0.33	27.97	28.14	28.38	28.16	0.07	0.21
30	38.56	0.19	12.58	12.65	12.73	12.65	0.03	0.16
40	39.46	0.20	9.64	9.52	9.80	9.65	0.02	0.12
45	58.14	0.29	16.17	46.53	16.44	26.38	0.07	0.23
60	65.07	0.32	24.41	24.94	24.89	24.75	0.06	0.19
75	44.11	0.22	13.13	13.30	13.53	13.32	0.03	0.15
90	50.89	0.25	17.03	17.14	17.38	17.18	0.04	0.17
120	81.50	0.40	31.13	31.16	31.31	31.20	0.08	0.19
150	51.51	0.25	16.66	16.78	17.17	16.87	0.04	0.16
180	55.73	0.28	9.06	9.12	9.34	9.17	0.02	0.08
240	41.64	0.21	16.55	17.12	16.77	16.81	0.04	0.20
300	58.75	0.29	21.72	21.70	22.33	21.92	0.05	0.19
930	29.36	0.15	9.92	10.06	10.05	10.01	0.02	0.17
1260	31.66	0.16	9.59	9.78	9.74	9.70	0.02	0.15

Table 9.29. Values of the temporal evolution of the diluted domino cyclization of ester **31** (reaction 5.2, figure 5.8) recorded with UHPLC-UV/Vis spectroscopy. All signals were standardized to the amount of substrate **32** used for the individual setup.

substrate **31**	reference		measurements			average		standardized
time / min	$m_{31,Start}$ / mg	$n_{31,Start}$ / mol	$m_{31,1}$ / mg	$m_{31,2}$ / mg	$m_{31,3}$ / mg	$\bar{m}_{31}$ / mg	$\bar{n}_{31}$ / mol	$\frac{\bar{n}_{31}}{n_{31,Start}}$
10	25.91	0.13	19.89	18.14	18.31	18.78	0.09	0.72
15	29.37	0.15	23.23	24.11	24.07	23.80	0.12	0.81
30	25.61	0.13	16.93	17.19	17.75	17.29	0.09	0.68
45	18.48	0.09	11.64	11.52	11.79	11.65	0.06	0.63
60	47.98	0.24	13.32	13.62	13.43	13.46	0.07	0.28
60	15.61	0.08	8.42	8.15	7.83	8.13	0.04	0.52
60	15.25	0.08	11.23	11.16	10.76	11.05	0.05	0.72
90	34.22	0.17	23.19	23.28	23.78	23.42	0.12	0.68
120	36.67	0.18	22.82	22.96	23.18	22.99	0.11	0.63
210	29.72	0.15	19.42	19.50	19.58	19.50	0.10	0.66
270	39.75	0.20	18.31	18.31	19.27	18.63	0.09	0.47
360	15.34	0.08	7.37	7.69	7.78	7.61	0.04	0.50
1110	32.37	0.16	20.25	20.21	20.53	20.33	0.10	0.63
1200	19.56	0.10	5.87	6.03	5.62	5.84	0.03	0.30
1320	18.47	0.09	6.56	6.50	6.82	6.63	0.03	0.36

monomer **32**	reference		measurements			average		standardized
time / min	$m_{31,Start}$ / mg	$n_{31,Start}$ / mol	$m_{32,1}$ / mg	$m_{32,2}$ / mg	$m_{32,3}$ / mg	$\overline{m}_{32}$ / mg	$\overline{n}_{32}$ / mol	$\frac{\overline{n}_{32}}{n_{31,Start}}$
10	25.91	0.13	0.86	0.82	0.86	0.85	0.00	0.03
15	29.37	0.15	0.83	0.83	0.9	0.85	0.00	0.03
30	25.61	0.13	1.52	1.46	1.49	1.49	0.01	0.06
45	18.48	0.09	1.21	1.25	1.31	1.26	0.01	0.07
60	47.98	0.24	7.28	7.38	7.36	7.34	0.04	0.15
60	15.61	0.08	0.82	0.87	0.84	0.84	0.00	0.05
60	15.25	0.08	0.62	0.53	0.54	0.56	0.00	0.04
90	34.22	0.17	1.92	1.97	1.97	1.95	0.01	0.06
120	36.67	0.18	4.15	4.15	4.23	4.18	0.02	0.11
210	29.72	0.15	1.72	1.67	1.66	1.68	0.01	0.06
270	39.75	0.20	4.94	5.05	5.05	5.01	0.02	0.13
360	15.34	0.08	1.77	1.74	1.8	1.77	0.01	0.12
1110	32.37	0.16	2.25	2.28	2.25	2.26	0.01	0.07
1200	19.56	0.10	3.41	3.48	3.26	3.38	0.02	0.17
1320	18.47	0.09	3.62	3.58	3.53	3.58	0.02	0.19

dimer **33**	reference		measurements			average		standardized
time / min	$m_{31,Start}$ / mg	$n_{31,Start}$ / mol	$m_{33,1}$ / mg	$m_{33,2}$ / mg	$m_{33,3}$ / mg	$\bar{m}_{33}$ / mg	$\bar{n}_{33}$ / mol	$\frac{\bar{n}_{33}}{n_{31,Start}}$
10	25.91	0.13	2.08	1.64	1.85	1.86	0.00	0.04
15	29.37	0.15	1.93	1.90	1.98	1.94	0.00	0.03
30	25.61	0.13	3.83	3.83	3.88	3.85	0.01	0.08
45	18.48	0.09	2.58	2.62	2.59	2.60	0.01	0.07
60	47.98	0.24	17.81	18.19	18.25	18.08	0.04	0.19
60	15.61	0.08	3.57	3.54	3.65	3.59	0.01	0.12
60	15.25	0.08	1.48	1.54	1.60	1.54	0.00	0.05
90	34.22	0.17	4.58	4.61	4.58	4.59	0.01	0.07
120	36.67	0.18	5.37	5.35	5.37	5.36	0.01	0.07
210	29.72	0.15	3.19	3.15	3.15	3.16	0.01	0.05
270	39.75	0.20	11.78	11.96	12.01	11.92	0.03	0.15
360	15.34	0.08	2.53	2.59	2.68	2.60	0.01	0.09
1110	32.37	0.16	5.01	4.97	5.11	5.03	0.01	0.08
1200	19.56	0.10	6.33	6.38	5.95	6.22	0.02	0.16
1320	18.47	0.09	4.64	4.74	4.76	4.71	0.01	0.13

9.5 List of reaction names – Original data in the lab journals

Synthesis

scheme	reaction	starting materials	product	yield	journal
3.3	3.1	molononitrile, propargylbromide	alkyne **2**	37%	J1 P105
3.4	3.2	alkyne **2**	deuterated alkyne $\mathbf{2_{deut}}$	79% (41%D)	J2 P29
3.4	3.3	alkyne **2**	deuterated alkyne $\mathbf{2_{deut}}$	80% (94%D)	J2 P37
3.5	3.4	alkyne **2**	phenyl alkyne $\mathbf{2_{Ph}}$	50%	J2 P15
3.6	3.5	*trans*-2-pentenal $\mathbf{1_A}$, alkyne **2**	cyclopentene carbaldehyde $\mathbf{6_A}$	83%	J0 P13
3.6	3.6	*trans*-2-hexenal $\mathbf{1_B}$, alkyne **2**	cyclopentene carbaldehyde $\mathbf{6_B}$	53%	J0 P15
3.6	3.7	*trans*-2-cinnamaldehyde $\mathbf{1_D}$, alkyne **2**	cyclopentene carbaldehyde $\mathbf{6_C}$	16%	J0 P17
3.6	3.8	DMAC $\mathbf{1_E}$, alkyne **2**	cyclopentene carbaldehyde $\mathbf{6_D}$	> 12%	J0 P43 J0 P51

scheme	reaction	starting materials	product	yield	journal
3.6	3.9	*trans*-2-pentenal **1_A**, deuterated alkyne **2_{deut}**	cyclopentene carbaldehyde **$6_{A,deut}$**	31% (56%D)	J2 P33
3.6	3.10	*trans*-2-pentenal **1_A**, phenyl alkyne **2_{Ph}**	cyclopentene carbaldehyde **$6_{A,Ph}$**	> 9%	J2 P25
3.7	3.11	*trans*-2-pentenal **1_A**, alkyne **2**	Michael product **4_A**	83%	J1 P137
3.7	3.12	*trans*-2-pentenal **1_A**, alkyne **2**	Michael product **4_A**	83%	J1 P139
3.7	3.13	*trans*-2-pentenal **1_A**, alkyne **2_{Ph}**	Michael product **$4_{A,Ph}$**	50%	J2 P73
4.2	protection	Boc-Hyp-OH	^{t}Bu-Boc-Hyp-OH **7**	99.8%	J3 P33
4.2	protection	Boc-Hyp-OH	^{t}Bu-Boc-Hyp-OH **7**	15%	J2 P177
4.2	protection	Boc-Hyp-OH	^{t}Bu-Boc-Hyp-OH **7**	67%	J3 P9
4.2	mesylation	^{t}Bu-Boc-Hyp-OH **7**	^{t}Bu-Boc-Hyp-OMes **8_A**	99%	J3 P17
4.2	tosylation	^{t}Bu-Boc-Hyp-OH **7**	^{t}Bu-Boc-Hyp-OTos **8_B**	93%	J2 P163
4.2	S_N2	1-Methyl imidazole, 1-Bromoethanol	MeIm-C_2-OH **9**	100%	J2 P125
4.3	4.1	^{t}Bu-Boc-Hyp-OMes **8_A**, 1-Butanol	^{t}Bu-Boc-Hyp-O-C_4 **12**	-	J3 P1
4.3	4.2	^{t}Bu-Boc-Hyp-OMes **8_A**, 1-Octanol	^{t}Bu-Boc-Hyp-O-C_8**13**	-	J3 P5
4.4	4.3	^{t}Bu-Boc-Hyp-OMes **8_A**, TBSO-C_4-OH	^{t}Bu-Boc-Hyp-O-C_4-OTBS **14**	x	J3 P23
4.5	4.4	1-Butanol	C_4-OMes **15**	81%	J3 P13
4.5	4.5	1-Methyl imidazole, C_4-OMes **15**	MeIm-C_4-OMes **16**	100%	J3 P15
4.6	4.6	^{t}Bu-Boc-Hyp-OMes **8_A**, 1,2-dibromoethane	^{t}Bu-Boc-Hyp-O-C_2-O-Hyp-Boc-^{t}Bu **17**	x	J2 P175
4.7	4.7	TBSO-C_4-OH	TBSO-C_4-I **18**	79%	J3 P39
4.8	4.8	^{t}Bu-Boc-Hyp-OH **7**	^{t}Bu-Boc-Hyp-I **19**	-	J3P27
4.10 / 4.13	4.9	^{t}Bu-Boc-Hyp-OMes **8_A**, TBSO-C_4-I **18**	^{t}Bu-Boc-Hyp-O-C_4-OTBS **14**	-	J3 P53
4.11 / 4.13	4.10	^{t}Bu-Boc-Hyp-O-C_4-OTBS **14**	^{t}Bu-Boc-Hyp-O-C_4-OH **20**	-	J3 P65 J3 P57
4.12 / 4.13	4.11	^{t}Bu-Boc-Hyp-O-C_4-OH **20**	^{t}Bu-Boc-Hyp-O-C_4-OMes **21**	< 5% over three steps	J3 P67

If a yield is marked with - instead of a percentage, it was not determined. If an x was placed in the yield coulumn, the reaction was not successful.

Mass spectra

figure	MS	name	journal
3.2a	EI	cyclopentene carbaldehyde **$6_{A,Ph}$**	J2 P25
3.2b	EI	vinyl product **$5_{A,Ph(E)}$**	J2 P25
3.2c	EI	Michael product **$4_{A,Ph}$**	J2 P25
3.6a	EI	cyclopentene carbaldehyde **6_A**	J1 P177

figure	MS	name	journal
3.6b	EI	Michael product **4**$_A$	J1 P179
3.7	ESI(+)	overall reaction *trans*-2-pentenal **1**$_A$ and alkyne **2**	J2 P139
3.8a	CID	598	J2 P31
3.8b	CID	664	J2 P31
3.8c	CID	786	J1 P153
3.9a	CID	526	J0 P43
3.9b	CID	592	J1 P153
3.9c	CID	696	J1 P153
3.10	CID	721	J2 P33
3.11a	CID	1105	J2 P3
3.11b	CID	1226	J1 P141
3.11c	CID	1684	J1 P141
3.12a	CID	1431	J1 P151
3.12b	CID	1432	J2 P33
3.12c	CID	1459	J2 P39
3.13	CID	1021	J2P31
3.14a	ESI(+)	overall reaction *trans*-2-pentenal **1**$_A$ and deuterated alkyne **2**$_{deut}$	J2 P33
3.14b	ESI(+)	overall reaction *trans*-2-pentenal **1**$_A$ and phenyl alkyne **2**$_{Ph}$	J2 P17
3.15a	ESI(+)	overall reaction *trans*-2-hexenal **1**$_B$ and alkyne **2**	J2 P39
3.15b	ESI(+)	overall reaction *trans*-2- octenal **1**$_C$ and alkyne **2**	J1 P103
3.15c	ESI(+)	overall reaction *trans*-2-cinnamaldehyde **1**$_D$ and alkyne **2**	J2 P143
3.22a	ESI(+)	Michael addition *trans*-2-pentenal **1**$_A$ and phenyl alkyne **2**$_{Ph}$	J2 P19
3.22b	ESI(+)	Michael addition *trans*-2-pentenal **1**$_A$ and phenyl alkyne **2**	J1 P179
3.22c / 3.22d	ESI(+)	5-*exo*-*dig*-cyclization Michael product **4**$_A$	J1 P187
3.24a	ESI(+)	5-*exo*-*dig*-cyclization Michael product **4**$_A$ solely gold	J1 P139
3.24b	ESI(+)	5-*exo*-*dig*-cyclization Michael product **4**$_A$ solely gold with 10 mol% pyridine	J1 P171
3.24c	ESI(+)	5-*exo*-*dig*-cyclization Michael product **4**$_A$ solely gold with 10 mol% TEA	J2 P35
3.25	CID	944	J2 P33
3.31a	ESI(+)	overall reaction *trans*-2-octenal **1**$_E$ and alkyne **2** with 10 mol% pyridine	J2 P7
3.31b	ESI(+)	overall reaction *trans*-2-octenal **1**$_E$ and alkyne **2** with 50 mol% benzoic acid	J2 P3
3.32a	ESI(+)	Michael addition *trans*-2-pentenal **1**$_A$ and phenyl alkyne **2** with 10 mol% pyridine	J1 P175
3.32b	ESI(+)	Michael addition *trans*-2-pentenal **1**$_A$ and phenyl alkyne **2** with 50 mol% benzoic acid	J1 P153

figure	MS	name	journal
3.33a	ESI(+)	5-*exo-dig*-cyclization Michael product $\mathbf{4_A}$ with 10 mol% pyridine	J1 P159
3.33b	ESI(+)	5-*exo-dig*-cyclization Michael product $\mathbf{4_A}$ with 50 mol% benzoic acid	J1 P143
4.4a	ESI(+)	S_N2 reaction crude after distillation	J3S35
4.4b	ESI(+)	S_N2 reaction first combined organic layers	J3S35
4.4c	ESI(+)	S_N2 reaction crude second combined organic layers	J3S35
4.4d	ESI(+)	S_N2 reaction crude first aqueous layer	J3S35
4.4e	ESI(+)	S_N2 reaction crude second aqueous layer	J3S35
4.6a	ESI(+)	TBAF deprotection crude after extraction	J3 P47
4.6b	ESI(+)	TBAF deprotection crude after filtration over silica	J3 P47
4.8	ESI(+)	mesylation	J3 P49
4.9	HR ESI(+)	mesylation	J3 P67
9.1	EI	deuterated alkyne $\mathbf{2_{deut}}$	J2 P29
9.2	EI	deuterated alkyne $\mathbf{2_{deut}}$	J2 P37
9.3	EI	cyclopentene carbaldehyde $\mathbf{6_{A,deut}}$	J2 P33
9.7	ESI(+)	5-*exo-dig*-cyclization Michael product $\mathbf{4_A}$ solely gold with 50 mol% benzoic acid	J1 P163
9.10	HR ESI(+)	S_N2 test reaction 1-butanol crude	J3 P1
9.11	HR ESI(+)	S_N2 test reaction 1-butanol crude	J3 P5

Gas chromatograms, ^{1}H NMR spectra, UHPLC-coupled UV/Vis measurements and other data

figure	method	name	journal
3.1	gas chromatogram	overall reaction *trans*-2-pentenal $\mathbf{1_A}$ and phenyl alkyne $\mathbf{2_{Ph}}$	J2 P25
3.3	DEPT	cyclopentene carbaldehyde $\mathbf{6_{A,Ph}}$	J2 P25
3.5a	gas chromatogram	overall reaction *trans*-2-pentenal $\mathbf{1_A}$ and alkyne **2**	J1 P177
3.5b	gas chromatogram	Michael addition *trans*-2-pentenal $\mathbf{1_A}$ and phenyl alkyne **2**	J1 P179
3.16 / 3.17 / 3.18 / 3.19 / 3.23 / 3.27 / 3.28	GC monitoring	overall reaction *trans*-2-pentenal $\mathbf{1_A}$ and alkyne **2**	J2 P63
3.17	GC monitoring	overall reaction *trans*-2-hexenal $\mathbf{1_B}$ and alkyne **2**	J2 P39
3.17	GC monitoring	overall reaction *trans*-2-octenal $\mathbf{1_C}$ and alkyne **2**	J2 P143
3.17 / 3.18	GC monitoring	overall reaction *trans*-2-cinnamaldehyde $\mathbf{1_D}$ and alkyne **2**	J2 P85
3.19	GC monitoring	overall reaction *trans*-2-pentenal $\mathbf{1_A}$ and deuterated alkyne $\mathbf{2_{deut}}$	J2 P33

figure	method	name	journal
3.20	GC monitoring	overall reaction *trans*-2-pentenal **1_A** and phenyl alkyne **2_{Ph}**	J2 P159
3.21	GC monitoring	overall reaction *trans*-2-pentenal **1_A** and phenyl alkyne **2_{Ph}** (doubled equivalents)	J2 P55
3.23	GC monitoring	Michael addition *trans*-2-pentenal **1_A** and alkyne **2**	J2 P65
3.23	GC monitoring	5-*exo*-*dig*-cyclization Michael product **4_A**	J2 P53
3.26	GC monitoring	5-*exo*-*dig*-cyclization Michael product **4_A** solely gold	J2 P147
3.26	GC monitoring	5-*exo*-*dig*-cyclization Michael product **4_A** solely gold with 10 mol% pyridine	J2 P149
3.26	GC monitoring	5-*exo*-*dig*-cyclization Michael product **4_A** solely gold with 10 mol% triethylamine	J2 P151
3.27	GC monitoring	overall reaction *trans*-2-pentenal **1_A** and alkyne **2** with 50 mol% benzoic acid	J2 P61
3.27	GC monitoring	overall reaction *trans*-2-pentenal **1_A** and alkyne **2** with 10 mol% pyridine	J2 P59
3.28	GC monitoring	overall reaction *trans*-2-pentenal **1_A** and alkyne **2** with 50 mol% benzoic acid (Michael product **4_A**)	J2 P61
3.28	GC monitoring	overall reaction *trans*-2-pentenal **1_A** and alkyne **2** with 10 mol% pyridine (Michael product **4_A**)	J2 P59
3.29	GC monitoring	Michael addition *trans*-2-pentenal **1_A** and alkyne **2** with 50 mol% benzoic acid	J2 P69
3.29	GC monitoring	Michael addition *trans*-2-pentenal **1_A** and alkyne **2** with 10 mol% pyridine	J2 P67
3.30	GC monitoring	5-*exo*-*dig*-cyclization Michael product **4_A** with 50 mol% benzoic acid	J2 P51
3.30 / 9.9	GC monitoring	5-*exo*-*dig*-cyclization Michael product **4_A** with 10 mol% pyridine	J2 P49
5.1a	^{1}H NMR	example for domino cyclization with oxidative coupling in CD_2Cl_2	J1 P33 NMR V6
5.1b	^{1}H NMR	example for domino cyclization with oxidative coupling in CD_2Cl_2 with isopropanol as internal standard	J1 P59 NMR V9
5.3a	^{1}H NMR monitoring	domino cyclization with oxidative coupling measurements in dichlrormethane-d_2 (10 mg/mL)	J1 P33 NMR V 8
5.3b	^{1}H NMR monitoring	domino cyclization with oxidative coupling measurements in dichlrormethane-d_2 with isopropanol as standard (10 mg/mL)	J1 P59 NMR V9
5.4a	^{1}H NMR monitoring	domino cyclization with oxidative coupling measurements in dichlrormethane-d_2 (1 mg/mL)	J1 P81 NMR V12B
5.4b	^{1}H NMR monitoring	domino cyclization with oxidative coupling measurements in dichlrormethane-d_2 with isopropanol as standard (1 mg/mL)	J1 P81 NMR V12B
5.5a	^{1}H NMR monitoring	domino cyclization with oxidative coupling measurements in benzene-d_6 (1 mg/mL)	J1 P69 NMR V11
5.5b	^{1}H NMR monitoring	domino cyclization with oxidative coupling measurements in tetrahydrofurane-d_8 (1 mg/mL)	J1 P81 NMR V12A
5.6	UHPLC	example for the detection of substrate **31**, monomer **32** and dimer **33**	J1 P97
table 5.1	UHPLC calibration	dilution series for substrate **31**, monomer **32** and dimer **33**	J1 P107
5.7	UHPLC monitoring	domino cyclization with oxidative coupling (20 mL/mmol)	J1 P109
5.8	UHPLC monitoring	domino cyclization with oxidative coupling (100 mL/mmol)	J1 P117

figure	method	name	journal
9.4	^{1}H NMR	cyclopentene carbaldehyde $\mathbf{6_{A,Ph}}$	J2 P25
9.5	^{13}C NMR	cyclopentene carbaldehyde $\mathbf{6_{A,Ph}}$	J2 P25
9.8	GC monitoring	5-*exo*-*dig*-cyclization Michael product $\mathbf{4_A}$ solely gold with 50 mol% benzoic acid	J1 P163
9.12	^{1}H NMR	TBAF deprotection of **20**	J3 P11
table 9.2a	mesylation	separation with cyclohexane : ethyl acetate 1 : 1	J3 P49
table 9.2b	mesylation	separation with cyclohexane : ethyl acetate 2 : 1	J3 P49
table 9.2c	mesylation	separation with cyclohexane : ethyl acetate 9 : 1	J3 P55
table 9.2d	mesylation	separation with cyclohexane : ethyl acetate 6 : 1	J3 P55
table 9.2e	mesylation	separation with cyclohexane : ethyl acetate 6 : 1 + 5% triethylamine	J3 P55
table 9.2f	mesylation	separation with cyclohexane : ethyl acetate 9 : 1 + 5% methanol	J3 P55
table 9.2g	mesylation	separation with cyclohexane : ethyl acetate 19 : 1 + 5% methanol	J3 P55
table 9.2h	mesylation	separation with cyclohexane : ethyl acetate 49 : 1 + 5% methanol	J3 P55 J3 P67
table 9.2i	mesylation	separation with cyclohexane : ethyl acetate 99 : 1 + 5% methanol	J3 P61 J3 P63
9.13	UHPLC calibration	calibration curves for substrate **31**, monomer **32** and dimer **33**	J1 P107